Alma Mater Studiorum – Università di Bologna

DOTTORATO DI RICERCA IN

Scienze Biotecnologiche e Farmaceutiche

Ciclo XXXI

Settore Concorsuale: 06/A3 - MICROBIOLOGIA E MICROBIOLOGIA CLINICA

Settore Scientifico Disciplinare: MED/07 - MICROBIOLOGIA E MICROBIOLOGIA CLINICA

TITOLO TESI
"Human Parvovirus B19: from the development of a reverse genetics system to antiviral strategies"

Presentata da: Ilaria Conti
Matricola n. 0000772499

Coordinatore Dottorato	**Supervisore**
Chiar.mo Prof. **Santi Mario Spampinato**	**Chiar.mo Prof.** **Giorgio Gallinella**

Esame finale anno 2019

Abstract

Dott. Ilaria Conti

Supervisor: Prof. Giorgio Gallinella

PhD course: Scienze Biotecnologiche e Farmaceutiche, XXXI ciclo

Thesis: "Human Parvovirus B19: from the development of a reverse genetics system to antiviral strategies"

Human Parvovirus B19 (B19V) is a human pathogenic virus which belongs to the *Parvoviridae* family. It is worldwide distributed and is responsible of various clinical manifestations in human, although neither an antiviral therapy nor a vaccine are available. The virus is not well adapted to grow in cellular cultures and this causes difficulties for its propagation, maintaining and characterization. B19V has a narrow tropism for the erythroid progenitor cells of human bone marrow and very few cellular systems can support the viral replication (such as, UT7/EpoS1 cells which is a megakaryoblastoid cell line).

In this research, a reverse genetic approach was developed to allow the generation of mature and infectious viral particles from an established *consensus sequence*. Synthetic clones that differ for the length and isomerism of their terminal regions (ITRs) were constructed. After their transfection in UT7/EpoS1 cells, the obtained viral particles were used to infect EPCs (erythroid progenitor cells) in serial passages, in order to evaluate the capability for each clone to generate a new viral stock and to propagate it. Mature and functional viral particles, with properties comparable to the native virus, were obtained by clones containing the almost full length ITRs. Indeed, clones codifying ITRs that were extended till the symmetry sites could generate new B19V functional particles, only whether the terminal regions had different isomerisms.

Not only a deep investigation of the virus, but also the study of its target cells is important for Human Parvovirus B19 characterization. Actually, the virus can productively infect cells in a "restricted window" within the erythroid differentiation lineage. Cellular factors and mechanisms change along their differentiation and this variation probably influences the cellular susceptibility and permissiveness to the virus. The expression of the globoside receptor, the coreceptor (receptor for the viral VP1u protein), transferrin (marker of endocytosis) and pSTAT5 (EpoR pathway) was evaluated in both EPCs and UT7/EpoS1 cells during this research. These markers were commonly detected among the cells, although only a portion of them were infected by the virus. These results suggested the presence of other factors that determined a cell as permissive and susceptible to the B19V.

Characterization of both the virus and the cells allows investigation of new strategies for the development of specific antiviral compounds. In this research, different molecules were tested that acted on different targets: i) re-targeted drug: *Hydroxyurea* (an inhibitor of the available deoxyriboncleotides); ii) lipid conjugate of a broad range drug: *Brincidofovir* (acyclic nucleoside phosphonate analogue); iii) screening of small chemical library; iv) investigation of DNA G4 structures and possible ligands.

The retargeted drug *Hydroxyurea* (HU) and the broad range analogue *Brincidofovir* (BCV) showed an antiviral activity toward B19V. A potent and selective antiviral action was especially observed for *Brincidofovir,* which totally inhibited the viral replication without effect on the cells. Both the drugs are already available and used for other purposes, such as the treatment of sickle-cell disease for HU, and as a broad-range antiviral compound against other dsDNA viruses for BCV. The identification of these compounds as antiviral agents can also lead advances towards a more selective B19V antiviral strategy.

Investigation of other strategies did not allow to identify a compound with comparable inhibitory activity against the Human Parvovirus B19V. Small-scale screening of newly synthesized molecules (such as, coumarin analogues) were performed and led to identification of compounds with suboptimal activity, which however can form the basis for the further development. Presence of G-quadruplex structures (G4) were predicted within the B19V ITRs by computational tool and they could be considered as target for new antiviral compounds, although both chemical and biological studies in presence or not of known G4 ligands did not fully corroborate the computational predictions and did not suggest a relevant role for putative G4 structures in the viral lifecyle.

Further investigation of the virus-cells complex and the biological characteristics of B19V will allow to increase the knowledge of the virus for continuing the development of an antiviral strategy.

Table of Contents

1. Introduction

2. Aim of the Research

3. B19V Synthetic Genome and Virus

7. Materials and Methods

8. References

1. Introduction

1.1 Taxonomy and Evolution

Human Parvovirus B19 (accepted acronym = B19V) is probably the smallest non-enveloped human pathogen among the pool of viruses that are known at the moment; according to this, *parvum* means *small* from Latin.

This little virus was discovered by Yvonne Cossart and colleagues in 1974 in England during the screening of blood samples for hepatitis B antigens; at first, the "new agent" was confused with hepatitis virus both morphologically and serologically [Cossart et al.; 1975] The naming of B19V was just due to the label of a sample in this study: number 19 in panel B [Heegaard et al; 2002]. In 1979, it was independently characterized in Japan as "Nakatani" virus but subsequent testing proved the two viruses to be identical [Okochi et al.; 1984]. Although Human Parvovirus B19 was originally labeled *"serum parvovirus-like particle"* or *"human parvovirus"*, it was officially recognized as a member of the *Parvoviridae* family and given the name B19 by the International Committee on Taxonomy of Viruses in 1985 [Siegl et al; 1985]. Due to the fact that B19V is the only well-known parvovirus to cause disease in humans, it became one of the most important member of the *Parvoviridae* family.

The *Parvoviridae* family is divided into two different subfamilies: *Parvovirinae* and *Densovirinae*. These two subfamilies are distinguished primarily by their respective ability to infect vertebrate and arthropod hosts [Cotmore et al.; 1986 - Cotmore et al.; 2014].

Inside the *Parvovirinae* subfamily (figure 1.1), eight different genera could be identified according to the phylogenetic analysis of the amino acid sequence of the large nonstructural protein NS [International Committee on Taxonomy of Viruses, 2014]. All the viruses that belong to a given genus should have >30% of identical NS amino acid sequence or <30% of identical NS amino acid sequence to those of other *parvovirus* genera. Within a given species, >85% identity of the NS protein is required. Based on this identity, the eight different genera are: *Protoparvovirus*, *Amadoparvovirus*, *Aveparvovirus*, *Bocaparvovirus*, *Copiparvovirus, Dependoparvovirus*, *Erythroparvovirus*, and *Tetraparvovrivurs*. Among them, the parvovirus genera that infect humans are *Erythroparvovirus* (such as, B19V), *Bocaparvovirus* (such as, HBoV1-4), *Protoparvovirus* (BuV) and *Tetraparvovirus* (such as, PARV4) [Qiu et al; 2017].

B19V is now classified as a member of the *Erythroparvovirus* genus, since its replication only occurs in erythrocyte precursors (*Erythro* means *red* from Greek, referring to red cell tropism [ViralZone]). Indeed, it is the only accepted member and type species [International Committee on Taxonomy of Viruses; 2000] of the this genus; actually, other viruses have

been proposed to belong of the *Erythroparvovirus* genus: simian parvovirus (SPV), pig-tailed macaque parvovirus (PtPV) and rhesus macaque parvovirus (RhPV) [Gallinella; 2013].
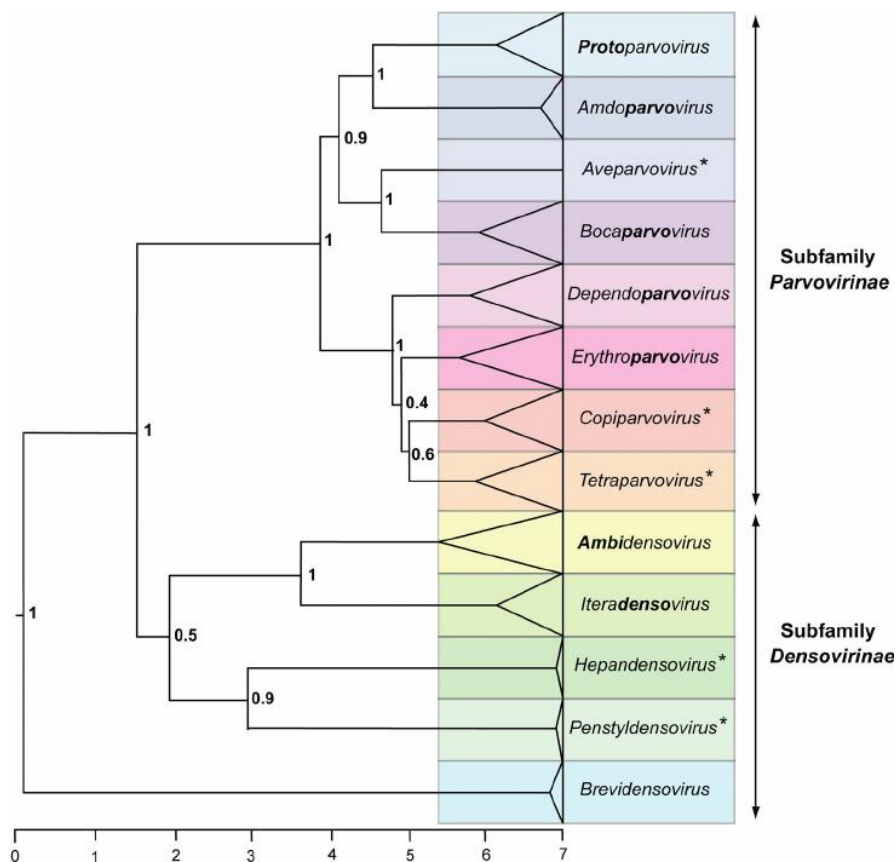
Figure 1.1: Phylogenetic tree of the family *Parvoviridae*: phylogenetic analysis based on the amino acid sequence of the viral non-structural protein which contains a conserved helicase domain. Bayesian trees were calculated over one billion iterations using BEAST; probability scores were indicated at statistically significant nodes. Asterisks denoted the names of the new genera [Cotmore et al; 2014].

The genome of B19V is a 5596 bases long single-stranded DNA, with two inverted repeated terminal regions flanking a unique region which codifies for structural and non-structural proteins. The genome was originally characterized by sequencing a viral isolated called "*pvbaua*" obtained from the serum of a child with homozygous sickle cell disease during the early stages of aplastic crisis in 1985 [Shade et al;1986]. A large number of isolates were sequenced after that and the reported B19 genomes were all intimately clustered showing only 6% divergence among themselves. The non-structural gene was found well conserved, while the capsid genes occasionally showed a variability of 2 to 3% [Hemauer et al; 2000].

In 1990s, the new V9 isolate was identified and it showed to divergence more than 11% from the previous B19V isolates [Nguyen et al; 1998]. Later in 2002, two isolates (they were called LaLi and A6, respectively) were characterized to belong another B19V variant [Servant

et al; 2002]. The three variants were identified as sequence models for three different genotypes: the prototypical B19V isolates for the genotype 1, the LaLi and A6 isolates for the genotype 2 and the V9 isolate for the genotype 3.

The continuous development of innovative sequencing techniques has led to identify a constant increasing number of B19V genomes that could be allocated to one of the three previous mentioned variants. In this way, three clearly separated clusters have been found [Servant et al; 2002]. The region coding for the non-structural protein is well conserved, consistent with a required role in virus propagation, while the structural protein regions may show a greater variability [Mori et al; 1987].

There are about 100 complete or almost complete genomes of Human Parvovirus B19 in NCBI database thanks to polymorphism analysis, sequencing of cloned viral genomes, sequencing of cloned PCR amplification products and direct sequencing of PCR amplification products. Considering alignment of consensus sequences obtained from available complete genomes, the genetic distance between clusters is about 10% for genotype 1 and 5-6% for genotypes 2 and 3. At the same level, the genetic distance within clusters is generally less than 2% for genotype 1 and, in the range 3-10% for genotypes 2 and 3 (figure 1.2). Besides, the constant input of new genomic sequences into databases has allowed for further subdivisions into subtypes. So, within the genotype 1, the majority of isolates belong to genotype 1a, while few isolates from Asia belong to a separate cluster called 1b [Parsyan et al; 2007]. Also genotype 3 is divided into two subtypes: 3a and 3b [Toan et al; 2006].
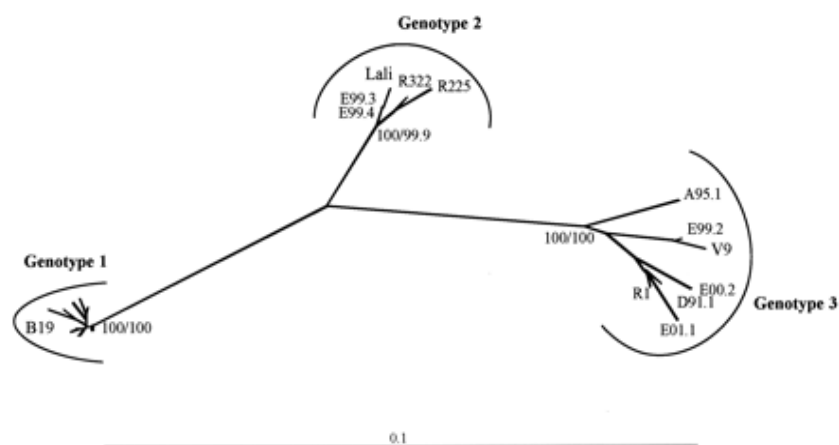
Figure 1.2: Tree graphic of different B19 genomes divide in three genotypes; each genotype is identified by a different cluster [Servant et al; 2002].

All the three B19V genotypes appear to circulate together worldwide but they are different for the frequency and their spatial and temporal distribution is not uniform [Candotti et al; 2004]. The genotype 1a is the most common and it is present in all geographic areas. Since

1960s, the genotype 2 has been rarely found in acute infections or blood but it can frequently be detected within various tissues of people born before 1972; for example, B19V was recently found in 45% of 106 old bones of Finnish victims from World War II [Toppinen et al; 2015]. Finally, the genotype 3 can be frequency detected in Western Africa (such as Ghana) and at lower frequency in other geographic areas including Europe, Brazil, India and South Africa. Although not very probable, the possibility of concomitant infection of more than one genotype cannot be completely excluded [Schneider et al; 2008]. Among the Parvovirus B19 genotypes, genotype 3 seems to be the most divergent and probably this could indicate a longer evolutionary history than the other genotypes [Hubschen et al; 2009].

A completely different situation appears when the viral genotype is analyzed from other sources than blood, indeed long-term persistence of B19V DNA in human tissue is a well-known feature. The residual viral DNA can remain in tissue for decades or even lifelong (bioportfolio), after acute infection [Norja et al; 2006]. In these instances, the frequency of viral DNA and abundance of different genotypes could help us to understand the spread of the virus and its epidemiology in the past; for example, the frequency of genotype 2 was normally higher than now. In particular, genotype 2 is widespread mostly in people born before 1960-1970, while genotype 1 has become prevalent after these years in Europe; so, there was a global replacement of genotype 2 with genotype 1 [Parsyan et al; 2007].

The DNA of Parvovirus B19 type 1 was detected by epidemiological studies in plasma, blood and tissue pools from Danish and Finnish donors, while genotype 3 was initially detected only in African patients (especially from Ghana). Moreover, a different tissue distribution emerges between genotype 1 and 2: the DNA of B19V type 1 persists in numerous tissue types like synovial tissue, skin, liver, brain, muscle and myocardial tissue; the DNA virus type 2 persists especially in skin. Recent studies have shown a lifelong persistence of both the two types of B19V and that they have circulated equally in north and center Europe until 1960s, after that, virus type 2 disappeared. Differently, virus type 3 did not circulate in these large areas during the last 70 years [Ekman et al; 2007]. The molecular basis for these epidemiological differences is unknown and till now, no correlation between specific disease symptoms and B19 sequence has been detected.

Entering in the detail of the phylogenetic history and evolutionary dynamics, a high evolutionary speed, with approximately 10^{-4} nucleotide substitutions per site per year, was observed [Duffy et al; 2008]. This rate is characteristic of the *Parvoviridae* family but it's similar to that of RNA viruses. Moreover, it can lead to a rapid evolutionary dynamics, possibly with the formation of a viral-quasi species (a "quasi-species" is a group of closely

related viral genomes subjected to a continuous process of genetic variation relative to the parents, competition among the offspring generated and their selection in a given environment [Domingo et al; 2012]; by contrast, in a "species" most of the offspring are copies of the parents) and an expansion of the population in the sequence space around master sequences. In a recent study, where the rates of sequence change in plasma-derived virus populations was compared to those resident persistently in tissues, the plasma B19V isolates showed the substitution rate of 4 x 10^{-4} and a synonymous substitution rate of 18 x 10^{-4}; slow or absent sequence change was detected for the tissue-derived viral samples. Besides, the last common ancestor for currently circulating genotype 1 was predicted to exist around 1956-1959, confirming the previous analysis of B19V bioportfolio [Suzuki et al; 2009].

The rate of synonymous substitutions is higher than non-synonymous mutations, indicating for a strong selective pressures on B19 virus. In this way, it is guaranteed both uniformity in the biological behavior and immunogenicity of the diverse genotype [Ekman et al; 2007]. However, a slow and gradual accumulation of point mutations can lead to periodical and dynamic replacement of strains with higher sequence divergence.

1.2 Genome and Transcriptome

Molecular studies on the B19V genome at the electron microscopic observation confirmed the presence of a single-stranded, linear genome as the other members within the *Parvoviridae* family. Subsequent molecular cloning and sequencing allowed to learn more about the genome structure and its organization. The B19V ssDNA molecule is 5596 bases in length of either positive or negative polarity. Molecules of different polarity are incapsidated in icosahedral virions at the same frequency (figure 1.3) and can anneal in solution forming linear double-stranded DNA molecules [Deiss et al; 1990].
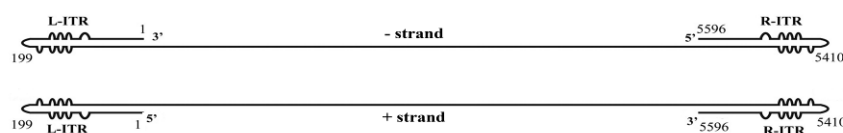
Figure1.3: Genome of Parvovirus B19 of positive or negative polarity. The hairpin ITRs are diagrammed at the two ends of the genomes with unpaired or mismatched bases in the palindromes represented by "bulges" or "bubbles", respectively [Deiss et al; 1990].

Using scanning force microscopy (SFM), which is also known as "atomic force microscopy" (AFM), the results showed that most of the DNA molecules extracted from the viral capsids had a linear form, few molecules had one "fold-back" end and none molecule showed two bifurcated ends (figure 1.4). Probably, the linear form of the DNA is due to its association with the capsid viral proteins.
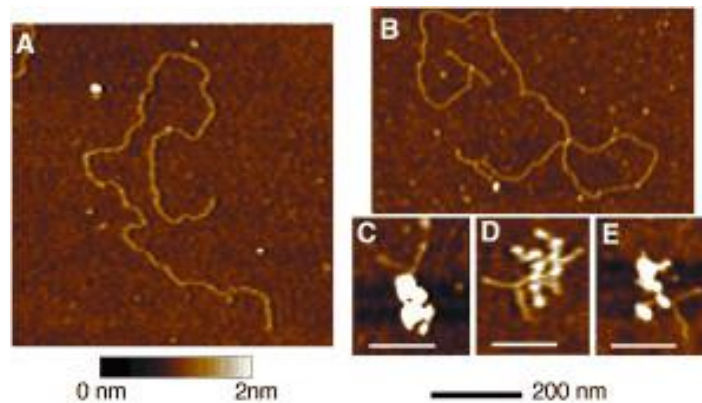
Figure 1.4: TM-SFM (Tapping-mode scanning force microscopy) images of purified B19V DNA adsorbed on the surface of mica before and after heat denaturation. A) Linear double-stranded molecule purified from virions: in most of the molecules, no terminal structures are evident; B) A linear reannealed double-stranded molecules after heat denaturation showing forked double-stranded termini; C-E) Reannealed coiled single-stranded B19V DNA after heat denaturation presenting forked termini protruding from their irregular and compact coiled bodies (the size bars are 100 nm long in these enlargements) [Zuccheri et al; 2001].

The viral genome is composed of a unique internal region (IR) of 4830 nucleotides, which contains all the coding sequences and is flanked by two repeated, inverted terminal regions (ITRs). Each terminal region is 383 nucleotides long and its last 365 bases are an imperfect palindrome due to the sequence asymmetries. The ITRs can fold back on themselves assuming hairpin duplex configurations and serving as primers for the synthesis of the complementary strand [Astell et al; 1990]. Actually, the terminal regions can be present in either one of the two alternative sequences, each is inverted complement of the other and they are usually labeled as flip/flop. As a result of the combination of these alternative sequences at both termini, four different genome isomers can be identified for Human Parvovirus B19. The presence of these self-complementary sequences in the terminal regions allows to adopt different conformations to the single-stranded DNA: terminal loop and stem structures [Zuccheri et al; 2001] (figure 1.5). The mismatched bases in the ITRs probably introduce distortions in these "double.stranded" structures, so the diverse B19V isomers might differ depending on the distortion introduced.

Differences within the three genotypes have been found not only in the internal region, but also along the inverted terminal regions: genotype 2 has variations in the ITRs in comparison to genotype 1 [Tsuikawa et al; 2012], while at present, no ITR sequence of genotype 3 has been reported.
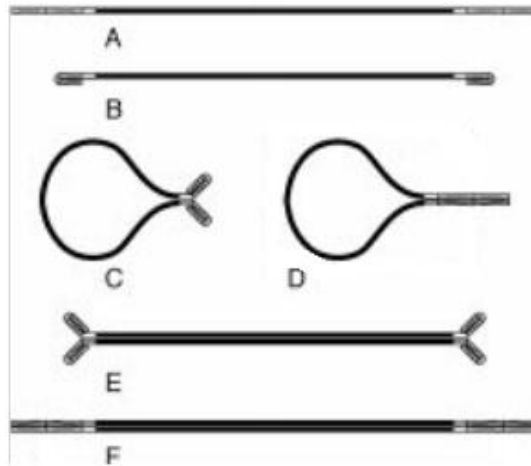
Figure 1.5: Scheme of the different structural possibilities of parvovirus B19 DNA (the grey parts are the terminal palindromes; the white ones in the terminal regions are the non-palindromic parts of the inverted regions). A) A single-stranded molecule with extended termini; B) A single-stranded molecule with the palindromic ended regions fold back themselves; C) A single-stranded molecule with" fold-back ends"; D) A single-stranded molecule with double-stranded linear ends; E) A double-stranded molecule with "fold-back" ends; F) A completely annealed double-stranded molecule [Zuccheri et al; 2001].

The ITRs contain the origin of replication (Ori) which works as active replicative origin in double-stranded DNA during B19V replication. The internal region of 4830 nucleotides has a single promoter, (P6, transcription start is at nt 531) and contains all open reading frames (ORF) that codify for viral proteins: two major and a number of minor reading frames are present. In particular, the viral non-structural protein NS is codified in the left half of the genome and the two viral capsid proteins VP1 and VP2 are codified in the right half of the genome. Additional minor reading frames are present in the center and right end of the genome and they potentially codify for smaller non-structural proteins: 11 kDa, 9 kDa and 7.5 kDa. During evolution, the virus was probably constrained to maintain the large structural and non-structural proteins rather than the small non-structural polypeptides. Actually, the nucleotide substitutions are more common where nucleotide sequence is shared by two overlapping ORFs (between the ORF which codifies for a big protein and the one for a small protein, as NS/7,5 kDa, VP1/9kDa, VP2/11kDa) usually resulted in amino acid changes that are more frequent in the small protein (5-8 changes in the 7,5, 9 and 11 kDa proteins,

respectively) than in the large protein (2, 6 and 0 changes in NS, VP1 and VP2 proteins, respectively) [Servant et al; 2002].

Various enhancer elements upstream of the P6 promoter bind the cellular transcription factors CREBP, C-Ets, GATA, YY1, Oct-1, Sp1, Sp3 and their action improve the P6 promoter activity [Raab et al; 2001]. Viral NS protein binds NS-binding elements (NSBEs), which is rich in C and G nucleotides, at nt 337 to 354 (figure 1.6): these are located inside the ITRs and, together with NS protein-Sp factors interaction act to transactivate the P6 promoter [Tewary et al; 2014]. Finally, a hypoxic environment may also increase the activity of the promoter [Pillet et al; 2004].
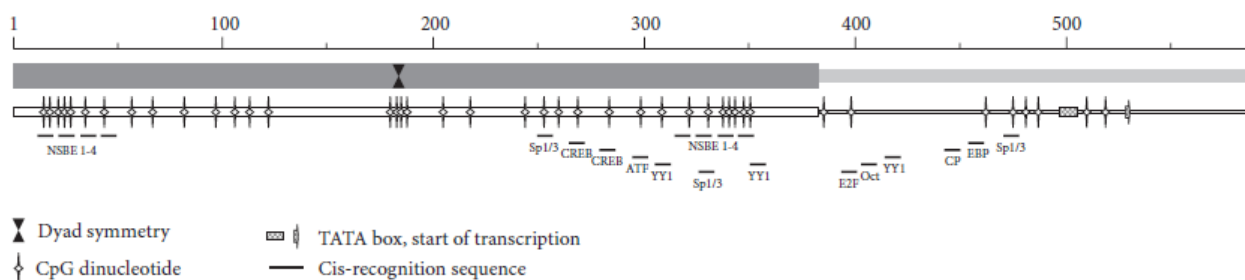
Figure 1.6: Schematic representation of the left terminal region of B19V within CpG dinucleotides, TATA box and start of transcription, a selection of cis-recognition sequences for eukaryotic transcription factors and NS protein-binding elements. Thick box) left inverted terminal region with indication of the dyad symmetry; Thin box) internal region [Gallinella et al; 2012].

Sequencing analysis of clinical samples (amniotic fluid, fetal blood and sera from different patients) showed that the P6 promoter region was markedly divergent between B19 and V9 viruses, as well as Lali and B19 virus and between Lali and V9 virus. Indeed, the fourth GC box inside the V9 promoter region was deleted compared to the B19 virus P6 (a putative binding site for the cellular factor Sp1 located just upstream of the TATA box). Within the P6 region analyzed, the other identified binding motifs for transcription factors were preserved, although some nucleotide substitutions [Servant et al; 2002].

From the promoter P6, a single precursor mRNA (pre-mRNA) is transcribed, which generates several mature mRNA transcripts due to alternative splicing and polyadenylation. Two sites, named pAp (proximal site; in the middle of the genome) and pAd (distal site; in the right end of the genome) respectively, are responsible for the polyadenylation. The pAp controls the internal polyadenylation and is divided into the two sites pAp1 and pAp2, respectively. The pAp1 site contains a non-consensus hexanucleotide core motif (AUUAAA) and for its efficient function, it requires both downstream and upstream cis-acting elements;

indeed, it is further influenced by a second adjacent non-consensus motif (AAUAAC). On the contrary, pAp2 contains a canonic hexanucleotide core-motif (AAUAAA) [Yoto et al; 2006]. Cleavage at pAp1 will generate the most abundant classes of viral mRNAs, cleavage at pAp2 will occur at tenfold lower frequency and generates alternative mRNAs potentially including the small ORF of the 9 kDa protein.

The pre-mRNA contains two introns with two splicing donor sites (D1 and D2), each followed by two alternative splice acceptor site (A1-1/2 and A2-1/2). All the spliced viral transcripts have a common 60 nucleotides long leader sequence at their 5' end spliced from the D1 splice site to the central exon. When polyadenylated at pAp site, the unspliced mRNAs encode the large NS protein, while of the small mRNAs spliced at D1 to A1-2 those that are spliced only at the A1-1 acceptor can potentially encode the small 7.5 kDa protein [St Amand et al; 1993 - Luo et al; 1993].

The first intron is spliced out from all the mRNA with polyadenylation at the pAd site. The mRNAs resulting from this polyadenylation encode capsid protein VP1. The mRNAs that are polyadenylated at pAd and excise both the first and the second small intron (D2 to A2-1) encode VP2, while those that are polyadenilated at pAd site and excise the first and the second large introns (D2 to A2-2) encode the 11 kDa protein. (figure 1.7).

All these events are in relation to the viral DNA replicative process. Without replication, the internal polyadenylation at pAp sites is favored, while during the replication, the overcoming of pAp is enhanced and the polyadenylation occurs at the distal site pAd. So, replication of the genome would increase the generation of transcripts that encode the viral capsid proteins and the 11 kDa non structural protein [Bua et al; 2016].

Serine-arginine (SR) protein-binding GAA motifs have been found in the central exon to act as exonic splicing enhancers/intronic splicing enhancers (ESEs/ISEs , respectively) elements. Of these, ISE1 and ESE1 elements have been identified in the region between A1-1 and A1-2 and facilitates splicing at the A1-1 acceptor site. ESE2 and ESE3 have been identified in the region between A1-2 and D2 site: ESE2 facilitates the splicing at the A1-2 acceptor site, while ESE3 is important for recognition of the D2 donor site. The G/GU rich region next to the D2 site acts as ISE2. The frequency of recognition events can provide the basis for regulatory splicing during B19V pre-mRNA processing [Guan et al; 2011].

Alternative splicing coordinates polyadenylation: for example, splicing of the pre-mRNA within the first intron (D1-A1) stimulates polyadenilation at the pAp site, while the splicing of the second intron (D2-A2) leads to polyadenylation at the pAd site. So, splicing of the second intron competes with polyadenylation at the pAp site [Guan et al; 2011].
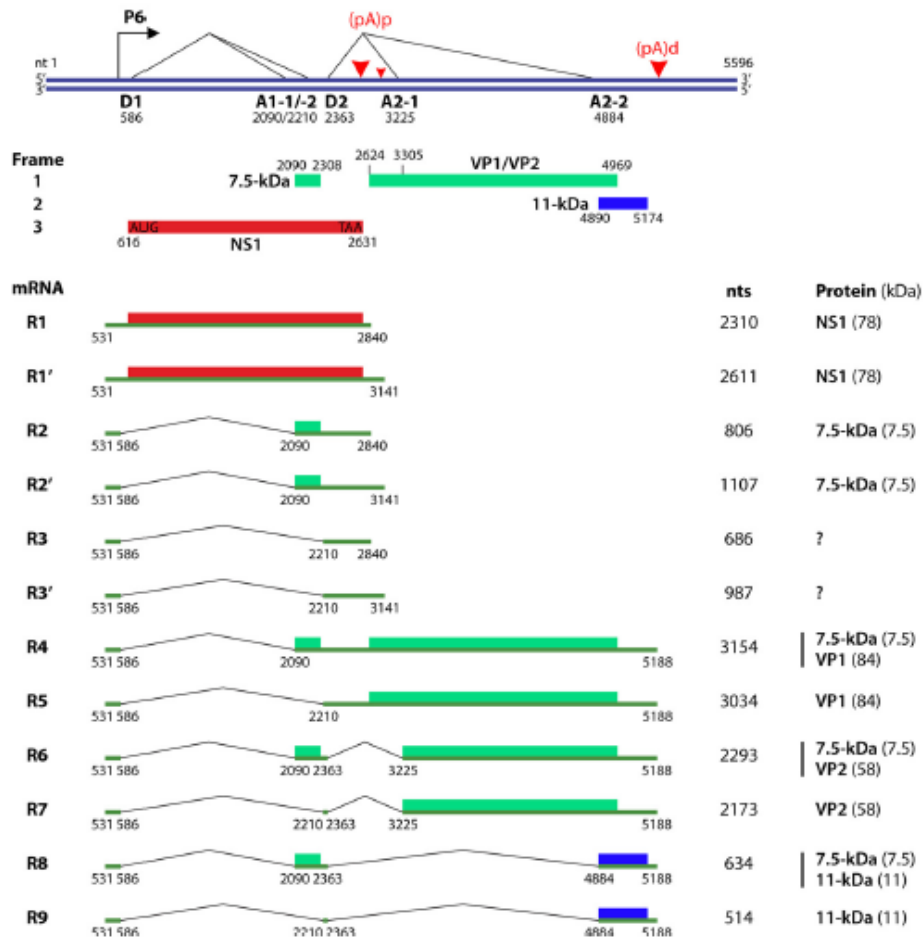
Figure 1.7: Schematic diagram of the double-stranded replicative form of the B19V genome. The P6 promoter, the RNA initiate site, the splice donor and the splice acceptor sites, polyadenilation sites and the resulting nine major and three minor RNAs (R1 to R9 and R1' to R3', respectively) are indicated. Proteins encoded by each mRNA and their molecular masses are shown on the right; different ORFs are identified in different colors [Qiu et al; 2017].

Different patterns of splicing and polyadenylation has been observed in B19V-permissive and non-permissive cells. In particular in non-permissive cells, most of the mRNAs are polyadenylated at pAp site, and thus the mRNAs encoding capsid proteins are produced in low level; in permissive cells, most B19V mRNAs encode for VP1, VP2 and 11 kDa proteins due to the reading through the pAp site coupled to the viral replication. Indeed, the early blocking of full-length mRNAs production has been identified as a mechanism of virus tropism. In a viral permissive environment, two distinct patterns in the viral mRNA production has been revealed: i) at an early phase of infection, a block at the pAp site leads to higher-level production of NS-mRNAs; ii) at a late phase of infection, the read through of pAp is more efficient and it leads to a higher-level production of VP1-, VP2- and 11 kDa-

mRNAs. The mechanism implicated to overcome the transcription block in B19V permissive cells is still not known [Bua et al; 2016].

CpG DNA methylation can be an epigenetic modification which play a role in the control of gene expression. Indeed the Human Parvovirus B19 ITRs show all the features of a genomic CpG island. The effects of DNA methylation on the regulation of viral genome were investigated by transfection of two viral DNAs in a model cell line, unmethylated or methylated in vitro, respectively: the results showed that methylation of viral DNA caused a lower expression levels of the viral genome. Besides, the same correlation was found in different B19V infected cellular environments *in vitro* and in natural infected bioptic samples *in vivo*. The methylation of B19V genome in a typical CpG island and the presence of an epigenetic level of regulation of viral genome expression, probably correlate with its silencing and contributing to the maintenance of the virus in tissues [Bonvicini et al; 2012].

1.3 Morphology

As previously mentioned, the B19V ssDNA is enclosed inside a small capsid which is a common characteristic for the parvoviruses. The non-enveloped viral particles are 24-25 nm in diameter and show an icosahedral symmetry due to the combination of 60 protein subunits: 20 triangular faces, 12 pentagonal vertices in each of which converge 5 protein subunits (penton). They are made of two structural proteins (VP1 and VP2) in different amount: the larger VP1 proteins contributes for about the 5% of the virion mass, while the smaller VP2 constitutes the remaining 95% of the virion [Cotmore et al; 1986]. Cryoelectron microscopy and crystallographic X-ray diffraction studied on VP2-only B19 capsids (VLP: viral like-particles), together with capsid sequence alignment and comparison with known molecular structure, allowed the structural prediction of the B19V capsid shell. More recently, native virions both empty and full for viral DNA, have been purified and crystallized (figure 1.8).

The parvovirus capsid comprises 60 subunits called capsomers composed by the VP1 and VP2 capsid proteins that assemble into a T=1 icosahedral symmetry. The two proteins are codified by the same open reading frame but they differ only in the N-terminal extension of VP1, which is longer of 227 aa than VP2 and it is called the unique region (VP1u). However, this VP1u region is exposed only after receptor binding, heat or low-pH treatment; whereas this region seem to be always accessible in VLPs.
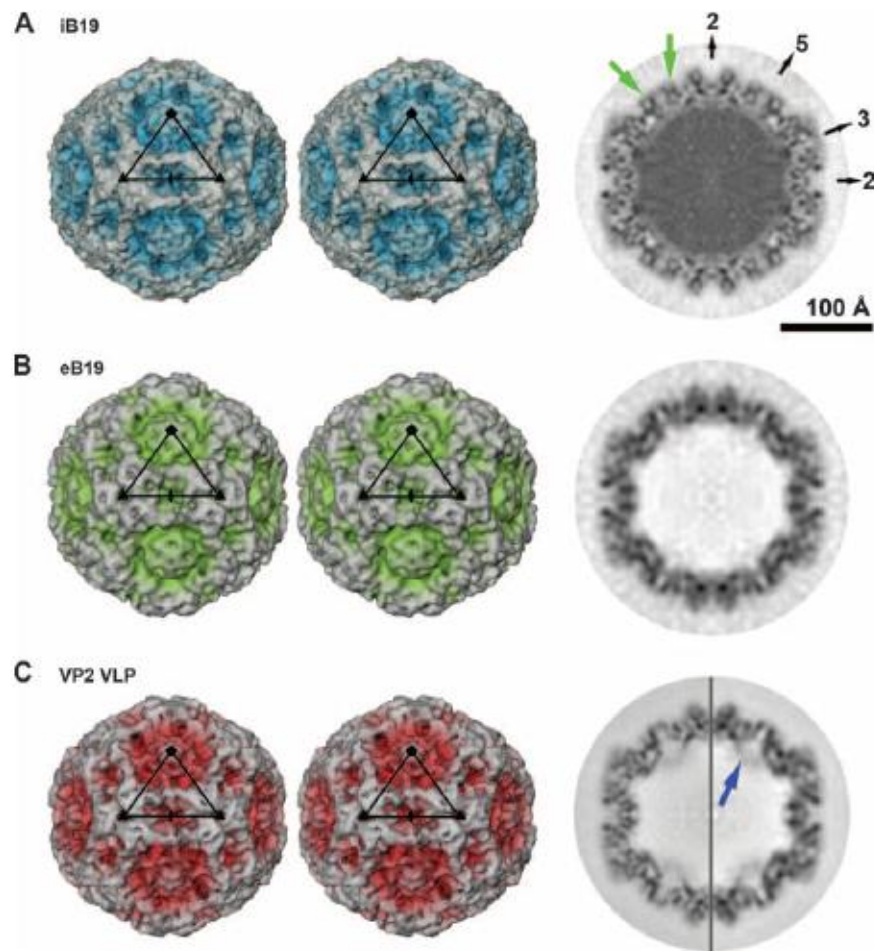
Figure 1.8: 3D image reconstruction of Parvovirus B19 = A) Intact B19V particle (iB19) at 7,5 Å resolution: The black triangle identifies an icosahedral asymmetric unit (left); darker coloring in the central cross-section (right) corresponds to higher electron density. The positions of 2-, 3-, 5-fold axis are indicated by black arrows. Densities near the viral surface are highlighted with green arrows. Darker coloring in the central cross-section corresponds to the higher electron density; B) Empty B19V particle (eB19) at 11,3 Å resolution; C) Recombinant B19V VP2 VLP (VP2 VLP) at 7,7 Å resolution: differences between wild-type B19V particles and VP2 VLP are located around the icosahedral 5-fold axes. Blue arrow identifies a density due to an internally located VP2 termini. The equatorial slice divides the 7,7 Å resolution (left) and 11,3 Å resolution (right) resolution [Kaufmann et al; 2008].

VP2 alone is sufficient to form icosahedral virus-like particles with all the parvovirus surface features, like protrusions and depressions. VP2 contains an antiparallel eight-stranded β-barrel consisting of the arrangement of two β-sheet. This motif is approximately in the same position relative to the icosahedral symmetry axis and large insertions (loops) connecting the strands of the β-barrel are responsible for the contacts among the subunits, so they determine the topography and specific structures at the 5-, 3- and 2-fold symmetry axis (figure 1.8 and 1.9).
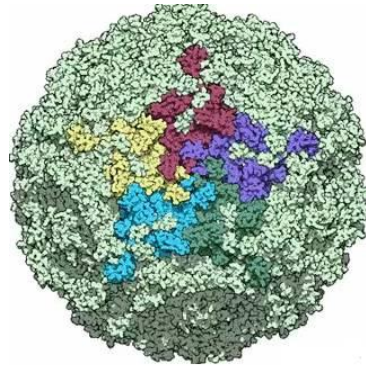
Figure 1.9: Distribution of the 5 viral proteins (red, yellow, purple, light blue, dark green) within a capsomer (penton unit) [PDB: 1s58].

The capsid appears to be stabilized by the presence of the neighboring VP2 molecules where loops 3 and 4 of loop GH of one subunit are closely connected with loop 1 of loop BC and a portion of another loop GH of a 3-fold symmetry-related subunit (figure 1.10). Most of the C-terminal 50 residues of VP2 are accessible on the particle surface, but the final 4 amino acids are buried inside the shell; the N-terminus of the VP2 structure is located within the capsid too and closed to a 5-fold axis [Kaufmann et al; 2004].
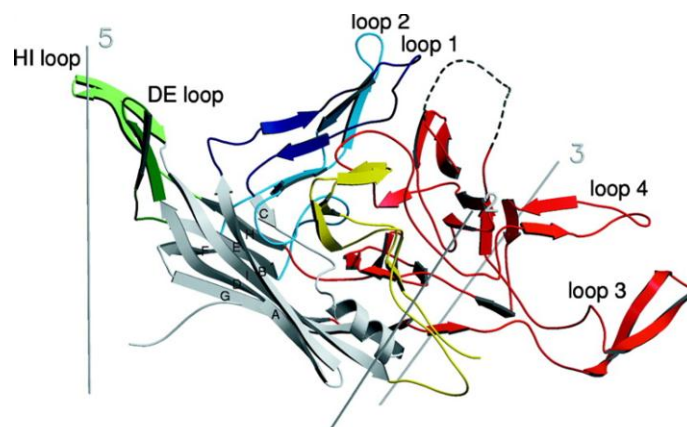
Figure 1.10: Ribbon diagram of VP2. The strands of the β-barrel (gray) are labeled A to I. The surface loops connecting the strands of the β-barrel are labeled by color: dark blue (BC loop), dark green (DE loop), light blue (EF loop), red (GH loop), light green (HI loop), yellow (C-terminal amino acids). The position of the disordered loop (amino acids 301–313) (dashed line) was modeled based on the corresponding AAV-2 loop [Kaufmann et al; 2004].

Parvovirus B19 is characterized by the absence of prominent spikes at the 3-fold axis and a general smooth surface; a dimple-like depression occurs at each 2-fold axes. A cylindrical

structure is present at the 5-fold axis, it is surrounded by a "canyon-like" depression and it acts as a gated channel connecting the interior and outer surface of the virion.

The 5-fold channel is constructed by five copies of the DE loop, it is occupied by a conserved glycine-rich region and it is suggested to be involved in the externalization of the N-terminal VP1. The channel seems to be usually closed by a gate of threonines at the outer viral surface. The three glycine (aa 136-138) immediately following the gating residues might provide the necessary structural flexibility to switch the channel from closed to open and leading the externalization of one in five of the N terminus VP proteins in the presence of VP1 or DNA or during cell entry [Kaufmann et al; 2008]. The role and the importance of this glycine-rich motif is confirmed by its preservation within erythroviruses: the only significant amino acid change in the DE loop is the gating residue 135 which is a threonine in human viruses and a proline in non-human viruses.

Different densities at electron microscopy were found around the icosahedral 5-fold axis comparing native B19 viruses and VLPs. In particular, a positive density extending toward and into the 5-fold pore was present only in native virions and this was probably as a result of the presence of VP1 and/or DNA, that are absent in the VLPs. However, the positive density was not found to continue through the 5-fold channel to the viral surface, but it continued to the surface of the adjacent 5-fold β-cylinder.

Both VP1- and VP2-N termini are not represented by a crystal structure mainly because their positions are different in each particle and because of the low copy number of the VP1 molecules. Measuring the binding of monoclonal antibodies against VP1u and the phospholipase activity (PLA2) of VP1u, it has been suggested that this protein changes its conformation during virus entry, although this has not been structurally confirmed [Ros et al; 2006]. However, cryoelectron microscopy studies of MVM (minute virus of mice) and AAV-2 (adeno.associated virus type 2) suggested that VP1u is located inside the wild-type particle and a conserved glycine-rich portion close to the VP2 N terminus has been modeled (figure 1.11).

Moreover, a non-conventional nuclear localization signal (NLS; aa 493-503) has been identified in the C-terminal region of VP, which is well conserved within erythroviruses and it is probably involved for the transport of the new viral protein from the cytoplasm to the nucleus. The NLS is exposed on the surface of an isolated VP2 for the recognition by cellular nuclear import molecules, but after assembly, it is hidden in the inner capsid surface [Pillet et al; 2003].
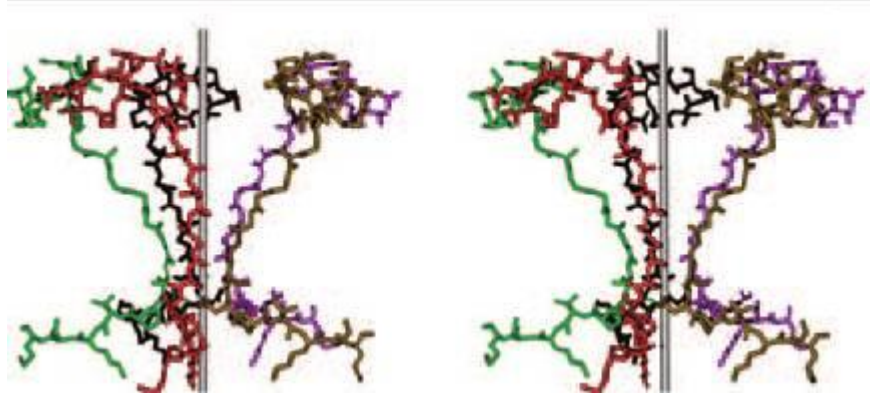
Figure 1.11: Organization ofresidues 1 to 24 of VP2 termin at a 5-fold axis. On the left) the position of the VP terminus makes possible for VP externalization; On the right) the position of VP terminus closes the base of the 5-fold channel [Kaufmann et al; 2008].

Viral particles change their structure during or after cell entry by receptor-mediated endocytosis and this leads to the exposure of the VP termini and genome release. Similar structural changes can be induced in vitro by physiochemical treatment of full DNA-containing virions [Mani et al; 2007].

1.4 Viral Proteins

A total of six ORFs are distributed along the B19V genome and on the three positive strand frames that encode for the structural (capsid proteins) and non-structural viral proteins. In the left half of the genome, the major ORF in frame 1 codifies for the non-structural NS protein. The right half of the genome contains a major ORF in the frame 2 which codifies for the VP1 and VP2. Both the capsid proteins are codified from the same ORF and mRNA splicing events lead to obtain one instead of the other protein. VP1 and VP2 have the same core region but they differ for the unique region at the N terminus of VP1 which is called precisely VP1u. Two ORFs in frame 3 are in the middle and right end of the genome; they code for a putative 9 kDa (X protein) and an 11 kDa protein, respectively. A small additional ORF is in frame 2 and at the beginning of the ORF for the VP proteins: it has the potential to code for a7,5 kDa protein (figure 1.12).
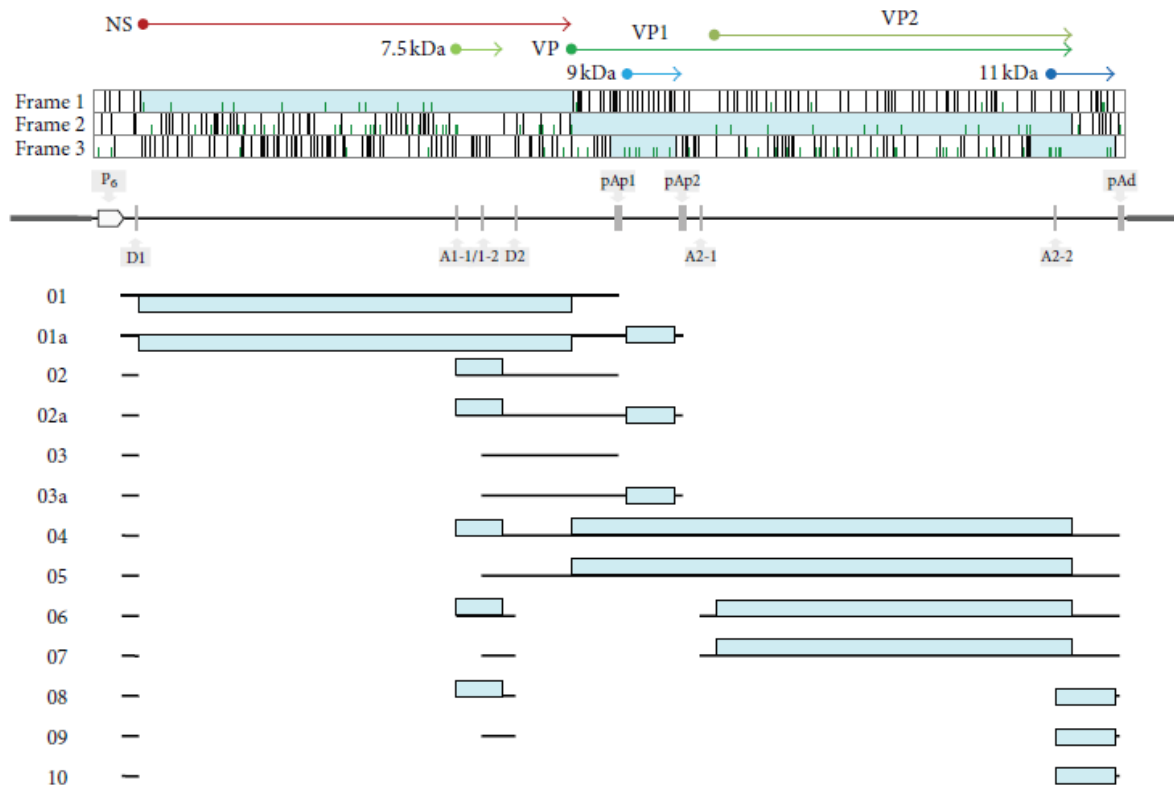
Figure 1.12: Schematic representation of B19V genome organization and functional mapping. Top) Open reading frames identified in the positive strand of genome; arrows indicate the coding region for viral proteins positioned on the ORF map; Center) Genome organization with distinct representation of the terminal regions indication of the position of the promoter (P6), splice donor (D1, D2), splice acceptor (A1-1-1/2, A2-2/2), and cleavage-polyadeniliation (pAp1, pAp2 and pAd) sites; Bottom) Viral mRNA species; black boxes indicate the exon composition and light boxes indicate the ORFs contained within mRNAs [Gallinella et al; 2013].

NS protein. The large B19V non-structural protein NS is composed of 671 amino acids and has a molecular weight of about 74 kDa. A nuclear localization signal (NLS) has been detected at aa 177 to 180 (KKPR) and it is responsible for the predominant localization of the NS protein to the nucleus [Brown; 2005]. Moreover, the non-structural protein contains an SF3 helicase domain, although it has not been solved for NS. A SF3 helicase domain is normally composed by five stranded parallel β-sheet flanked by several α-helices and it is usually associated with an origin-binding domain in small viruses such as parvovirus, polyomavirus and papillomaviruses. Structural and functional predictions indicate the presence of DNA binding/endonuclease domain at the N terminus, an helicase/ATPase-nucleoside triphosphate (NTP)-binding/hydrolisis motif of 160 aa in the central region and a putative transactivation domain (TAD) at the C terminus [Tewary et al; 2014-Momoeda et al; 1994 – Lou et al; 2012]. A suggested mechanism for NS action is that, thanks to its helicase

domain, the protein binds to the viral origin of replication leading to DNA unwinding, then cellular replications proteins are recruited for the final replication of the viral genome.

B19V NS is essential for viral generation, actually its mutations blocks viral replication; it is produced early in the replication of B19V but is detectable along all the time course of infection. Within the infected cells, it could be present in additional forms of lower molecular weight, but neither post-translational modification nor processing has been documented.

The NS non-structural protein is involved in several activities and interacts with different factors inside the cells, in addition to the regulation of viral gene expression by binding the promoter P6 together with Sp1/Sp3 cellular factors. NS protein promotes an inflammatory response, for example inducing the production of inflammatory cytokine interleukin-6 (IL-6) binding a NF-kB binding site in the cytokine promoter, in K562 cells [Moffatt et al; 1996]. While in the monocyte cell line U937, it promotes the production of tumor necrosis factor alpha (TNF-α) protein.

B19V NS induces apoptosis involving caspase-3 and caspase-9 in erythroid lineage K562, UT7/Epo (semipermissive to B19V) and HepG2 cells (nonpermissive to B19V). The NTP-binding motif of the protein has been suggested in NS-induced apoptosis, indeed its mutation could abolish the cytotoxic activity. In human erythroid progenitor cells, NS expression induced DNA damage response (DDR) and block of the cell cycle in the G2 phase, that were probably responsible for the killing of the cells. Here, the viral induced apoptosis was inhibited by caspase 3, 6 and 8 inhibitors [Sol et al; 1999].

VP1 and VP2 proteins. As previously mentioned, the capsid shell is composed by two proteins (VP1 and VP2), that are codified by the same ORF but differ for the additional part of 227 aa at the N terminus of VP1 (known as VP1 unique region or VP1u). In the VP1/VP2 common region, these proteins have a β-sandwich structure consisting of 8 β-strands in two sheets; interactions between their domains allow the formation of 5-fold assemblies and so to an T = 1 icosahedral capsid (figure 1.13). The major capsid protein VP2 is of 554 aa and has a molecular mass of 58 kDa. The minor capsid protein VP1 is of 781 aa and has a molecular mass of 84 kDa. The N terminus of VP1 (aa 1 to 100) of VP1u is important in viral binding and internalization during B19V entry into the cells; while the central portion of VP1u (aa 128 to 160) contains a motif with PLA2 activity. This phospholipase activity (PLA2) has probably a role during intracellular trafficking to escape late endosome for nuclear entry.
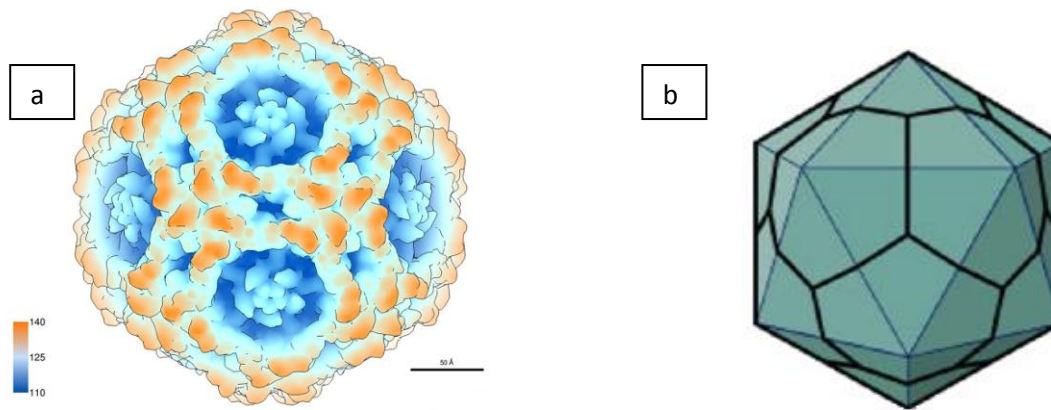
Figure 1.13: a) Structure of Human Parvovirus B19 at X-ray diffraction with 3,5 Å resolution [PDB 1S58]; b) Schematic representation of an icosahedral capsid with T = 1 geometry [VirusWorld – ViralZone].

Both proteins are produced and accumulated into the cellular cytoplasm during the replicative cycle, but they are carried into the nucleus thanks to a nonconventional NLS motif (KLGPRKATGRW) at their C termini. Here, they assemble into empty capsids. However, VP2 alone can assemble virus-like particles (VLPs) in the baculovirus expression system and its truncations destroy the ability to form particles. VP1 protein can be incorporated in VLPs in a percentage from the normal 5% up to 40%, but it cannot self-assemble in regular capsids [Kawase et al; 1995].

Small nonstructural proteins. Additional ORFs are present in B19V genome other than NS and VP proteins: two are in frame 3 in the center and right end of the internal region, that have the potential to codify for a 9 kDa and 11 kDa protein, respectively; a small ORF is in frame 2 overlapping with the NS coding sequence and which potentially codify for a 7,5 kDa protein. All these three ORFs are maintained in other *Erythroparvoviruses* (as V9), indicating that these proteins might be functionally important for the virus [Servant et al; 2002].

The 11 kDa protein is translated as a family of proteins (94-85 aa) due to the presence of multiple start codons in its ORF, and it is expressed in a huge amount in B19V-infected erythroid progenitor cells (EPCs) where it is localized more in the cytoplasm than in the nucleus. It is proline rich and it contains three consensus SH3 (Src homology 3)-binding sites; however, it is not required for DNA replication but its role seems related to post-transcriptional events, such as obtaining adequate amounts and a correct distribution of capsid proteins. Besides, the 11 kDa protein can alter the cellular environment to favor viral replication and maturation in receptor-binding protein-2 (Grb2) and it is a potent inducer of apoptosis which involves caspase-10 in virus infected EPCs [Fan et al; 2001 – Chen et al; 2010].

The ORF encoding the 7,5 kDa protein (74 aa) was discovered on the left side of the viral genome completely overlapping the one of NS and two small RNAs of B19 virus were demonstrated to regulate its expression [Luo et al; 1993]. Currently, nothing is known about the function of the 7,5 kDa protein during viral infection and it is not required for B19V DNA replication in UT7/EpoS1 cells that were transfected by pB19-M20 infectious clone [Zhi et al; 2006].

A third short ORF overlapping the VP1 coding region is predicted to encode a putative "X protein" of 9 kDa (81 aa). Although, no evidence shows that this ORF is expressed in B19, it is common in all the viruses of the *Parvovirus* genus and it is structurally similar to the "small alternatively translated protein (SAT)" of PPV (Porcine Parvovirus). Protein X knockout mutants did not show any differences compared to wild-type with respect to B19V infectivity and DNA replication, while in heterologous expression system, this protein exerts a transactivating effect on the P6 promoter comparable to that of NS protein [Dong et al; 2012]; indeed, mutations of SAT in PPV caused a "slow-spreading" phenotype [Zadori et al; 2005]. Probably, this protein could be involved in B19V pathogenesis or life cycle.

1.5 Cellular tropism and Viral life cycle

Human Parvovirus B19 can only be grown in culture with difficulty due to its limited tropism and restricted replicative ability. The main target cells are erythroid progenitors cells (EPCs) in the bone marrow that provide a susceptible and permissive environment to B19 infection (figure 1.14). Actually the virus is detectable in infected progenitor cells, and B19V purified from viremic sera inhibits erythropoiesis *in vitro* and the colony formation of late erythroid progenitors as well as the more primitive burst-forming erythroid progenitors (BFU-E) [Young et al; 1984 – Mortimer et al; 1983].

A higher viral replication can be supported by enrichment of erythroid progenitor cells from bone marrow but susceptible and permissive EPCs to B19V infection can also be obtained from a variety of sources including peripheral blood [Schwarz et al; 1992], fetal liver [Yaegashi et al; 1989] and from umbilical cord blood [Srivastava et al; 1992]. Besides, it is possible to produce pure populations of CD36^{+} EPCs ex vivo expanded and differentiated from circulating peripheral blood haematopoietic stem cells (HSCs) isolated from either human bone marrow or peripheral blood mononuclear cells (PBMCs) [Filippone et al ; 2010].

Erythropoietin (Epo) is required to maintain viral replication and the susceptibility of erythroid progenitors to viral infection increases with differentiation [Takahashi et al; 1990].
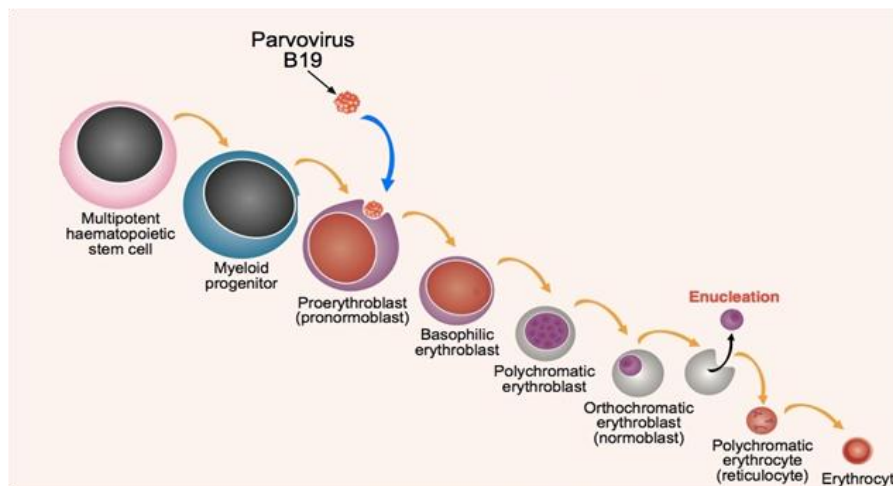
Figure 1.14: Erythroid differentiation and susceptibility/permissiveness to Human Parvovirus B19 infection.

In addition, hypoxic conditions, about 1% O_2, significantly increase B19 infectivity in $CD36^+$ EPCs mimicking the native infection of erythroid progenitors in human bone marrow [Chen et al; 2011]. Despite the high viral yield obtained after B19V infection, all these systems are primary cellular cultures and as a consequence they are not suitable for long-term maintaining and propagation of virus.

Few myeloblastoid cell lines can support Human Parvovirus B19 infection for its studying *in vitro*: the MB-02 cells [Munshi et al; 1993], the UT7/Epo cells and its subclone the UT7/EpoS1 (megakaryoblastoid cell lines) [Shimomura et al; 1992], the JK-1 cells [Takahashi et al; 1993] and the Ku812Ep6 cells (the latter two are erythroid-leukemia cell lines) [Miyagawa et al; 1999]. They all require Epo both for cellular growth and differentiation, in addition to its role for B19V permissiveness. All these cell lines are semi-permissive to B19V infection: actually, the virus can infect them but a very low viral yield is obtained due to the cellular limited ability to propagate the virus [Wong et al; 2006].

Human Parvovirus B19 uses globoside (globotetraosylceramide; Gb4Cer) as its cellular receptor. Globoside is a neutral glycosphingolipid found predominantly on erythroid cells or their progenitors, where it is known also as "blood group P antigen" (figure 1.15).

Red cells contain more than 400 antigens, many of them are membrane proteins or oligosaccharide structures that are classified into families known as "blood group". Some blood-group antigens are attachment site for pathogens, especially bacteria; however, the

large antigens' heterogeneity may act to protect human populations against viral, bacteria and protozoa infections [Brown et al; 1994].

The P blood group was discovered in 1927 by Landsteiner and Levine and it contains two common antigens (P^1 and P) and a rare antigen (P^k). Individuals with *P^1* phenotype have P and P^1 antigens, individuals with $P^k{}_1$ phenotype have P^1 and P^k antigens, individuals with P^2 phenotype have only P antigen, while individuals with the rare *p* phenotype lack all the three antigens. The P^1 and P^2 phenotypes are both very common while the other two phenotypes are very rare but they are more frequent in Japan, Sweden and among the Amish in the USA. Blood and bone marrow of individuals without the P antigen or with the *p* phenotype cannot be infected by Parvovirus B19 [Brown et al; 1995] while purified globoside or monoclonal antibody direct against it prevents the binding of the virus to erythroid cells.
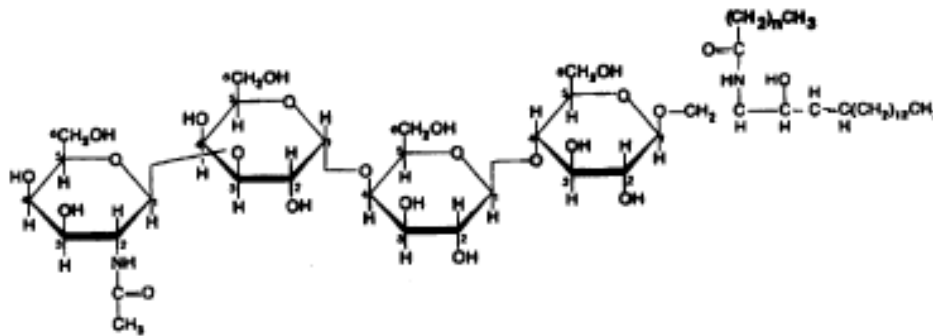
Figure 1.15: Structure formula of Globoside = Gal-N-Ac β(1-3) Gal α(1-4) Gal β(1-4) Glc β(1-1') Cer; where Gal-N-Ac is N-acetylgalactosamine, Gal is galactose, Glc is glucose and Cer is ceramide; n= 16, 18, 22 or 24 [Chipman et al; 1996].

However, P antigen is necessary but not sufficient in mediating B19V infection [Weigel-Kelley et al; 2001]. Globoside can be expressed on several cell types but not all of them are permissive to infection by Parvovirus B19. Actually other primary cells such as human umbilical vein endothelial cells (HUVEC) and normal human lung fibroblasts (NHLF) or various cell lines have this antigen on their plasma membranes. Virus can bind these cells due to the presence of the receptor globoside, without correlation between the amount of globoside expression and efficiency of binding, but these systems are not permissive to B19V entry.

A relevant phenomenon is antibody-dependent enhancement of infectivity (ADE) which leads to internalization of the virus in a non-permissive environments via c1q receptor [Von Kietzell et al; 2014]. Possible effects on cells can be a consequence of the innate immune recognition, while specific pathological effects can occur if the virus can replicate. The ADE was first identified in U937 cell model and after in other cells such as endothelial cells and B

lymphocytes from tonsillar tissue. In particular, endothelial cells are a diffuse B19V target and they are involved for the persistence of the virus within various tissues and for some clinical manifestations [Bua et al; 2017].

Therefore, it is believed that globoside acts as a primary receptor that mediates the initial attachment of B19 on the target cells while the viral entry is allowed by the binding to a specific coreceptor. Both $\alpha_5\beta_1$ integrin and Ku80 have been proposed as possible B19V coreceptors. The $\alpha_5\beta_1$ integrin functions as receptors for the extracellular matrix component fibronectin and they are normally expressed on the surface of viral susceptible cells, such as erythroid progenitor cells or they can be induced in other cell lines as K562 (cells derived from human blood with chronic myelogenous leukemia disease). After ligand binding, different cellular functions are activated, including anchoring, trafficking, proliferation and differentiation. The integrin function on B19V entry is enhanced by clustering of co-expressed β2 and β3 integrins to β1 or by Rap1 GTP in the erythroid progenitor cells [Weigel-Kelley et al; 2006 – Weigel-Van Aken et al; 2009]. Ku is a heterodimeric DNA-binding protein consisting of a 70 kDa (Ku70) and an 80 kDa (Ku80) subunit and was originally identified as a nuclear antigen in patients with systemic *lupus erythematosus* and scleroderma. Ku is a DNA-protein kinase which is involved in several nuclear processes including DNA repair, chromosome maintenance and transcription regulation. In addition to its nuclear functions, Ku80 was found on the surface of different B19 binding cells, such as erythroblasts, T cells, B cells, macrophages in bone marrow. Its inhibition in Ku812Ep6 which are sensitive to B19V caused a reduction on viral infection and its expression in transfected HeLa cells allowed B19V entry into the cells [Munakata et al; 2005]. However, more recent experiments showed that the expression of both Ku80 and $\alpha_5\beta_1$ integrin only vaguely correlate with the B19V tropism and cannot explain the restricted internalization profile of the virus [Chen et al; 2010 - Leisi et al; 2016]. In addition, the internalization of B19V is inefficient in non-erythroid cells such as endothelial cells, although the cells express P antigen, ku80 and $\alpha_5\beta_1$ integrin on their surface in a similar amount of those in UT7/EpoS1 cell line [Von Kietzell et al; 2014].

This suggests the presence of a still unknown receptor responsible for the specific viral internalization into early erythroid progenitors cells. VP1u has been identified as possible responsible of the viral binding to the "new and unknown" coreceptor in UT7/Epo cell line and in CFU-E cells. The measurement of the PLA$_2$ activity of VP1 suggests that this region is normal buried within the B19V capsid shell but becomes exposed after treatment with heat and low pH or binding on human red blood cells (RBCs). Actually the region from 5 to 80

amino acids of VP1u is required and sufficient for binding and internalization into susceptible UT7/Epo cells. Further truncations from both termini led to a gradual decrease of the binding and internalization capacity; the critical regions is located between amino acids 20 - 68 of the VP1u [Leisi et al; 2013 - Leisi, Di Tommaso et al; 2016]. VP1u internalization was not affected by the inhibitory antibodies against $\alpha_5\beta_1$ integrin and the decreasing of B19 virus binding and internalization in CFU-E cells in a competition assay with the recombinant VP1u demonstrated that VP1u is the responsible and only significant uptake pathway for B19V infections [Leisi, Von Nordheim et al; 2016]. However, the expression pattern of the receptor globoside or the proposed coreceptors ($\alpha_5\beta_1$ integrin and Ku80 antigen) does not correlate with the binding pattern of the VP1u, suggesting that these receptors are not directly involved in the internalization process of Human Parvovirus B19.

The low affinity binding to globoside might further facilitate tissue spreading and dissemination of the virus by attachment to circulating red blood cells, while the binding of the capsid to additional receptors might stabilize the virus attachment to the cell surface and thus indirectly facilitate the virus internalization by the VP1u. Though, the importance of binding to globoside should not be underestimated; attachment of B19V to cells or its incubation with Gb4Cer triggered conformational changes in the capsid leading to the accessibility of the N terminus of VP1 to antibodies. Moreover the N-terminal part and the PLA$_2$ motif at C-terminal part of VP1u could became exposed upon mild heat and low-pH treatments without capsid disassembly [Ros et al; 2006].

As mentioned previously, the 5-fold axis pore has been suggested to facilitate the externalization of VP1u; this occurs in all Parvoviruses during the intracellular trafficking of the capsid caused by the acidification of the endosomal environment. Instead, for Human Parvovirus B19 the conformational changes do not occur inside the cell but probably at the cell membrane, actually the 5-fold channel is normally closed in the B19V particle. However a rearrangements during infection which may expand or open a flexible pore could not be excluded, as observed in AAV-2 capsids with heparin [Levy et al; 2009].

Only a small proportion of cell-bound viruses were internalized, while the majority detached from the receptor. The capacity of the virus to detach and reattach again enhances the probability of productive infection, actually the receptor-detached virus showed an increase cell binding capacity when they were added to no-infected cells and were more infectious than the native virus [Bonsch et al; 2010].

A mechanism of "detachment-reattachment" has suggested to explain the B19V strategy to avoid repetitive "abortive" attachments to the same receptor and increase the probability of

productive viral binding and subsequent internalization (figure 1.16). At first, Parvovirus B19 binds to globoside, which leads changes in the VP1u conformation; the structurally altered capsid is ready for a further interaction, which involves binding of the N-terminal part of VP1u with the coreceptor. However, the virus detaches from the globoside in situations where the interaction with the coreceptor is not possible; the "detachment-reattachment" procedure is repeated until the second interaction is possible and virus can be internalized. The exposition of VP1u region after binding to its receptor is critical for viral internalization since capsids without VP1 can bind the cells but are not internalized [Bonsch et al; 2010]. So the Gb4Cer is not only the primary B19V receptor but it's also the mediator of capsid rearrangements required for a successful viral internalization.
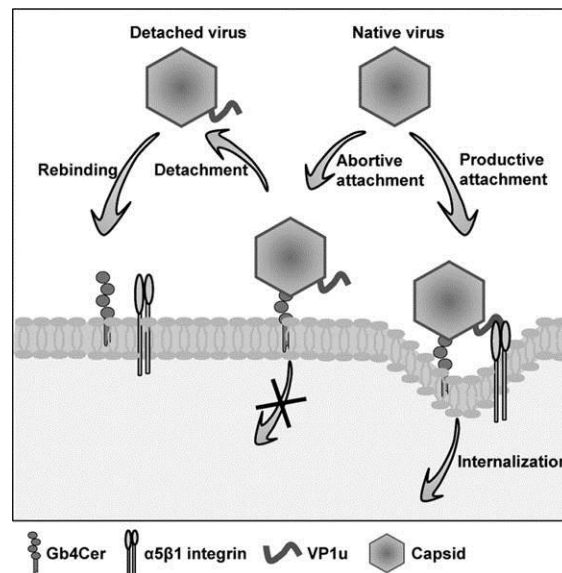
Figure 1.16: Schematic representation of the "detachment-reattachemnt" mechanism = the virus binds to the Gb4Cer receptor which leads to expose of VP1u. However, if the interaction with the coreceptor is not possible, the virus detaches from the Gb4Cer while keeping VP1u accessible at the surface. Cycles of detachment and reattachment are repeated until the second interaction with the coreceptor occurs and after which, the virus is internalized [Bonsch et al; 2010].

The early steps of Human Parvovirus B19 infection were investigated in UT7/Epo cells. In particular, the complex B19V-receptor globoside associated with lipid rafts, especially of the noncaveolar types (figure 1.17). Actually, degradation of the lipid rafts by pharmacological treatments inhibited viral infection when the drug was added prior to virus attachment. B19V is internalized by clathrin dependent endocytosis and enters into the endocytic pathway reaching the lysosomal compartment within few minutes. A substantial proportion of B19 virions are degraded by the lysosomal action. A viral-induced permeabilization of the

endocytic vescicles was not observed, so the viral particles practice a mechanism of endosomal escape without apparent membrane damage.

Drugs as Bafilomycin-A1 and compounds as NH_4Cl prevented endosomal escape increasing the endosomal pH with the accumulation of B19V inside lysosomes and blocking of viral infection as a result. On the contrary, chloroquine prevented the transfer of viruses from late endosomes to lysosomes, so the viral DNA was not degraded and the infection was boosted. The viral DNA was associated rapidly within the nucleus already reaching a plateau by 3 hours post-internalization [Quattrocchi et al; 2012].
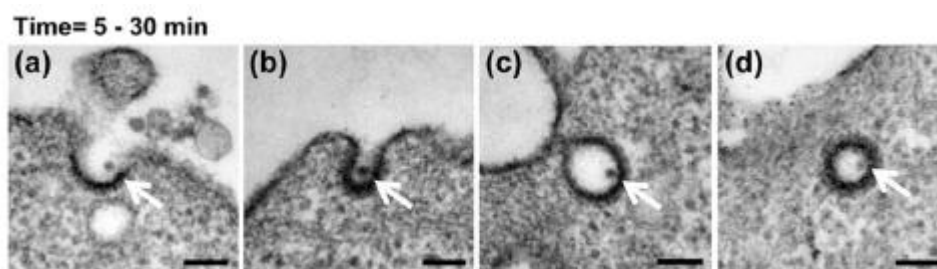
Figure 1.17: Electron micrographs of B19V internalization in UT7/Epo cells by clathrin-mediated endocitosis. a) early coated pit; b) coated pit; c) newly formed coated vesicle; d) coated vesicle in cytoplasm (black bar = 100 nm) [Quattrocchi et al; 2012].

VP1u shows phospholipase activity during the transport of the virus along the endosomal pathway but all the steps of B19V intracellular trafficking are not yet well known. However, the action of PLA_2 as well as the mechanism for endosomal escape and the role of the lipid rafts in the process of virus entry requires further investigations.

Once the viral genome is inside the nucleus, its transcription and its replication occur using the cellular machinery due to absence of both a viral DNA and a viral RNA polymerase. It is assumed that these activities require S-phase specific cellular factors and an actively replicating cells, as for the other members of the *Parvoviridae* family. Several S-phase factors, such as PCNA (proliferating cell nuclear antigen), MCM (minichromosome maintenance complex), cyclin A, RFC1 (replication factor complex 1) colocalize in B19V replication centers [Luo et al; 2013]. However, B19V has the ability to modulate progression through the cell cycle to its own advantage and alter various cell signaling pathways (for example: erythropoietin signaling [Ganaie et al; 2017], the DDR [Lou et al; 2012] and cell cycle progression [Luo et al; 2013]) for efficient viral replication.

The first step of the replicative cycle is the conversion of the incoming parental single-stranded genomes into a double-stranded DNA, which has either an "extended" or a "turn-around" form of the terminal regions (extended or closed conformation, respectively). Both

positive and negative B19V nucleotide sequences have inverted terminal repeats so they are functionally equivalent. The "double-stranded" terminal hairpin structures provide the priming structure for DNA polymerases to synthesize the complementary strand. NS protein binds to cis-recognition elements at the ITRs and presumably nicks ssDNA to generate a free 3'-OH end that primes the DNA extension [Cotmore et al; 2014]. The replication proceeds via a "rolling-hairpin mechanism" (figure 1.18), through cycles of terminal resolution and hairpin-primed strand displacement synthesis where the endonuclease and helicase activity of NS protein are necessary for the terminal resolution process and strand-displacement synthesis. Null mutations of NS blocks viral replication [Heegaard et al; 2002] while it is not yet known the role of the sequence asymmetries within the palindromic ITRs during viral replication and transcription.
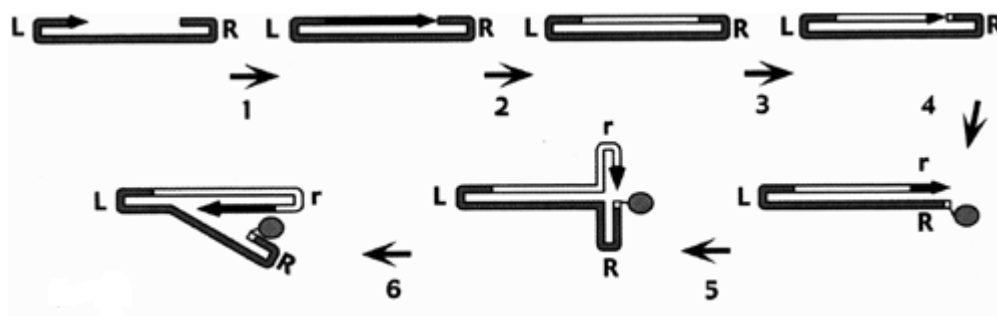
Figure 1.18: Schematic representation of Human Parvovirus B19 replication by "rolling-hairpin mechanism" = 1-6) ssDNA is converted into dsDNA using one ITRs as starting sequence, NS protein nicks the newest strand and acts with its helicase activity to displace strands for a new replication cycle (L = left ITR; R = right ITR; r = newest right ITR) [Knipe et al; 2007].

A replicative intermediate of B19V has not been well isolated. Actually ssDNA, monomeric dsDNA and dimeric dsDNA forms are all detected in productively infected cells, but it is known that the formation of a dsDNA intermediate generates a template active for transcription. Starting from the unique promoter P6, the transcription is directed from the left to the right end of the genome. The P6 promoter, although most efficient in erythroid cells, is relatively generic and conversely might promote expression of the viral genome even in non-permissive environment. The permissiveness to viral replication could be related to the presence of specific elements or, alternatively, to the relative inefficiency of cellular restriction factors [Bua et al; 2017]. Difference in the expression profile of B19V genome may occur during the viral replicative cycle due to restriction posed by different environments. Hypoxia enables B19V-infected cells to yield a higher level of progeny than under normoxia. In human bone marrow, where hypoxia is physiological, the response of

B19V to the oxygen reduction can be regarded as an adaptation of the virus to the environment of its primary target cells [Pillet et al; 2004]. EPO (erythropoietin) is a hormone secreted by renal tissue in response to hypoxia, it is essential for survival and differentiation of EPCs and it is essential to B19V replication. Actually EPO binding to EPO-R (EPO Receptor) activates JAK2-signal transducer (Janus Kinase 2) and STAT5 (activator of transcription 5) in addition to PI3K (phosphatidylinositol 3-kinase) and ERK (extracellular signal-regulated kinase) pathways. Simultaneous up-regulation of STAT5 signaling and down-regulation of MEK/ERK signaling boost the level of B19V infection in erythroid progenitor cells under normoxia to that in cells under hypoxia. JAK2 predominantly phosphorylates STAT5A in the cells of erythroid lineage, and this is involved in increasing of B19V replication in cells under hypoxia condition where STAT5A is overexpressed. Actually, STAT5 interacts with the MCM complex and recruits the helicase complex of the cellular DNA replication machinery to viral DNA replication centers, which facilitates viral DNA replication. The inhibitor of STAT5 phosphorylation, pimozide, abolished the viral DNA replication in B19V-infected CD36^{+} EPCs reducing the STAT5-MCM complex interaction [Ganaie et al; 2017].

  Analysis of viral nucleic acid from infected UT7/EpoS1 cells had made possible to establish an early model of B19V genome expression [Shimomura et al; 1993]. Genome transcription and replication could be divided in early and late events. RNA transcription precedes DNA replication of B19 parvovirus with viral RNA detected about 6 hours after infection (hpi) while dimer replicative intermediate forms of DNA did not appear until more than 16 hpi after infection. Besides, the non-structural protein RNA appeared earlier (6 hpi) compared to capsid protein RNA that were detected 24 hpi [Bonvicini et al; 2008]. The addition of an inhibitor of protein synthesis to block production of nonstructural protein abolished both the capsid protein RNA transcription and the DNA replication. The differences in the viral nucleic acids expression profile among permissive and non-permissive cellular environments indicate that B19V virus genome should be considered a single replicative and transcriptional unit and it is characterized by a "two-state expression profile". Actually both viral DNA and RNA were constantly represented in permissive environments as bone marrow mononuclear cells, UT7/EpoS1, KU812Ep6; while only earlier RNAs and no DNAs were detected in non-permissive cells, such as TF-1 cells [Bonvicini et al; 2006]. The block of B19V genome replication in non-permissive cellular environments can also be overcome and enhanced by other viruses, such as adenovirus infection [Guan et al; 2009]. Human fibroblasts and human umbilical vein endothelial cells (HUVEC) are normally not permissive for B19V replication,

but different growth factors or cytokines could allow a complete B19V infection [Zakrzewska et al; 2005].

The last steps of viral replicative cycle are not well characterized. The VP proteins are transported from the cytoplasm to the nucleus and they assembly into capsids. The correctly assembled capsids incorporate the viral genome of positive or negative polarity, and then, they are re-exported in the cytoplasm before the egress by lysing the cell (figure 1.19). These terminal phases are probably tightly regulated and may require helper functions [Morey et al; 1993].
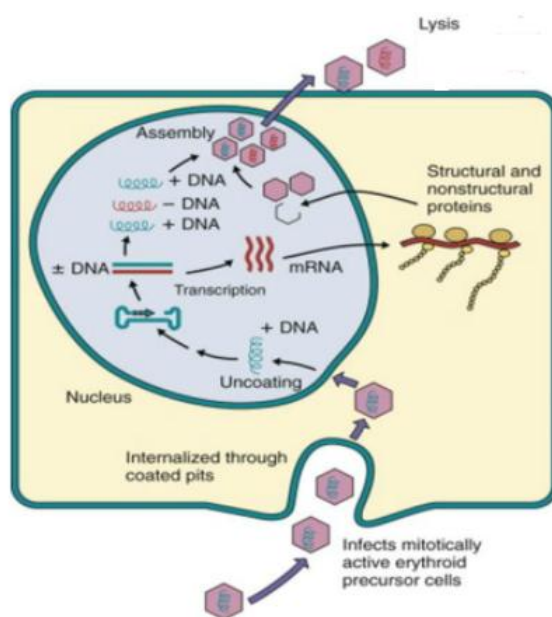
Figure 1.19: Schematic representation of a complete B19V replicative cycle [Murray et al; 2005].

In UT7/EpoS1 cells and EPCs, B19V infection induces block in G2/M arrest, a cell cycle status with 4N DNA content. Cyclin A, cyclin B1 and phosphorylated cdc2 accumulate in these cells and the kinase activity of the cdc2-cyclin B1 complex increases. The accumulation of cyclin B1 inside the cytoplasm reduces its nuclear import resulting in cell cycle arrest at the G2 phase and preventing progression to M phase [Morita et al; 2001]. B19V infection was shown to induce also an arrest in G1 phase of the cellular cycle. In particular NS expression increases p21/WAF1 expression as consequence of the interaction NS − transcription factor Sp1. The p21/WAF1 is a cyclin-dependent kinase inhibitor which induces the G1 arrest.

B19V acts downregulating the activating E2F transcription factors (E2F1 to E2F3a) and upregulating the repressive E2Fs (E2F4 to E2F8) in EPCs. Interaction between NS and E2F4 or E2F5 enhances the nuclear import of these repressive E2Fs and induces G2 arrest. This G2 block is independent of p53 activation and leads to increased viral replication, but the

activation of G2-related transcription factors and/or DNA repair proteins may cause activation of the p53 signal transduction and upregulation of E2F7 and E2F8 contributing to the block of cell cycle progression [Wan et al; 2010].

As mentioned previously, B19V infection triggers a DDR (DNA-damage response) with activation of ATM (ataxia-telangiectasia mutated), ATR (ATM and Rad3 related) and DNA-PKcs (DNA-dependent protein kinase catalytic subunit) signaling. Other than recognizing the damaged cellular DNA, the DDR is also activated by various DNA viruses to facilitate viral DNA replication [Trigg et al; 2015]. Only the ATR and DNA-PKcs signaling pathways are important for B19V replication, while ATM pathway is dispensable [Luo et al; 2011]. In particular DDR pathway is involved in cell cycle arrest at late S phase [Luo et al; 2013]; while ATR activation is responsible in B19V NS-induced G2 phase arrest through the ATR-Chk1-Cdc25c-Cdk1 pathway [Xu et al; 2017].

Additionally to NS protein. apoptosis is caused also by the nonstructural 11 KDa protein in EPCs and UT7/EpoS1 cells. Both B19V infection and NS transfection induced apoptotic cell death which involved caspase-3, -6 and -8 activation (extrinsic apoptosis pathway). Moreover the 11 KDa protein activates the caspase 10, which is also an initiator caspase of the apoptotic extrinsic pathway [Chen et al; 2010]. Hence viral NS and 11 KDa proteins synergistically act to induce the apoptosis in B19-infected cells. Additionally, B19V infection induced mitochondrial autophagy and the formation of an intracellular autophagosome; inhibition of autophagy significantly facilitated B19V infection-mediated cell death [Nakashima et al; 2006].

A cellular gene expression profile has recently obtained by *Gene Ontology* analysis of B19V-infected primary human erythroid progenitors. At the early time point of infection (6 hpi), the most significantly enriched pathways were those associated with the response to oxygen levels and the response to hypoxia. At the 12 hpi, the differentially expressed genes were significantly enriched in pathways associated with apoptosis and cell death, that remained at high levels for the following 24 hpi and 48 hpi. At 24 hpi, the response to DNA damage stimulus was also enriched. At 48 hpi, the most significantly enriched pathways were the immune response-related regulation pathways, including the inflammatory response [Zou et al; 2018].

1.6 Epidemiology and Pathogenesis

B19V is a global and common infectious pathogen in humans and the virus is generally spread in the community by the respiratory route. The virus can be detected in the saliva in the acute phase of infection, but it is currently unknown how B19V overcomes the respiratory epithelium barrier to reach its main target cells. Vertical transmission occurs from mother to fetus or the virus could be spread by blood transfusions or blood-derived products (such as platelets, intravenous immunoglobulin, fibrin products or solvent/detergent-treated plasma units).

Circulation of the virus is higher during the months of late winter and early spring and epidemic cycles occur every 4-5 years. Close contacts among people and especially with children (for example: school, household, etc.) favor transmission of Parvovirus B19 with attack rates as high as 50% [Chorba et al; 1986]. The viral transplacental transmission from mother to fetus has an estimated rate of transmission in the range of 29-39%, while the risk of adverse fetal outcome has been reported from 3% to 12% [Bonvicini et al; 2017]. Another setting where B19V could spread quickly are hospitals, where staff or susceptible patients can be exposes to source-infected individuals [Blumel et al; 2010].

The course of infection was first investigated involving healthy human volunteers, who were inoculated with B19V via intranasal route and followed with respect to their virological, immunological, hematological and clinical parameters. After the contact via the respiratory route, the virus enters in the blood stream. Persistence of the viral DNA has been detected in tonsillary tissues but it is not known if tonsils are the true portal of entry; an alternative mechanism of access could be transcytosis through respiratory epithelia [Manning et al; 2007]. The virus gains access to the primary target organ: the bone marrow, where it can infect erythroid progenitor cells achieving a productive infection (primary viremic phase). The cytopathic effect of infection is manifested as giant pronormoblasts (alternately referred to as lantern cells), first recognized in bone marrow in 1948 [Koduri; 1998]. Giant pronormoblasts are early erythroid progenitor cells with a diameter of 25 to 32 μm, large eosinophilic nuclear inclusion bodies, cytoplasmic vacuolization, and occasionally "dog-ear" projections (figure 1.20).
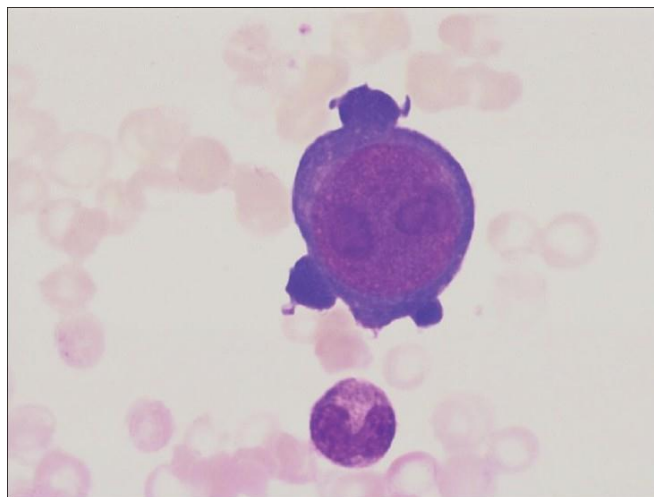
Figure 1.20: Bone marrow aspirate showing a giant pronormoblasts with multiple intranuclear inclusions and cytoplasmic projections (dog ear) [Gadage et al; 2011].

The virus inhibits the formation of bone-marrow derived erythroid colonies at the BFU-E and CFU-E stages and its effects are due to the ability of B19V to induce cell-cycle arrest, block of erythropoiesis and eventually apoptosis. Viral replication and its cytotoxic effects increase with the progression of erythroid differentiation [Takahashi et al; 1990 – Bua et al; 2016]. Bone marrow supports a productive infection and the viral progeny is released in the blood, leading to a secondary viremia which can reach high viremic levels (10^{12} virus/mL) in the acute phase of infection. Through the bloodstream, the B19V can be distributed inside all human body causing the possible clinical manifestations of infection that can involve mainly skin and synovia, even if the virus has been implicated in disease in almost all organs and tissues. Secondary target cells have been identified (such as, endothelial cells) but persistence of viral DNA has been detected in up to 50% of biopsy specimens of spleen, lymph nodes, tonsils, liver, heart, synovial tissues, skin, brain and testes [Corcioli et al; 2008]. During the systemic phase of infection, cells of mesodermic origin are mainly involved and of these endothelial cells may play a central role. Actually endothelial cells are normally non-permissive but they can be infected by B19V and be a site of persistence of the viral genome; additionally, endothelia constitutes a diffuse tissue that can account for the wide distribution of virus and its detection in various organs. So B19V may enter and persist in non-erythroid lineage tissues, but there is not clear evidence that infection is productive. The interplay with the immune systems (innate and adaptive recognition mechanisms) may lead to the development of immunopathological mechanisms or autoimmune processes.

The two classical manifestations of B19V infection are erythema infectiosum or fifth disease (also named as "slapped cheek" disease), typical of children and arthropathies, typical of

adults. Arthritis and arthralgias are more frequent in females than males, in most cases they involve symmetrically the small joints of hands and feet; chronicization is more frequent in adult patients with up to 20% of cases in affected women. In recent years, interest for B19V as a cardiotropic virus has been raised [Andreoletti et L, 2009]. Parvovirus B19 is the most prevalent virus detected in the heart and it has been recognized as etiologic agent in acute myocarditis both in pediatric and adult populations [Bock et al; 2010].

The globoside (viral receptor) is present on the villous trophoblast layer of human placenta and it may help transcytosis of the virus to the fetal circulation, since the trophoblasts are not permissive to the B19V. However, the expression of globoside changes during the pregnancy reaching highest level in the first trimester and progressively decrease until vanishing in the third trimester. This temporal change correlates with the frequency of transmission of Parvovirus B19 to the fetus [Wegner et al; 2004]. Inside the fetus, the virus can infects erythroid progenitor cells in liver and/or bone marrow depending on the gestational age and can be detected both in several tissues and in amniotic fluid. The block in fetal erythropoiesis can be severe due to the combination of an expanded erythropoietic compartment and an immature immune response. Typical fetal damages include fetal anemia and hydrops, cardiomegaly and pericardial effusion, hydropic or non-hydropic intrauterine fetal death. Infections occurring at earlier stages (weeks 9-20) can result in fetal death at the highest rate, up to 16%.; while the development of hydrops (fluid accumulation in fetal compartments such as subcutaneous, pericardial, pleural and abdominal) is more frequent in the central part of pregnancy. Hydrops may lead to fetal death or the fetus may recover without persistent damage. Fetal death accompanied by hydrops is commonly observed in case of maternal infection within week 20 [Enders et al; 2010]. Presently, there is no sufficient data assessing a role for B19V in neurodevelopmental defects in congenitally infected children and the virus is not regarded as a teratogen [Lassen et al; 2013]. However, the natural course of fetal infection is affected by several factors: i) the immune status of the mother which is assumed to be protective towards infection of the fetus; ii) the gestational age, for example infections in the first two trimesters have rapid rate of transmission because of different expression of globoside on placenta; iii) developmental stage of the fetus, depending on the expansion of the erythroid compartment and maturity of fetal immune response.

As mentioned previously, the B19V target cells in bone marrow are CD36+ cells and are mostly susceptible when in differentiating phase (erythroblasts). The fact that the least differentiated cells are relatively resistant to infection ensures that the block in erythropoiesis is temporary and can be solved by a neutralizing immune response. Actually a balance is

established between cell population dynamics and viral replication, but this can be lost due to alterations in the erythropoiesis process or defects in the immune response (figure 1.21).
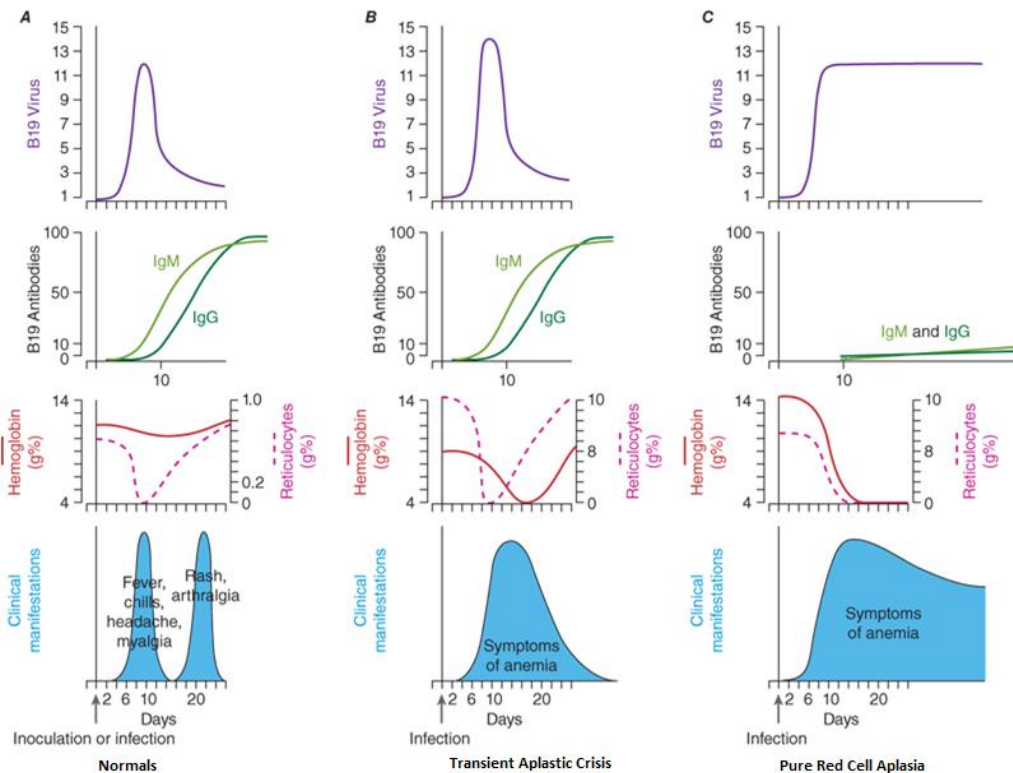
Figure 1.21: Schematic representation of B19V clearance, immune response, level of hemoglobin and clinical manifestation in the three different conditions = a) normal individuals; b) individuals with alterations in the erythropoiesis process; c) individuals with defects in the immune response [Young et al; 2004].

a) In an individual with physiological erythropoiesis and normal immune system, infection is limited and controlled by prompt development of a specific immune response. Levels of hemoglobin only marginally is reduced and the production of antibodies with neutralizing activities are important for the clearance of infection which takes usually 3-4 months, decreasing progressively. Viral DNA can still be detected in the bone marrow after this period, but persistence of viral DNA implicates active chronic infection only in the presence of viremia [Musiani et al; 1995]. b) An acute episode of profound anemia occurs in situations where the number of erythroid progenitors and their replication rate are increased because of a reduced lifespan of erythrocytes. Hemoglobinopathies, thalassemia, enzymatic defects, iron deficiencies, coinfection with other viruses/microorganisms/parasites are favorable situations to the development of anemia and aplastic crisis. c) Congenital and acquired immunodeficiencies (for example HIV infection), malignancies, in the course of chemotherapy or of immunosuppressive treatments (for example in bone marrow or solid

organ transplant recipients) are typical situations where the immune system could not control and clear the viral infection. Herein in these cases, the B19V infection can become persistent with active viral replication and involves the erythroid compartment in different degrees: depression of erythropoiesis can be manifest with severe levels of anemia (Pure Red Cell Aplasia) but also compensated and unapparent [Gallinella; 2013].

In pure red cell aplasia, as well as in transient aplastic crisis, clinical evidences of a persistent infection are less shown. Actually the typical symptoms of B19V infection (such as fever, malaise, cutaneous eruption and join pain) are usually mediated by immune complexes; these last ones do not form in absence of antibodies against the virus.

1.7 Immune Response

Human Parvovirus B19 is capable of establishing a long-term relationship with its host depending on the interplay and balance between the pathogenic ability of the virus and the control mechanism of the immune system.

Following the B19V infection, an immune response is developed to control and clear the virus with both its innate and its adaptive immunity. The role of the innate immunity has not been well investigated but in general, B19V might be recognized through its PAMPs (Pathogen Associated Molecular Patterns) by cellular PRRs (Pattern Recognition Receptors). For example, the viral ITRs are GC rich and can possibly be recognized by receptors such as TLR9 inducing the accumulation of the erythroid cells in S and G2/M phase. NS was shown to play a major role in inducing both short- and long-term upregulation of defensins and TLR9; some effects on innate immunity activation are played also by VP2 [Hsu et al; 2011].

Antibodies are the major components of the adaptive immune response to B19V. In naïve individuals, neutralizing antibodies are produced early after the infection and progressively lead to clearance of B19V infection. In particular, IgM are produced first and can usually remain for about 3-6 months after the infection, while the IgG are produced after the previous one, they are more specific, with higher avidity and long-lasting. IgA can also be detected in body fluids.

Viral capsid proteins are the major antigens recognized by the immune system. Epitopes on VP common region are mainly conformational and are distributed on the all capsid surface, while epitopes on VP1u region are mainly linear and are located at the N-terminus of the VP1 protein. A mature and effective immune response shows the presence of antibodies directed

against VP2-conformational and VP1u-linear epitopes [Manaresi et al; 2001]. Antibodies to NS protein are also produced probably as a result of prolonged stimulation. In addition B cell memory is maintained against conformational epitopes of VP2 and linear of VP1 but is absent against linear epitopes of VP2.

The development of a neutralizing activity is typical of a mature and effective immune response, while antibodies with incomplete neutralizing activity are typical of persistent infections. A common phenomenon is the production of autoantibodies that can also induce autoimmune diseases. Heterologous, cross-reactive and self-reactive antibodies can normally be produced: normally they do not play a substantial role in the pathogenic process but, in some cases, autoantibodies may persist and trigger autoimmune disease [Lehmann et al; 2003].

The cellular component of the adaptive immunity showed a HLA class II CD4+ T-cell response directed against the capsid proteins VP1 and VP2 in recent as well as remote B19V infected patients. In addition the CD4+ T-cell activation by HLA class II was most vigorous among the recently infected patients but not confined inside the acute phase [Franssila et al; 2001].

Also CD8+ T-cells are involved in the control of B19V infection. Actually, CD8+ T-cell responses were observed especially against NS protein and in less amount against the VP common region in acutely infected individuals where they were maintained or increased over months after the resolution of acute disease. In persistently infected individuals, the higher reactivity was observed against viral capsid protein epitopes [Isa et al; 2006].

Over the first year after infection, up to 4% of T-cell population was of CD8+ T-cells, that possessed strong effector function and intact proliferative capacity. B19-specific cytotoxic T-lymphocytes were also detectable in individuals many years after infection, at frequency lower than 0,5% of CD8+ T-cells. A highly T-cell response is important to identify and eliminate the B19V and for the control of viral infection.

Both the viral capsid proteins can stimulate Th cells to proliferate and to secrete IFN-γ and IL-10. In recently and remotely B19V-infected subjects, the ability to stimulate Th cells was measured: B19V specific IFN-γ responses were generally stronger than IL-10 activation in both recent and remote infection, while patients with subsequent infections or persisting symptoms showed even lower IL-10 responses. IFN-γ specific responses against VP1u were very strong in recently infected individuals, but absent in the remotely infected ones [Franssila et al; 2004- Franssila et al; 2005].

An initial peak of proinflammatory cytokines (IL-1β, TNF-α, IL-6 and IL-8 was found during the acute phase of B19V infection. IL-2, IL-12 and IL-15 (Th1 type of cytokines) were in the early phase, while the Th2 type of cytokines (IL-4, IL-5 and IL-10) and IFN-γ remained low in the same period. Although the reduced Th2 cytokines, IgG antibodies were produced and probably induced by a low-grade IL-6 response or other cytokines , such as TGF-β [Isa et al; 2007].

CD4+ T-cells were identified as the main central memory of the immune system and this is also relevant for the definition of the pathogenic mechanisms of B19V infection. Hence, the activation of CD4+ T-cells during the acute phase of infection is functional to the development of antibodies and may contribute to the clinical manifestations including the development of immunopathological or autoimmune processes. The development of a CD8+ T-cells immune response would limit the viral replication, so reduce CD4+ T-cells activation and eventually contribute to the control of viral persistence.

1.8 Diagnosis

The virus is not adapted to grow in cell cultures and for diagnosis of infection, specific viral components, viral genome or proteins are detected in addition to the detection of the specific immune response. IgM and IgG antibodies detection is still considered the standard and most widely used laboratory diagnosis that may allow for distinguishing active, recent or past B19V infection. At first, immunological assays were established using native viruses as antigens [Cohen et al; 1983] but their limitations rapidly appeared. Recently, enzyme immunoassays or chemiluminescent immunoassays can use VLPs to allow detection of antibodies to VP2 conformational or also VP1u linear epitopes [Manaresi et al; 2004]. In addition, NS can be used as antigen to detect the presence of specific IgG antibodies late in infection and so the NS-antibody test is useful to exclude very recent infections in patients with an unclear serology [Venturoli et al; 1998].

However, the detection of the viral genome in peripheral blood, bone marrow or tissues can be considered the more direct and appropriate approach to the diagnosis of infection. Nowadays, the real-time quantitative PCR techniques must be considered the standard analytical methods [Gallinella et al; 2004].

Both *in situ* hybridization for viral nucleic acids and immunocytochemistry for the detection of viral proteins can be useful as a complement to PCR techniques. *In situ* hybridization can

identify productively infected cells, while immunocytochemistry is useful to detect viral NS or VP proteins, elucidating if the B19V is able to express its genome and hypothesize a role for viral proteins in pathogenesis [Bua et al; 2017].

The continuous technical development will lead to novel molecular detection methods and analytical platforms to improve performances and to reduce time and costs.

1.9 Treatment and Prophylactic Options

B19V infection is normally considered a benign clinical situation. In fact, the virus is widely diffuse, in most case infection is asymptomatic or unnoticed and therapeutic intervention not required due to the immune response activity. Sometimes, acute phase symptoms may require treatments: transfusions of red blood cells are preferred to treat the anemia in transient aplastic crisis or prolonged anemia while nonsteroidal anti-inflammatory drugs are used in case of arthalgias or other atypical inflammatory complications. Red blood cells and platelets intrauterine transfusion (IUT) are indicated in cases of fetal infections and hydrops [Melamed et al; 2015].

Another situation is present in the course of chronic infections, that may depend on the inability of the immune system to develop a neutralizing response. In this case, passive immunization by IVIG (intravenous immunoglobulins) administration can be considered as an effective means of reducing the viral load (figure 1.22). These preparations usually contain high levels of neutralizing anti-B19V antibodies since they are derived from large pools of donors. IVIG therapy also has been described as a successful treatment of fetal hydrops [Matsuda et al; 2005]. However, the treatment is still empirical and may not be normally effective in the complete clearance of the virus, so in many instances the administrations have to be repeated [Crabol et al; 2012]. Alternatively, human monoclonal antibodies have been developed but their therapeutic or prophylactic use has not been evaluated [Gigler et al; 1999].

At the moment no specific antiviral therapy has been developed for B19V, although it could be useful for reducing the inflammatory and pathological aspects of acute and chronic infections. Viral NS protein or the PLA_2 domain in the VP1u region constitute potentially relevant targets due to their involvement in the viral infectivity and their responsibility to pathogenetic effects. Their specific inhibition would probably reduce the capacity of the virus to replicate, its cytotoxicity and its proinflammatory activity [Gallinella et al; 2013].
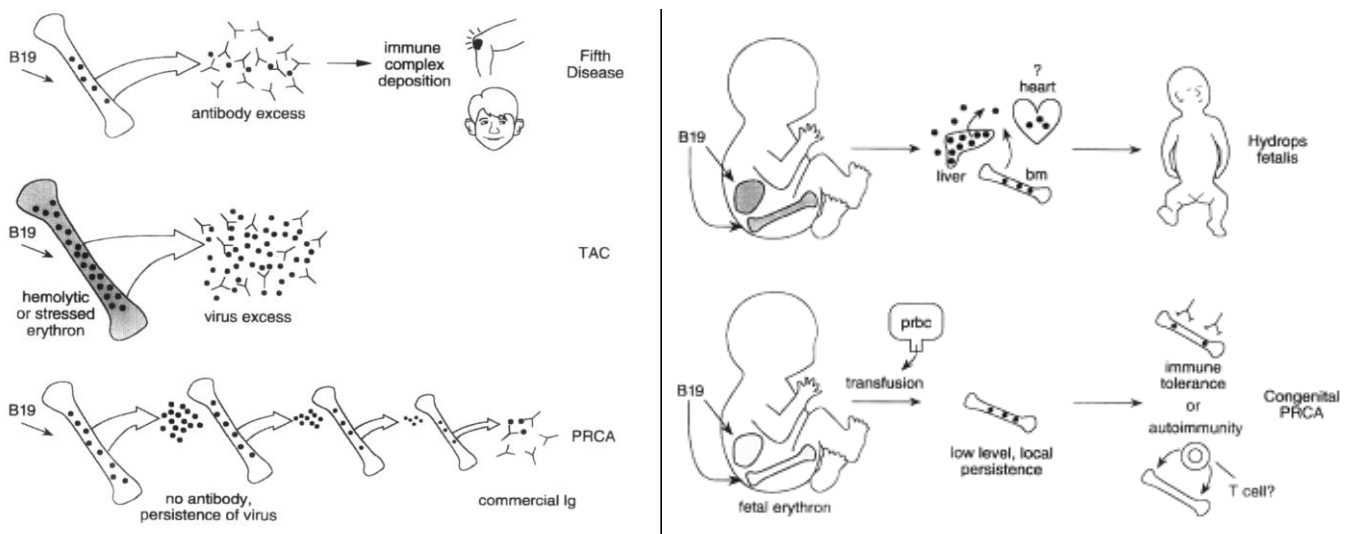
Figure 1.22: Summary of some B19V clinical manifestations and the related treatments [Brown et al; 1995].

B19V is a virus adapted exclusively to human host, it is transmitted by closed contact and effectively neutralized by the immune response. A vaccine would prove useful to protect at-risk populations, such as patients with hematological disorders and women of childbearing age. Preliminary work on vaccine development has been done especially considering the viral capsid proteins, with their VP2 conformational and VP1u linear epitopes. In fact, viral capsid proteins expressed in eukaryotic systems form VLPs that are antigenically similar to native virions. A VLP formulation composed by VP1 and VP2 proteins (MF59C.1) were produced from insect cells and they were immunogenic in the animal experimental model (mice) in the presence of the MF59 adjuvant. Phase I studies showed their immunogenicity and relative safety in humans [Ballou W. R. et al; 2003]; however, phase II studies showed a reactogenicity [Bernstein et al; 2011] probably due to insect cell contaminants. New studies for a B19V vaccine are developing with the expression of VP1+VP2-VLPs from *Saccharomicies cerevisiae.* Immunization of mice showed a strong neutralizing response in the presence of the adjuvant MF59 [Chandramouli S. et al; 2013].

In addition to an accurate diagnosis of infection and therapeutic actions, prophylactic and monitoring options are required. Actually, the B19V is transmitted not only by respiratory route, but also by blood-, blood components- or blood products-transfusions. Two major factors are important for the clinical outcome: 1) the total amount of virus transfused or infused to recipients; 2) the immune status and competence of patients. The viral concentration of about 10^7 International Units (IU) per mL is the identified threshold level

necessary for transmission of B19V infection. However, the presence of specific antibodies in the donated blood and a previous immunity in recipients interferes with infectivity. Although the probability of infection by single blood or blood components unit is low and screening unjustified in terms of costs, high-risk patients (such as patients with immune deficiencies or hematological disorders and pregnant women) would take advantage by single-donor screenings. A different situation is for blood products that are manufactured from large pool of donations. In this case, an high probability of high-titer viremic units is expected and dilution during the manufacturing process is not sufficient to decrease the viral concentration [Gallinella et al; 2013].

To reduce the risk of transmission, a safety threshold at 10^4 IU/mL has been indicated by regulatory offices. Quantitative molecular detection methods and physical removal or heat/chemical inactivation steps are normally introduced during the manufacturing processes to implement blood products safety. B19V is a small virus, resistant to solvent and detergent treatments but only relatively resistant to heat treatment due to the physical conditions and composition of the medium [Blumel et al; 2010].

2. Aim of the Research

2.1 B19V Synthetic Genome and Virus

Human Parvovirus B19 is still not a well characterized virus although its worldwide distribution, clinical relevance and its relatively low complexity. As mentioned previously, B19V is difficult to maintain and propagate *in vitro* due to its very strict tropism for the cells within the erythroid lineage. EPCs from the bone marrow or from other sources are not immortal cells (they can be maintained about 16-20 days in culture *in vitro*) and their susceptibility and permissiveness to B19V changes along the differentiation process, so this system is not adapted to maintain and propagate the virus for long period. In addition to EPCs, other few myeloblastoid cell lines can support viral replication, such as the UT7/EpoS1 cells, but only a very limited production of infectious virus is obtained by these cell lines.

The availability of native virus from clinical isolates is still the major requirement for in vitro infectious experiments and genetic studies. Hence, other approaches are required to overcome the problem of limited propagation of B19V *in vitro* and to become independent from the viremic sera of infected patients, such as the generation of molecular clones and recombinant viral particles. Actually the construction of complete genomic clones with infectious capability was possible for the *Dependoviruses* (adeno-associated viruses: AAVs) and other viruses of the *Parvoviridae* family.

The first molecular clone of B19V was constructed without the two ITRs and it was very useful for exploring its connection with the other mammalian parvoviruses [Cotmore et al; 1984]. Subsequently, other B19V clones were generated within either incomplete or rearranged terminal regions, but they were not functional and they were not able to complete a full replicative cycle after transfection in cells. For example, an AAV-B19 hybrid was built from a B19V genome in which the defective ITRs were replaced with the full-length inverted terminal repeats from a nonpathogenic human parvovirus, the adenoassociated virus 2 (AAV2) [Srivastava et al; 1989]. A full-length B19V genome (J35 isolate) called pB19-M20 was cloned with the two ITRs; pB19-M20 replicated and produced infectious virions in semi-permissive UT7/EpoS1 cells [Zhi et al; 2004].

For studying capsid structure and assembling dynamics, eukaryotic expression systems were used to produce B19 viral capsid proteins that can self-assembly and form viral like particles (VLPs) comparable to native virions. Different heterologous systems were developed: at first, capsid protein expression was obtained by genetically engineered "Chinese hamster ovary"

cell line [Kajigaya et al; 1989] or B19V-SV40 hybrid vectors that were transfected into COS-7 cells [Cohen et al; 1995]. However, the baculovirus expression system in eukaryotic insect cells became the most widely used heterologous system for the production of B19V capsid proteins able to form VLPs [Brown et al; 1991].

These systems allowed conducting studies on sequence-structure correlation after mutational analysis in B19 genome, to understand the viral expression profile and viral protein functions, but they still did not lead to a high yield of infectious viral particles. Further studies, advanced biotechnological techniques and exploration of novel strategies were still required.

In this study, a new model genetic system for Human Parvovirus B19 was established. A synthetic approach was followed, from the design of a consensus reference genome sequence to the generation of the corresponding artificial construct which was cloned and subsequently transfected in UT7/EpoS1 cells in order to obtain infectious viral particles. These were further propagated by infecting EPCs to increase the yield of the recovered virus.

In particular, the B19V genome was constructed maintaining the complete and functional form of the virus and the entire process was optimized in order to obtain a stock of virus effectively comparable to the infectivity of native B19V. In addition, the synthetic approach was repeated using cloned genomes with different symmetries and with truncated ITRs. Progressive deletions of the terminal regions and the four different isomeries for every cloned genomes were investigated to evaluate their functional competence during the replicative cycle of Human Parvovirus B19 [Manaresi et al; 2017].

A functional B19V synthetic genome will provide the possibility to perform genetic studies to understand the correlation among the B19V genes and their relative functions through targeted mutagenesis within the viral genome, and also to investigate and to evaluate both the viral life cycle and the activity of putative antiviral molecules.

2.2 Cell Susceptibility and Permissiveness

The strict tropism of Human Parvovirus B19 for cells of the erythroid lineage can explain most of its pathological potential, but a debate has always been present whether this option was mainly dictated by receptor-mediated specificity or by restrictive intracellular events [Bua et al; 2017].

Different markers and factors are expressed by the cells along the various stages of the erythroid differentiation. B19V can not achieve a complete replicative cycle in all the

erythroid cells but it infects successfully cells that belong to a particular "window" of the differentiation process [Bua et al; 2016]. Besides, both viral and cellular factors are required to permit the B19V entry within the target cells, the escape from endosomes and possibly the blocking of cellular restriction factors for the production of the new viral progeny.

As mentioned previously, one of these factors is the VP1u specific coreceptor: after the binding to both the globoside receptor and to the VP1u specific coreceptor, the virus is internalized by clathrin-mediated endocytosis [Quattrocchi et al; 2012 - Leisi et al, n°61; 2016 – Leisi et al, n° 265; 2016]. A phospholipase activity by the PLA_2 domain in the central part of VP1u protein is necessary to escape late endosomes during the transport of the virus to the nucleus. B19V traffics rapidly through the endosomal compartment to the lysosomal compartment and the leakage from it is necessary to avoid the viral degradation inside the lysosomal vesicles.

Cell cycle arrest, elements of the cellular S-phase (such as cellular polymerase, accessory proteins, etc...) and erythroid-lineage specific host factors are important for efficient viral DNA synthesis [Qiu et al; 2017]. For example, the EPO-signaling which activates the JAK2-STAT5 pathway, positively regulates the B19V replicative cycle. Expression of STAT5 is upregulated during hypoxia and replication of B19V in human EPCs is facilitated by the hypoxic conditions as it happens in the bone marrow [Chen et al; 2011]. Human Parvovirus B19 needs EPO for its replication but erythroid lineage cells and B19V- semi permissive cell lines (such as UT7/EpoS1) depend on EPO for survival [Ganaie et al; 2018]. Hence, the virus has adapted to its target cell environment and benefits from the host machinery for its efficient replication.

However, not all the cells within the erythroid lineage are susceptible to B19V entry and/or are permissive for the production of new infectious particles. During erythropoiesis, pluripotent hematopoietic stem cells (HSCs, CD34$^+$) are differentiated into enucleated erythrocytes encompassing various stages: BFU-Es (Erythroid-Burst Forming Units), CFU-Es (Erythroid-Colony Forming Units), normoblasts, erythroblasts, reticulocytes and finally the mature erythrocytes [Ogawa et al; 1993]. Along the erythroid differentiation, both cellular markers expressed on the surface and signalling pathways inside the cell change, in addition to dimensional and functional modifications. The earlier stages of differentiation are EPO-independent and rely on factors like SCF (Stem Cell Factor), IL-6 and IL-3, while the late stage differentiation process requires EPO [Ganaie et al; 2018].

In this study, both the cellular and the viral factors were investigated to characterize the tropism of B19V and in particular the narrow "differentiation window" within the erythroid

lineage. Both viral elements (such as, the VP1u protein) and cellular constituents (such as, the globoside, the viral coreceptor, the endocytic pathway and the STAT5 pathway) are necessary to B19V to complete its replicative cycle. They are not expressed at every stages of the erythroid differentiation and they could increase or disappear in particular conditions or in a particular step within the lineage. These changes influence the susceptibility and permissiveness to B19V for the viral entry and its replication inside the cell, resulting in a higher or lower infectivity and so, progeny production.

2.3 Investigation of Antiviral Compounds

Nowadays, a vaccine for B19V has not been established yet, and no specific antiviral drugs have been developed for the treatment of B19V infection. IVIG therapy has been recognized as a current option because it offers a good source of neutralizing antibodies in immunocompromised patients exposed to B19V. Intravenous immunoglobulin substantially increase reticulocyte counts and hemoglobin levels. however, the IVIG treatment can become cost-prohibitive due to its repeated applications and despite this, the 33,9% of treated patients may have a relapse at a mean of 3 – 4 months. In principle, anti-B19V drugs should be useful to treat and protect the high-risk categories of population, such as patients with disorders at immune system and/or pathologies at hematopoietic compartment and pregnant women [De Clercq et al; 2016].

New antiviral drugs could be found through the applications of different strategies. In particular: i) rationale design of new molecules as direct antiviral agents; ii) screening of libraries of chemical compounds to identify drugs with an activity against B19V; iii) evaluation of an expanded spectrum of activity for available antiviral compounds; iv) the re-targeting against B19V of molecules that are already available to treat different diseases.

Previous work from our group identified an antiviral activity against B19V of the antiviral compound Cidofovir (CDV). The CDV is an acyclic nucleoside phosphonate active against dsDNA viruses; in particular, it is regulatory approved for the treatment of Cytomegalovirus retinitis in AIDS patients. *Cidofovir* has also been used as an off-label drug to treat many DNA virus infections such as HSV, adenovirus, poxvirus, polyomavirus, and papillomavirus infections. It is a cysteine analogue and its active metabolite (the *Cidofovir* diphopshate) inhibits viral replication by selectively inhibiting viral DNA polymerases. It also reduces the human polymerases but its action is weaker than the one against the viral enzyme.

Actually, in infected UT7/EpoS1 cells, the CDV inhibited the viral infectivity with an EC_{50} of about 41 μM [Bonvicini et al; 2015], while the action in EPCs was lesser however provoking a significant reduction on B19V DNA amounts at 500 μM both in EPCs extendedly exposed and in serially infected cells [Bonvicini et al; 2016]. Since the drug did not interfere with the cellular DNA synthesis and metabolic activity, the observed effect of CDV could be related to a specific antiviral effect.

The research of new anti-B19V drugs continues. In this study, both the antiviral action, directed against new targets such as G-quadruplex structures and, the effect on cellular viability and proliferation was evaluated for different compounds. In particular, various strategies were followed and molecules tested:

a) *Hydroxyurea* (HU): the HU is the only disease-modifying therapy approved for sickle cell disease (SCD) and it is usually used in the treatment of various cancers and myeloproliferative disorders. An anti-HIV activity was discovered due to its ability to induce cell cycle arrest through inhibition of ribonucleoside reductase [Lori et al; 1994]. HU is an inhibitor of the ribonucleoside-diphosphate reductase, which converts ribonucleosides in deoxyribonucleosides So its action could probably reduce the availability of deoxyribonucleosides diphosphates for the genome replication.

b) *Brincidofovir* (BCV): it is a novel lipid conjugate of CDV which showed antiviral activity against dsDNA viruses [Panter et al; 2012].

c) small chemical library screening: analogues of HU, coumarin derivatives and analogues of G-quadruplex ligand BRACO-19, and new synthesized compounds without an identified action and not characterize from a structural point of view (compounds were provided by the group of Professor A. Locatelli; FaBiT, University of Bologna).

d) G-quadruplexes ligands (BRACO-19 and PDS): they bind the G4 structures stabilizing them and leading to a block or an increase of the replication.

3. B19V Synthetic Genome and Virus

3.1 Design of a consensus sequence

To establish a model genetic system for Human Parvovirus B19, a reference sequence genome was designed for the purpose of obtaining a functional molecular clone. A total of 49 sequences (genotype 1a) deposited in the NCBI nucleotide database were analyzed by bionformatic tools. In particular, sequences were globally aligned using the ClustalW algorithm implemented within Clone Manager 9 and MEGA6 software packages. As result, an unambiguous global sequence alignment was obtained extending over all the genome sequence of B19V. Within the selected set, 40.2 hits per each of the 5596 nucleotide positions was the average coverage. The degree of sequence information available was different between the internal unique region (IR) and the terminal regions (ITR). For the IR, sequence from all the 49 isolates provided a relatively higher coverage of 46.0 hits/position. For the ITRs, only three complete sequences could be included in the dataset provided an average coverage as low as 5.8 hits/position. From the global sequence alignment, a Position Weight Matrix (PWM) was obtained and its Information Content (IC) was calculated for every nucleotide position; the value of the average IC in bit units was 1.966 (figure 3.1).
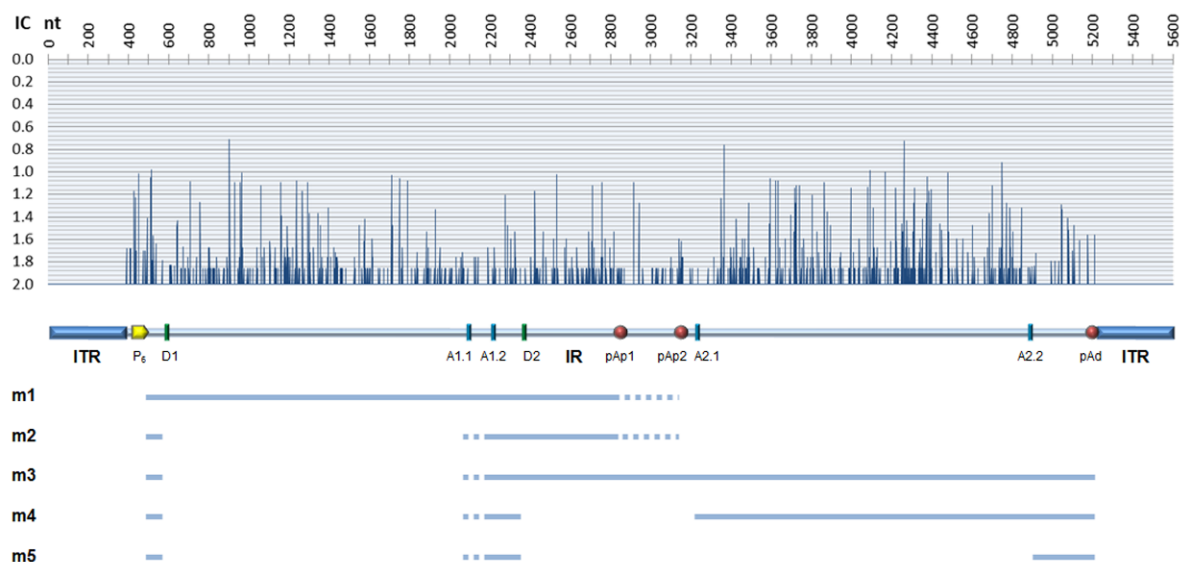
Figure 3.1: Sequence diversity and functional map of B19V genome. Top) Information Content (IC) profile of the Position Weight Matrix (PWM) obtained from the alignment of the set of 49 B19V whole genome sequences. For each position (w), and j $\in$ {T,C,G, A}, the IC(w) was calculated as: IC(w) = 2 + Σj pwj log$_2$p$_{wj}$ [*ClustalW*]; Center) A schematic diagram of B19V genome indicating the two inverted terminal regions (ITR), and the internal region (IR) with the distribution of cis-acting functional sites (P6, promoter; pAp1, pAp2,

proximal cleavage-polyadenylation sites; pAd, distal cleavage-polyadenylation site; D1, D2, splice donor sites; A1.1, A1.2, A2.1, A2.2, splice acceptor sites); Bottom) Transcription map of B19V genome indicating the five classes of mRNAs (m1-5) with respective alternative splicing/cleavage forms.

The subsequent analysis with MEGA6 allowed to determine other information on the genetic variance within the selected B19V genome set. Maximum Likelihood (ML) fits of different nucleotide substitution models were evaluated to describe the observed nucleotide substation pattern. A General Time Reversible (GTR) model, with Gamma Distribution (+G, 0.80) and invariant sites (+I, 0.66) gave the highest ML score and was used for further modelling. Pairwise distance distribution ranged continuously from 0.000 to 0.037, with average values for each sequence in the range 0.009-0.022 and an average overall value for the matrix of 0.013.

The global sequence alignment yielded a consensus sequence matching the highest IC profile for B19V genome, with the minimal average distance value from other sequences in the dataset (0.008, range 0.002-0.022) and coincident with a possible ancestral state as determined from a ML phylogenetic tree. This consensus sequence was used for the further studies as a reference B19V (1a) genotype.

3.2 Genome cloning

From the obtained B19V consensus sequence, a synthetic strategy was developed to construct a complete molecular clone. The insert was projected to contain a segment extending from position 136 to position 5461 of the B19V consensus sequence. Deletion of the external part of the ITRs was conceived in order to avoid difficulties in maintaining full-length and stable inserts, as experienced in previous experiments.

The cloned region included the complete internal region and extension of both ITRs beyond the sites of dyad symmetry (at nt 182/183 and 5413/5414) that allowed to maintain the potential to fold back in hairpin structures and preservation of flip/flop sequence heterogeneity (within nt 148-218 and 5379-5449).

To construct the projected molecular clone, gene blocks corresponding to segments of the viral genome were obtained by DNA synthesis, then the diverse inserts were progressively ligated into a single insert and cloned into the plasmid vector pIDT. As final result, four different plasmids were obtained (named pCK00-01-10-11), each containing the same insert corresponding to 136-5461 nt of B19V consensus sequence and differing for the diverse

combination of flip/flop terminal isomers. Plasmids were stably maintained in *SURE 2 Supercompetent Cells* strain without rearrangements or deletions, as confirmed by Sanger sequencing.

pCK plasmids were used to recover complete genomic inserts extending beyond the sites of dyad symmetry from nt 136-5461, by SacI restriction endonuclease cleavage (CK00-01-10-11) and the other inserts. In particular, truncated genomic inserts, extending up the sites of dyad symmetry from nt 184-5413 were recovered by BssHII cleavage (CH00-01-10-11) or by PCR amplification using the combination of the different HH0/HH1 primers due to the isomerism. A truncated genomic insert, extending within the sites of dyad symmetry from nt 242-5355 was recovered by AccIII cleavage (CI0 insert) or by PCR amplification (HI0 primers). In addition, a truncated genomic insert excluding the terminal regions (CJ0) was obtained by PCR amplification, extending from nt 367-5230 (figure 3.2).

Figure 3.2: Terminal regions sequence heterogeneity and extension of B19V inserts. Top) Schematic diagram of B19V genome indicating the extension of inserts relative to the two inverted terminal regions (ITR) and the internal region IR); Bottom) Schematic alignment of left terminal region sequences in flip/flop isomers. Triangles indicates the site of dyad symmetry within the ITR, underlined bases indicate the location of sites relevant for the definition of inserts.

3.3 Functional competence

- CK10: UT7/EpoS1 Nucleofection

Insert CK10 was selected to test the functional competence of the synthetic cloned genome in a time course experiment. $1x10^6$ UT7/EpoS1 cells were nucleofected with 1 µg of CK10 insert and maintained in culture for 12 days adding complete medium whether required. Cells and supernatants were collected at 1–3–6–9-12 dpt (day post-transfection) and analyzed for viral proteins and viral DNA expression. Meanwhile, UT7/EpoS1 cells were infected by B19V serum at moi (multiplicity of infection) of 10^4 geq/cell in order to control their susceptibility and permissiveness for viral infection.

IIF anti-VP assays at the different time points showed positive cells for viral capsid proteins expression since 1 dpt and a progressive increase from 3 to 6-9 dpt both in terms of number of positive cells and in term of fluorescence brightness. At 12 dpt, positive cells for VP expression were still present although in lower number compared to the previous days (figure 3.3).
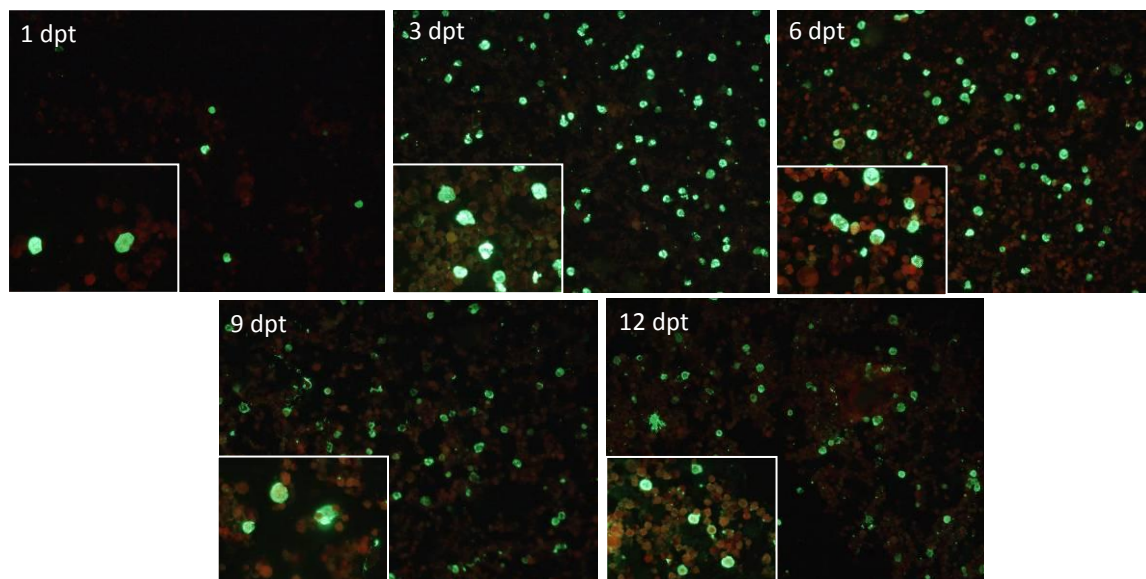
Figure 3.3: IIF anti-VP for CK10 nucleofected UT7/EpoS1 1-3-6-9-12 dpt = positive cells for protein production are in green while the negative cells are in red due to the staining with Evans Blue (10x and 40x magnification).

B19V DNA molecules were detected inside the transfected cells by a FISH assay, indicating that active viral replication could occur in transfected cells. At 1 dpt, few positive cells for B19V were shown, probably due to the low transfection efficiency; instead at 3 dpt, their number increased. Their fluorescence brightness was maximal at 6 dpt; however, progressive less number of B19V DNA positive cells were shown at 6, 9 and 12 dpt (figure 3.4).
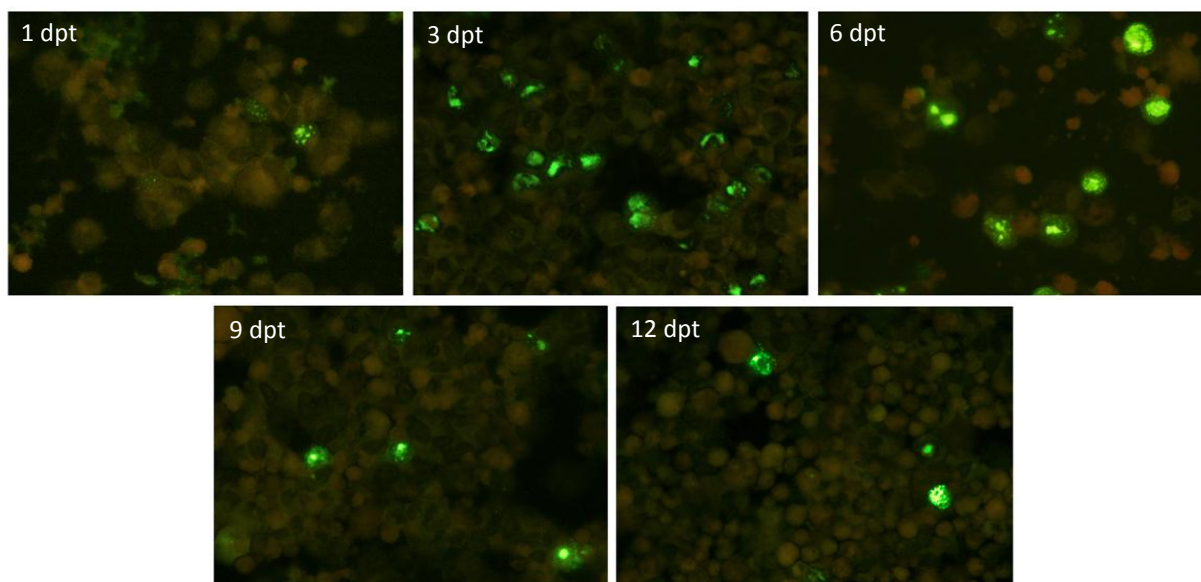
Figure 3.4: FISH assay of CK10 nucleofected UT7/EpoS1 at 1-3-6-9-12 dpt = Upper) Pictures of transfected cells: positive cells for protein production are in green while the negative cells are in red due to the staining with Evans Blue (40x magnification); Lower) Graphs representative of percentage of FISH positive cells: 1 dpt = 2.1%, 3 dpt = 6.7%, 6 dpt = 5.6%, 9 dpt = 4.3% and 12 dpt = 2.0%. Plotted values are mean of two experiments [*GraphPad Prism 6.0*].

The results by qPCR assay of viral nucleic acids extracted from transfected cells and supernatants were less informative. Actually, a high amount of B19V DNA was detected for every time points probably due to the high background of the initial transfected CK10 insert.

However, an increasing amount of benzonase-resistant DNA was present in supernatants from 3 dpt; the amount of B19V genomes at 6, 9 and 12 dpt were comparable. This indicated that a progressively higher fraction of viral DNA was encapsidated in mature virions and that these were released from cells into the medium. Confirmation of these data was obtained by Southern Blot analysis of viral nucleic acids extracted from UT7/EpoS1 cells: DpnI resistant DNA bands were shown for the cellular extracts at 6, 9 and 12 dpt (figure 3.5). Digestion with DpnI enzyme allowed to distinguish the newly synthesized DNA (GATC-DNA) from the bacterial one (GmATC-DNA).
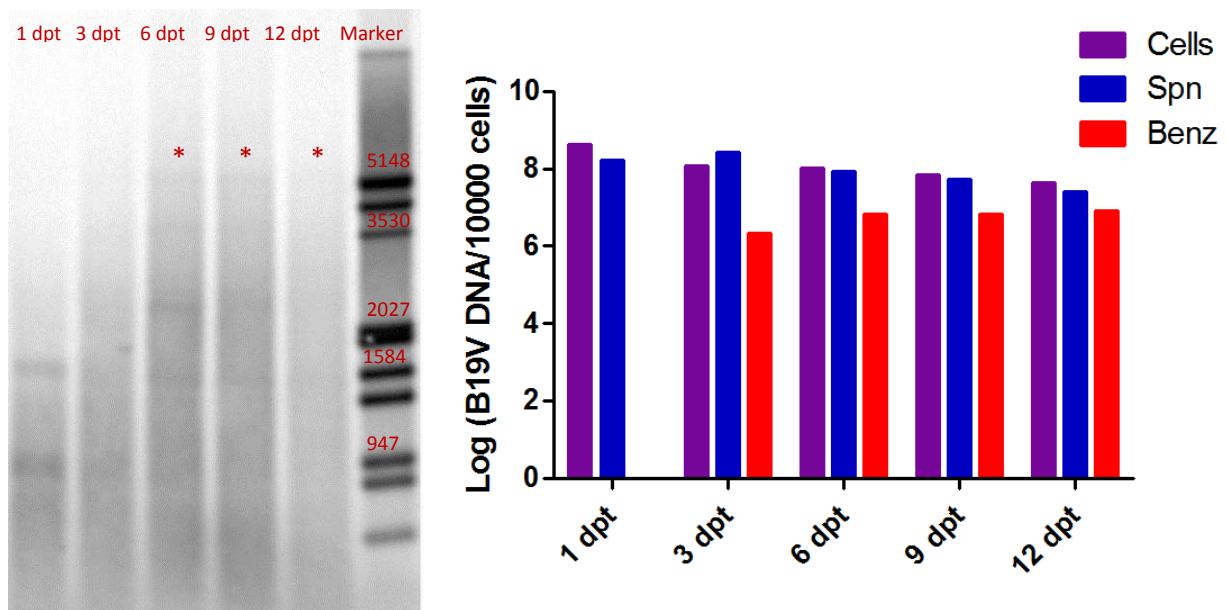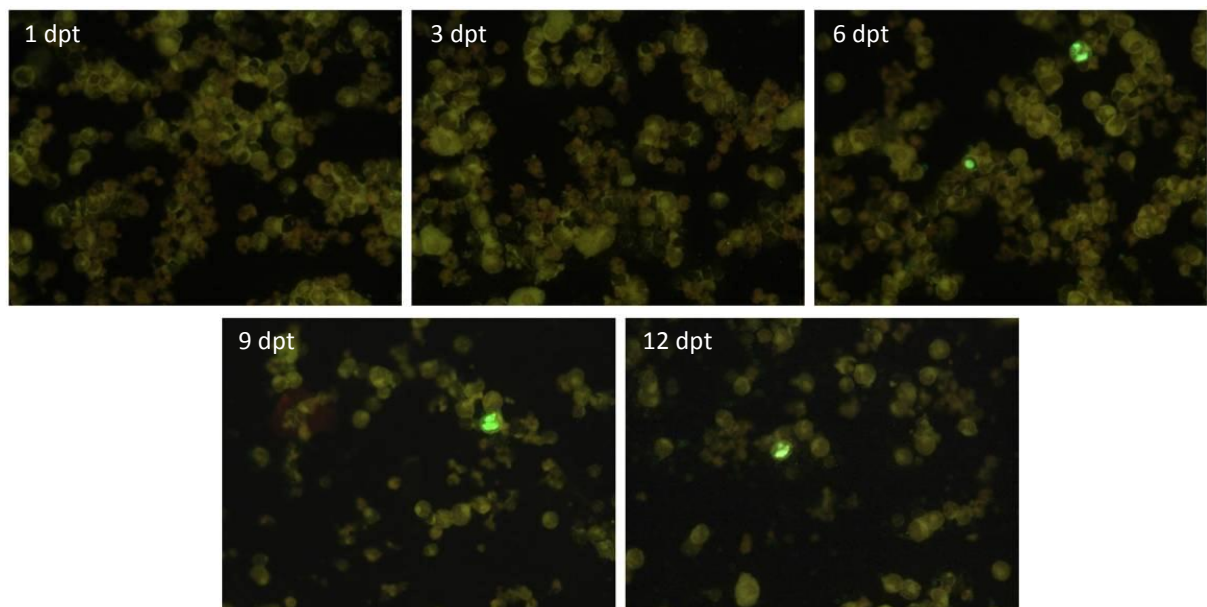

Figure 3.5: CK10 nucleofected UT7/EpoS1 cells 1-3-6-9-12 dpt = Left) Southern Blot analysis of DNA cellular extract digested by DpnI + EcoRI: bands at about 5000 bps (*) corresponding to DpnI resistant B19V DNA (newly synthesized sequences) for 6, 9 dpt and less evident at 12 dpt (*Marker III-Dig*, Roche); Right) B19V DNA amounts evaluated by qPCR assay in cells (purple; Log DNA geq/10^4 cells), supernatants (blue; Log DNA geq /10 µL) and benzonase resistant within supernatants (red; Log DNA geq/10 µL). Plotted values are mean of two experiments which are done in duplicate [*GraphPad Prism 6.0*].

- CK10: EPCs infections

Collected supernatants at different days post-transfection (1-3-6-9-12 dpt) were used to infect EPCs at day 8 of differentiation (ratio 75 µL of supernatants for 750.000 EPCs). Also in this situation, viremic serum at moi of 10^4 geq/cell was used to infect the cells, as positive control, for testing their susceptibility and permissiveness to B19V. Cells and supernatants were collected at the following different time points: 2 hpi, 48 hpi and 6 dpi (hpi = hour post-infection; dpi = day post-infection). The yield of infection was evaluated by IIF assay for the capsidic viral protein expression and FISH assay together with Southern Blots and qPCRs of

cellular and supernatants extracted nucleic acids, for viral DNA production. Few positive cells were detected by IIF anti-VP only for infected EPCs at 48 hpi by 6-9-12 dpt supernatants; their numbers increased at 6 dpi. No positive cells were shown for 1 dpt supernatants neither at 48 hpi nor at 6 dpi infected cells, while few positive cells were detected for 3 dpt supernatants only at 6 dpi infected EPCs.

Same results were obtained by FISH: an increasing number of positive cells for B19V DNA from 48 hpi to 6 dpi for 6-9-12 dpt infected EPCs, a lower number for 3 dpt infected cells but maintaining a progressive increasing from 48 hpi to 6 dpi, while no positive cells were detected by FISH assay for 1 dpt infected EPCs (figure 3.6). qPCR assay showed no significant increase in the amount of viral DNA for the 1 dpt and 3 dpt collected infected EPCs or supernatants, neither at 48 hpi nor at 6 dpi compared to their respective 2 hpi. However, a significant increase was shown for the 6-9-12 dpt infected EPCs at 48 hpi only in the cells and at 6 dpi both in the cells and supernatants. Actually, variations of +0,5 - 0,9 Log in the infected cells at 48 hpi, +2,6 - 3,0 Log in the cells at 6 dpi and + 2,9 – 3,2 Log in the supernatants at 6 dpi were found (figure 3.7).

Figure 3.6: Infected EPCs with nucleofected UT7/EpoS1 supernatants collected at 1-3-6-9-12 dpt (first round of infection) = Pictures of infected EPCs at 6 dpi: positive cells show a mainly nuclear distribution of B19V DNA among the negative cells that are in red due to the Evans Blue staining (40x magnification);
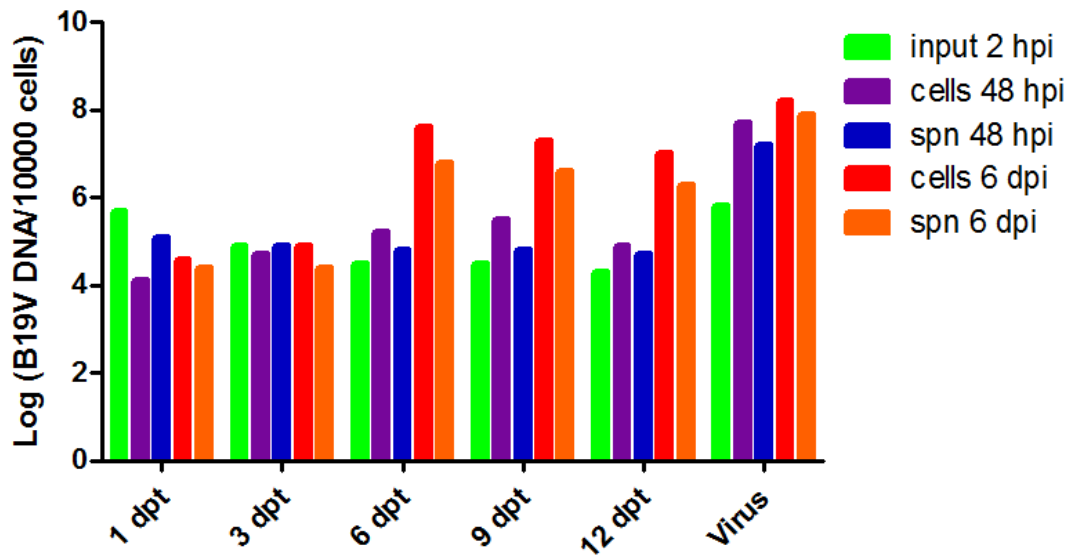
Figure 3.7: Infected EPCs with nucleofected UT7/EpoS1 supernatants collected at 1-3-6-9-12 dpt (first round of infection) = B19V DNA amount extracted from infected EPCs evaluated by qPCR assay, at different time points, in cells (Log DNA geq/10^4 cells) and supernatants (spn; Log DNA geq/10 µL). "Virus" is the amount of viral DNA detected in cells and supernatants of the positive control (viremic serum infected EPCs at moi = 10^4 geq/cell). Plotted values are mean of two experiments which are done in duplicate [*GraphPad Prism 6.0*].

Southern Blot assay of nucleic acids extracted from infected EPCs (2 hpi, 48 hpi and 6 dpi) showed bands, that corresponded to B19V DNA, only at 6 dpi (figure 3.9). So only the supernatants collected at this time point were used for a second round of infections.

For this purpose, 60 µL of supernatant from 6 dpi of each infection were used to infect 600.000 EPCs at day 5, in order to expand the previously obtained viral progenies. Meanwhile, cells were infected by viremic serum at moi of 10^4 geq/cell as positive control. Infected EPCs were cultured for 6 days adding complete medium whether necessary. Cells and supernatants were collected at 2 hpi, 48 hpi and 6 dpi and tested for B19V capsid protein expression and B19V DNA replication by IIF assay, FISH, Southern Blot and qPCR assay, respectively.

IIF assay anti-VP showed a large number of positive cells, that expressed B19V capsid proteins, for 6 dpi from 6-9-12 dpt supernatants infected EPCs (second round of infection), both at 48 hpi and at 6 dpi. In addition, their fluorescence brightness increased from 48 hpi to 6 dpi. No positive cells were detected for the EPCs that were infected by the supernatants of the first round of 6 dpi infected EPCs by 1 and 3 dpt supernatants.

FISH assay detected B19V DNA both at 48 hpi and at 6 dpi of 6-9-12 dpt infected EPCs, second round. However, lower number of B19V DNA positive cells was found for the 12 dpt than the 6 and 9 dpt second round infected EPCs (figure 3.8).
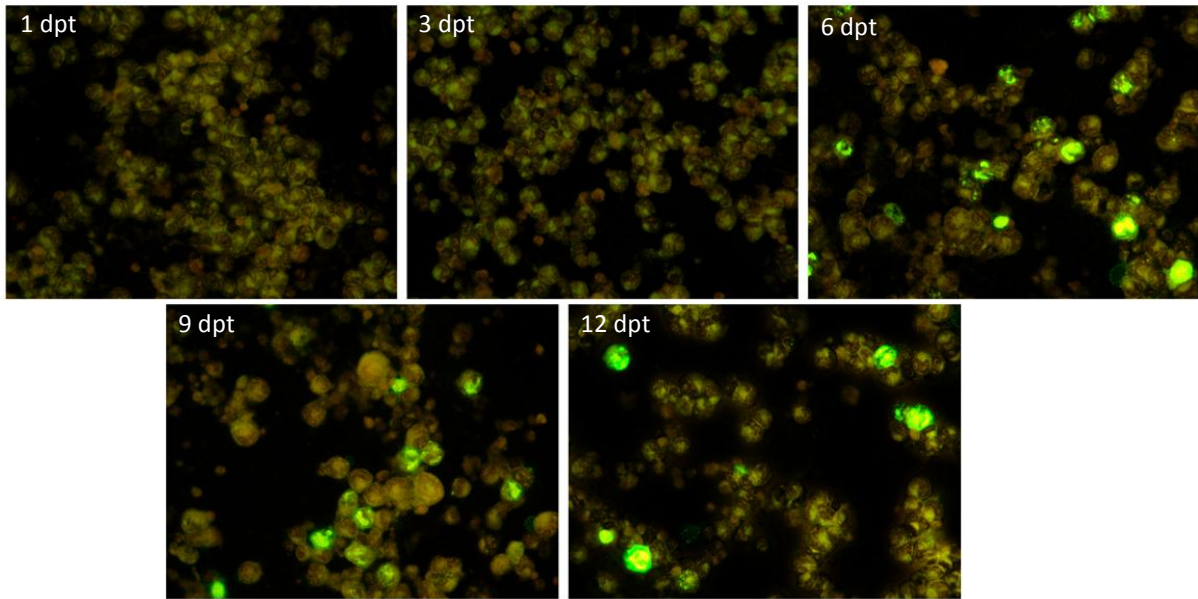
Figure 3.8: Pictures of FISH assay for 6 dpi infected EPCs by 6 dpi supernatants of infected EPC with 1-3-6-9-12 dpt supernatants (second round of infection). Positive cells show a mainly nuclear staining (40x magnification).

B19V correspondent bands were detected both at 48 hpi and at 6 dpi for 6 dpt infected second round EPCs by Southern Blot, with a higher intensity at 48 hpi rather than at 6 dpi (figure 3.9).
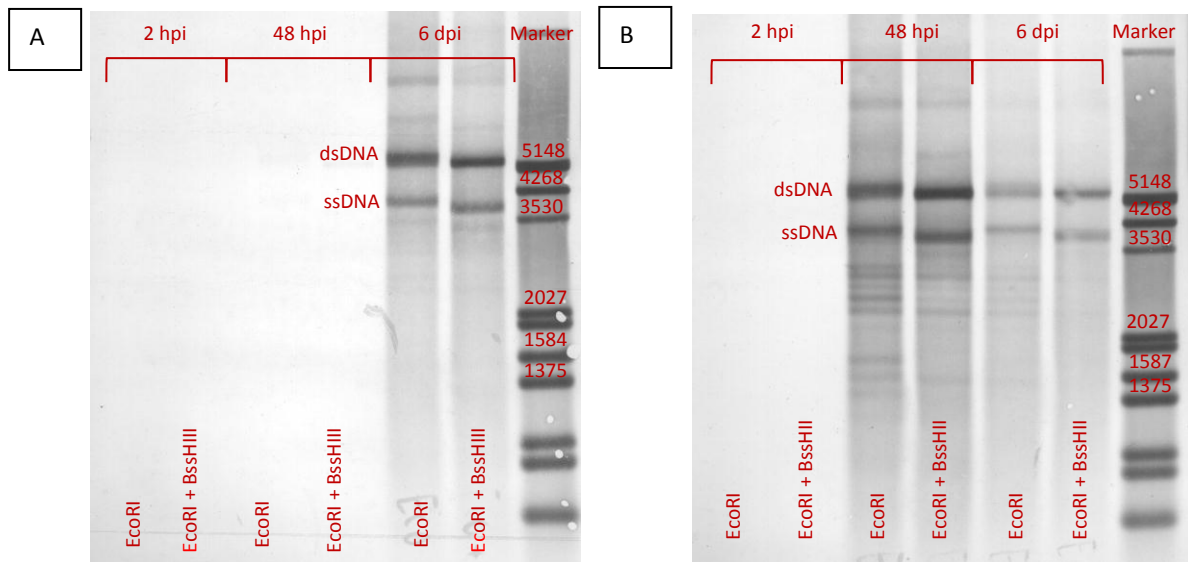
Figure 3.9: Southern Blot assay of 2-48 hpi and 6 dpi infected EPCs = nucleic acids extracted from cells and digested by EcoRI = 5596 bps or EcoRI + BssHII = 5231 bps + 365 bps. dsDNA and ssDNA are shown and it is visible the difference of height among the EcoRI and EcoRI/BssHII digested DNA due to the ITRs. *Marker III-Dig* (Roche) = A) First round of infection by 6 dpt supernatant: B19V bands only for 6 dpi extracts; B) Second round of infection by 6 dpi supernatants from EPCs infected by 6 dpt supernatant: B19V bands both at 48 hpi (more intensity) and at 6 dpi.

Same results were confirmed by qPCR: no significant increase in the amount of viral DNA was detected for the 1 dpt and 3 dpt cells/supernatants at 2 – 48 hpi or 6 dpi, while a significant increase was observed for the 6-9-12 dpt infected EPCs, already at 48 hpi both in cells and supernatants, only in supernatants at 6 dpi. In particular, variations of +3,4 - 3,7 Log were found in cells at 48 hpi, + 2,4 – 2,7 Log were found in supernatants at 48 hpi, +3,3 – 3,5 Log were found in cells at 6 dpi and + 3,9 – 4,1 Log were found in supernatants at 6 dpi (in comparison to the 2 hpi). So, from 48 hpi to 6 dpi, the amount of viral DNA was maintained stable within the cells, while it increased in supernatants, probably due to the egress of the new B19V progeny.

Indeed, these increases were higher than those obtained for native B19V (viremic serum). Actually, the amount of viral DNA increased of +2,1 Log in cells and +2,0 Log in supernatants at 48 hpi, +1,3 Log in cells and +2,3 Log in supernatants at 6 dpi in comparison to 2 hpi, for native B19V. Finally, the whole amount of B19V DNA was comparable between the CK10 progeny and native B19V (figure 3.10).
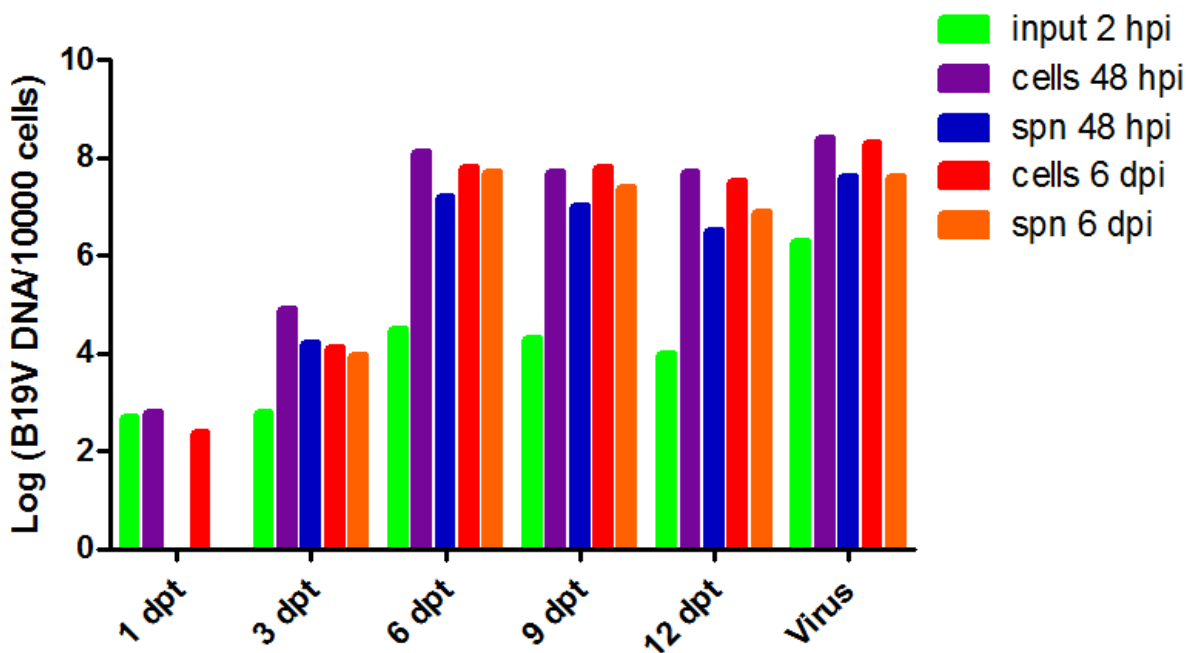
Figure 3.10: Second round of infection of EPCs = B19V DNA amount extracted from infected cells evaluated by qPCR assay, at different time points, in cells (Log DNA geq/10^4 cells) and supernatants (spn; Log DNA geq/10 µL). "Virus" is the amount of viral DNA detected in cells and supernatants of the positive control (viremic serum infected EPCs at moi = 10^4 geq/cell). Plotted values are mean of two experiments which are done in duplicate.

3.4 Comparative analysis

- **Comparative analysis: UT7/EpoS1 transfection**

A series of experiments was carried out to test the functional competence of the genomic inserts in dependence of the different isomer combinations and/or extension of the terminal regions.

The viral inserts were excised from their respective plasmids by SacI digestions (CK-inserts) or were obtained by PCR amplifications (CH-, CI0 and CJ0 inserts) . UT7/EpoS1 cells were transfected with the viral inserts using the *Amaxa System Nucleofector*, program T20 and reagent V (ratio 1 µg DNA every $1x10^6$ cells). Transfected cells and supernatants were collected at 3 and 6 dpt and analyzed for the viral proteins and DNA expression.

IIF anti-NS showed positive cells for the production of the B19V non-structural protein, in UT7/EpoS1 cells that were transfected with every clone, while the IIF assay against the VP capsid proteins detected positive cells for all the clones except CJ0 at both 3 dpt and 6 dpt (data is not shown).

The same results were observed with the FISH assay but indicating more diversity among the clones (figure 3.11 – figure 3.12). Actually, CK- clones could sustain a major viral replication, both for the amount of positive cells and in term of fluorescence brightness, while CH-clones and CI0 lower number of positive cells and lower fluorescence brightness, and very few positive cells were observed in CJ0 nucleofected cells.
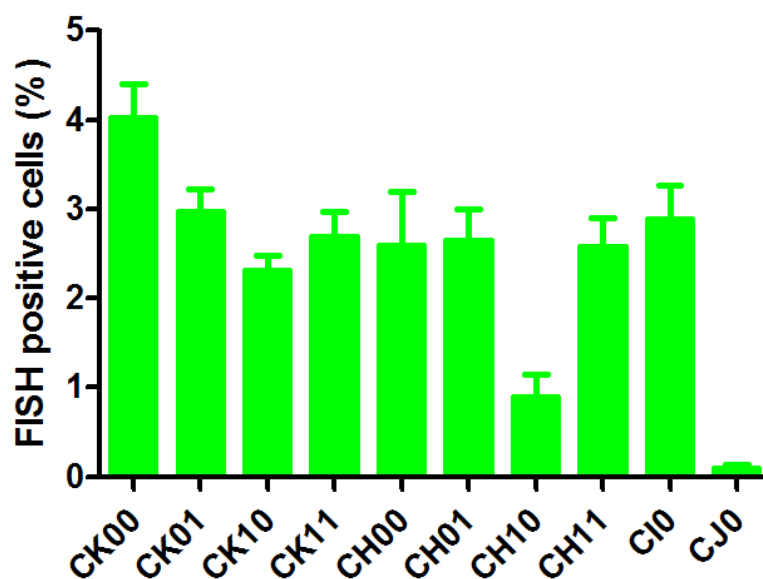

Figure 3.11: Graphs representative of percentage of FISH positive cells following the transfection with the indicated inserts, at 6 dpt = CK: 2,3 – 4,0%; CH: 2,3 – 3,2%; CI0: 2,9%; CJ0: 0,1% [*GraphPad Prism 6.0*].
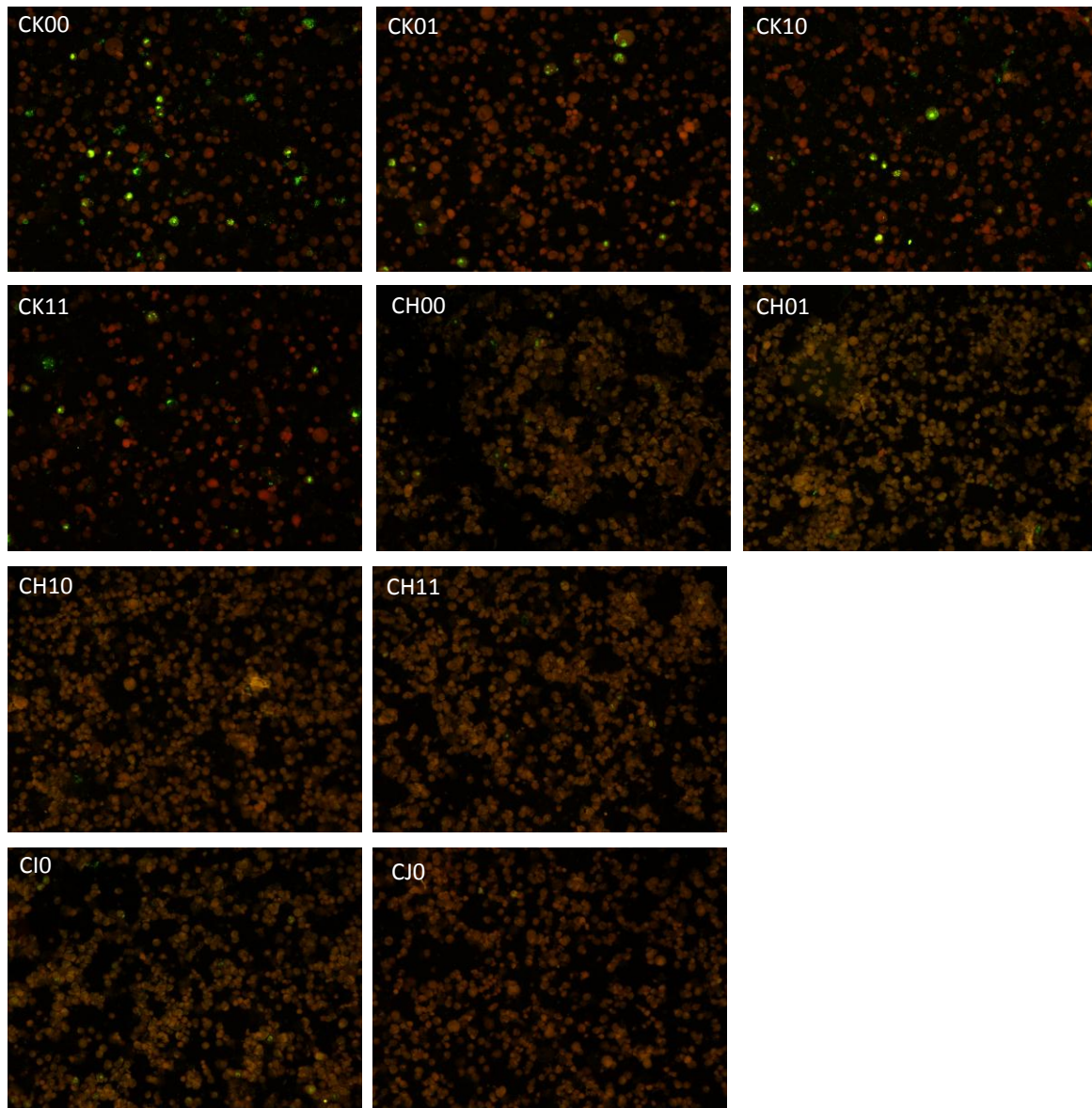
Figure 3.12: FISH assay for 6 dpt nucleofected UT7/EpoS1 by CK 00-01-10-11, CH 00-01-10-11, CI0 and CJ0 clones. Positive cells show a mainly nuclear staining with differences about the number and the fluorescence brightness among the various clones (40x magnification).

Also for these nucleofections, a high background of input DNA was detected by qPCRs both in the cellular and supernatant. However, the treatment with the Benzonase enzyme showed resistant viral DNA in supernatants from all the clones, but with significant differences among them. In particular, the highest values of Benzonase resistant nucleic acids were observed for the CK- clones (6,6 – 6,7 Log geq/10 µL) and lowest for CJ0 clone (5,0 Log geq/10 µL), while intermediate values were detected for the CH- group and CI0 clone (5,8 – 6,1 Log geq/10 µL) (figure 3.13).
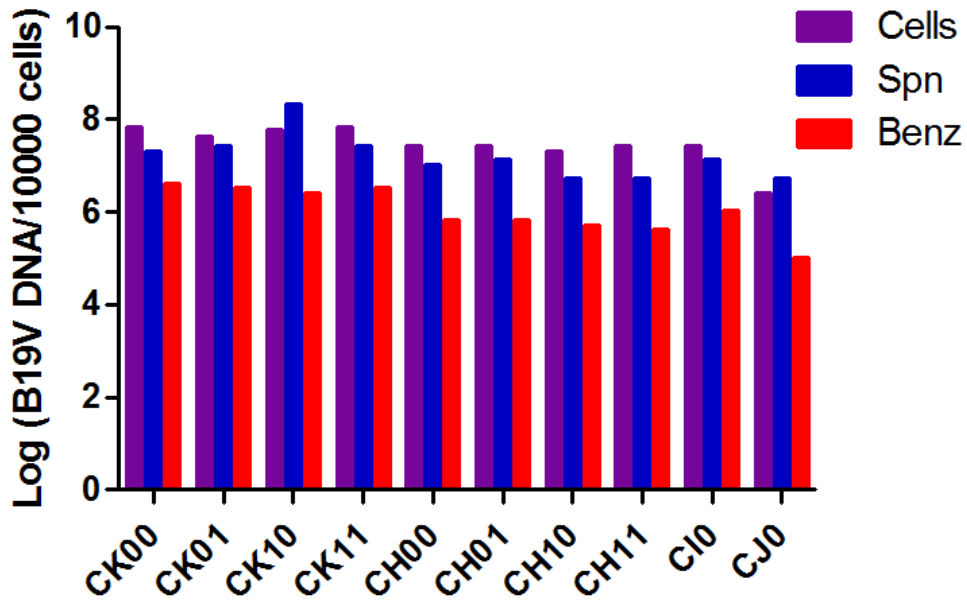
Figure 3.13: Transfection of UT7/EpoS1 by CK-00-01-10-11, CH-00-01-10-11, CI0, CJ0 at 6 dpt. B19V DNA amounts evaluated by qPCR assay in cells (purple; Log DNA geq/10^4 cells), supernatants (blue; Log DNA geq /10 μL) and benzonase resistant within supernatants (red; Log DNA geq/10 μL). Plotted values are mean of two experiments [*GraphPad Prism 6.0*].

Finally, Southern Blot analysis of nucleic acids extracted from nucleofected cells at 6 dpt showed DpnI resistant B19V molecules for all the clones except CJ0 (figure 3.14).
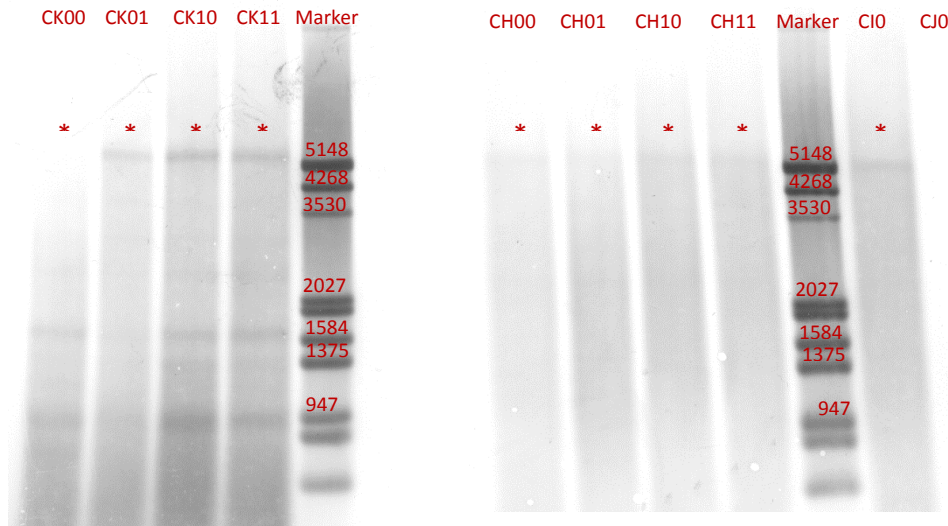
Figure 3.14: Southern Blot analyses for UT7/EpoS1 nucleofection by CK-00-01-10-11, CH-00-01-10-11, CI0, CJ0. DNA cellular extracts digested by DpnI + EcoRI = bands at about 5000 bps (*) corresponding to DpnI resistant B19V DNA (newly synthesized sequences) are shown for all clones except CJ0. CK00 shows a not very evident band; bands with less molecular weight appears for all CK- clones probably due to the initial transfected DNA which is digested by DpnI enzyme. *Marker III-Dig* (Roche).

- **Comparative analysis: EPCs infections**

Supernatants from CK 00-01-10-11, CH 00-01-10-11, CI0, CJ0 nucleofected UT7/EpoS1 cells were used to infect EPCs for a first round of infections. In particular, 30 µL of respective supernatants were used to infect 300.000 cells at day 8 of differentiation. The infected EPCs were kept in culture for other 6 days, collecting cells and supernatants at different time points. Samples of 48 hpi and 6 dpi were analyzed by IIF assay, FISH assay and qPCR for evaluating the expression of B19V proteins and nucleic acids, respectively.

IIF assay anti-VP at 48 hpi showed positive cells for CK clones, less positive cells for CH10 and CH01 infected EPCs, while no positive cells were observed for CH11, CH00, CI0 and CJ0 infected cells. The pattern was maintained at 6 dpi but with a decreasing in the yield of positive cells.

The data were confirmed with the viral DNA detection assays. By FISH assay: both at 48 hpi and 6 dpi positive cells for B19V DNA replication were found in all CK- clones, CH01 and CH10 infected EPCs with an increasing for the number of positive cells from 48 hpi to 6 dpi. Cells infected by CH00, CH11, CI0 and CJ0 supernatants did not show DNA viral expression. By qPCRs, increases of +1,9 − 2,5 Log was evaluated for all the CK infected cells and of +0,5 − 1,3 Log was detected for the supernatants; while +3,0 − 3,6 Log and +2,7 − 3,2 Log were the increases of the DNA amount at 6 dpi in the cells and supernatants, respectively. For CH01 and CH10, increases were observed both in the cells and in the supernatants at 6 dpi in the range of +2,8 − 3,0 Log and +2,0 − 2,5 Log, respectively. As for the previous results, CH00, CH11, CI0 and CJ0 clones showed any increases neither in the cells nor in the supernatants (figure 3.15).
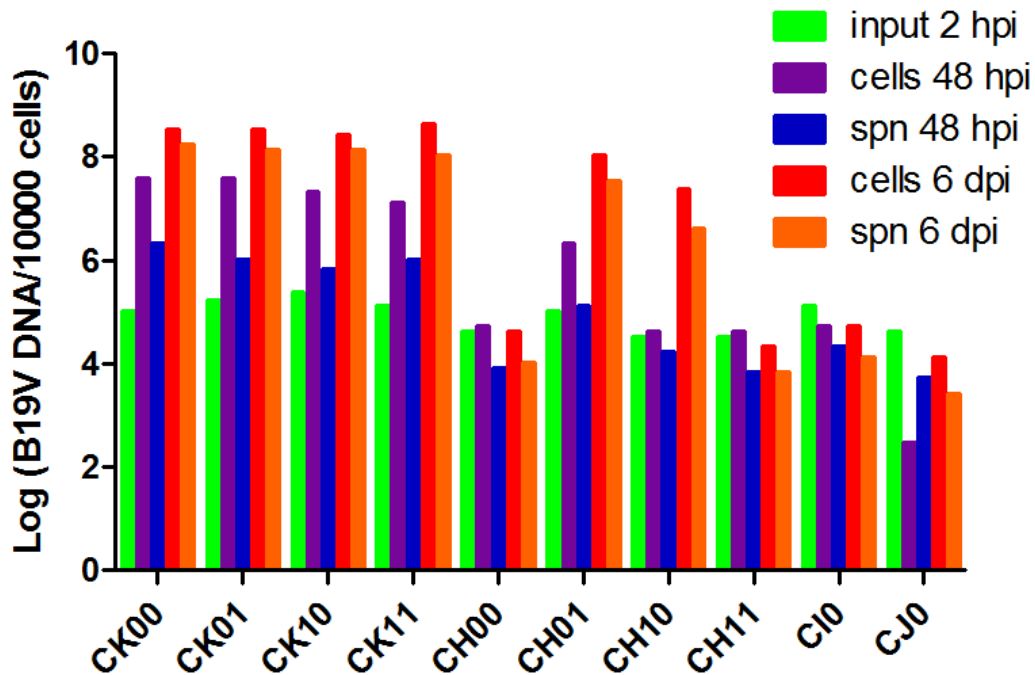
Figure 3.15: First round of EPCs that are infected by CK 00-01-10-11, CH 00-01-10-11, CI0, CJ0 nucleofected UT7/EpoS1 6 dpt = B19V DNA amount extracted from infected cells and supernatants evaluated by qPCR assay, at different time points (2 hpi, 48 hpi and 6 dpi), in cells (Log DNA geq/10^4 cells) and supernatants (spn; Log DNA geq/10 µL). Plotted values are mean of two experiments which are done in duplicate [*GraphPad Prism 6.0*].

Then, 30 µL of each 6 dpi supernatant was used to infect new EPCs for a second round of infections in order to propagate the viral progeny when possible and to confirm the obtained data from the first round of infection. Cells and supernatants were collected at 2 hpi, 48 hpi and 6 dpi and analyzed for B19V production.

Positive cells for viral DNA were observed by FISH assay for all CK-inserts, CH01 and CH10 with an increasing yield of positive cells from 48 hpi to 6 dpi. By qPCR, a comparable increase in the amount of viral DNA was evaluated for them in the range of +2,8 – 4,5 Log and +2,5 – 4,0 Log in cells and supernatants (both at 48 hpi and at 6 dpi), respectively (figure 3.16). CH00, CH11, CI0 and CJ0 inserts showed neither positive cells for viral DNA within nuclei by FISH assay nor increases in the amount of B19V DNA by qPCR.

Southern Blot assay of cellular extracts showed bands corresponding to B19V DNA for the active replicative inserts (all CK clones, CH01 and CH10) both at 48 hpi and at 6 dpi (figure 3.16).
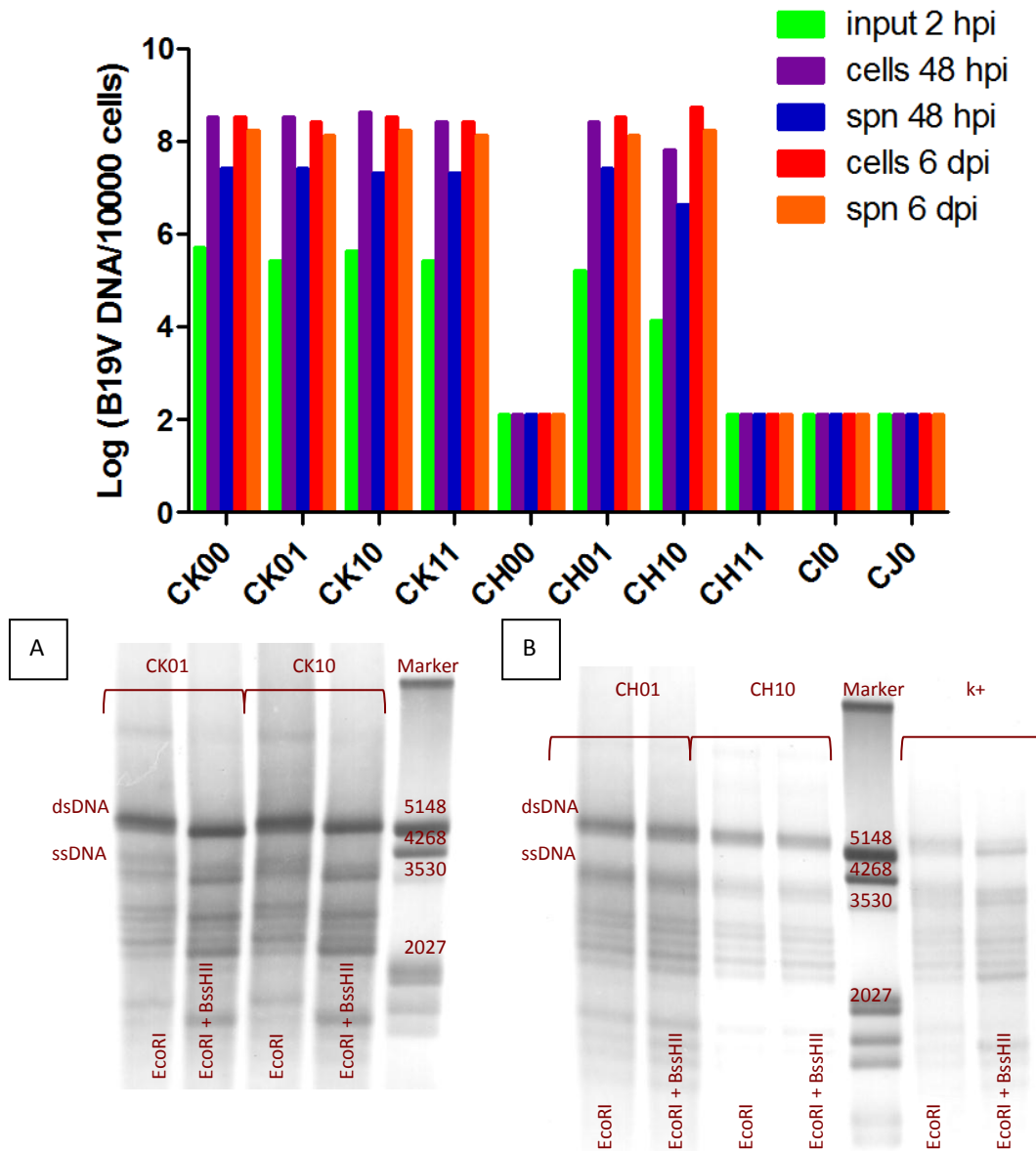
Figure 3.16: Second round of infection of EPCs by supernatants from 6 dpi infected EPCs = Upper) B19V DNA amount extracted from infected cells and supernatants evaluated by qPCR assay, at different time points (2 hpi, 48 hpi and 6 dpi), in cells (Log DNA geq/10^4 cells) and supernatants (spn; Log DNA geq/10 μL). Plotted values are mean of two experiments which are done in duplicate [*GraphPad Prism 6.0*]; Lower) Nucleic acids extracted from 48 hpi infected cells and digested by EcoRI = 5596 bps or EcoRI + BssHII = 5231 bps + 365 bps. The patterns among them are comparable with both dsDNA and ssDNA; it is visible the difference of height between the EcoRI and EcoRI/BssHII digested DNA due to the ITRs. *Marker III-Dig* (Roche) = A) CK01 and CK10 infected EPCs; B) CH01, CH10 and viremic serum (K+, moi = 10^4 geq/cell) infected EPCs.

3.5 Discussion

Difficulties for investigations on Human Parvovirus B19 are due to its strict tropism for the erythroid progenitor cells in the bone marrow. Both the propagation and the maintaining of the virus *in vitro* are limited from this differentiating and short-lived primary cellular populations, thus viremic sera from patients are normally used as source for the virus.

In the present research, a new model genetic system for B19V was established, leading from the design of a consensus reference genome sequence as a working tool, to molecular cloning of a respective synthetic construct in a complete and functional form and finally, to generation of fully competent virus that could be efficiently propagated in erythroid progenitor cells. In particular, a consensus sequence which possibly represented an ancestral B19V sequence was obtained by bioinformatic analysis on a set of B19V genomes (genotype 1a).

Synthetic techniques allowed the transition from in silico designed sequence to DNA. In the cloning strategy, the whole internal region of B19V sequence and only part of the terminal sequences were maintained in order to avoid instability in the vector plasmids. However, the cloned inserts extended beyond the sites of dyad symmetry with the conservation of the potential to fold back in hairpin structures and preservation of flip/flop sequence heterogeneity. Both these features were considered a priori as relevant for the generation of fully competent genomes. Different combinations of terminal isomers and progressively truncated inserts could be excised from vector plasmids and investigated.

Functional competence of the cloned synthetic genome was demonstrated by transfection in UT7/EpoS1 cells where the replication of the viral genome and enhanced release of the virus were related to the extension of the terminal regions. However, the system showed a limited efficiency of the de novo virus production possibly linked to both a relatively low efficiency of the transfection technique and to the semi-permissive characteristics of the UT7/EpoS1 cells [Wolfisberg et al; 2013].

A demonstration of the functional competence of the virus produced in UT7/EpoS1 cells and enhancement of the process efficiency were obtained by amplification in the primary target cells, the EPCs. Two successive rounds of infection confirmed both the infectivity and the maintenance of the infectivity of the virus produced and in addition, lead to a viral yield comparable to what could be obtained from native virus. Within this experimental system, inserts extending beyond the dyad symmetry, independently of their terminal isomer combinations (CK00-01-10-11), and also inserts extending up the site of dyad symmetry (CH clones) showed functional competence and ability to generate infectious virus. In this latter

case, only inserts containing heterogeneous terminal regions (CH01-10) were able to generate mature virions.

Irrespective of the starting inserts, the amount of virus produced per volume unit was of the same order of magnitude of what can be recovered from native isolates, the usual source of virus for in vitro infection experiments. Hence, both the potential to form hairpin structures and a full-representation of cis-elements appear to be critically required for viral replication, although further investigations will be required to understand the mechanistic details [Luo et al; 2015].

The developed model genetic system offers many advantages for further studies. The ease of cloning, possibility of simple manipulation and stability of the cloned genome make such system convenient to genetic engineering. Subsequently, the possibility of genetic engineering allows for refined sequence/function studies, both when considering the replicative competence following transfection and when considering the generation of infectious virus. A virus of defined sequence, generated in controlled conditions and free from all the contaminating substances of the biological matrices, can constitutes a reference system for investigation of the biological properties of the virus and for the research of specific antiviral strategies.

4. Cell Susceptibility and Permissiveness

4.1 Experimental Design

Human Parvovirus B19 has a narrow tropism for the erythroid progenitor cells of the human bone marrow. Within them, the virus can not conclude a complete replicative cycle in all the erythroid cells but it infects successfully cells that belong to a particular "window" of the differentiation [Bua et al 2016].

Different markers and factors are expressed by the cells along the various stages of the erythroid lineage and these can influence the permissiveness and susceptibility of the cells to the viral infection. One of these B19V susceptible factor is the VP1u specific coreceptor: after the binding to both the globoside receptor and to the VP1u specific coreceptor, the virus is internalized by clathrin-mediated endocytosis [Quattrocchi et al; 2012 - Leisi R. et al; n°61, 2016– Leisi R. et al; n° 265, 2016]. However, EPCs expressing the required receptors and coreceptors are not always permissive suggesting that the selective replication of B19V is determined by additional intracellular factors such as,the EpoR pathway [Chen et al; 2010 - Luo et al; 2011]. The high viremia which is tipically associated to B19V acute infection, exceeds occasionally 10^{13} geq/mL of plasma [Kooistra et al; 2011] suggesting that the virus can efficiently replicate in the target cells when all the required elements are present [Wolfisberg et al; 2013].

However, the specific cellular factors have not been yet reproduced in an established cell line. Cell lines such as the megakaryoblastoid UT7/EpoS1 cells [Shimomura et al; 1992] can be infected by the virus and used as system for its study. However, they did not allow to propagate the B19V *in vitro* in a productive and sustainable manner [Chen et al; 2011].

To determine the cellular factors that influence the cell susceptibility and permissiveness to B19V infection, the expression of some markers was evaluated in different cellular systems. In particular, the globoside receptor, the VP1u protein coreceptor, the endocytic pathway and EpoR signaling were investigated, in order to find a common factor which was responsible of the narrow B19V efficiency of infection.

4.2 VP1u production

ΔC128 and ΔN29/C128 were two VP1u derived proteins that were previously studied and developed for their different abilities to bind VP1u receptor (this research started within the

66

laboratory of the Prof. Carlos Ros who provided the materials for the further studies, University of Bern) [Leisi R. et al; n°61, 2016– Leisi R. et al; n° 265, 2016]. In particular, ΔC128 is a protein consisting in the first 128 aa of the VP1u sequence (VP1u protein: 227 aa long) which lost the PLA$_2$ domain, but maintain the ability to bind the B19V coreceptor. ΔN29/C128 is a truncated form, with a deletion of 29 aminoacids at N-terminus compared to ΔC128, which prevents its binding to cells. Both the VP1u derived proteins were produced adding a MAT-tag and a FLAG-tag (about 10 aa long each one) that can be used for their purification and for the development of the IIF assays.

Firstly, *BL21(DE3) Competent* bacteria were transformed with the plasmids encoding for the two proteins in order to produce and purify them. Ampicillin-resistant colonies were expanded, and selected by screening purified plasmids with restriction enzyme digestions and PCR amplifications for the VP1u region. For the PCRs, *Q5 High-Fidelity 2x Mix* (NEB) was used and the resulting amplifieds were checked by gel electrophoresis.

Selected colonies were expanded in 100 mL of LB Broth containing ampicillin and the expression of the proteins was induced by IPTG for 4 h at 37°C. After sonication for breaking the cells, the proteins were purified using *Ni-NTA Magnetic Agarose beads* (Qiagen). Actually, the Nickel beads allowed to bind Histidine of MAT-tag of the proteins and separated them from cellular debris and suspensions. Then, the proteins were purified using columns and eluted from the beads in 250 mM Imidazole solution obtaining the following concentrations:

[ΔC128] = 2,05 mg/mL

[ΔN29/C128] = 0,52 mg/mL

Finally, the purified proteins were checked by a SDS-PAGE followed by Coomassie staining in order to control and to evaluate their yield and quality of purification (data are not shown).

4.3 VP1u Binding/Internalization IIF assay in UT7/Epo

UT7/Epo cells were used at first for the development of the VP1u Binding/Internalization IIF assay. Proteins were bound directly to the cells followed by incubation with primary antibody, fixation/permeabilization of the cells by Methanol/Acetone 1:1 and incubation with the second antibodies. Better results were obtained when ΔC128 and ΔN29/C128 proteins were labeled to the anti-FLAG (primary antibody) before the incubation with the cells. Actually, the pre-labeling allowed to bind dimers of VP1u proteins to each primary antibody

molecule. So, for the pre-labeling, a ratio 1:1 between the proteins and the antibody was used, about 2×10^{12} anti-FLAG molecules (300 ng) were incubated with 3×10^{12} ΔC128 or ΔN29/C128 (75 ng). In addition, a better fluorescence brightness and less no-specific signal were obtained using goat serum diluted in PBS as blocking medium and, for the "Binding" IIF assay, carrying out the fixation/permeabilization step after the incubations with both the antibodies.

The temperatures of the incubations during the assays were important to distinguish the amount of VP1u protein which bound the own receptor on the cellular membrane ("Binding") from the one which was internalized within the cell after the binding ("Internalization").

The "Binding" IIF assay protocol was finally established including different steps: i) pre-labeling of ΔC128 or ΔN29/C128 with the anti-FLAG primary antibody; ii) adding of the proteins-antibody complex to the cells and incubation at +4°C; iii) incubation with the secondary antibody at +4°C; iv) fixation and permeabilization of the cells; v) staining with DAPI for distinguishing the nucleus from the cytoplasm within the cells.

The "Internalization" IIF assay protocol differed from the previous one, as the temperature of incubation with proteins-primary antibody complex occurred at +37°C for allowing the entry of the complex protein-antibody within the cells: i) pre-labeling of ΔC128 or ΔN29/C128 with the anti-FLAG primary antibody; ii) adding of the proteins-antibody complex to the cells and incubation at +37°C followed by trypsin treatment; iii) fixation and permeabilization of the cells; iv) incubation with the secondary antibody at RT; v) staining with DAPI for distinguishing the nucleus from the cytoplasm within the cells.

As control for the trypsin action and for detaching all the no-internalized proteins, cells were incubated with VP1u protein-primary antibody complex at +4°C followed by trypsin treatment.

In UT7/Epo cells, different positive signals were observed due to the diverse IIF assays. The "Binding" IIF showed the ΔC128 proteins bound on the cellular membrane, like "spots" on all the outside surface of the cell. The ΔN29/C128 did not show positive signal confirming its inability to bind the receptor.

A different result was observed for the "Internalization" IIF assay in which the positive signal appeared like a cluster of proteins-receptors within the cells near to the nuclei. Herein, this confirmed that the bound ΔC128 proteins were internalized. In this assay too, the ΔN29/C128 protein continued to act as negative control proving specificity of the internalization process (figure 4.1).
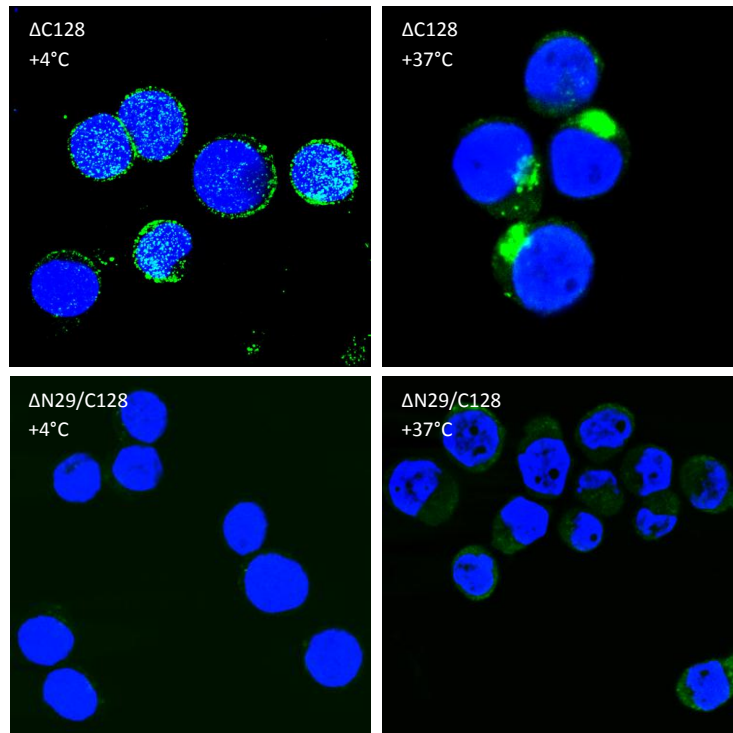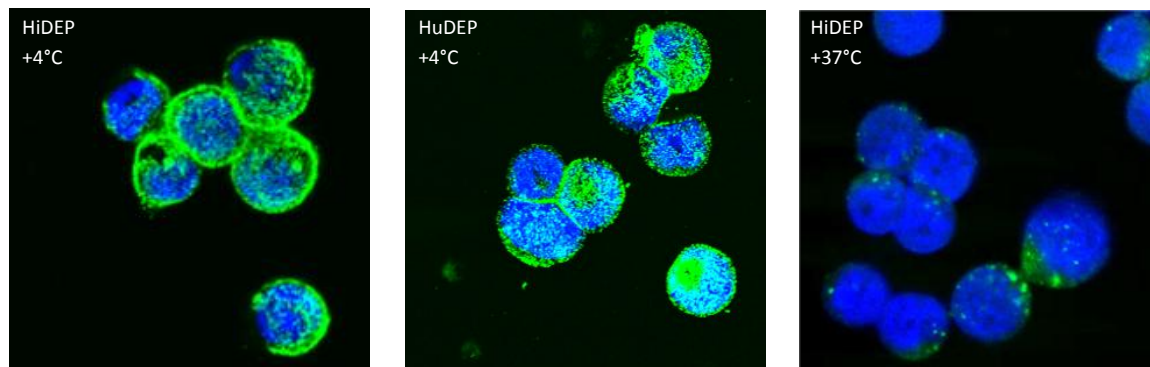
Figure 4.1: Pictures of ΔC128 or ΔN29/C128 proteins "Binding" and "Internalization" IIF assay in UT7/Epo cells = ΔC128 +4°C) Binding of ΔC128: green positive signals appear like "spots" on the cellular membrane; ΔC128 +37°C) Internalization of ΔC128: green positive signal is like a cluster near the cellular nuclei; ΔN29/C128 +4°C) Binding of ΔN29/C128: no positive signal; ΔN29/C128 +37°C) Internalization of ΔN29/C128: no positive signal. Nuclei are stained by DAPI; Confocal microscope (100x magnification).

The developed assays allowed to distinguish the binding of ΔC128 protein from its internalization with two different kind of signals: external for the first one and within the cells for the second one. So, the same protocols were applied to other cell lines in order to evaluate whether they worked and could be applied to systems other than UT7/Epo cells.

HuDEP and HiDEP cell lines are human erythroid progenitor cell lines derived from CD34^{+} hematopoietic stem cells and fibroblasts, respectively [Kurita et al; 2013]. They are at the end of the erythroid lineage and expressed erythroid markers so, they might act as possible target for Human Parvovirus B19V.

Although viral replication was not detected by qPCR assay after viral infection, these cell lines were tested for the "Binding" and "Internalization" IIF assays, previously developed. Both HuDEP and HiDEP showed a huge amount of positive signal for the ΔC128 "Binding" assay compared to the UT7/Epo cells, while, they showed less ΔC128 "Internalization" signal which appeared as little clusters that did not spread in all the cells, compared to UT7/Epo cells (figure 4.2). HuDEP and HiDEP cells belong to the erythroid lineage and in particular, they are at the end of the cellular differentiation stage. So, the different results for ΔC128

binding and internalization compared to the UT7/Epo cells could be caused by the lack of differentiation-related internalization pathways.

Figure 4.2: Pictures of ΔC128 protein "Binding" and "Internalization" IIF assay in HiDEP and HuDEP cells = HiDEP +4°C) Binding of ΔC128 in HiDEP cells: green positive signals appear like "spots" on the cellular membrane; HuDEP +4°C) Binding of ΔC128 in HuDEP cells: green positive signals appear like "spots" on the cellular surface; HiDEP +37°C) Internalization of ΔC128: green positive signal is like little clusters near the cellular nuclei. Nuclei are stained by DAPI; Confocal microscope (100x magnification).

4.4 VP1u Binding/Internalization and endocytosis marker in EPCs

EPCs are specific target for Human Parvovirus B19 and they can be infected only in a particular "window" of their differentiation, as previously mentioned. Viral and cellular factors important for B19V infection could change during their growth and differentiation influencing the susceptibility and permissiveness to the virus. In order to evaluate whether the expression of receptor for VP1u could change during the differentiation process, the previous developed "Binding" and "Internalization" IIF assays were applied to EPCs.

Erythroid progenitor cells from bone marrow were grown at first in complete medium without EPO (erythropoietin) to prevent their entry in the differentiation lineage (EPCs at day 0). The IIF assays for evaluating the binding and the internalization of ΔC128 and ΔN29/C128 proteins were applied and no positive signals were observed for any of them (data are not shown).

After that, EPCs were grown in complete medium in presence of EPO for inducing the differentiation; at different days of cultivation, both the "Binding" and the "Internalization" IIF assay were tested. At day 10 of differentiation, a huge amount of ΔC128 protein was

bound to the receptor of VP1u on the outer surface of the cells while its binding was reduced at day 15. At this last day, a reduced positive signal linked to the internalization of ΔC128 was detected, comparable to what was observed with the HuDEP and HiDEP cells. At day 15, only a fraction of the cells showed a positive signal due to the heterogeneous composition of these population. No positive signal was observed for both the IIF assays with ΔN29/C128 protein (figure 4.3).
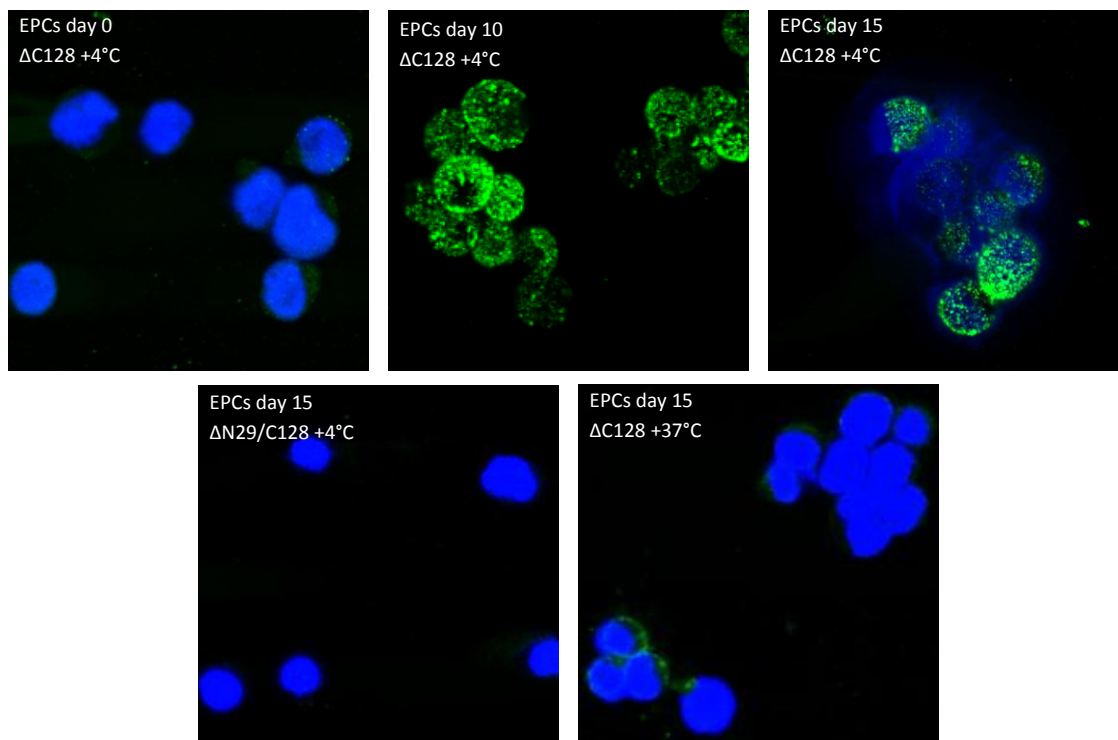

Figure 4.3: Pictures of ΔC128 and ΔN29/C128 proteins "Binding" and "Internalization" IIF assay in EPCs at different days of differentiation = EPCs day 0 ΔC128 +4°C) Binding of ΔC128: no positive signal; EPCs day 10 ΔC128 +4°C) Binding of ΔC128: huge amount of positive signal like green "spots" on the cellular membrane; EPCs day 15 ΔC128 +4°C) Binding of ΔC128: green "spots" on the cellular surface but with heterogeneity among the EPCs population; EPCs day 15 ΔN29/C128 +4°C) Binding of ΔN29/C128: no positive signal; EPCs day 15 ΔC128 +37°C) Internalization of ΔC128: reduce positive signal as few and little green "spots" within the cells and outside the nuclei but limited to some of the cells (heterogeneous population). Nuclei are stained by DAPI; Confocal microscope (100x magnification).

In order to investigate the cause of the reduction of VP1u protein internalization, the functionality of the endocytic pathway was firstly studied. As previously mentioned, B19V enters inside the cells by endocytosis, while erythroid progenitor cells lose most of their functional mechanisms during the differentiation. To understand whether the decreasing of ΔC128 internalization was linked to the reduction or loss of the endocytic pathway, "Binding"

and "Internalization" IIF assays were evaluated for transferrin. Actually, the transferrin is the typical marker for the studies of endocytosis.

  EPCs at different days of differentiation were studied for the binding and the internalization of both VP1u protein and *holo transferrin-FITC*. This last was the ligand for the transferrin receptor and it was directly conjugated to the FITC fluorophore. At day 8 of differentiation, the majority of the cells showed positive signal due to the binding of transferrin on the cellular membrane for the "Binding" IIF assay and a positive cluster within the cells for the "Internalization" IIF assay. The same results for the transferrin were observed at day 15 of EPCs' differentiation in medium with EPO, while less internalization for ΔC128 protein was detected confirming the previous results (figure 4.4). However, not all the cells both at day 8 and at day 15 of differentiation showed the same behavior for the transferrin and ΔC128 binding and internalization, due to the heterogeneity of the erythroid population.

  Hence the loss of VP1u protein internalization and its correlate reduction of B19V infectivity for EPCs during the erythroid lineage did not seem to be linked with a decreasing functionality of the endocytic pathway. Actually, the internalization of transferrin was observed without significant changes for all the tested differentiated cells.
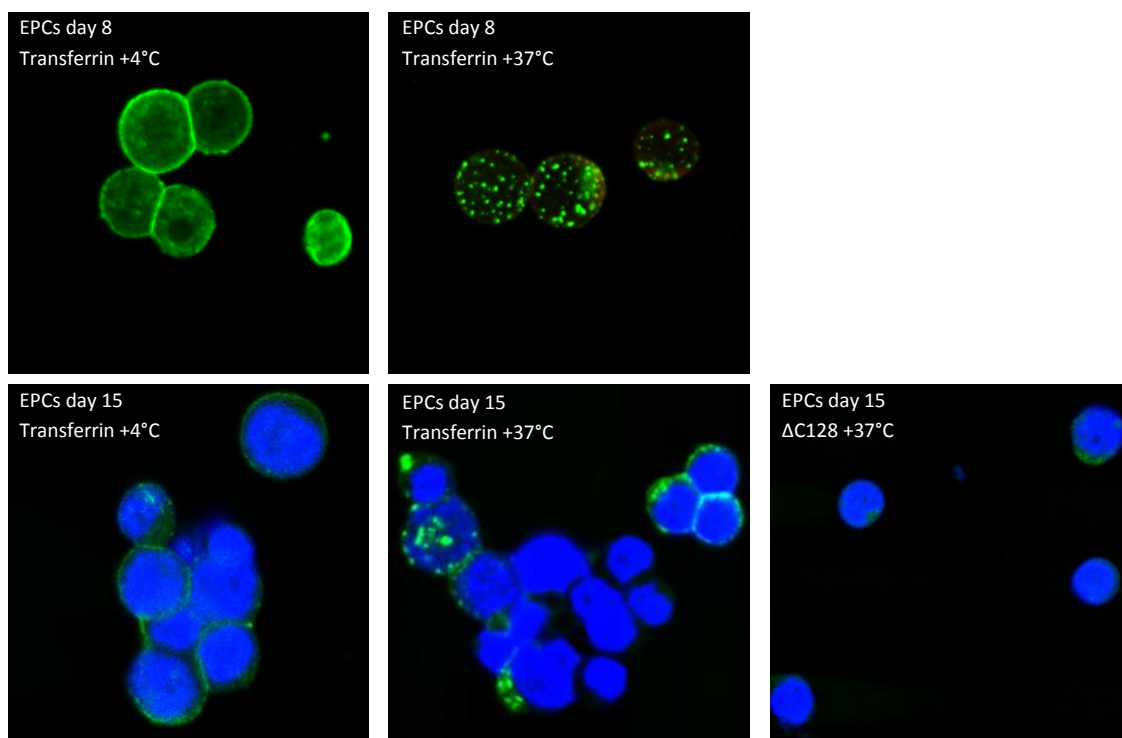
Figure 4.4: Pictures of ΔC128 and holo transferrin-FITC "Binding" and "Internalization" for EPCs at different days of differentiation: EPCs day 8 Transferrin +4°C) Binding of holo tranferrin-FITC = positive signal appears as a huge amount of green little "spots" on the cellular membrane; EPCs day 8 Transferrin +37°C) Internalization of holo transferrin-FITC = positive signal appears as several green clusters; EPCs day 15

Transferrin +4°C) Binding of holo transferrin-FITC = positive signals (green little "spots") on the cellular surface for the major of the treated cells (heterogeneous population), probably less amount of positive signal than the cells at day 8 of differentiation; EPCs day 15 Transferrin +37°C) Internalization of holo transferrin-FITC = the major of the cells shows green cluster within them and near their nuclei as positive signal (heterogeneous population); EPCs day 15 ΔC128 +37°C) Internalization of ΔC128 = few positive signal is shown compared to the holo transferrin-FITC at the same day of cellular differentiation. Nuclei are stained by DAPI; Confocal microscope (100x magnification).

4.5 pSTAT5 in addition to cellular and viral markers in UT7/EpoS1 cells

To further investigate other factors that could influence and determine the B19V infection, the expression of pSTAT5 was studied alone and in combination with other markers. As mentioned previously, pSTAT5 is usually activated by the EPO receptor (EpoR) after the binding of its ligand to induce the DNA synthesis. Human Parvovirus B19 infects cells that require EPO and the virus itself requires EPO ligand and EpoR signaling to complete its replicative cycle [Chen et al; 2010].

UT7/EpoS1 cells were analyzed for the expression of pSTAT5, globoside, VP1u coreceptor and transferrin. By IIF assay, all the analyzed cells showed expression of globoside, VP1u receptor and transferrin, as a common characteristic, while pSTAT5 was expressed in different amounts among the UT7/EpoS1 cells and it appeared with especially a cytoplasmic localization (figure 4.5). In particular, the globoside receptors was detected in all the cells but with differences about the expression levels within the cells. The "Binding" and "Internalization" assays of ΔC128 were performed together with transferrin (ΔN29/C128 was used as negative control): both the markers were expressed in all the cells and they co-localized both on the outer surface and within the cells. The expression of pSTAT5 was less homogeneous and diffuse, since it was not observed in all the cells and within them it was detected in different amounts.
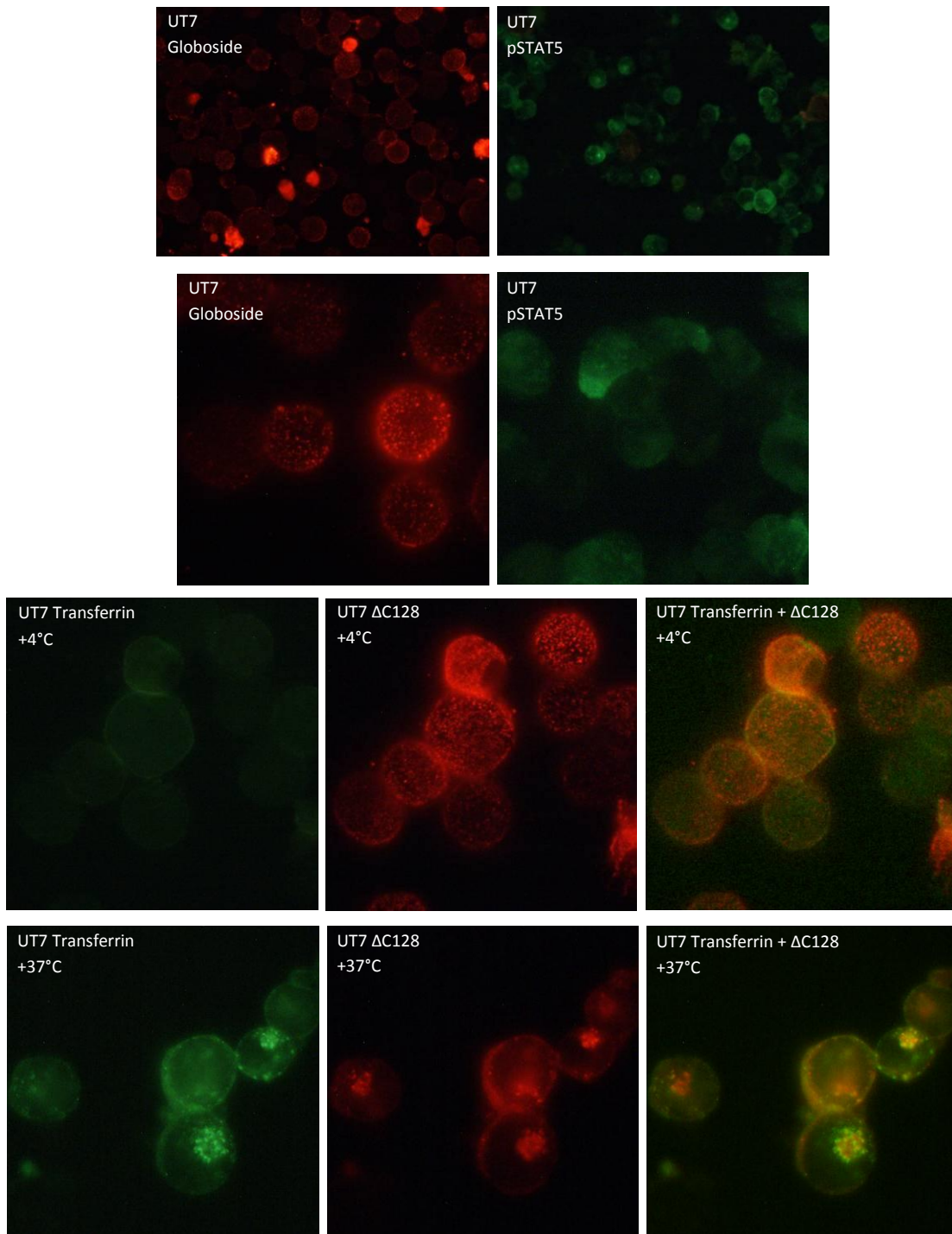
Figure 4.5: Pictures of globoside, pSTAT5, VP1u coreceptor and transferring expression in UT7/EpoS1 cells (40x and 100x magnification) = UT7 Globoside) The globoside receptor (red) is detected in all the cells but with differences about its expression level; UT7 pSTAT5) pSTAT5 (green) is not observed in all the UT7/EpoS1 cells; Transferrin, ΔC128, Transferrin + ΔC128) Binding (+4°C) and Internalization (+37°C) assays shows the diffuse expression of Transferrin (green) and ΔC128 (red; VP1u coreceptor) among the cells; their co-localization is shown with yellow colour.

In order to investigate whether pSTAT5 was required for DNA synthesis allowing viral replication, the UT7/EpoS1 cells were infected by B19V at moi of 10^4 geq/cell and cultured for 72 hours. Following the incubation, the cells were analyzed for capsid protein production together to pSTAT5 expression, by IIF assay. Not-infected cells were used as control. qPCR assay on nucleic acids extracts was performed to evaluate and confirm viral replication ($\Delta Log_{72-2 \text{ hpi}} = 1,83$ log).

By IIF assay, pSTAT5 was observed both in B19V infected UT7/EpoS1 and not-infected cells without any significant difference between them, as positive and negative cells for pSTAT5 expression were detected in both the conditions. Combining the two staining, viral infected cells at 72 hpi (that were positive for VP capsidic proteins) did not show expression of pSTAT5 (figure 4.6). Probably, the infected cells at 72 hpi were at very late phase of B19V infection and near their lysis or apoptotic phase, so they were not anymore in an active metabolic condition.
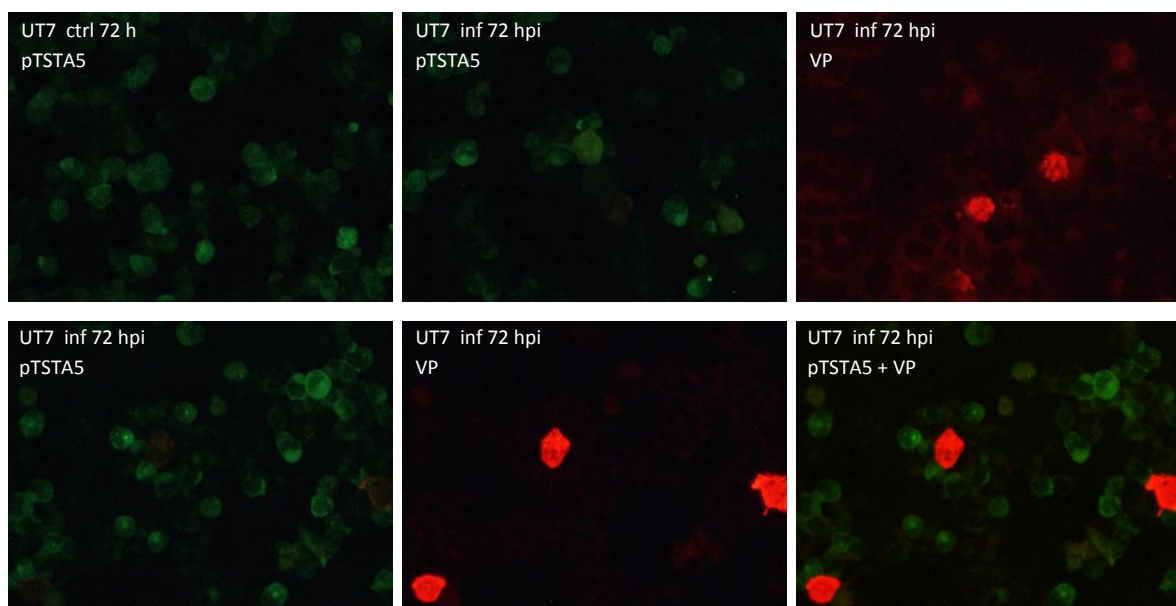
Figure 4.6: Pictures of pSTAT5 (green) and VP (red) expression in UT7/EpoS1 cells and B19V infected UT7/EpoS1 cells (40x magnification) = Up) pSTAT5 (infected and no-infected cells: "inf 72 hpi" and "ctrl 72 h", respectively) and VP proteins are stained separately; Bottom) pSTAT5 and VP are stained together. The two markers do not co-localize.

4.6 pSTAT5 in addition to cellular and viral markers in EPCs

The same experiments were performed also for the erythroid progenitor cells in order to investigate whether a different marker expression was shown in comparison to UT7/EpoS1

cells. The expressions of the globoside receptor, VP1u coreceptor, transferrin and pSTAT5 were analyzed in EPCs at day 7 of erythroid differentiation, by IIF assays. Since the erythroid progenitors are a heterogeneous population, the globoside, the VP1u receptor and transferrin were not expressed among all the analyzed cells, and different amounts of these markers were observed within the population. Indeed, the "Binding" and "Internalization" of VP1u receptor (ΔC128 protein; ΔN29/C128 protein was used as negative control) and transferrin were not detected among all the EPCs. However for ΔC128 and transferrin positive cells, the two markers co-localized. Unexpected, pSTAT5 was not detected within cultured cells (figure 4.7).
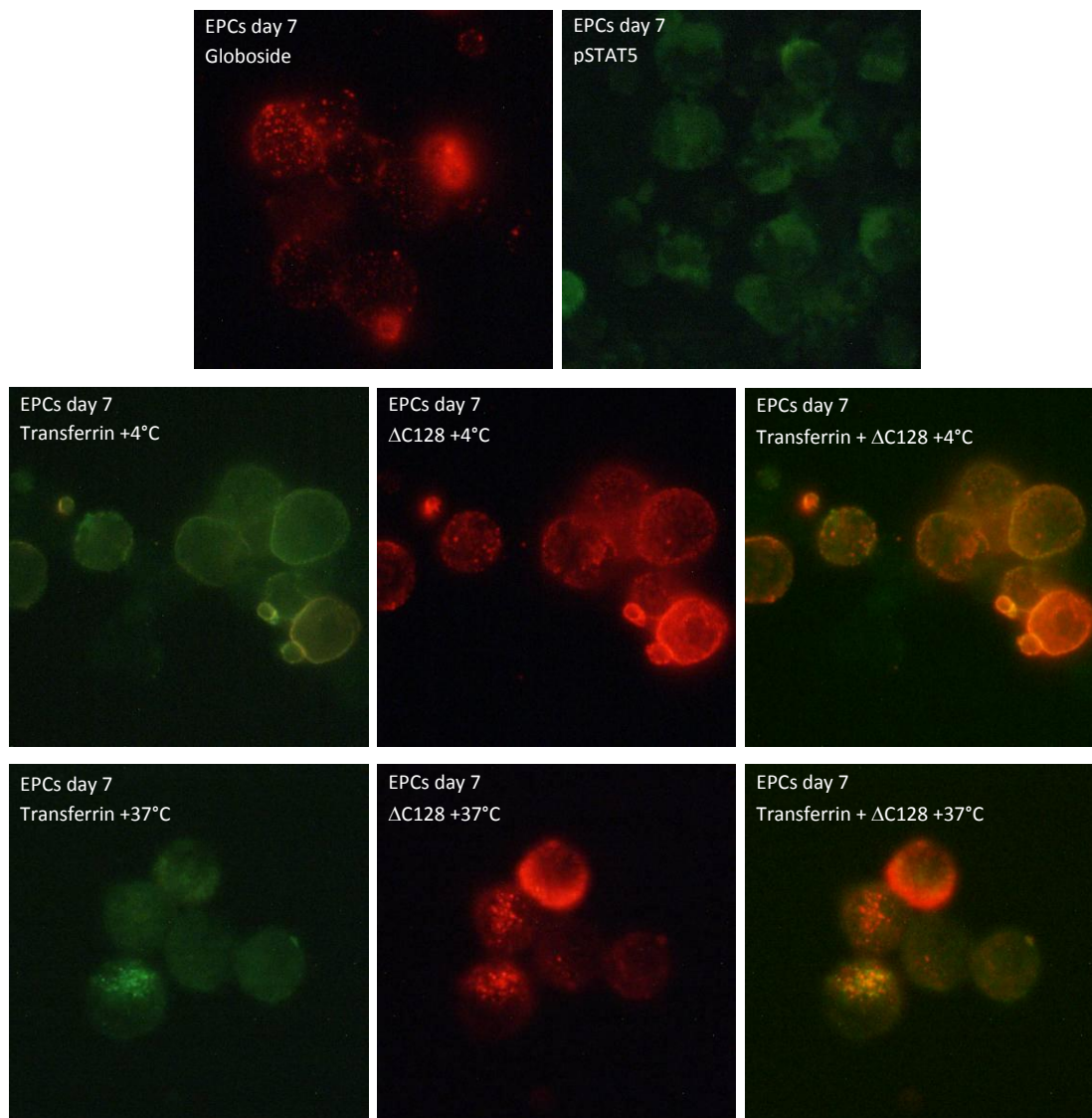
Figure 4.7: Pictures of globoside, pSTAT5, VP1u coreceptor and transferrin expression in EPCs at day 7 (100x magnification) = EPCs Globoside) The globoside receptor (red) is detected in several cells but with differences about its expression level; EPCs pSTAT5) no positive signal for pSTAT5 (green); Transferrin, ΔC128, Transferrin + ΔC128) Binding (+4°C) and Internalization (+37°C) assays shows the diffuse expression

of Transferrin and ΔC128 (red; VP1u coreceptor) among the cells but not in all of them; their co-localization is shown with yellow colour.

Meanwhile, EPCs at day 7 were infected by B19V at moi of 10^4 geq/cell and cultured for 48 hours. Cells were collected at different time points (2-24-48 hpi) and analyzed for the expression of viral and cellular markers by IIF assay and FISH assay (figure 4.8). qPCR assay on nucleic acids extracts was performed to evaluate and confirm viral replication ($\Delta Log_{48\text{-}2 \text{ hpi}}$ = 3 log). By IIF assay, EPCs expressed the viral capsid proteins from 24 hpi, while pSTAT5 could not be detected, as previously. By incubating the infected cells with ΔC128 at +4°C before their fixation (Binding IIF assay), the VP1u receptor was observed in the majority of the EPCs, compatibly with the characteristic of a heterogeneous population; ΔN29/C128 did not show a positive signal acting as negative control. Combining the evaluation of B19V DNA detection by FISH assay together with the expression of VP1u coreceptor, the expression of VP1u coreceptor was detected both in infected and no-infected cells within the same sample (FISH positive and negative cells, respectively), suggesting the necessity of other factors for allowing a complete viral replication.
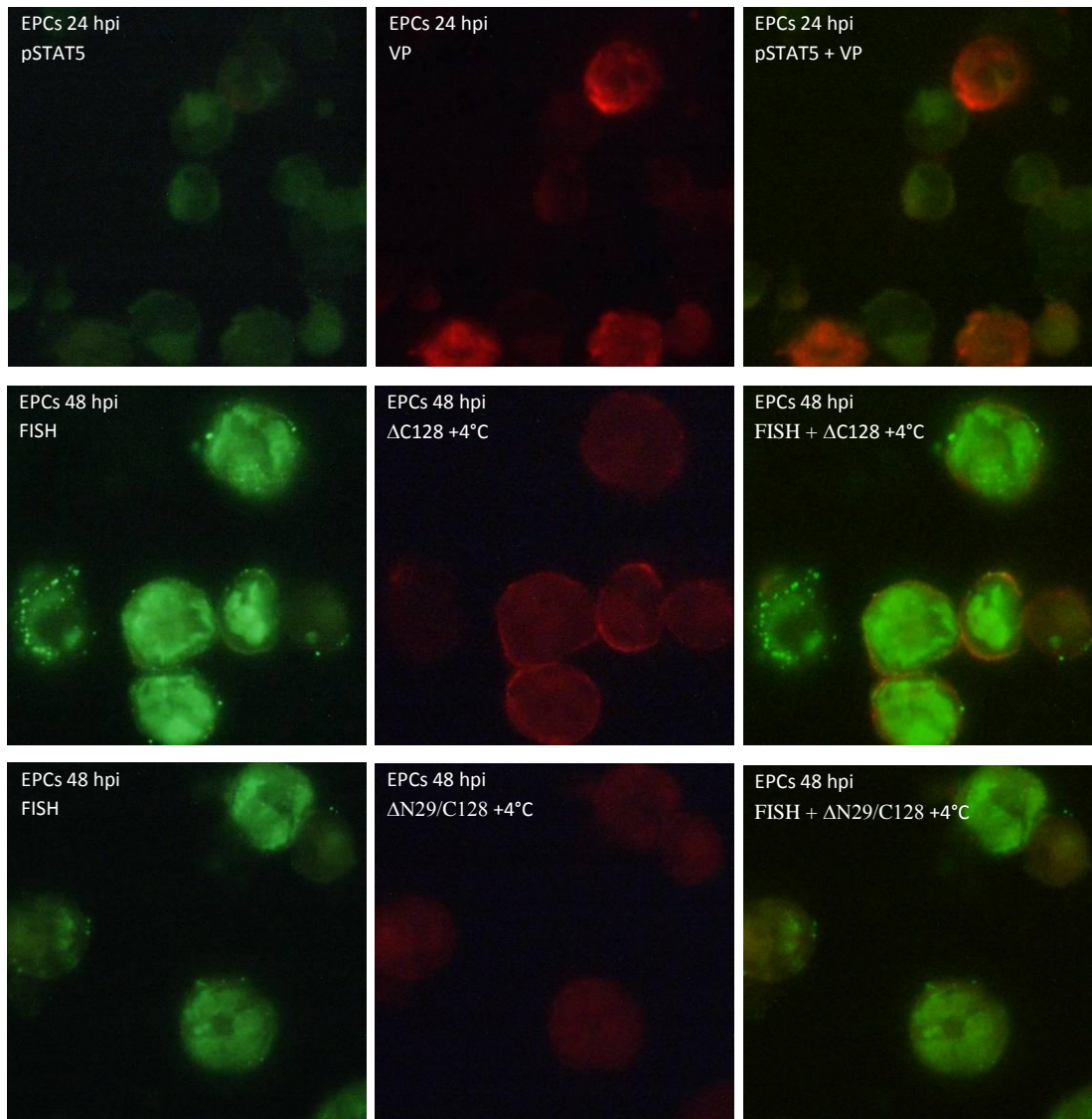
Figure 4.8: Pictures of pSTAT5, VP, VP1u coreceptor expression and by IIF assay and B19V DNA replication by FISH assay in infected EPCs at different time points (100x magnification) = pSTAT5, VP, pSTAT5 + VP) Positive cells are detected for VP capsidic protein (red) but not for pSTAT5 (green); FISH, ΔC128, FISH + ΔC128) Many positive cells are observed for viral DNA by FISH (green) showing a nuclear staining, while VP1u receptor is expressed on the surface of the major of the cells (ΔC128; red); FISH, (ΔN29/C128, FISH + ΔN29/C128) Many positive cells are observed for viral DNA by FISH (green) showing a nuclear staining, while no positive signal is due to the negative control ΔN29/C128 (red).

4.7 Discussion

Human Parvovirus B19 exploits the target cells for the production of new progeny. From the entry by cellular receptors to the egress of the new mature viral particles by lysis of the cell itself, the virus depends on the cellular constituents and function. However, B19V does not infect all the cells of the human body or in some cases it can enter within the cells without

completing its replicative cycle (such as in endothelial cells). The main viral target are the erythroid progenitor cells from the human bone marrow, and within this population, the virus productively infects only cells in a particular "window" along the erythroid differentiation [Bua et al; 2016].

From erythroid progenitors, cells undergo changes till the final state of erythrocytes (red cells). Along the erythroid differentiation, the cells change the markers that they express and the mechanisms that they acquire or lose. At the end of the lineage, the erythrocytes lack cellular nuclei and most of their organelles in order to have more useful space for accommodating hemoglobin. They become only receptacles for delivering oxygen to the body tissues and carbon dioxide from them to the lungs. Changes within the target cells due to their differentiation cause changes in cellular susceptibility and permissiveness to the Human Parvovirus B19 infectivity. Hence, not only studies of B19V itself are necessary, but also knowledge of the cellular targets is important to characterize and understand the virus lifecycle.

In the second part of this research, assays for evaluating the expression of cellular elements that are involved during the B19V infection and their correlation with the virus itself were developed and further applied to identify elements that constitute a viral susceptible and permissive cellular system and to distinguish their changes along the differentiation lineage of B19V target cells. At first, indirect immunofluorescence assays were developed for evaluating the expression of the VP1u coreceptor in UT7/Epo cells and its behavior by simulating a viral infection using different incubation temperatures. The different temperatures allowed to distinguish the diverse steps of the infection mechanism: in particular, the pre-labeled VP1u peptide binds its cellular receptor remaining on the outer cellular surface at +4°C ("Binding assay"), while it can be internalized, probably by endocytosis vesicles, after incubation at +37°C ("Internalization assay").

Once that the two IIF assays were developed, they were tested for other cellular systems for evaluating their versatility. In HuDEP and HiDEP cells, a larger "binding" signal and a smaller "internalization" signal were observed in comparison to UT7/Epo cells. HuDEP and HiDEP cells are erythroid progenitor cells derived from human umbilical cord and human iPS (induced pluripotent stem cells that were obtained from human fibroblast), respectively [Kurita et al; 2013], engineered as source of red blood cells to replace human transfusions in therapy. So, they were at the termination of the erythroid differentiation pathway, maintaining the Human Parvovirus B19 coreceptor but losing other cellular mechanisms, such as the internalization pathway of the endocytosis. Keeping the HuDEP and HiDEP obtained results

as model, the same experiments were applied in EPCs at different days of erythroid differentiation, also including the evaluation of binding and internalization of transferrin used as a marker for endocytic pathway. Along the erythroid differentiation, the signal for VP1u peptide binding and internalization changed; unlike what happened for transferrin which was internalized without particular change.

Whether the loss of the endocytosis was excluded as a cause of the decrease for the VP1u peptide internalization, other viral and cellular components were studied to understand the reason of narrow susceptible and permissive cellular tropism within the B19V target cells. In particular, the expression of globoside receptor, pSTAT5 (marker of EPO receptor pathway activation), of the viral capsid proteins and of the viral DNA was evaluated in infected and not infected cells together to the "Binding" and "Internalization" assays for VP1u peptide and transferrin. UT7/EpoS1 cells showed a widespread distribution of globoside receptor, VP1 coreceptor and transferrin receptor in all the cells. pSTAT5 was observed within all the UT7/EpoS1 cells but with different expression amounts; however, it was not expressed within infected cells due to their stage at the apoptotic/lysis phase of the B19V replicative cycle.

In EPCs at day 7, the globoside receptor was widespread distributed as well as the binding of transferrin and VP1u peptide. However, they were detected in a limited fraction of all the cells, compatibly with the heterogeneity of the erythroid population. pSTAT5 was not observed both in infected and not-infected erythroid progenitor cells probably due to a difficulty of detection correlated to its smaller amount of expression in EPCs in comparison to UT7/EpoS1 cells. The myeloid cells have developed a regulated serine protease which generates exclusively C-terminally truncated STAT5 proteins, the expression of which is essential for the maintenance of these cells in an immature and undifferentiated state [Mitchell et al; 2005]. The distribution of the VP1u coreceptor was the same within both B19V infected and not-infected EPCs and it was not influenced by the replicating virus (as detected by FISH assay).

Hence the globoside receptor, the VP1u coreceptor and the endocytosis pathway are necessary for the viral infection, but they are commonly diffuse within the susceptible and permissive cells. The expression of VP1u coreceptor was maintained unchanged in EPCs after the viral infection. pSTAT5 which is activated by EPO ligand and hypoxia was widespread observed only in UT7/EpoS1 cells, so it was not probably a factor determinant for the narrow viral tropism, although its expression decreased after B19V infection, probably due to the cellular lysis/apoptotic condition. However, none of them could be identified as a key factor determining the B19V restricted permissiveness. Further research will be necessary to

understand whether other cellular mechanisms such as the trafficking or the permeability of the nucleus could be the restrictive factors responsible of the narrow tropism of B19V. Studies about the changes of these factors along the erythroid lineage will be important to investigate the complex and not yet well known virus-cell interactions.

5. Investigation of Antiviral Compounds

Different strategies are commonly investigated to find molecules acting as drugs for various purposes such as antiviral agents or therapies for pathologies. In this research, we pursued several strategies, in some cases leading to identification of molecules that could show an antiviral activity against Parvovirus B19:

1. Retargeting: Hydroxyurea
2. Expanded spectrum antivirals: BCV
3. Small chemical library screening
4. Investigation of DNA G4 structures and possible ligands

5.1 Antiviral activity of *Hydroxyurea*

Hydroxyurea (HU) is a FDA-approved drug commonly used for the treatment of the chronic myeloid leukemia [Jain et al; 2013]. It is actually used for treating the ovarian cancer and certain types of skin cancers, such as melanoma and squamous cell carcinoma of the head and neck [Madaan et al; 2012]. Indeed, it increases the fetal haemoglobin (HbF) in β-thalassemia affected patients [Pule et al; 2015] and is currently used as disease-modifying drug for treatment of this class of patients.

HU can inhibit viral replication due to its mechanism of action. In particular, HU acts on viral replication inhibiting the Reductase Ribonucleotides enzyme (RNR), which is responsible of the reduction of ribonucleotides to triphosphate deoxyribonucleotides (dNTPs). As result, the DNA synthesis is blocked due to the decrease of available triphosphate deoxyribonucleotides (figure 5.1).
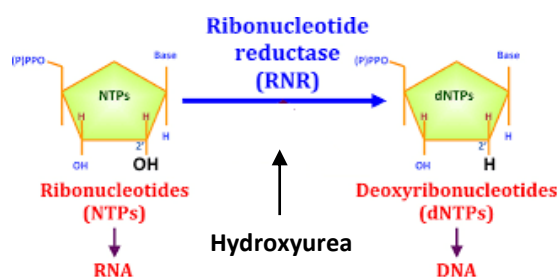
Figure 5.1: Schematic representation of the reactions where RNR enzyme is involved; HU acts blocking the enzyme action reducing the amount of available dNTPs.

Since an antiviral activity was discovered for *Hydroxyurea* due to its inhibiting action against the Ribonucleotide Reductase enzyme, in our work it was also tested against Human Parvovirus B19 replication. Firstly, cell proliferation and viability were tested in UT7/EpoS1 cell line and EPCs: cells grew in presence of several dilutions of HU (0,1 µM - 50 mM) for 48 hours then the effects of the compound on the cells were tested. By CCK8 assay, *Hydroxyurea* induced the 50% reduction of the cell viability at comparable concentrations between the two cellular systems (581,90 µM and 584,80 µM, respectively in UT7/EpoS1 and EPCs). By BrdU assay, cellular DNA replication was affected in a dose-dependent manner by HU leading to a 50% decrease of DNA synthesis at 706,90 µM and 494,00 µM (CC_{50} values: cytostatic concentration) in UT7/EpoS1 and EPCs, respectively. However, the compound at all the dilutions did not cause the loss of membrane integrity in UT7/EpoS1 cells measured by LDH assay, while a cytotoxic effect was observed at concentrations higher than 500 µM in EPCs but never reaching a 50% of cell damage (figure 5.2).
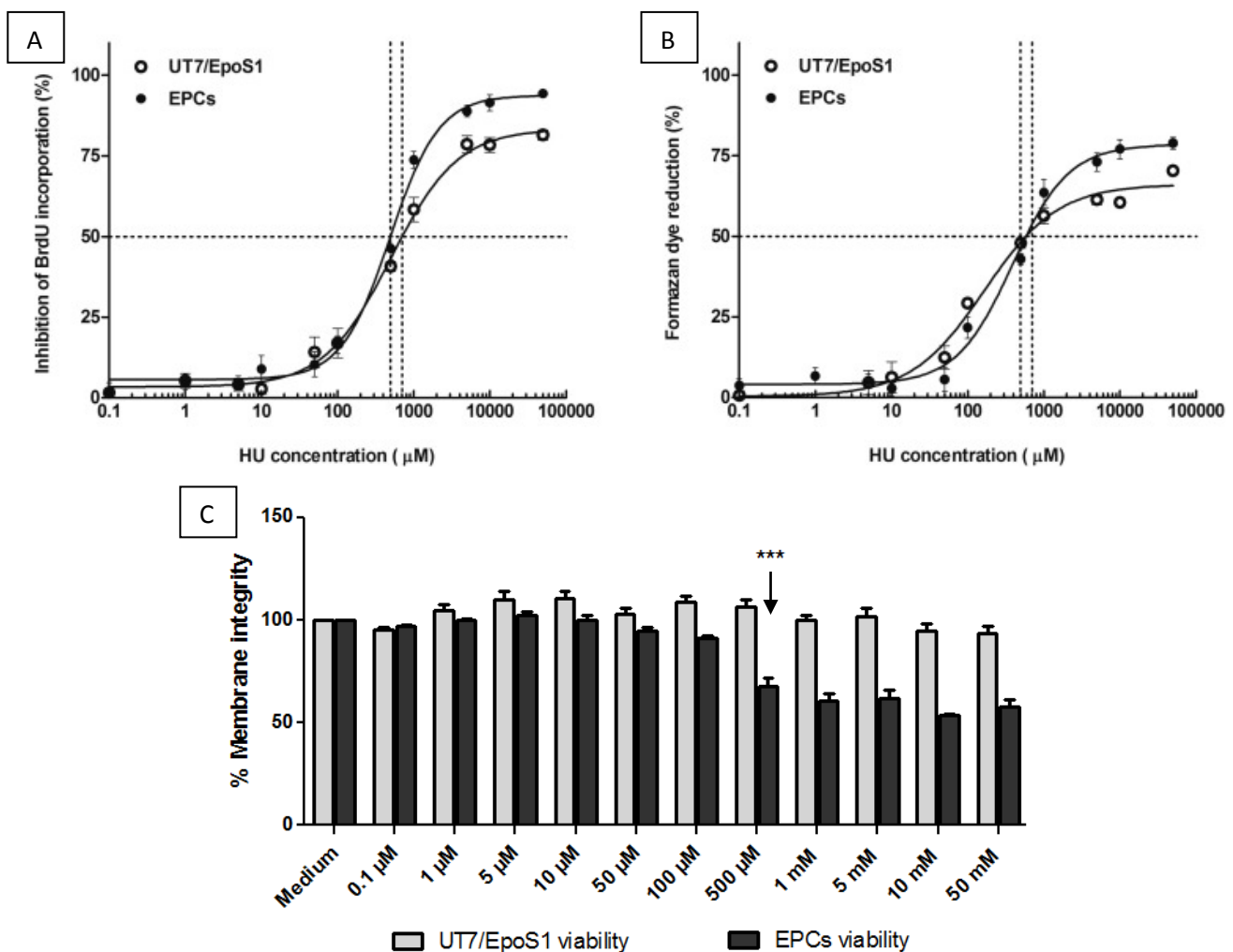
Figure 5.2: Representative graphs of the effects of HU on cellular viability and proliferation = A) BrdU incorporation assay: 50% inhibition of cellular DNA replication is at 706,90 µM (95% confidence interval: 579,50-880,40 µM; R^2 0,95) for UT7/EpoS1 and 494,00 µM (95% confidence interval: 422,20-571,50 µM; R^2

0,95); B) Cell viability by CCK8 assay: 50% reduction of cellular viability is at 581,90 µM (95% confidence interval: 426,50-812,30 µM; R^2 0,95) for UT7/EpoS1 and 584,80 µM (95% confidence interval: 478,50-722,30 µM; R^2 0,95); C) Membrane Integrity by LDH assay: UT7/EpoS1 cells do not display changes in presence of HU, while EPCs show loss of membrane integrity since 500 µM HU (citotoxicity values ranged from 25,60% at 500 µM to 40,40% at 50 mM) [*GraphPad Prism 6.0*]. Plotted values are mean of at least two experiments done in triplicate; ***p value < 0.0001.

Effect of *Hydroxyurea* on B19V replication was tested by IIF assay and qPCR assay in infected UT7/EpoS1 cells and EPCs. Both cellular infections were carried out by viremic serum at moi of 10^4 geq/cell; cells were collected at different time points (2 and 48 hpi) and analyzed for viral capsid protein and DNA production. By IIF assay, a decrease in the number of positive cells for the VP protein expression was observed for concentrations of the compound major than 10 µM and 100 µM respectively for UT7/EpoS1 cell line and EPCs. Total inhibition of capsid proteins expression was detected from HU 5 mM for UT7/EpoS1 cells and 10 mM for EPCs (figure 5.3).
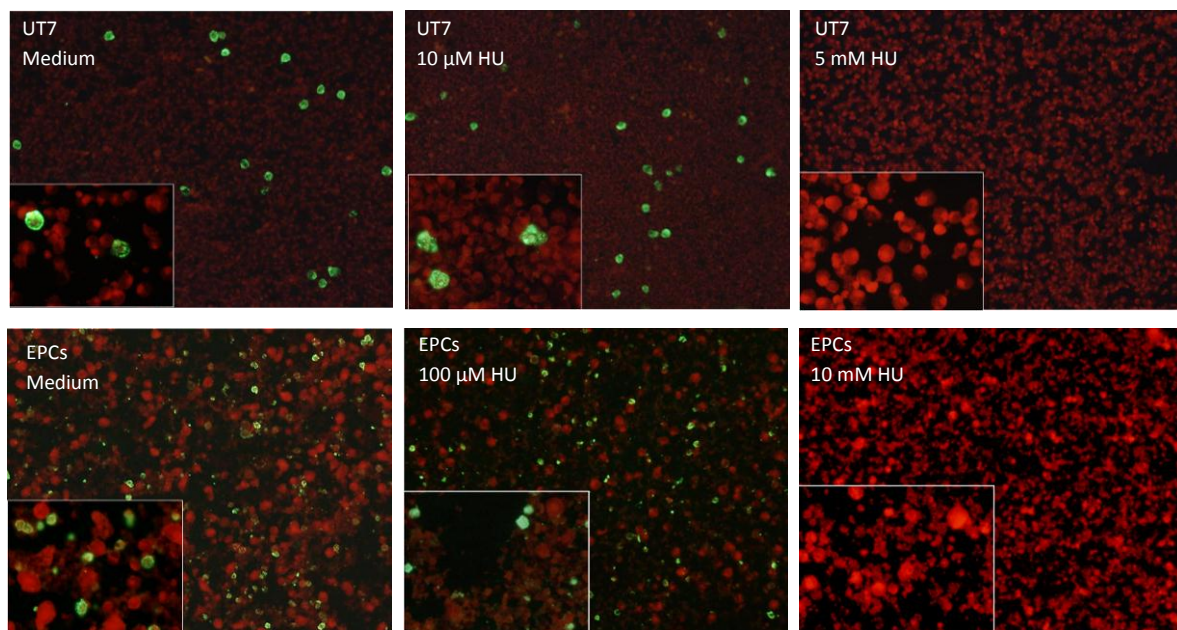
Figure 5.3: Pictures of IIF anti-VP assay for B19V infected UT7/EpoS1cell line and EPCs (48 hpi) that are grown in different HU concentrations (10x and 40x magnification) = UT7 Medium) Cells grown in absence of HU (control); UT7 HU 10 µM) UT7 grew in presence of HU 10 µM, the number of positive cells for VP proteins are comparable to the control; UT7 HU 5 M) UT7 grew in presence of HU 5 mM, no positive cells are detected; EPCs Medium) Cells grew in absence of HU (control); EPCs HU 100 µM) EPCs grew in presence of HU 100 µM, the number of positive cells for VP proteins are comparable to the control; EPCs HU 10 mM) EPCs grew in presence of HU 10 mM, no positive cells are detected.

The same results were obtained by qPCR assay: a progressive decrease of B19V DNA amounts in dependence of HU was observed in both cellular systems. In particular, DNA

amounts extracted from cells treated with HU concentration major than 1 mM were lower than input DNA (2 hpi). No bands for B19V genome were detected by Southern-Blot assay at HU concentration major than 500 μM (figure 5.4).

Non-linear regression curves were generated by expressing the dose dependent relationship between HU concentration and B19V amounts as percentage inhibition of replication relative to the untreated control (0 μM HU). 50% inhibitions of B19V replication were evaluated at 96,20 μM and 147,10 μM of HU concentration (EC_{50} values: effective concentrations) for UT7/EpoS1 cells and EPCs, respectively (figure 5.4).
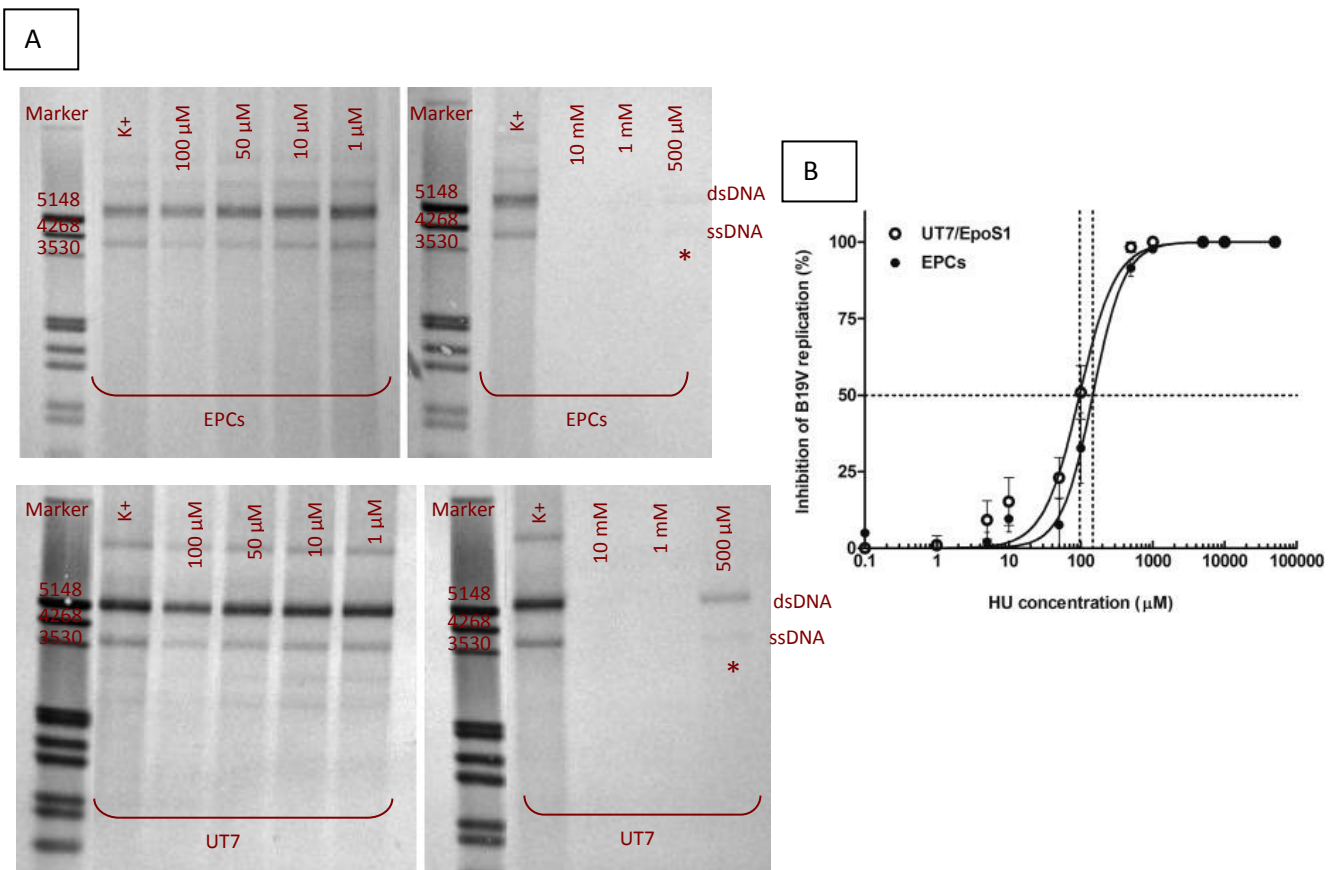
Figure 5.4: B19V replication in infected UT7/EpoS1 and EPCs in response to the different HU concentrations. A) Sothern-Blot assays of B19V DNA extracted from cells (48 hpi) = no viral DNA bands are detected at concentration major than 500 μM (*) in both cellular systems. Digestions by EcoRI = 5596 bps; both dsDNA and ssDNA bands are detected and comparable to the control (K+ 48 hpi); *Marker III-Dig* (Roche); B) Non-linear regression curves obtained by expressing B19V amounts as percentages of inhibition relative to the untreated control. EC_{50} values are 96,20 μM (95% confidence interval: 81,50-118,10 μM; R^2 0,95) and 147,10 μM (95% confidence interval: 121,40-190,40 μM; R^2 0,95) for UT7/EpoS1 cells and EPCs, respectively. Plotted values are obtained from five independent experiments [*GraphPad Prism 6.0*].

Hydroxyurea inhibited B19V replication at lower concentrations than those affecting cellular proliferation, thus acting as a selective Human Parvovirus B19 antiviral agent. In

order to better characterize the effects of the compound on the cells, the expression of erythroid differentiation lineage markers and the cell cycle were evaluated by flow cytometric analysis. In particular, EPCs at day 8 were grown for 48 hours in presence of the compound at established CC_{50} and EC_{50} values (HU 494,00 μM and 147,10 μM, respectively). EPCs before and after the treatment were collected and analyzed for the expression of CD36, CD71 and CD235a markers. Cells grown in the absence of compound were used as control. By flow cytometric assay, an increase of cells expressing the specific differentiation markers were observed for the control (without HU), while their reductions were observed for the HU treated cells. In particular, a significant decrease was observed for both CD71 and CD235a markers in presence of the highest HU concentrations, confirming the previous data on cytostatic effect of HU on cell population.

B19V infected cells were then investigated to evaluate whether different cellular effects could be observed due to the replicating virus in presence of the same established *Hydroxyurea* concentrations. In the absence of HU, the fraction of cells positive for CD36, CD71 and CD235a markers were the same both before and after viral infection, suggesting that B19V inhibited the maturation and expansion of erythroid progenitors. In the presence of HU, a further decrease of the cells that expressed markers, especially for CD71, was observed within the infected EPCs (figure 5.5).
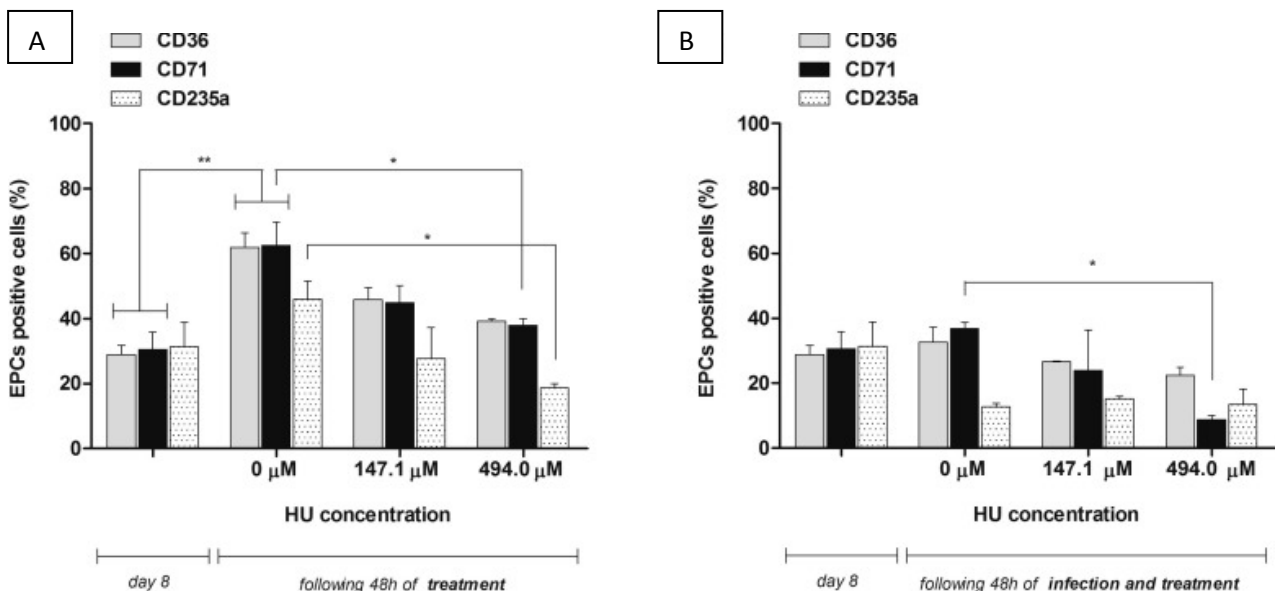
Figure 5.5: Expression of the erythroid lineage specific markers CD36, CD71 and CD235a in EPCs by flow cytometric analysis. A) EPCs grown in presence of HU (0, 147,1 and 494,0 μM); B) B19V infected EPCs grown in presence of HU (0, 147,1 and 494,0 μM). Plotted values are means of two experiments; *p value<0.01-0.05; **p value<0.001 [*GraphPad Prism 6.0*].

Finally, by PI staining, the percentage of cells in G2/M phase was observed to increase in both not-infected and B19V infected EPCs in absence of HU. In presence of HU, cells were blocked in G1/phase and a decreased percentage was detected in G2/M phase both in infected and not-infected cells. Probably, G1/S phase blocked cells (2N DNA content) were not competent to support B19V replicative cycle, increasing the antiviral effect of the reduction of available deoxyribonucleotides due to the presence of HU.

Cell cycle	EPCs (0 h)	mock-infected (48 hpi)			B19V-infected (48 hpi)		
	0 µM HU	0 µM HU	147.1 µM HU	494.0 µM HU	0 µM HU	147,1 µM HU	494.0 µM HU
G0/G1	77.9%	74.7%	70.5%	77.1%	73.0%	67.2%	76.7%
S	17.3%	17.0%	22.5%	19.2%	17.7%	24.3%	18.5%
G2/M	4.8%	7.6%	6.4%	3.5%	8.9%	7.2%	4.1%

- Discussion

Hydroxyurea is a FDA-approved drug which is usually used for the treatment of chronic myeloid leukemia and other pathologies such as thalassemia and several kinds of cancers. Since it interferes the DNA synthesis inhibiting the enzyme responsible for the production of deoxyribonucleotides, an inhibiting action against different viruses was identified.

Importantly, *Hydroxyurea* is widely used as a disease-modifying drug for the treatment of sickle-cell disease. A recent research showed beneficial effect in sickle cell disease (SCD) patients that were also infected by B19V. In particular, HU reduced requirements of blood transfusions and attenuate transient aplastic crisis caused by B19V infection in SCD patients [Hankins et al; 2016].

In the present study, the activity of *Hydroxyurea* against the Human Parvovirus B19 replication was investigated in the two relevant systems UT7/EpoS1 cell line and EPCs. HU showed a specific anti-B19V activity in absence of cellular toxicity combining both its inhibiting action on Ribonucleotide Reductase enzyme and its blocking action on cell cycle. In this last case, HU probably prevents the "G2/M arrest" (cell cycle status with a 4 N DNA content) which is triggered by B19V infection presumably to provide S phase factors for viral replication [Luo et al; 2013]

In SCD population, HU probably enhances the production of fetal hemoglobin which prevents the formation of sickle-shaped red blood cells and improved blood flow through the circulatory system, reducing the need for transfusions and the frequency of painful crises [Green et al; 2014]. Since the treatment in SCD patients requires a plasma concentration of the drug within the range of 276-709 µM, based on the results of the present research, HU is not responsible of both reduction of cellular viability and proliferation during the therapy.

This is of relevance in the perspective of its use in the treatment of B19V-caused diseases. In B19V infected children with SCD, HU treatment minimizes symptoms of severe anemia, attenuates clinical symptoms during TAC episode experiences with improved hematological indices, decrease frequency of red blood cells transfusions and normal immunological response [Hankins et al; 2016]. Hence, HU might determine a dual beneficial effect on SCD patients, not only for the treatment of the disease but also against a virus responsible for severe complications [Bonvicini et al; 2017].

5.2 Antiviral activity of *Brincidofovir*

Previous research allowed to identify the known broad-spectrum antiviral drug *Cidofovir* (CDV) as agent inhibiting the Human Parvovirus B19 replicative cycle. The acyclic nucleoside phosphonate *Cidofovir* [(S)-1-(3-hydroxy-2-phosphonylmethoxpropyl)cytosine: HPMPC] is a broad-range antiviral drug. Actually, it has shown activity against viruses belonging to all families of human dsDNA viruses, such as Cytomegalovirus (CMV), Herpes viruses (HSV-1 and HSV-2), varicella-zoster virus (VZV), Epstein-Barr virus (EBV), Papillomavirus (HPV), viruses that belong to *Poxviridae* and *Polyomaviridae* families. However, the drug has been approved by FDA only for the treatment of retinitis in Cytomegalovirus infected patients with AIDS [De Clercq; 2007 – De Clercq et al; 2005].

CDV is a monophosphate cytidine nucleotide analogue, which contains a phosphonate group bound through a P-C-O bond to the acyclic nucleoside. This P-C-O bond is not susceptible to the digestion by cellular hydrolases and so it is more stable than the natural P-O-C phospho-ester bond. Following the uptake by endocytosis, two phosphate groups are added to the drug for a total of three phosphate groups (CDVp and CDVpp); the second derivative (CDVpp) is the antiviral active compound. For the production of the final molecule, CDV is different from the other acyclic nucleoside analogues (ANPs e.g. *Aciclovir*, *Penciclovir*, *Ganciclovir*) that require the addition of all the three phosphate groups [De Clercq et al; 1998]. Both viral and cellular polymerases can recognize the CDVpp as substrate and they can add it at the 3'-terminus of the newly synthesized DNA [Magee et al; 2012]. In particular, CDVpp acts as competitive inhibitor of the triphosphate deoxycytidine natural substrate (dCTP) causing a deceleration of the DNA synthesis rather than a total block when it is added (figure 5.6). However, incorporation of two consecutive CDVpp molecules causes the arrest of synthesis [Xiong et al; 1997].
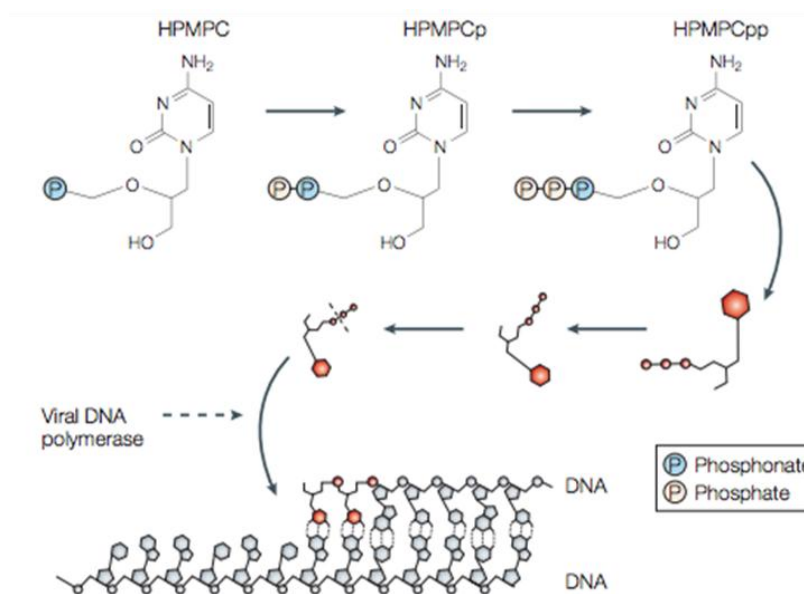
Figure 5.6: Schematic representation of the mechanism of action for CDV (HPMPC) [De Clercq et al; 2005].

Recent research from our group has expanded the antiviral range of *Cidofovir* toward also ssDNA viruses in addition to the dsDNA viruses. In particular, antiviral activity was observed for CDV against the Human Parvovirus B19 in infected UT7/EpoS1 cell line and EPCs without significantly altering the proliferation and viability of both the cellular systems [Bonvicini et al; 2015]. Moreover, a decreased infectivity was shown for the released B19V particles in long-term infected erythroid progenitor cells [Bonvicini et al; 2016]. B19V is highly dependent on cellular machinery for its replication and offers few virus specific targets, but a broad range antiviral compound has the possibilities to interfere within its biological activity in a very complex and not yet fully characterized virus-cell interaction network.

Recently, a novel lipid conjugate (*Brincidofovir*; BCV) has been developed in order to increase and speed up the compound entry through the cellular membrane. CDV in transported into the cells by fluid phase endocytosis, a relatively inefficient method [Connelly et al; 1993]. By previous research, conjugation of the lipid (3-hexadecyloxy-1-propanol) to the phosphonate moiety of CDV to produce BCV resulted in significant decreases in EC_{50} values relative to those of CDV. Once BCV is inside the cells, CDV is liberated by phospholipase cleavage of the lipid ester linkage and activated by two successive phosphorilations (figure 5.7), first to *Cidofovir* monophosphate (CDVp) and then to *Cidofovir* diphosphate (CDVpp) [Cihlar et al; 1996].
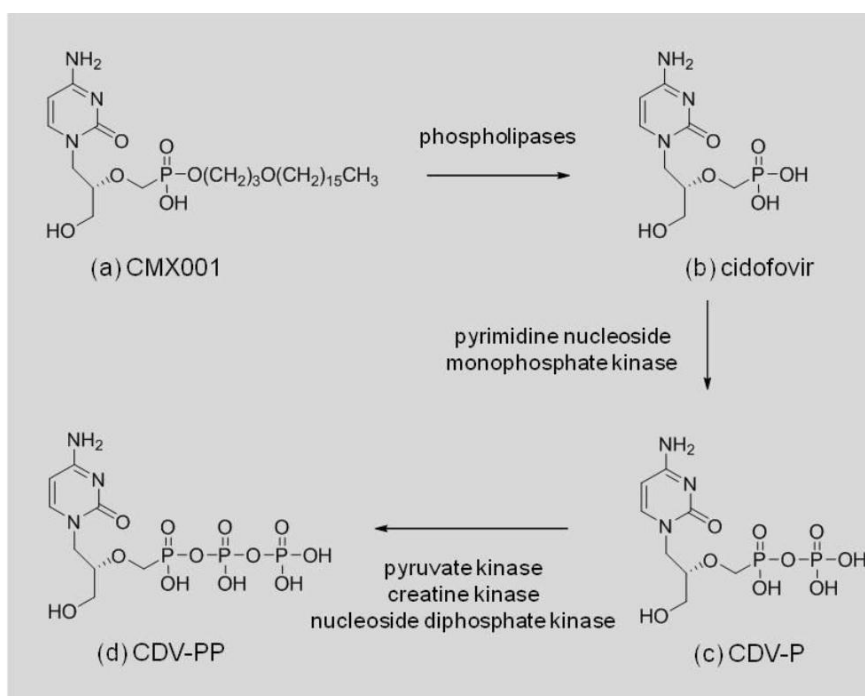
Figure 5.7: BCV (CMX001) cleavage and anabolism by host cell enzymes [Lanier et al; 2010].

The present study investigated the activity of the lipid conjugate BCV to assess its potential as an antiviral agent against B19V. Its inhibitor effect is directly correlated to CDVpp which acts as an alternative substrate for viral DNA synthesis [Magee et al; 2005]. The incorporation of CDV into newly synthesized DNA reduces the nucleic acid replication or induces chain termination. These mechanisms are possibly responsible of its antiviral action against viruses, such as B19V, that do not possess a DNA polymerase [De Clercq et al; 2005]

At first, effect of BCV-S (the active stereoisomer) and CDV were tested on viability and proliferation of both UT7/EpoS1 cells and EPCs. Cells were grown in presence of several dilutions of BCV and CDV (range 0,1-500 μM) for 48 hours, then analyzed; cells cultured without compounds were used as control. By CCK8 assay and BrdU assay, BCV and CDV caused a decrease in cellular viability and proliferation for both the cellular systems but with a higher effect due to BCV rather than CDV. In particular, BCV reduced totally the cell proliferation and viability in UT7/EpoS1 cell line at ≥100 μM concentration, while its effects were lower in EPCs. Instead, cell proliferation and viability were decreased by CDV but never reaching the 50% of inhibition (figure 5.8).
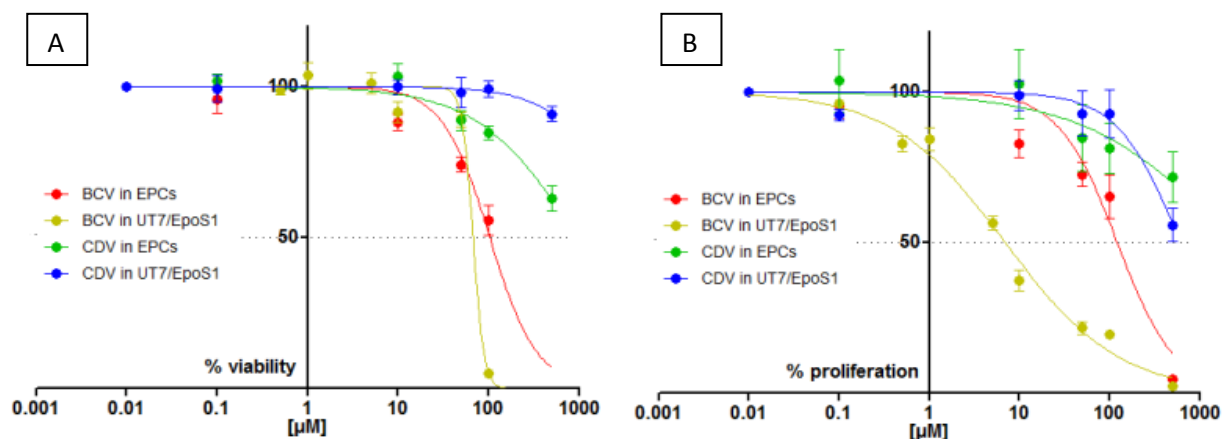
Figure 5.8: Representative graphs of the effects of BCV and CDV on cellular viability and proliferation (data are normalized to the control) = A) CCK8 assay: 50% reduction of cellular viability is at 102,90 μM (95% confidence interval: 87,60-120,80 μM; R^2 0,93) and 66,80 μM (95% confidence interval: 62,00-72,90 μM; R^2 0,98) for BCV in EPCs and UT7/EpoS1, respectively; for CDV > 500 μM for both. B) BrdU incorporation assay: 50% inhibition of cellular DNA replication is at 121,60 μM (95% confidence interval: 91,70-161,30 μM; R^2 0,89) and 6,90 μM (95% confidence interval: 5,70-8,40 μM; R^2 0,97) for BCV in UT7/EpoS1 and EPCs, respectively; for CDV > 500 μM for both. Plotted values are mean of two experiments [*GraphPad Prism 6.0*].

Non-linear regressions were performed to determine 50% reduction of cellular viability and proliferation: for BCV, 102,90 μM and 66,80 μM were the CC_{50} values of cell viability in EPCs and UT7/EpoS1 cells, respectively; 121,60 μM and 6,90 μM were the CC_{50} values of cell proliferation respective to EPCs and UT7/EpoS1 cells. CC_{50} values of cell viability and proliferation were higher than 500 μM concentration for CDV in both the cellular systems.

The antiviral activities of BCV and CDV towards B19V were investigated in both cellular systems. UT7/EpoS1 cell line and EPCs were infected by Human Parvovirus B19 at moi of 10^4 geq/cell and incubated for 48 hours in presence of the compounds at the same previous established dilutions. Cells grown without compounds were used as control. At 2 hpi and 48 hpi, cells were collected and analyzed for viral DNA replication. By qPCR, the amount of B19V DNA decreased in presence of the compounds in both the cellular systems and in a dose-dependent manner. In particular, complete inhibition of viral replication was detected for BCV at concentrations ≥10 μM in UT7/EpoS1 and ≥500 μM in EPCs; while in presence of CDV, the viral replication was totally inhibited at concentration ≥500 μM in UT7/EpoS1 but not in EPCs at any tested compound concentration (figure 5.9). Non-linear regression curve allowed to calculate the 50% inhibition of B19V replication: EC_{50} values were established at 9,65 μM and 0,22 μM for BCV in EPCs and UT7/EpoS1, respectively, and at 320,50 μM and 16,10 μM for CDV in EPCs and UT7/EpoS1 cells respectively. As a result, the BCV acted as antiviral agent against Human Parvovirus B19, it had an enhanced action in comparison to its

progenitor (CDV) and with a higher inhibiting action in infected UT7/EpoS1 cell line rather than EPCs.

Furthermore, a study to evaluate the *Brincidofovir* activity against the virus was carried out in infected EPCs by different B19V concentrations. In particular, cells were infected by B19V at range of moi of 10^1–10^4 geq/cell and cultured in presence of the compound at different concentration (0,1-500 µM) for 48 hours. Cells were collected at different time points (2 and 48 hpi) and analyzed for B19V DNA replication; cells grown in absence of compound were used as control.

By qPCR assay, differences in the viral DNA amount were observed at the various time points due to both the initial infection moi and the concentration of the compound (figure 5.9). Amounts of B19V DNA increased with increasing of the concentration of the virus. Within each infection at a determined moi, the detected amount of B19V was influenced by the concentration of BCV. In particular, viral replication was inhibited in presence of increasing BCV concentration. It was completely inhibited in presence of BCV 500 µM at every viral moi, since DNA amounts at 48 hpi were lower than those at 2 hpi. Non-linear regression curve allowed to determine the 50% inhibition of B19V (EC_{50}) at the different moi: values ranged between 6,60 and 11,50 µM of BCV, yielded to a complex value of BCV 9,35 µM, as result.
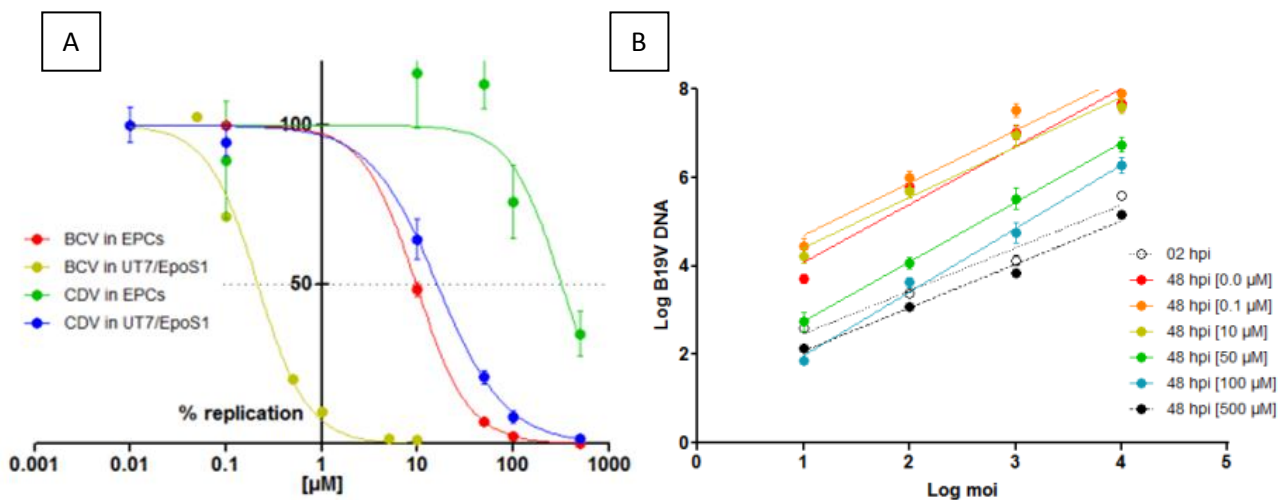
Figure 5.9: B19V replication in infected cells. A) Non-linear regression curves obtained by expressing B19V amounts as percentages of inhibition relative to the untreated control in infected UT7/EpoS1 cell line and EPCs in presence of BCV and CDV. EC_{50} values are: for BCV, 0,22 µM in UT7/EpoS1 cells (95% confidence interval: 0,19-0,25 µM; R^2 0,99) and 9,65 µM in EPCs (95% confidence interval: 9,15-10,20 µM; R^2 0,99); for CDV, 16,10 µM in UT7/EpoS1 cells (95% confidence interval: 12,90-20,20 µM; R^2 0,95) and 320,50 µM in EPCs (95% confidence interval: 173,90-590,70 µM; R^2 0,41). B) Linear regression analysis for Log B19V DNA

in EPCs as function of the different multiplicities of infection (Log moi) and in presence of several BCV-S concentrations. Plotted values are mean of two experiments [*GraphPad Prism 6.0*].

As mentioned previously, BCV can assume two different enantiomeric configurations: BCV-S (CMX001) and BCV-R (CMX029). In particular, BCV-S is the active one, which is converted in CDV and double phosphorylated within the cell, while BCV-R is not converted in CDVpp. Hence, the effects of both the enantiomers on the viral replication and on the cells were evaluated in EPCs and UT7/EpoS1 cells.

Cells were cultured in presence of different concentrations of both the molecules (range 0,01-100 μM) for 48 hours, then the cell viability was evaluated by CCK8 assay; cells that grew without compounds were used as control. Non-linear regression curve allowed to determine the 50% reduction of cellular viability at 93,40 μM and 59,90 μM in EPCs and UT7/EpoS1 cells respectively, for BCV-S; while CC_{50} values were calculated at 146,2 μM and 72,10 μM respectively in EPCs and UT7/EpoS1 cells, for BCV-R. Cells were infected by B19V at moi of 10^4 geq/cell and cultured in presence of the same previous BCV-S and BCV-R concentrations; cells cultured without compounds were used as control. At 2 hpi and 48 hpi, cells were collected and analyzed for B19V replication by qPCR. Non-linear regression curves were performed to determine the 50% inhibition of B19V replication values: EC_{50} values were calculated at 14,30 μM and 0,63 μM for BCV-S in EPCs and UT7/EpoS1 respectively, while at 93,00 μM and 54,70 μM for BCV-R in EPCs and UT7/EpoS1 cells (figure 5.10).
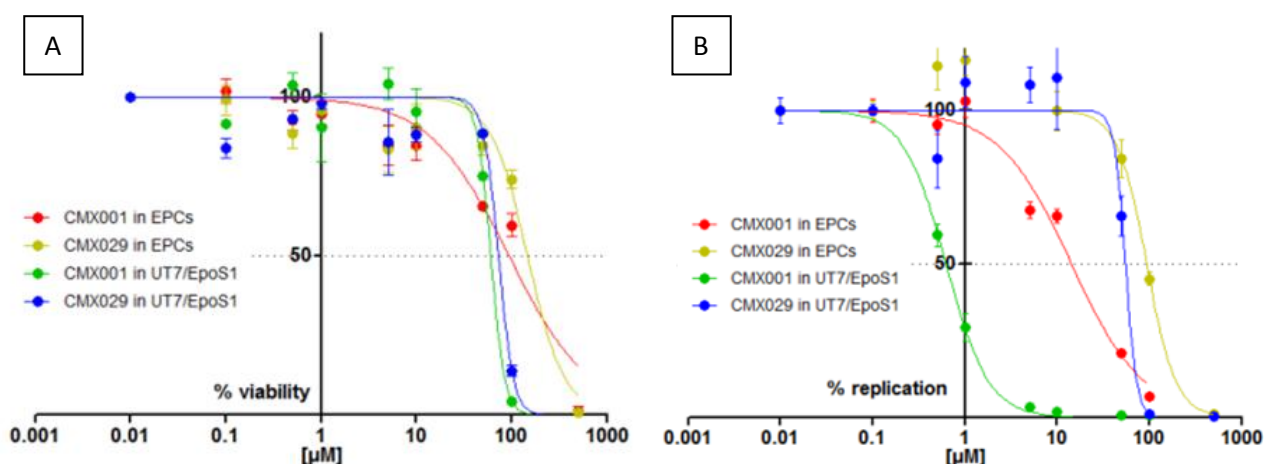
Figure 5.10: Effects of BCV-S (CMX001) and BCV-R (CMX029) on cellular viability and B19V replication (untreated cells were used as control to normalize the values). A) Non-linear regression curves obtained by CCK8 assay: CC_{50} values are for BCV-S at 93,40 μM in EPCs (95% confidence interval: 68,90-126,60 μM) and 59,90 μM in UT7/EpoS1 cells (95% confidence interval: 52,70-68,10 μM), for BCV-R at 146,20 μM in EPCs (95% confidence interval: 106,40-200 μM) and 72,10 μM in UT7/EpoS1 cells (95% confidence interval: 62,50-

83,10 μM). B) Non-linear regression curves obtained by qPCR assay: EC_{50} values are for BCV-S at 14,30 μM in EPCs (95% confidence interval: 11,80-17,30 μM) and 0,63 μM in UT7/EpoS1 cells (95% confidence interval: 0,58-0,68 μM), for BCV-R at 93,00 μM in EPCs (95% confidence interval: 77,40-111,80 μM) and 54,70 μM in UT7/EpoS1 cells (95% confidence interval: 42,70-69,90 μM). Plotted values are mean of two experiments [*GraphPad Prism 6.0*].

To determine the enantiomeric configuration which acted as a more specific B19V antiviral agent, their selective index (S.I. = CC_{50}/EC_{50}) were calculated. In EPCs, the S.I. values were 6,50 μM for BCV-S and 1,60 μM for BCV-R, while in UT7/EpoS1 cell line, the S.I. values were 95,10 μM for BCV-S and 1,30 μM for BCV-R. Since the selective index reflects the amount of the compounds which inhibited the viral replication without acting a cytotoxic effect on the cells, higher S.I. values mean that the compounds inhibited the virus rather than provoking a reduction of cellular viability. In both the cellular systems, BCV-S had a bigger S.I. than BCV-R suggesting that the S stereoisomer (CMX001) was selective for inhibiting B19V infection. Indeed, its inhibitory activity was higher in viral infected UT7/EpoS1 cells than EPCs, probably due to the different permeability, conversion and phosphorylation mechanism of the compound within the two different cellular systems.

- **Discussion**

Recently, the FDA-approved drug *Cidofovir* (CDV) was identified as antiviral agent toward Human Parvovirus B19 [Bonvicini et al; 2015 – Bonvicini et al; 2016]. To overcome the difficulty of cellular uptake for CDV and its cellular toxicity, the newly lipid conjugate of this acyclic nucleoside phosphonate (named *Brincidofovir*, BCV or CMX001) was synthesized. As well as CDV, BCV is active against all the five families of double-stranded DNA viruses that cause human morbidity and mortality [Lanier et al; 2010]. Actually, the lipid chain of BCV facilitates its efficient uptake into the cells, and it is then followed by metabolism of BCV to CDVpp [Painter et al; 2012]. Within the cells, BCV is firstly converted in CDV and then double phosphorilated to obtain the active antiviral molecule which acts as a competitive, an alternative substrate inhibitor of the DNA directed DNA polymerases [Xiong et al; 1997].

Hence the addition of the lipid chain at the CDV helps and speeds up its cellular uptake without changing its antiviral properties. Actually, BCV inhibited the B19V replication within both the studied cellular systems and with an enhanced effect at lower concentrations in infected UT7/EpoS1 probably due to the different cellular permeability and processing of the compound within the cells compared to what happened in EPCs. In addition, in the EPCs only BCV and not CDV achieved a complete inhibition of viral replication. Accordingly, the

effects of BCV on cell viability and proliferation were measurable at lower concentrations compared to CDV in both cellular systems.

The present results are of relevance in order to use BCV as B19V antiviral therapy with highly favorable properties. Administration of BCV produces low circulating plasma concentration of CDV, which greatly reduces the nephrotoxicity associated with administration of intravenous CDV [Tippin et al; 2016].

Between the two BCV stereoisomers, BCV-S (CMX001) was evaluated as the selective antiviral agents towards Human Parvovirus B19. The inhibition of viral replication compared to the induction of cell cytotoxicity is restricted to BCV-S supporting the hypothesis of an active and selective antiviral role of CDVpp derived from BCV rather than an inhibition of viral replication related to a non-specific cytotoxic effect. Actually, the metabolism of both the two enantiomers of BCV (BCV-S and BCV-R) result in formation of CDV, however only in the case of BCV-S, the two phosphorilations occur and CDVpp is formed [Bua et al; 2019].

As for CDV, these results expand the spectrum of viral targets BCV including also a ssDNA virus (B19V) other than dsDNA viruses within their spectrum allowing their possible applications towards other viruses.

5.3 Small chemical library screening

5.3.1 Initial screening

As an alternative, 'serendipity' approach, a small chemical library was selected for evaluation of their putative antiviral activity against Human Parvovirus B19. Actually, a set of 8 different compounds was selected and provided by the group of Professor. A. Locatelli (FaBiT, University of Bologna). The 8 compounds (A to H) and could be divided into different groups due to their common characteristics, including: i) molecules comparable to *BRACO-19* (known G4 ligand) = A, B, E, F; ii) coumarin derivative = D; iii) cyclic urea derived compounds = G, H; iv) molecule without a reference molecule = C.

They were provided as powder, hence firstly the compounds were solubilized in 100% DMSO till the common concentration of 14,3 mg/mL which was previously used for their study at NMR. However, before the biological studies, it was determined the maximal concentration at which the compounds could be maintained in solution, without forming precipitates, in cellular cultures:

Compound	Compound	Concentration (µM)	% DMSO
A	BIS ARPy2G.2HCl	60	0,75
B	AR24EGG.2HCl	20	0,09
C	MM-67IFUR	150	0,38
D	AR-CUM	91,25	0,19
E	IS-INDIND	30	0,1
F	5M-BIM	20	0,05
G	IND-5Cl-Nmet-34-PIRIMEt	64	0,19
H	ARCI-34-PIRIMEtAL	20	0,09

Then, compounds at different concentrations were tested for their effects on cell viability, using the UT7/EpoS1 cells as a test system.

Compound	Compound	Concentration (µM)	% DMSO
A	BIS ARPy2G.2HCl	50	0,63
B	AR24EGG.2HCl	20	0,06
C	MM-67IFUR	10	0,01
D	AR-CUM	50	0,10
E	IS-INDIND	20	0,10
F	5M-BIM	20	0,05
G	IND-5Cl-Nmet-34-PIRIMEt	50	0,19
H	ARCI-34-PIRIMEtAL	20	0,10

Indeed, previous studies based on CCK8 assays showed that concentrations equal or major to the 3% DMSO induced a decrease in the vitality of UT7/EpoS1 cells, and therefore all the tested concentrations of the newly synthesized compounds had DMSO content lower than 3.

UT7/EpoS1 cells were cultured for 48 hours in presence of the maximal concentration of each compound and their viability was evaluated by CCK8 assay. Cells cultured with only complete cellular medium or medium in presence of the maximal % DMSO among the various conditions were used as controls. Compared with the controls, the C, D and E compounds showed a reduction in the cellular vitality: 40%, 53% and 67%, respectively (figure 5.11).
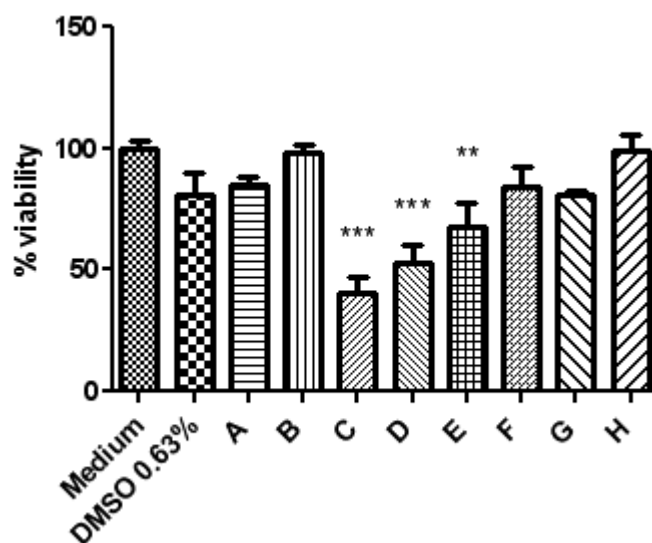
Figure 5.11: Representative graph of the percentages of the living UT7/EpoS1 cells due to the composition of the medium by CCK8 assay. C, D and E compounds show reduction of the cellular viability in comparison to the medium (100% vitality), which is more significant for C compound. % viability = Medium: 100%, 0,63% DMSO: 89,66%; A: 85,01%; B: 98,60%; C: 40,75%; D: 52,88%; E: 67,43%; F: 84,45%; G: 81,00%; G: 99,40% [*GraphPad Prism 6.0*]. The statistical analysis is done by Dunnett test (variance test based on multiple comparison; *one-way ANOVA*). Plotted values are mean of at least two experiments done in triplicate; **p value < 0.001, ***p value < 0.0001.

UT7/EpoS1 cells were then infected by Human Parvovirus B19 at moi of 10^4 geq/cell and cultured for a 48 hour time course of infection in medium containing the compounds at the same concentration tested for the viability assay. Cells were collected at different time points (2 hpi and 48 hpi); viral proteins production and B19V replication were evaluated by IIF assay and qPCR, respectively.

Positive cells for IIF against VP proteins were observed for infected UT7EpoS cells in presence of all the compounds (figure 5.12). The C compound induced a huge reduction of the number of the positive cells but this could be related to its significant effect on the cellular viability. Indeed, less amount of positive cells for IIF assay anti-VP was observed also for the D compound.
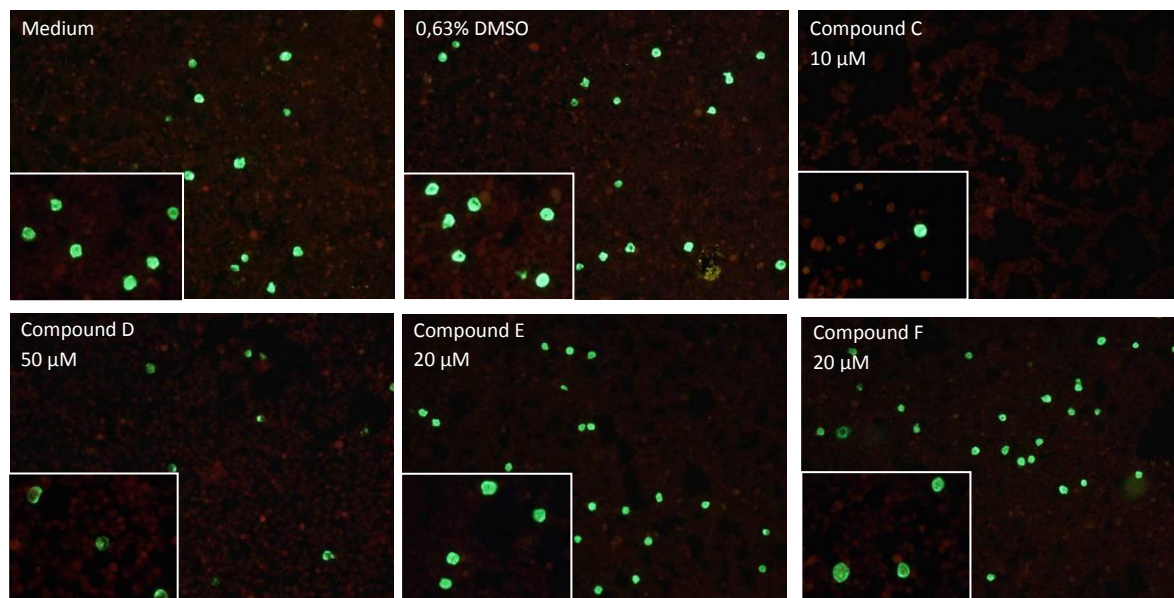

Figure 5.12: Pictures of IIF anti-VP assay for B19V infected UT7/EpoS1 (48 hpi) that are grown in different conditions (10x and 40x magnification) = Medium) UT7/EpoS1 complete culture medium without compounds (control); 0,63% DMSO) UT7/EpoS1 medium added with DMSO: the amount of positive cells is comparable to the control ("Medium"); Compound C 10 µM) Compound C at concentration of 10 µM: less amount of positive cells than the other compounds and the controls; Compound D 50 µM) Compound D at concentration of 50 µM: less amount of positive cells than the controls; Compound E 20 µM) Compound E at concentration of 20 µM: amount of positive cells is comparable to both the controls ("Medium" and 0,63% DMSO) and the other compounds (example: F); Compound F 20 µM) Compound F at concentration of 20 µM as example of the other compounds (A, B, G, H): the number of positive cells is comparable to both the controls ("Medium" and 0,63% DMSO).

qPCR assay on cellular extracts at 2 and 48 hpi showed active B19V viral replication in presence of all the different compounds, without a significant antiviral activity compared to the controls for most of the compounds. Some inhibition of B19V replication was detected in presence of the compound D (50 µM) and E (20 µM), while a relative major viral DNA reduction was observed in presence of the compound C (10 µM). This last was also responsible for a cytotoxic effect on the UT7/EpoS1 cells, hence the decrease of viral replication was probably correlate on the effect of the compound on cellular viability more than an its direct action on viral replication (figure 5.13).
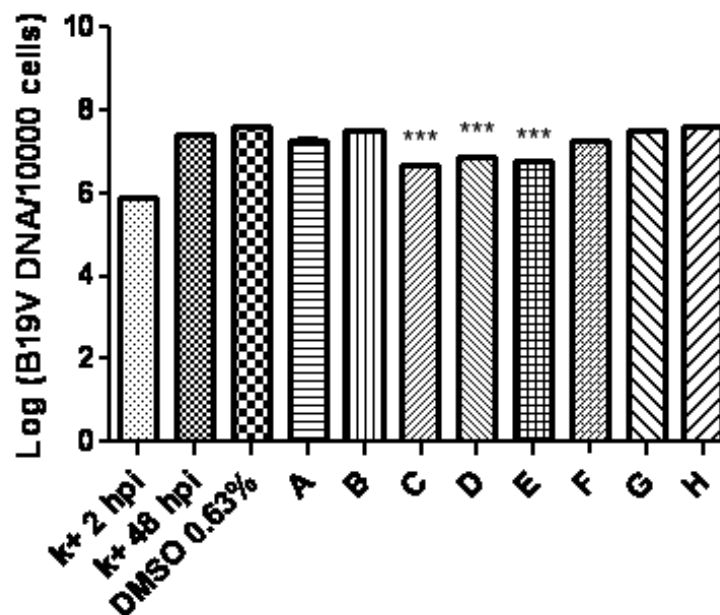
Figure 5.13: Representative graph of the amount of B19V DNA evaluated from cellular extracts by qPCR. Mean values are expressed as Log B19V geq/10.000 cells: +5,91 Log for k+ 2 hpi, +7,42 Log for k+ 48 hpi, +7,65 Log for 0,63% DMSO, +7,36 Log for A, +7,52 Log for B, +7,09 Log for C, +7,15 Log for D, +6,94 Log for E, +7,33 Log for F, +7,60 Log for G, +7,60 Log for H [*GraphPad Prism 6.0*]. The statistical analysis is done by Dunnett test (variance test based on multiple comparison; *one-way ANOVA*). Plotted values are mean of at least two experiments; data are normalized in 10.000 cells following the qPCR for the cellular ribosomal DNA (5.8S primers); ***p value < 0.0001.

5.3.2 Antiviral activity of Coumarin derivatives

Based on results of the initial screening, compound D was selected for further evaluation. As previously mentioned, D compound (AR-CUM or 4 compound) was a derivative of Coumarin molecules that have been found to inhibit different viruses such as HIV, hepatitis viruses, etc. Since a decrease in the amount of Human Parvovirus B19V replication and VP protein production was detected for the D compound (AR-CUM) in infected UT7/EpoS1 cells, a group of its derivatives were studied for their potential activity in a selective inhibition of Human Parvovirus B19 replication.

A set of 8 other molecules (named from 4a to 4h) in addition to the D compound were provided as powder by the group of Professor A. Locatelli Locatelli (FaBiT, University of Bologna). Firstly, they were resuspended in DMSO till the common concentration of 5 mM and the maximal concentrations of solubilization in cell culture conditions were determined for each compound. In particular from the stock solutions, 8 serial dilutions with a ratio 1:2 were prepared within the range from 50 to 0,39 μM, in cellular medium containing 1% DMSO (final volume of 100 μL, in 96 wells-plate). Actually, the common concentration of

1% DMSO in cultured medium was important to reduce the variability of the system among the different compounds.

Meanwhile, the same test was done in cellular medium added with 1% DMSO in presence of UT7/EpoS1 cells or EPCs (50.000 cells in 100 µL, in 96 wells-plate). After 48 hours of incubation at 37°C, the concentrations of compounds that did not show crystals at optical microscopy observation were selected as maximal concentrations for the following experiments.

Compound	Compound	Concentration (µM)
4	ARCUM	12,20
4a	ARCUM-A	6,25
4b	ARCUM-H	0,78
4c	ARCUM-5M	12,50
4d	2MCUM	1,56
4e	2MCUM-A	0,78
4f	2MCUM-H	3,13
4g	2MCUM-5M	12,50
4h	2MCUM-67	6,25

For each molecule, the action on effect on viability of the two cellular systems, UT7/EpoS1 cells and EPCs, was evaluated by CCK8 assays. In particular, cells were cultured in medium added with 1% DMSO and in presence of the different molecules at the previous established concentrations. Cultured cells in both medium without compounds and medium with 1% - 10% DMSO were used as controls.

In UT7/EpoS1 cells, decrease of cellular viability was observed in presence of the compounds 4, 4c, 4g and 4h with percentage of vitality of about 60 - 70%. 1% DMSO did not act on the vitality while 10% DMSO caused a reduction to 16,97% of living UT7/EpoS1 cells (figure 5.14).

The same assay was performed for EPCs: cells were cultured for 48 hours in presence of the compounds at the established concentrations; 1% - 10% DMSO and medium without compounds were used as controls. Reduction of cellular vitality was observed for compounds 4, 4c and 4g as for EPCs; in particular, a significant cytotoxic effect was observed for the compounds 4 and 4g (less than 50% of cellular viability). Higher cellular vitality was observed in presence of 4h compound in EPCs with respect to what happened in UT7/EpoS1 cells, in addition a relative toxic effect was observed for the 4a and 4f compounds (figure 5.15). Also for EPCs, 1% DMSO did not influence the vitality while 10% DMSO caused the 98% of EPCs mortality.
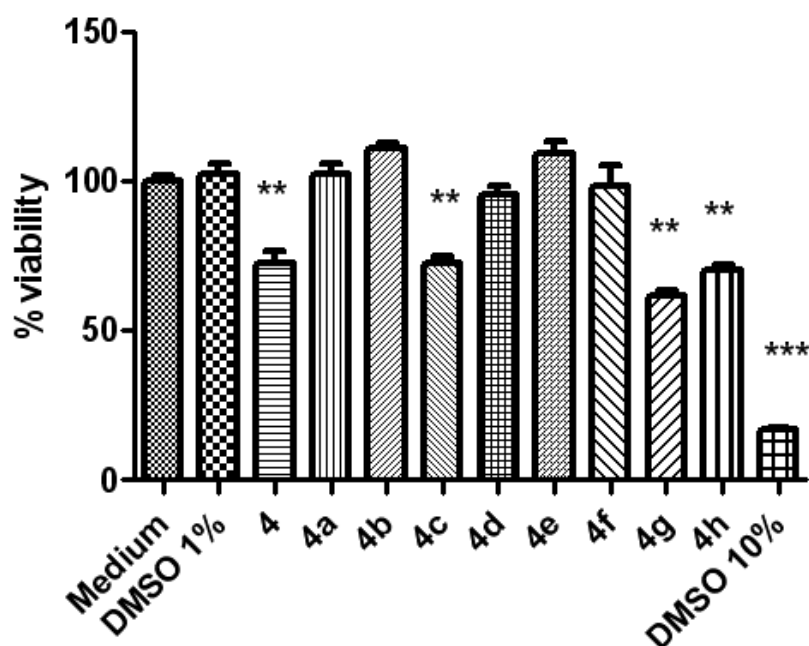
Figure 5.14: Representative graph of the percentages of the living UT7/EpoS1 cells due to the composition of the medium by CCK8 assay = 4, 4c, 4g and 4h compounds show a reduction of the cellular viability. % viability = Medium: 100%; 1% DMSO: 102,35%; 4: 72,29%; 4a: 102,74%; 4b: 111,28%; 4c: 72,50%; 4d: 95,74%; 4e: 109,34%; 4f: 98,44%; 4g: 61,46%; 4h: 70,07%; 10% DMSO: 16,98% [*GraphPad Prism 6.0*]. The statistical analysis is done by Dunnett test (variance test based on multiple comparison; *one-way ANOVA*). Plotted values are mean of two experiments done in triplicate; **p value< 0.001, ***p value < 0.0001.
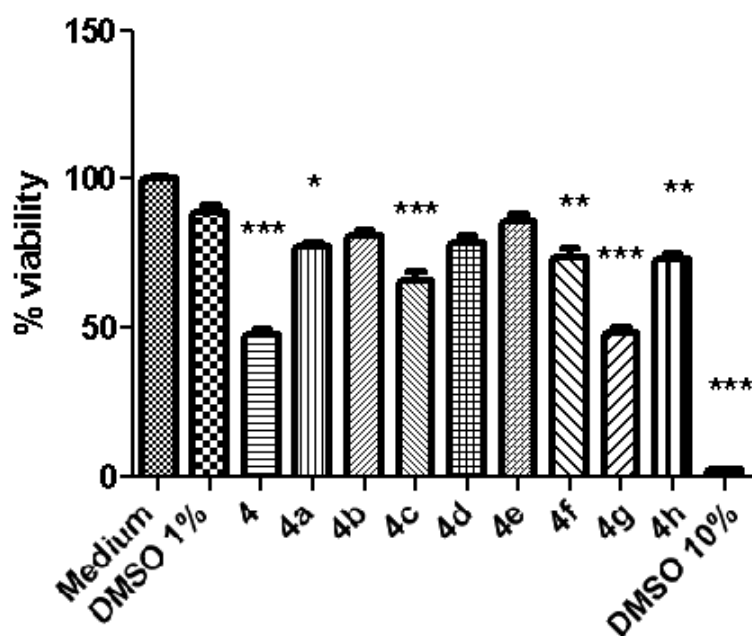
Figure 5.15: Representative graph of the percentages of the living EPCs due to the composition of the medium by CCK8 assay = 4, 4c, 4g compounds show a significant reduction of the cellular viability. % viability = Medium: 100%; 1% DMSO: 88,86%; 4: 47,93%; 4a: 77,26%; 4b: 81,13%; 4c: 65,92%; 4d: 78,46%; 4e: 85,55%; 4f: 73,39%; 4g: 48,20%; 4h: 73,32%; 10% DMSO: 2,34% [*GraphPad Prism 6.0*]. The statistical analysis is done by Dunnett test (variance test based on multiple comparison; *one-way ANOVA*). Plotted values are mean of two experiments done in triplicate; *p value< 0.01-0.05, **p value< 0.001, ***p value < 0.0001.

Meanwhile, effects of compounds on B19V replication was evaluated. Both UT7/EpoS1 cells and EPCs were infected by Human Parvovirus B19 at moi of 10^4 geq/cell for 2 hours; then after wash of the inoculum, the cells were cultured in medium in the presence of the compounds at their maximal concentration of use. Infected cells cultured only in medium or in medium added with 1% DMSO were used as controls. Cells were collected at different time points (2 hpi and 48 hpi) and the viral proteins expression and replication was evaluated by IIF anti-VP assay and qPCR assay, respectively.

In infected UT7/EpoS1 cells, expression of VP capsid proteins was observed in presence of all the compounds. However, less positive cells were observed for the 4, 4c, 4g and 4h compounds, but this could be related to their relative cytotoxic effect (figure 5.16).
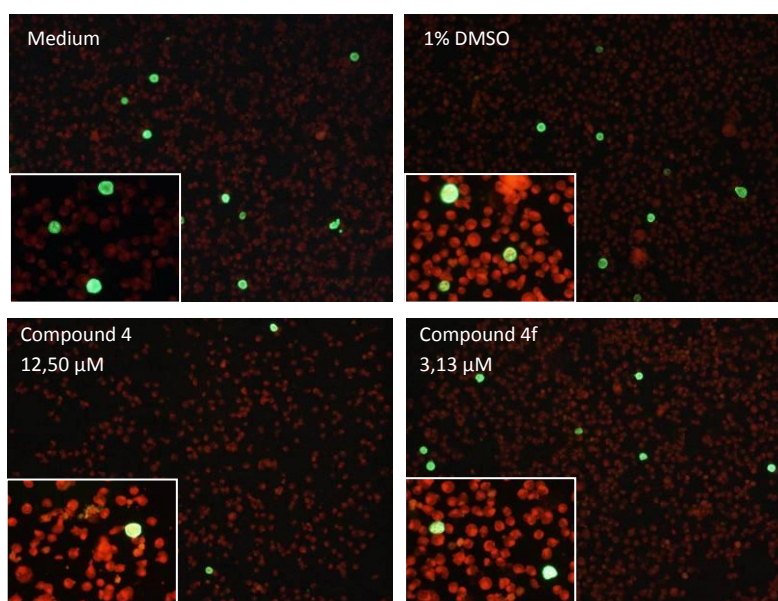
Figure 5.16: Pictures of IIF anti-VP assay for B19V infected UT7/EpoS1 (48 hpi) that are grown in different conditions (10x and 40x magnification) = Medium) UT7/EpoS1 complete culture medium without compounds (control); 1% DMSO) UT7/EpoS1 medium added with DMSO: the amount of positive cells is comparable to the control ("Medium"); Compound 4 12,50 µM) Compound 4 at concentration of 12,50 µM: less amount of positive cells than the other compounds and the controls; Compound 4f 3,13 µM) Compound 4f at concentration of 3,13 µM (as example of the other compounds): the number of positive cells is comparable to both the controls ("Medium" and 1% DMSO).

By qPCR assay, none of the compounds caused a complete inhibition of viral replication at 48 hpi in infected UT7/EpoS1 cells; actually, the amount of B19V DNA in presence of the molecules was increased respect to the 2 hpi of the control (medium without compounds). 1% DMSO did not alter the viral replication while a reduction in the amount of B19V DNA at 48 hpi occurred in the presence of the compounds 4, 4c, 4f, 4g and 4h (figure 5.17). In particular, compounds 4 and 4c showed a significant decrease of viral replication: in their presence, the

B19V virus maintained the capacity of replicate in the percentage of 53,31% and 33,42%, respectively. However, this action on B19V replication could also be related to the effects on the cells and not on their direct action against the virus.
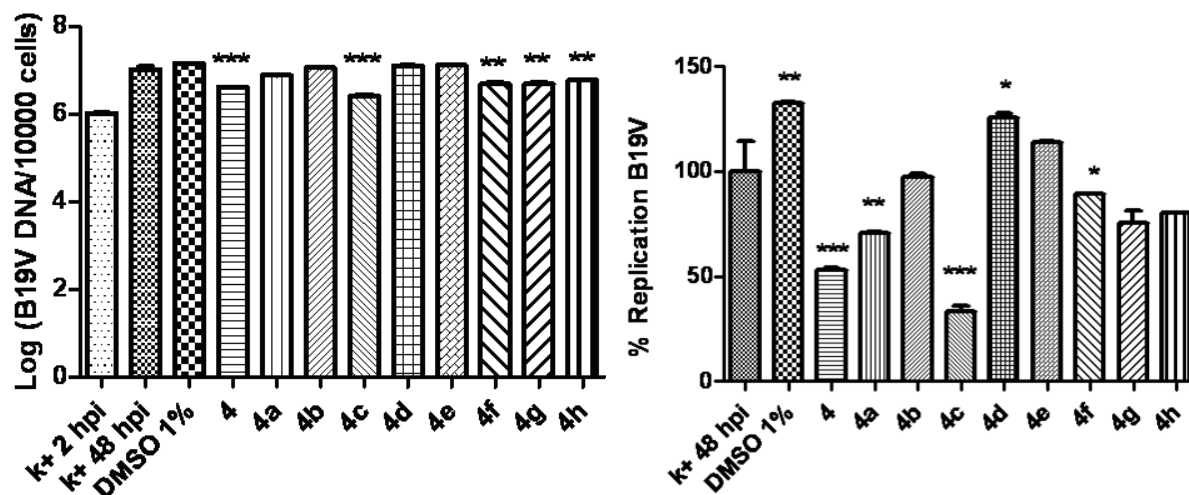
Figure 5.17: Infected UT7/EpoS1 at 48 hpi with B19V at moi = 104 geq/cell. Left) qPCR assay of the amount of B19V DNA evaluated from cellular extracts. Mean values are expressed as Log B19V geq/10.000 cells: +6,03 Log for k+ 2 hpi, +7,03 Log for k+ 48 hpi, +7,16 Log for 1% DMSO, +6,62 Log for 4, +6,89 Log for 4a, +7,07 Log for 4b, +6,42 Log for 4c, +7,11 Log for 4d, +7,13 Log for 4e, +6,97 Log for 4f, +6,70 Log for 4g and +6,78 Log for 4g; Right) Percentage of B19V replication corrected by the cell viability: compounds 4 and 4c cause a decrease of viral replication (53,31% and 33,42%, respectively), in comparison to both the controls. The other percentages: 4a: 70,75%, 4b: 97,60%, 4d: 125,75%, 4e: 114,13%, 4f: 89,61%, 4g: 75,35%, 4h: 80,11% [*GraphPad Prism 6.0*]. The statistical analysis is done by Dunnett test (variance test based on multiple comparison; *one-way ANOVA*). Plotted values are mean of two experiments; * p value < 0.01-0.05, ** p value < 0.001, ***p value < 0.0001.

In infected EPCs, VP capsid protein production were observed in all the different conditions of the medium by IIF assay at 48 hpi. Actually, a higher amount of positive cells was even detected in infected EPCs in presence of the compound 4d, by IIF assay(figure 5.18).

Figure 5.18: Pictures of IIF anti-VP assay for B19V infected EPCs (48 hpi) that are grown in different conditions (10x and 40x magnification) = Medium) EPCs complete culture medium without compounds (control); Compound 4d 1,56 µM) Compound 4d at concentration of 1,56 µM: major amount of positive cells

than the other compounds and the controls; Compound 4f 3,13 μM) Compound 4f at concentration of 3,13 μM (as example of the other compounds): the number of positive cells is comparable to both the controls.
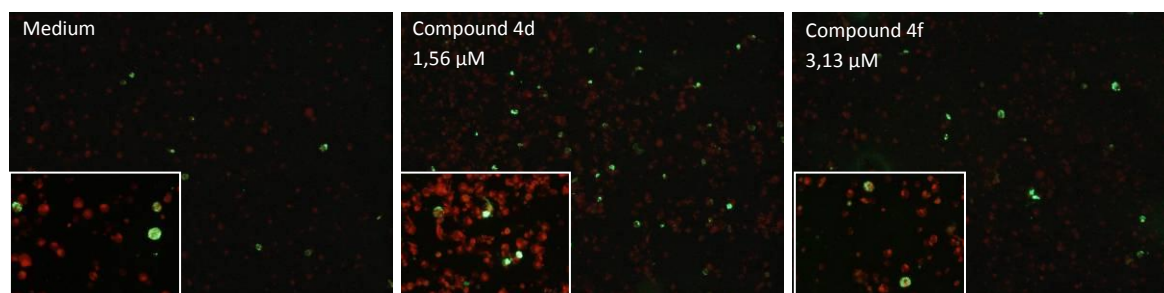
By qPCR assay, none of the compounds showed to inhibit completely the B19V replication at 48 hpi. However, the effects of the molecules on infected EPCs were in some cases different compared to what happened in UT7/EpoS1 cells. Actually, reduction on viral replication was observed in presence of the compounds 4, 4c, 4e, 4f, 4g and 4h at 48 hpi compared to the control (medium without compounds). In particular, a significant decrease occurred only in presence of the compound 4f (figure 5.19). However, also for infected EPCs, this action which limited the viral production could be related to the effects of the compounds on cellular viability. In addition compounds 4b and 4d showed an increase on viral DNA amount at 48 hpi, favoring the B19V replication. 1% DMSO did not alter the viral replication, hence the evaluated amount of B19V was due to the presence of the compounds.
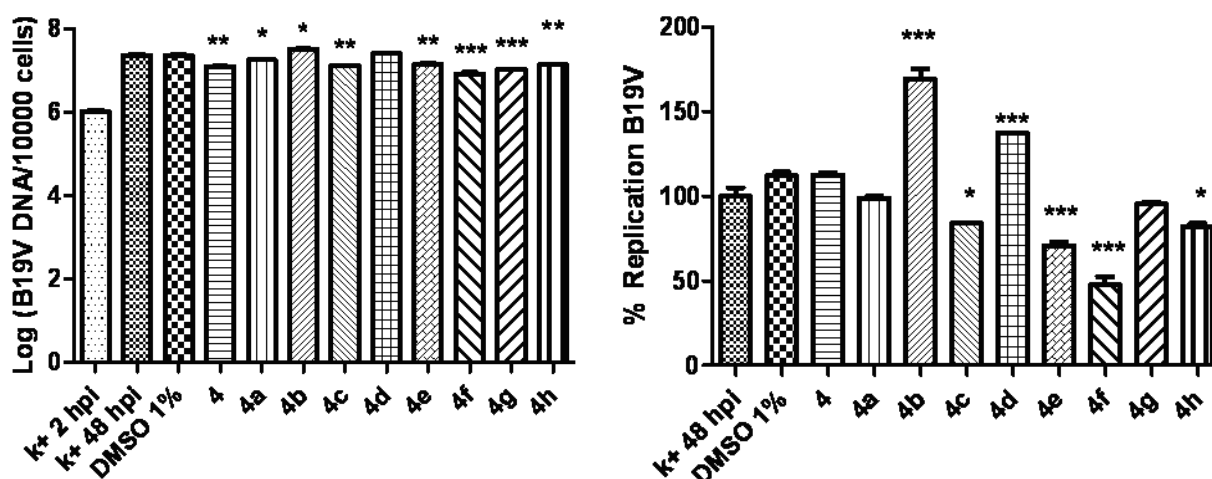
Figure 5.19: Infected EPCs at 48 hpi with B19V at moi = 10^4 geq/cell. Left) qPCR assay of the amount of B19V DNA evaluated in cellular extracts. Mean values are expressed as Log B19V geq/10.000 cells: +6,03 Log for k+ 2 hpi, +7,37 Log for k+ 48 hpi, +7,37 Log for 1% DMSO, +7,11 Log for 4, +7,26 Log for 4a, +7,51 Log for 4b, +7,11 Log for 4c, +7,40 Log for 4d, +7,16 Log for 4e, +6,92 Log for 4f, +7,04 Log for 4g and +7,15 Log for 4g; Right) Percentage of B19V replication corrected by the cell viability: compounds 4b and 4d cause an increase of viral replication (169,21% and 137,18%, respectively) while the 4f cause the major decrease (47,52%), in comparison to both the controls. The other percentages: 4: 112,37%, 4a: 98,99%, 4c: 83,95%, 4e: 70,63%, 4g: 95,47%, 4h: 82,23% [*GraphPad Prism 6.0*]. The statistical analysis is done by Dunnett test (variance test based on multiple comparison; *one-way ANOVA*). Plotted values are mean of two experiments, *p value < 0.01-0.05, ** p value < 0.001, ***p value < 0.0001.

By correcting the percentage of B19V replication relative to cell viability (ratio v/r), a relevant (v/r >2) and a significant selectivity was observed only for compounds 4 and 4c, in UT7/EpoS1 cell line. In EPCs, only the compound 4f showed a relevant (v/r >2) and

significant selectivity; while compound 4b confirmed its pro-viral effect (v/r <0,66) (figure 5.20).
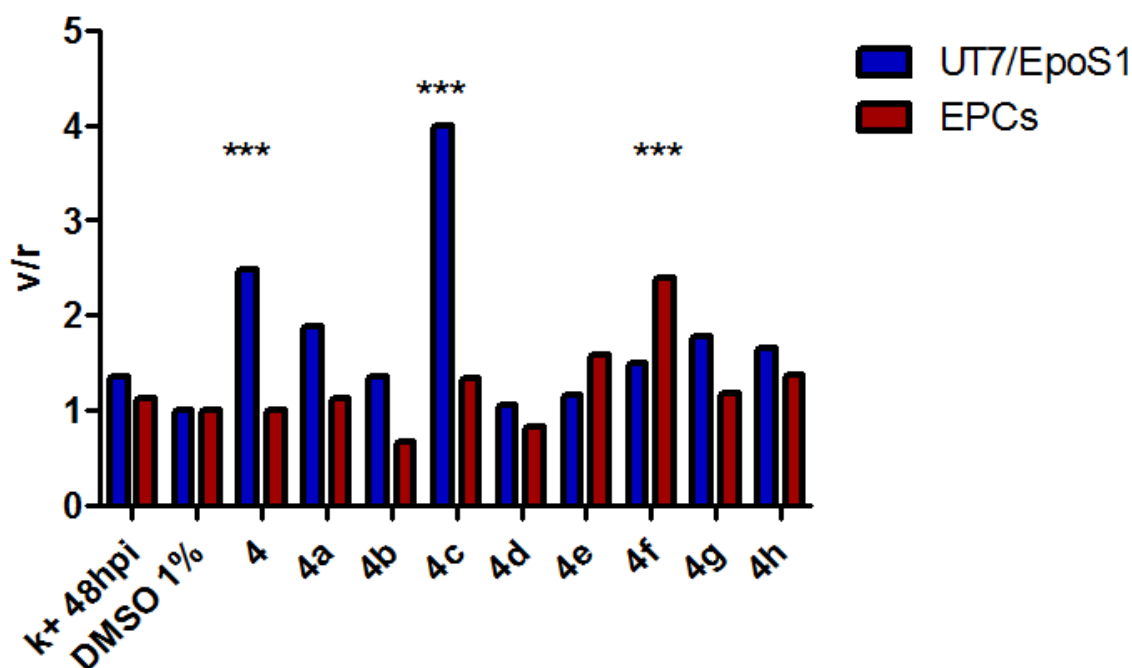
Figure 5.20: Percentage of B19V replication relative to cell viability in UT7/EpoS1 and EPCs cells for different compounds. i) v/r values for UT7/EpoS1: k+48 hpi = 1,36; DMSO = 1,00; 4 = 2,49; 4a = 1,88; 4b = 1,35; 4c = 3,99; 4d = 1,05; 4e = 1;16; 4f = 1,49; 4g = 1,77; 4h = 1,66. ii) v/r values for EPCs: k+48 hpi = 1,12; DMSO = 1,00; 4 = 1,00; 4a = 1,13; 4b = 0,66; 4c = 1,34; 4d = 0,82; 4e = 1;58; 4f = 2,39; 4g = 1,18; 4h = 1,37. The statistical analysis is done by Dunnett test (variance test based on multiple comparison; *one-way ANOVA*). Plotted values are mean of two experiments; ***p value < 0.0001.

5.3.3 Discussion

Another approach for searching antiviral compounds is constituted by screening of chemical libraries. Due to the difficulties in the cell culture systems and evaluation of viral replication, the screening of large libraries is precluded, but a serendipity approach in the screening of small libraries is feasible and justified.

By this approach, at first, 8 newly synthesized molecules (named A to H) were tested. They could be divided into different groups due to their characteristics: i) A, B, E and F were molecules comparable to a known G4 ligand (*BRACO-19*); ii) D was a coumarin derivative; iii) G and H were compounds derived since cyclic urea; iv) C had not a reference molecule.

A common protocol for screening of libraries was developed: starting from the solubilization and determination of the concentration of use for each molecules, up to the evaluation of their effects on viral replication and cells viability.

The maximal concentration of each compound at which they did not precipitate and did not cause the total cell death was first determined. At these established concentrations, the molecules were analyzed for their inhibiting action on B19V replication and for their effects on cellular system. Only the compound D showed an inhibiting action against the B19V which was not completely related to a cytotoxic effect on the cellular proliferation and viability. Actually in presence of the compound C, the B19V replication decreased significantly but this was due to the reduction of the cell viability and proliferation.

Based to the results of the first small chemical libraries, a second library of compounds derived from the coumarin analogue (compound D) was investigated for an antiviral activity against B19V.

Comarins (benzo-α-pyrone) are already used as therapeutic agents in human. Actually, they are considered a privileged structure for designing novel orally bioavailable and non-peptidic antiviral agents featuring the characteristic of a pharmacophore: a planar hydrophobic aromatic nucleus connected with a lactone group which is both responsible for hydrogen bone formation and a facilitator of a protein ligand binding [Penta et al; 2015]. Coumarin nucleus is the base of many natural products and synthetic molecules that showed inhibitory effects against replication of diverse viruses such as, HIV [Zhou et al; 2012], hepatitis [Tsay et al; 2016], herpes simplex 1-2, chikungunya and influenza A [Hassan et al; 2016]. However, the mechanism of antiviral action of coumarins is not well known; they can probably bind the RNA polymerase reducing the RNA and protein production. Actually, its structure with two rings exhibited binding interaction with the TP-1 allosteric site within the NS5B RNA polymerase of HCV and inhibited the polymerase function [Nichols et al; 2013].

A second library of 9 molecules containing the compound D or 4 and its 8 derivatives (named from 4a to 4h) were investigated using the previous established protocol. Reduction of viral replication were detected in infected UT7/EpoS1 cells and EPCs in presence of some of them, but this inhibition could be more related to the decrease of the cellular viability rather than a direct action of the compounds on the virus itself. Different effects were observed between the two cellular systems regarding both the inhibitory action on viral replication and reduction of cellular viability. Compounds 4, 4c, 4g and 4h caused a reduction in the viability of the UT7/EpoS1 cells and for the compounds 4 and 4c a selective reduction in viral replication was induced. Compounds 4, 4c and 4g caused also a reduction of cell viability in EPCs while compounds 4e and 4f induced a reduction in viral replication. However, only compounds 4 and 4c in UT7/EpoS1 cells and 4f in EPCs showed a significant and relevant inhibitory action against the replication of B19V that was not related to their

cytotoxic effect. The different effects observed within the two cellular systems could be related to different permeability and uptake mechanisms resulting in different intracellular concentrations, or to different molecules processing or interference mechanism towards replication machineries formed by a complex of the viral NS and cellular proteins.

Serendipity approach in the screening of small libraries does not always allow to identify a candidate molecule as new antiviral agent. However, serendipity is very useful for the evaluation of molecules that show partially the required purpose. Actually, these molecules could constitute the starting scaffolds for further molecular modifications in order to obtain new specific compounds with relevant antiviral activity.

5.4 Investigation of DNA G4 structures and possible ligands

5.4.1 DNA G4 structures

DNA can form several secondary structures besides the classical double helix: one that has obtained much interest in recent years is the G-quadruplex (G4). Since a hundred years ago, it was reported that concentrated guanylic acid can self-assemble, but only in 1960s the G4 phenomenon was elucidated and linked to several biological functions [Gellert et al; 1962].

The basic unit of the G4 is the G-tetrad: a planar array of four guanine bases that are linked together by Hoogsteen-bonded and stabilized by monovalent cations (figure 5.21).
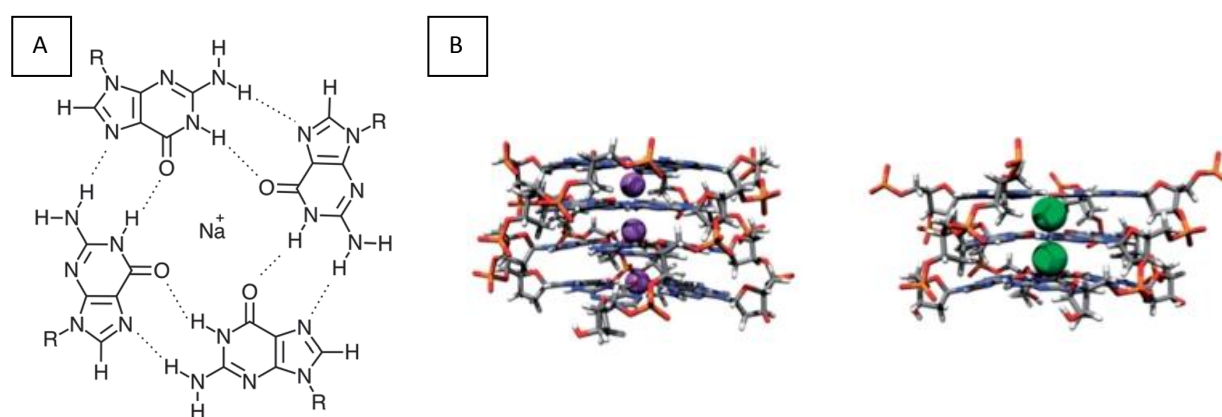
Figure 5.21: G-quadruplex structure = **A)** The basic unit of the G4 is the G-tetrad stabilized by a cation [Harris et al; 2015]; B) Parallelstacked quartets with Na^+ stabilization (purple spheres) or with K^+ stabilization (green sphere) [Lane et al; 2008].

Each G-tetrad stacks on the top of one another to form the G4 structure itself [Lane et al; 2008]. The stacked G-tetrads are connected by loops formed from mixed-sequence nucleotides: these loops can differ in both size and sequence from one G4 to another. The four strands comprising the G4 may originate from one, two or four separate strands of DNA or RNA and with a relevance for the directionality of the strands (running from the 5' end to 3' end); hence, the G4s can be inter- or intra-molecular structures [Lynne et al; 2015]. Finally, the kind of monovalent ion is important for the stability of the structure: K^+ ion gives more stability than Na^+ and Li^+ ($K^+ > Na^+ > Li^+$) [Mergny et al; 1998].

Different topologies has been identified among the G4s due to the conformation of glycosidic bonds of guanine bases in G-tetrads, the cations present and the number of stacked G-tetrads (figure 5.22). A quadruplex stem is a *parallel-stranded quadruplexes* (group I) when its strands progress in the same direction and it is characterized by guanosines with the

same glycosidic bonds angle. Instead, *antiparallel quadruplexes* can be characterized as belonging to two different types: group II and group III, respectively. In the first type (group II), the G4s are characterized by containing both sequences of guanosines with glycosidic bonds of the same types (such as *anti-anti* and *syn-syn*) as well as of different type (such as *syn-anti* and *anti-syn*). While the antiparallel quadruplexes of the group III are characterized by consecutively stacked guanosines of distinct glycosidic bonds [Karsisiotis et al; 2011].

A long-standing question has been whether this structures form and persist from the relatively stable DNA double helix. For this occur, G4 structure formation must be preceded or accompanied by localized unwinding of the double helix. Actually, active transcription results in a negative superhelicity behind the transcriptional machinery, and this can provide the torsional stress required for unwinding of the double helix and the formation of G4s [Sun et al; 2009].
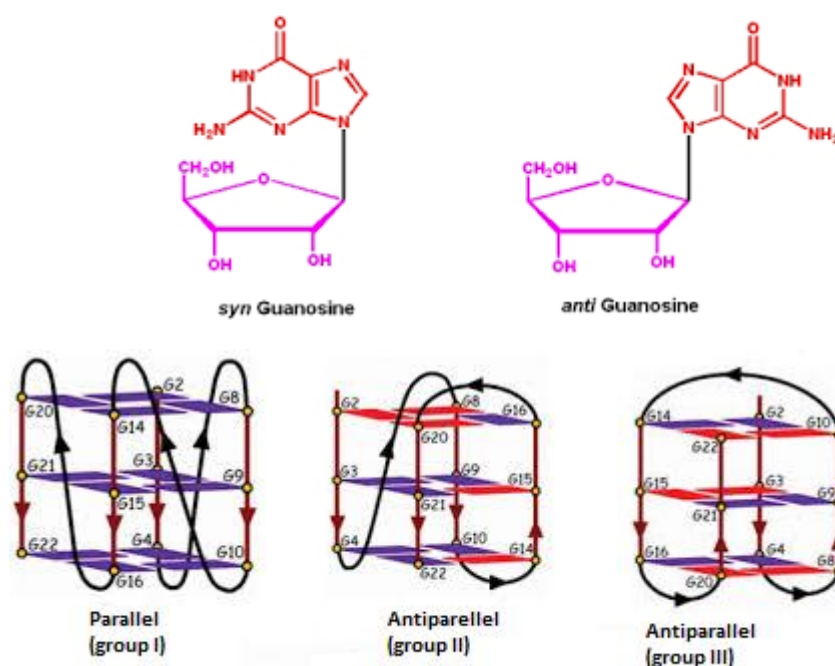
Figure 5.22: Top = chemical structures of *anti* and *syn* glycosidic bonds. Bottom = schematic representation for the three structurally determined G-quadruplezes topologies. Guanosines in red are *syn*, and those in blue are *anti* [Singh et al; 2016].

In theory, G4 structures can arise anywhere in the nucleotide sequences where sufficiently long stretches of single-stranded G-rich DNA/RNA are exposed during replication, transcription and recombination [Henderson et al; 2014]. Predictive algorithms, such as QGRS Mapper, have been developed to identify "putative quadruplex sequences" (PQS) within nucleic acid sequences of different length and within oligonucleotides [Kikin et al; 2006]. Use of these algorithms has revealed that PQS are overrepresented in gene regulatory

regions, such as telomeres. RNA G4s are present in transcripts associated with telomeres, in non-coding regions of primary transcripts and also in mature transcripts.

The regions in which PQS occur are linked to the specific functions of G4s at these locations. For example, G4 structures are proposed to be involved in telomere maintenance at both DNA and RNA level [Huppert et al; 2007]. G-rich telomeric repeats can form G4s and protect telomeres forming the telomere capping in *Saccharomyces cerevisiae,* when natural capping is compromised, preventing their identification by cellular surveillance mechanism, as unwanted DNA breaks. In addition, telomeric G4s protect the telomeric 3' single-stranded DNA overhang from being recognized by telomerase activity and so, they are important to regulate the telomerase activity [Smith et al; 2011].

In promoter regions, the behavior of G4s may be directly involved in gene regulation at the level of transcription. For example, c-MYC is a transcription factor whose expression is linked to cell proliferation and tumorigenesis. Its major regulator of transcription contains a PQS that forms G4 *in vitro* and which represses the transcription of c-MYC. Additionally, the G4s ligand TMPyP4 [Mesotetra(N-methyl-4-pyridyl)porphine] reduces c-MYC expression stabilizing the G-quadruplex structure in lymphoma cell lines [Siddiqui-Jain et al; 2002].

Certain helicases possess G4-resolving activity to aid transcription through these four-stranded structures. Disruption of G4-resolving helicases (such as FANCJ) in human cell lines results in genetic instability and elevates DNA damage [Henderson et al; 2014]. Hence, it is hypothesized that G4s could be used alongside inhibitors of DNA repair or associated pathway to inhibit tumorigenesis.

In RNA transcripts, G4s may play roles in pre.mRNA processing, translation and RNA turnover. In addition, they can contribute to telomere heterochromatinisation. Actually, human telomeres are transcribed to produce long, noncoding telomeric containing RNAs (TERRAs), that consist of G-rich sequences and adopt a G4 RNA structure [Lynne et al; 2015].

Other than a number of helicases that preferentially bind and disrupt DNA G4s, many proteins and molecules have been identified which interact physically and/or functionally with G4s stabilizing them in a variety of organisms. Compounds that induce and/or stabilize G4 formation can be used to investigate the biological roles of G4s, such as the acridine derivative *BRACO-19* and PDS (*Pyridostatin*). *BRACO-19* binds the G4 structures showing antiviral activity against HIV [Perrone et al; 2015] and also an anti-tumor activity both in 21NT human breast cancer cells and in mice bearing advanced stage of A431 human vulval carcinoma [Gowan et al; 2002]. PDS induces DNA damage and cell cycle arrest binding the

G-quadruplexes. Hence, it exhibits antiproliferative effects and induces dysfunctional telomeres in various cancer cell lines [Rodriguez et al; 2012].

G-quadruplexes affect also virulence processes in many bacterial and viral pathogens; for example the disruption of the G4s through site-directed mutagenesis prevented the recombination during the antigen variation in *Neisseria gonorrhoeae* [Cahoon et al; 2013]. This process is important for pathogens to express different versions of their surface epitopes in order to evade detection by the host immune system. Other than antigenic variation, G4s have been proposed to contribute to antigenic diversity. Actually, the failure to resolve G4 structures during the genome replication can lead to error-prone recombinational repair that may result in the diversification of antigens repertoires of *Saccharomyces cerevisiae* [Lopes et al; 2011], or changing in the epigenetic state of adjacent chromatin [Paeschke et al; 2013]. Interestingly, replication-dependent instability of G4 motifs was affected by the direction of the replication fork: it occurs only when the G4 was in the leading-strand template (figure 5.23).
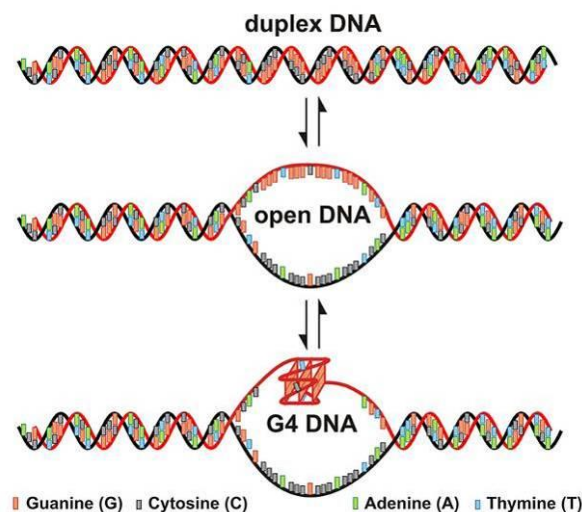
Figure 5.23: Negative superhelicity behind the transcriptional/replicational machinery provide the torsional stress for the formation of G-quadruplex structures within the leading strand.

Recent research suggests that viruses may use G4s as cis-acting regulatory elements in gene-expression. The HIV-1 Long Terminal Repeat (LTR) controls viral transcription and it contains two-intramolecular G4s within its promoter region. Mutations that disrupt G4s or the addition of a G4-stabilising ligand (*BRACO-19*) resulted in increased and decreased promoter activity, respectively, suggesting that G4s may regulate HIV-LTR promoter activity [Perrone et al; 2013]. G4s may also play a role in the latency program of herpers-viruses influencing the expression of mRNAs that are known to regulate their self-synthesis in Epstein-Barr virus

(EBV) [Murat et al; 2014] and in herpes simplex-1 (HSV-1) [Artusi et al; 2016]. Finally, G-rich regions of some human papillomavirus (HPV) genomes are able to form G4 structures that may be responsible of regulatory functions in this virus [Tuckova et al; 2013].

Many tools have been developed to analyze G4s at both genome-wide and sequence-specific levels. In addition to the predictive algorithms, several experimental techniques can determine whether the biophysical features of a putative PQS are consistent with G4 structure formation. These include thermal denaturation, ultraviolet spectroscopy, dimethylsulfate footprinting, circular dichroism spectroscopy and nuclear magnetic resonance [Lynne et al; 2015]. G4-structure specific antibodies have been developed to visualize G4s in both genomic DNA and cytoplasmic RNA of a range of mammalian cells [Biffi et al; 2013 – Henderson et al; 2014] and in viral infected cells, such as HSV-1 infected Vero cell line [Artusi et al; 2016].

5.4.2 G4 in B19V DNA: Bioinformatic Analysis

The genome of Human Parvovirus B19 was analyzed by the web-based server *QGRS Mapper* which allowed to predict the presence of G-quadruplex (G4) structures in nucleotides entries. In particular the predictions by this open source Software were based by using the following motif: $G_xN_{y1}G_xN_{y2}G_xN_{y3}G_x$

Different parameters were set: 30 bases as length of the G4 structure, 2 as minimum number of Guanine and 15 nucleotides as maximum length of the loop. As result, the QGRS Mapper gave predictions of putative G4 structures within the B19V ITRs and in particular in the region near the asymmetry site (figure 5.24).

For each prediction, the software gave a score (from 0 to 100) that evaluated the capability of the PQS predictions (PQS: Putative Quadruplex Sequence) to form a stable G-quadruplex and so to exist in nature. However, a clear definition of "good" or "bad" score and so good or bad G-quadruplex candidates was not indicated by the *QGRS Mapper*. Hence, higher was the score and better candidates were the PQSs (for example, a G-score of 100 was linked to a nucleotide sequence made of only Guanine and not present in nature).
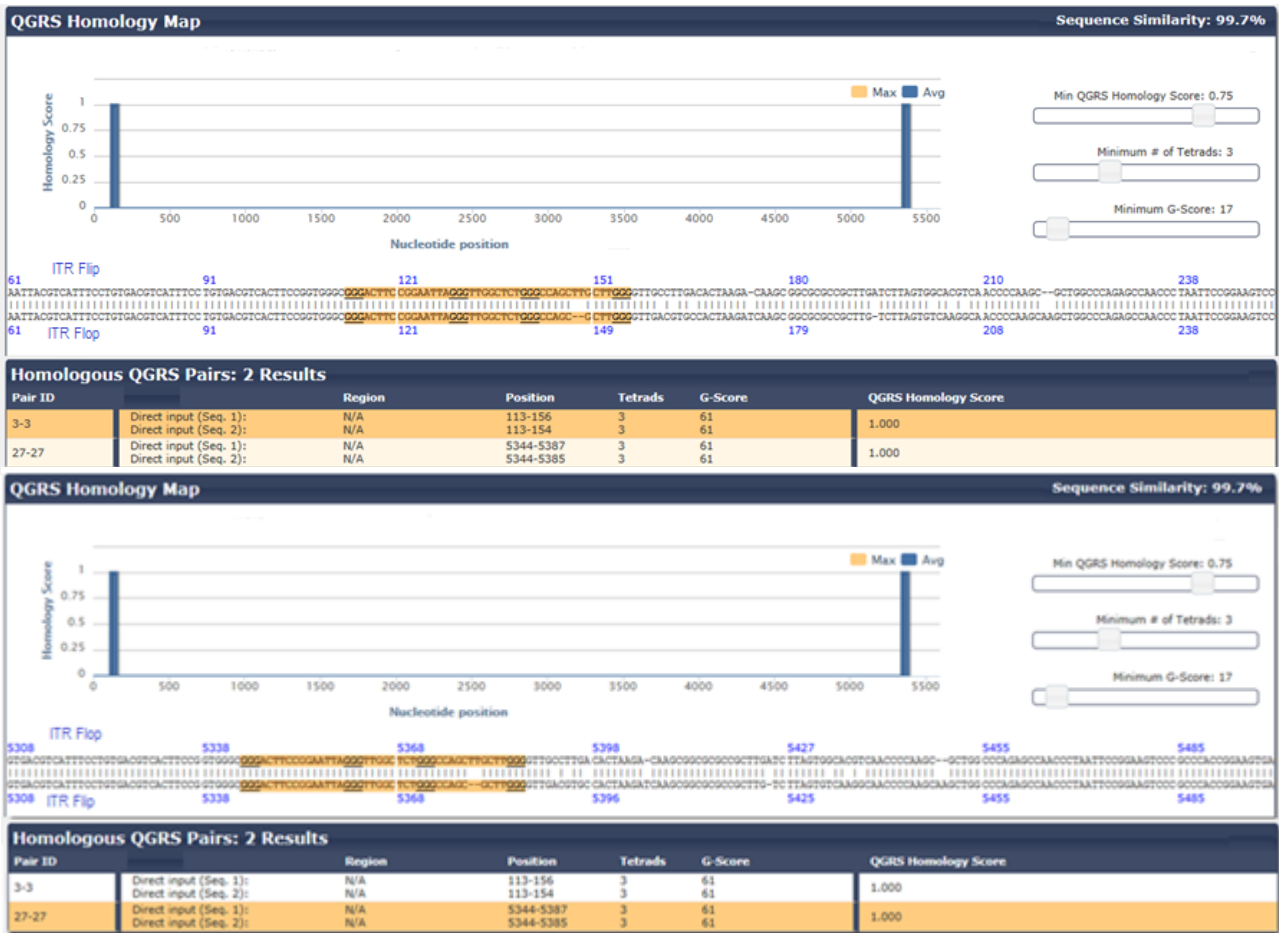
Figure 5.24: PQS predictions on B19V ITRs by QGRS Mapper = regions with higher score are near the asymmetry sites, as shown by the bars in the diagrams.

The results of the predictions within the B19V ITRs together with a known parallel G-quadruplex structure (LTR-II HIV; [Perrone et al; 2013]) are shown in the following table:

Oligos	Length	QGRS	G-Score
PQS113	42	**GGG**ACTTCCGGAATTA**GGG**TTGGCTCT**GGG**CCAGCGCTT**GGG**	67
PQS140	44	**GGG**CCAGCTTGCTT**GGGG**TTGCCTTGACACTAAGACAAGC**GG**	14
PQS68	45	**TCATTTCCTGTGACGTCATTTCCTGTGACGTCACTTCCGGTGGGC**	0
LTR-II HIV	33	**GGGG**ACTTTCCA**GGG**A**GGCGTGGCCT**GGG**C**GGG**	62

5.4.3 Analysis of G-quadruplex structures and interaction with G-quadruplex ligands

As mentioned previously, computational analysis by *QGRS Mapper* software allowed to predict putative G-quadruplex sequences (PQS) within the ITRs of Human Parvovirus B19, in

the region close to the asymmetry site. G-quadruplex ligands are available: hence, two of them (*BRACO-19* and *Pyridostatin*) were tested for their putative interactions with the predicted B19V putative G4 sequences both in chemical and in biological studies.

In order to confirm the bioinformatic predictions, B19V oligonucleotides containing the PQS were synthesized and analyzed by Circular Dichroism (CD). In fact, CD analyses consent to detect the G4 structures and to distinguish among their different conformations (parallel and antiparallel). In particular, the three oligonucleotides from B19V DNA were synthesized and analyzed: 1) PQS68: a 45 bases long oligonucleotide from the 68 position within B19V DNA (MW = 13752 Da) and with a G-score of 0 by QGRS Mapper, so it acted as negative control; 2) PQS113: a 45 bases long oligonucleotide from the position 113 within B19V DNA (MW = 14012 Da) and with a G-score of 67; 3) PQS140: a 44 bases long oligonucleotide from the 140 position within B19V DNA (MW = 13630 Da) and with a G-score of 13. In addition, a 33 bases long from LTR-II HIV (MW= 10349 Da) was synthesized and analyzed as positive control since it was already detected as parallel G-quadruplex by circular dichroism study and its interaction with *BRACO-19* and PDS (*Pyridostatin*) was confirmed [Perrone et al; 2013]. The synthesized oligonucleotides with their respective G-scores are shown in the previous table.

The oligonucleotides were diluted at concentration of 2 μM in 70 mM KCl buffered with 20 mM KAc at pH 6.8 and they were analyzed by CD with or without the G-quadruplex ligands. Actually, the K^+ ions were important for the study of the G-quadruplexes by CD analysis because the positive charges stabilized their structures allowed their identification. The same stabilization should be done by the G4 ligands (all the CD analysis were performed by the group of Professor M. Bartolini; FaBiT, University of Bologna).

Firstly, the four oligonucleotides were analyzed by circular dichroism without *BRACO-19* and PDS, in order to compare their spectra and to confirm the capacity of CD analyses for identifying G-quadruplexes. The CD spectrum of LTR-II HIV can be interpreted as the overlap between the contribution of a parallel G4 structure (containing a strong positive band at around 265 nm) and the profile of a GC-rich (76%) ssDNA in B-form, confirming it as positive control. The spectrum for PQS68 was comparable to that of the B-form ssDNA without any particular structures, so it acted as negative control. PQS113 and PQS140 showed different spectra in comparison to LTR-II HIV and PQS68 (figure 5.25).
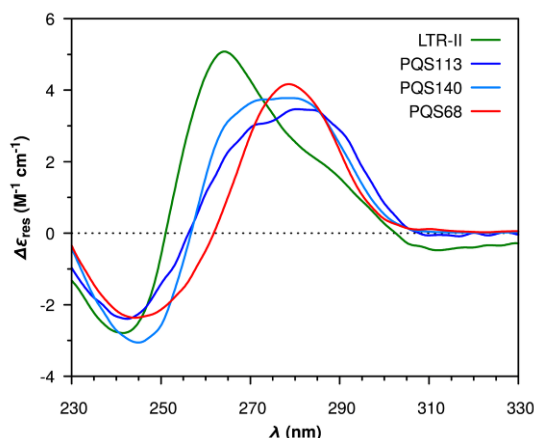
Figure 5.25: Circular dichroism analysis of the 4 synthesized oligonucleotides = LTR-II HIV (green) shows a typical parallel G4 spectrum with a positive peak at λ= 265 nm and a negative peak at λ= 245 nm; PQS68 (red) shows a spectrum comparable to the one identified for the form B of double helix DNA with a positive peak at about 290 nm and a negative peak at about 240 nm; PQS113 and PQS140 show different spectra than both the positive and the negative control. Obtained spectra are obtained by subtracting the buffer spectrum [*Jasco Spectra Manager 2*].

CD analyses of the oligonucleotides were also obtained in presence of different concentrations of *BRACO-19* and PDS. In particular, 10 and 20 μM of the compounds were added to the previously denatured oligonucleotides (respectively, ratio compound/oligonucleotide = 5:1 and 10:1) in order to allow their interactions whether possible. LTR-II HIV showed both an increase of the signal and a shift of the positive peak towards λ= 295 nm (CD signal for antiparallel G4) for the CD spectrum in presence of *BRACO-19* while the variation of the CD spectrum in presence of PDS was more difficult to interpret due to the interference of the "induced CD signal". This last was caused by a new signal due to the interactions between the two analyzed molecules. PQS68 did not show changes of the CD spectrum in presence of *BRACO-19* while PDS probably formed aggregates. Finally, changes in CD signal were detected for the oligonucleotides of interest (PQS113 and PQS140) in presence of *BRACO-19*: an increase of the positive peak and its shift towards λ=285 nm was observed for PQS113 and a new positive peak at about 300 nm was evaluated for both (figure 5.26). The signal caused by PDS was more difficult to evaluate due to its "induced circular dichroism". Indeed, both *BRACO-19* and PDS did not show CD signals when they were analyzed alone, hence the CD changes in presence of the oligonucleotides were possibly caused by their interactions.
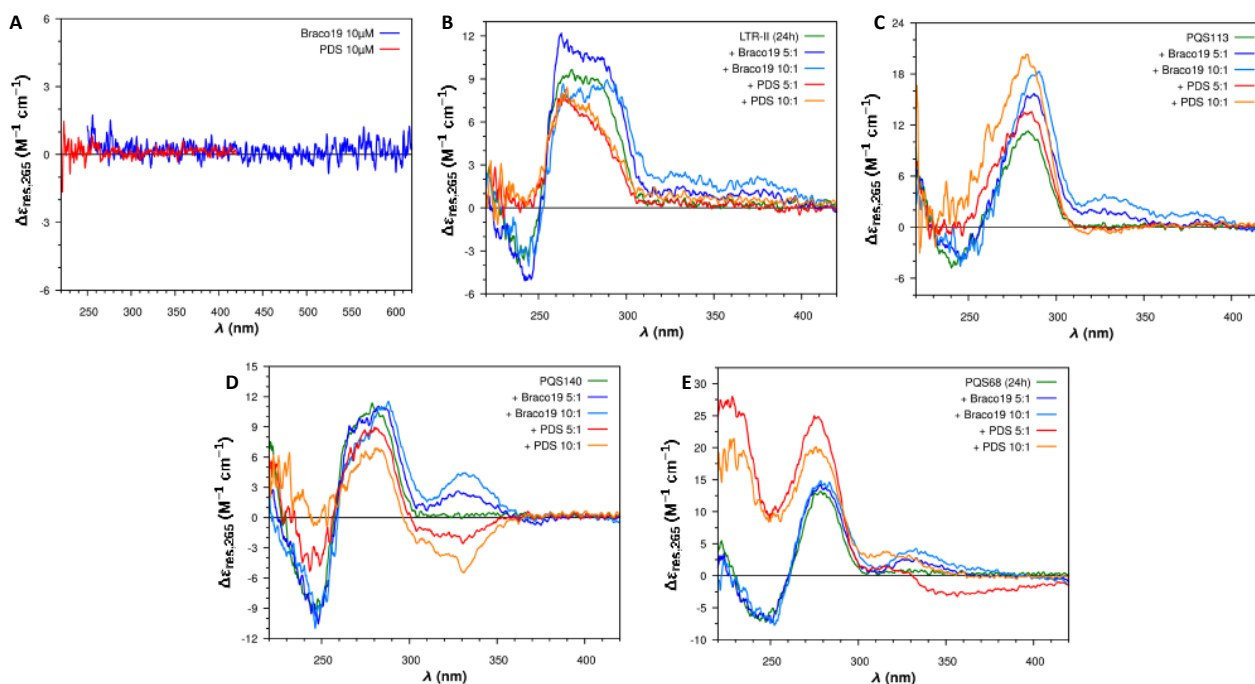
Figure 5.26: Circular dichroism analysis of the 4 synthesized oligonucleotides in presence of *BRACO-19* and *Pyridostatin* (G4 ligands) = A) CD spectra of only *BRACO-19* (blue) and PDS (red) at 10 μM of concentration: the compounds alone do not show CD signals; B) LTR-II HIV shows an increase of the signal and a shift towards 295 nm in presence of *BRACO-19*; C) PQS113 increases its positive peak and shows a shift towards 285 nm in presence of *BRACO-19*, an increase of CD signal at 330 nm is observed; D) PQS140 shows a positive peak at 330 nm in presence of *BRACO-19*; E) PQS68 does not change CD spectrum in presence of *BRACO-19*;. PDS causes a "induced Circular Dichroism" signal which interferes and alters the analysis. Spectra are obtained by subtracting the buffer spectrum.

Then, the 4 oligonucleotides were analyzed for their melting temperature without and with *BRACO-19*. Actually, GC-rich sequences melt at higher temperatures than AT-containing ones and compounds that bind double-strand DNA selectively stabilize this form in comparison to the single stranded random-coil, so increasing its melting temperature [Rachwal et al; 2007].

LTR-II HIV, PQS68, PQS113 and PQS140 were diluted at 2 μM concentration, in the presence of 70 mM KCl buffered with 20 mM KAc at pH 6.8. Oligonucleotides with/without *BRACO-19* were analyzed; as for CD, G4 ligand was added at 10 μM concentration, after a denaturation step of 30 minutes at 95°C. Data were collected during both melting ("heating curve") and annealing ("cooling curve") in order to assess the reversibility of the transition.

The CD melting curves of LTR-II HIV at 265 nm confirmed the presence of the ordered DNA secondary structure, both in absence and in the presence of *BRACO-19*. In particular, the G-quadruplex showed a clear disruption upon thermal denaturation (figure 5.27) and a

fully reversible profile upon renaturation. In presence of the compound, the parallel G4 structure was stabilized, actually, the T_m of the melting curves shifted of about +7°C toward higher values (figure 5.28).

The CD melting profiles of PQS113 at 290 nm in absence of *BRACO-19* showed a conformational transition upon denaturation and renaturation at low temperature, indicating an intrinsic degree of instability. This data was confirmed by the large uncertainty of its T_m value determined by non-linear regression on the cooling ramp (figure 5.28). A reversible conformational transition upon thermal denaturation/renaturation was detected within the CD melting profiles of both PQS140 and PQS68, in absence of *BRACO-19*. However, the magnitude of the change for these latter oligos in CD response at 285 nm along the temperature ramp was smaller than that observed with LTR-II HIV (figure 5.28). Indeed, the CD profiles during the heating ramp of all the B19V oligonucleotides suggested the presence of a ssDNA in B-form with no clear contribution from G-quadruplex structures (figure 5.27); the differences among the CD profiles were probably due to their different primary structures [Kypr et al; 2009].
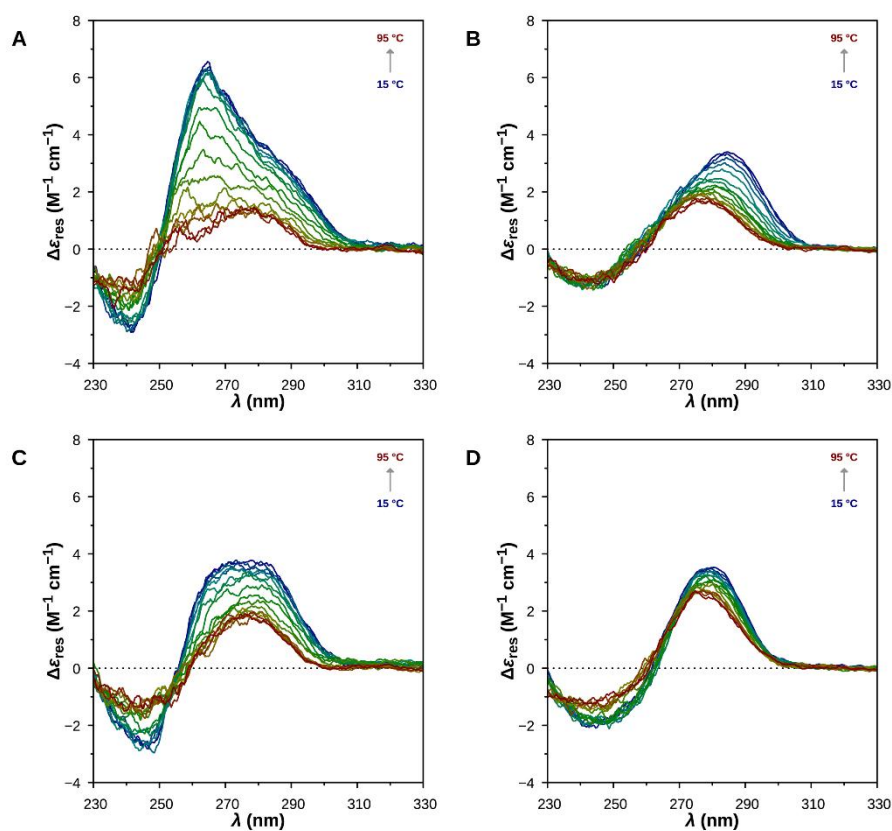
Figure 5.27: Circular dichroism analysis of the oligonucleotides (2 μM) during the heating ramps of the melting assays = A) LTR-II HIV; B) PQS113; C) PQS140; D) PQS68. The CD spectrum of LTR-II HIV shows the higher disruption upon thermal denaturation in comparison to the other oligonucleotides.

118

In presence of *BRACO-19*, the CD melting profiles of the oligonucleotides of interest suggested the occurrence of binding. The melting curves of PQS140 and PQS68 were not reversible, with the T_m values derived from the heating ramps higher than the T_m determined from the cooling ramps. Probably, this phenomenon of hysteresis was due to a slower kinetics of denaturation/renaturation induced by the presence of the G4 ligand [Mergny et al; 2003]. PQS113 added of BRACO-19 showed the more complex CD melting profile, with a possible two-state conformational transition that precluded the accuracy of the non-linear regression on the melting ramps.
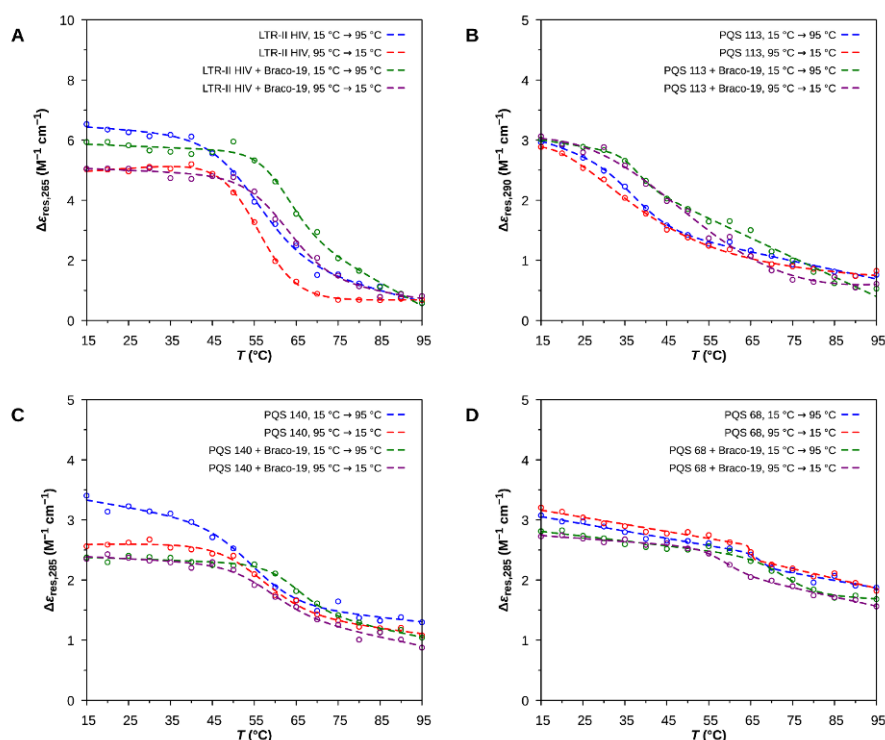
Figure 5.28: CD melting curves for the oligonucleotides under investigation (2 μM), both in absence or in the presence of BRACO-19 (10 μM) = A) LTR-II HIV; B) PQS113; C) PQS140; D) PQS68.

The Mid-transition temperatures (T_m, in °C) for the oligonucleotides under investigation, both in the absence or in the presence of *BRACO-19* (10 μM), as determined by CD melting assays are described in the following table:

	$\lambda_{\Delta_{max}}$ (nm)	Isolated oligonucleotide (2 μM)		Oligonucleotide (2 μM) + Braco-19 (10 μM)	
		15 °C → 95 °C	95 °C → 15 °C	15 °C → 95 °C	95 °C → 15 °C
LTR-II HIV	265	55.0 ± 1.4	55.9 ± 0.4	61.8 ± 1.5	62.4 ± 1.6
PQS 113	290	37.4 ± 2.4	0.3 ± 81.5	37.3 ± 2.5	45.3 ± 16.7
PQS 140	285	54.6 ± 2.3	56.2 ± 1.8	64.7 ± 1.7	57.8 ± 2.8
PQS 68	285	67.3 ± 2.8	65.0 ± 6.6	73.3 ± 3.3	58.1 ± 1.4

Since the experimental results suggested the absence of G-quadruplex structures within the B19V ITRs and the previous research showed difficulty of *Pyridostatin* solubilization and analysis, the CD melting assays were not done in presence of this latter compound.

5.4.4 Biological studies

In addition to the chemical studies (CD measurements), biological studies about G-quadruplexes within the viral DNA were performed. In particular, the two G4 ligands *BRACO-19* and PDS were investigated for their putative activity against Human Parvovirus B19 replication. Firstly, their action on cellular viability was tested for the UT7/EpoS1 cells. Different dilutions from 500 µM to 1 µM of the compounds in the respective cellular medium were prepared. UT7/EpoS1 cells were cultured in presence of the *BRACO-19* or PDS at the established concentration for 48 hours; after that, the cellular vitality was analyzed by CCK8 assay. Cells cultured in medium without compounds and medium with 10% DMSO were used as controls.

In UT7/EpoS1 cells, both *BRACO-19* and PDS were toxic for the cells at concentrations ≥100 µM: actually, the viability of the cells was reduced to 46 – 22% at 250 µM in presence of *BRACO-19* or PDS, respectively; a decrease below the 5% of viability (1,62 – 3,16%, respectively) was detected at 500 µM of both the compounds (figure 5.29).
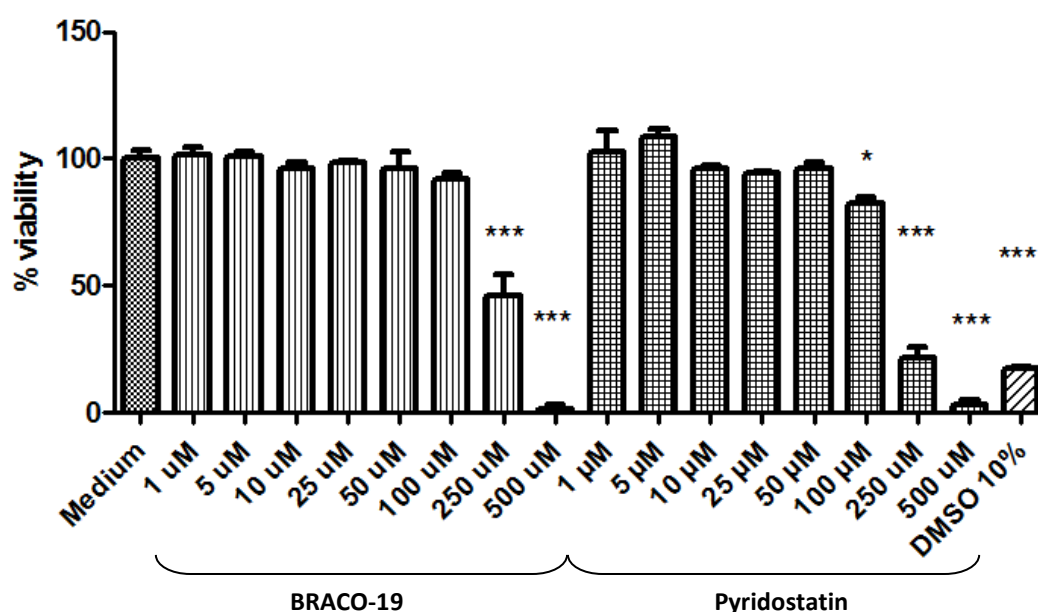
Figure 5.29: Representative graph of the percentages for the living UT7/EpoS1 in presence of different dilutions of G4 ligands by CCK8 assay: i) Medium = 100%; ii) BRACO-19 = 1 µM 101,53%, 5 µM 100,99%, 10 µM 96,22%, 25 µM 98,61%, 50 µM 96,42%, 100 µM 91,84%, 250 µM 46,17%, 500 µM 1,62%; iii) PDS 1 µM 102,46%, 5 µM 108,96%, 10 µM 95,95%, 25 µM 94,10%, 50 µM 96,30%, 100 µM 82,38%, 250 µM

21,39%, 500 µM 3,16%; iv) 10% DMSO = 17,53%. The statistical analysis is done by Dunnett test (variance test based on multiple comparison; *one-way ANOVA*). Plotted values are mean of one experiment done in triplicate each one; *p value < 0.01-0.05, ***p value < 0.0001 [*GraphPad Prism 6.0*].

Since the 250 and 500 µM of both compounds were toxic for UT7/EpoS1 cells, dilutions starting from 100 µM were tested to evaluate the G4 ligands effect on EPCs viability. As previously, EPCs were cultured in presence of *BRACO-19* and PDS at the established concentrations and after 48 hours, the cellular vitality was tested by CCK8 assay. Cells cultured in medium without compounds or medium with 10% DMSO were used as controls.

In EPCs, *BRACO-19* and PDS were more toxic than in UT7/EpoS1 (figure 5.30). Actually, the EPCs viability was reduced to 1,43% at ≥50 µM of *BRACO-19* (1% of viability with 100 µM of the compound); while PDS caused the decrease of cellular viability to 71,59% at 1 µM of concentration, 24,62% at 5 µM and below 10% at 10 µM (8,11% at 10 µM and around 0% at 50 µM and 100 µM).
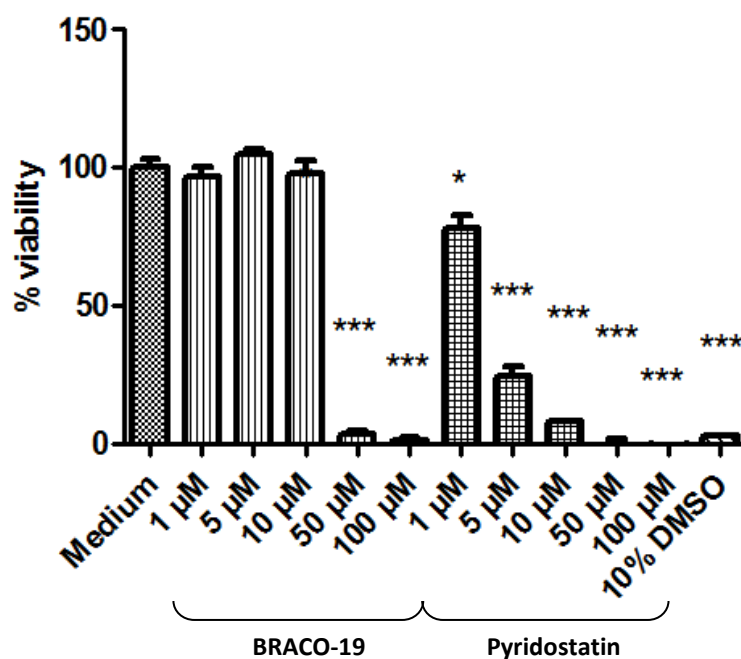
Figure 5.30: Representative graph of the percentages for the living EPCs in presence of different dilutions of G4 ligands by CCK8 assay: i) Medium = 100%; ii) BRACO-19 = 1 µM 96,87%, 5 µM 104,87%, 10 µM 97,95%, 50 µM 3,60%, 100 µM 1,02%; iii) PDS = 1 µM 77,92%, 5 µM 24,62%, 10 µM 8,11%, 50 µM 0,08%, 100 µM 0,00%; iv) 10% DMSO = 1,68%. The statistical analysis is done by Dunnett test (variance test based on multiple comparison; *one-way ANOVA*). Plotted values are mean of three experiments done in triplicate each one; *p value < 0.01-0.05, ***p value < 0.0001 [*GraphPad Prism 6.0*].

Both the cellular systems were infected by B19V viremic serum at moi of 10^4 geq/cell and were grown for 48 hours in presence of the two G-quadruplex ligands at the diverse

concentrations. Infected cells grown in complete medium without compounds were used as controls. Cells were collected at different time points (2 and 48 hpi) and used for evaluating viral capsid proteins production and DNA replication by IIF assay and qPCR assay, respectively.

By IIF assay, positive cells for VP capsid proteins were observed in infected UT7/EpoS1 in presence of all *BRACO-19* tested concentrations (10-50-100 μM) and comparable to the control. A lower number of VP positive cells were detected in presence of PDS, especially at 100 μM concentration (figure 5.31). However, this effect could be due to the presence of compound precipitates and to the difficulty for detecting VP positive cells caused by a high background staining by the compound itself.
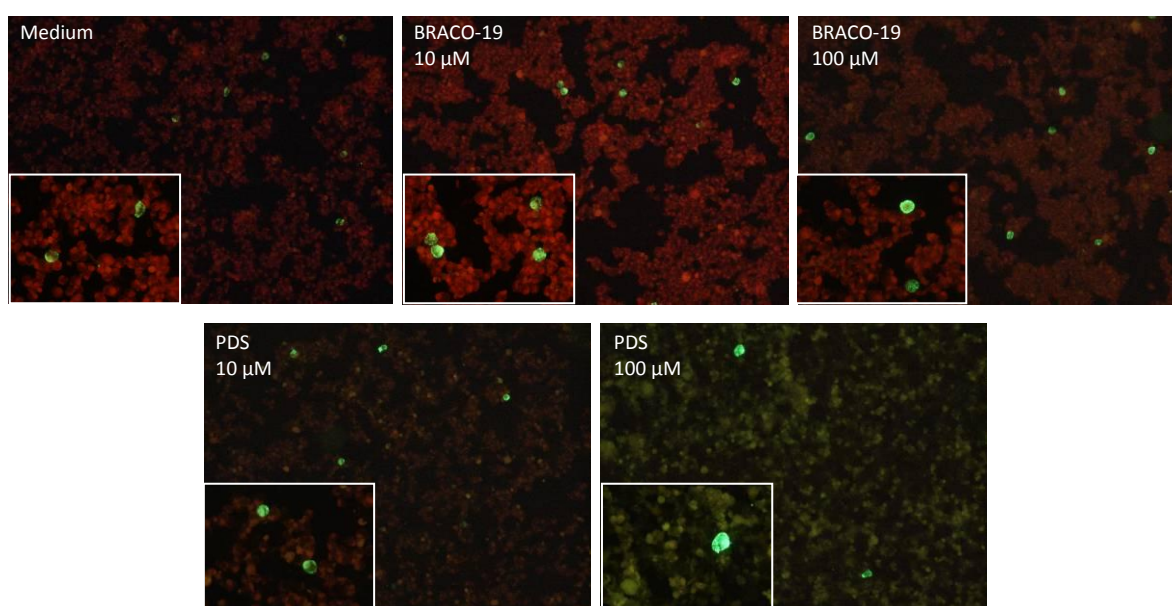
Figure 5.31: Pictures of IIF anti-VP assay for B19V infected UT7/EpoS1 (48 hpi) that are grown in different conditions (10x and 40x magnification) = Medium) UT7/EpoS1 complete culture medium (control); BRACO-19 10 μM) Ligand BRACO-19 at concentration of 10 μM: number of VP positive cells is comparable to the control; BRACO-19 100 μM) Ligand BRACO-19 at concentration of 100 μM: number of VP positive cells is comparable to the control; PDS 10 μM) Ligand Pyridostatin at concentration 10 μM: number of positive cells is comparable to the control and the negative cells are less red in colour for the Evans Blue staining due to the G4 compound; PDS 100 μM) Ligand Pyridostatin at concentration 100 μM: number of positive cells is lower than the control and the negative cells are white in colour for the G4 compound precipitation.

Concordant results were obtained by qPCR assay: *BRACO-19* did not interfer on B19V replication in UT7/EpoS1 cells, while a decrease of viral DNA was detected only in presence of 50 and 100 μM of PDS in cellular extracts at 48 hpi, however without inhibiting completely the viral replication. Correcting the viral DNA production for the cell viability

evaluated by CCK8 assay, lower percentages of B19V replication were obtained for 50 and 100 μM PDS (figure 5.32).
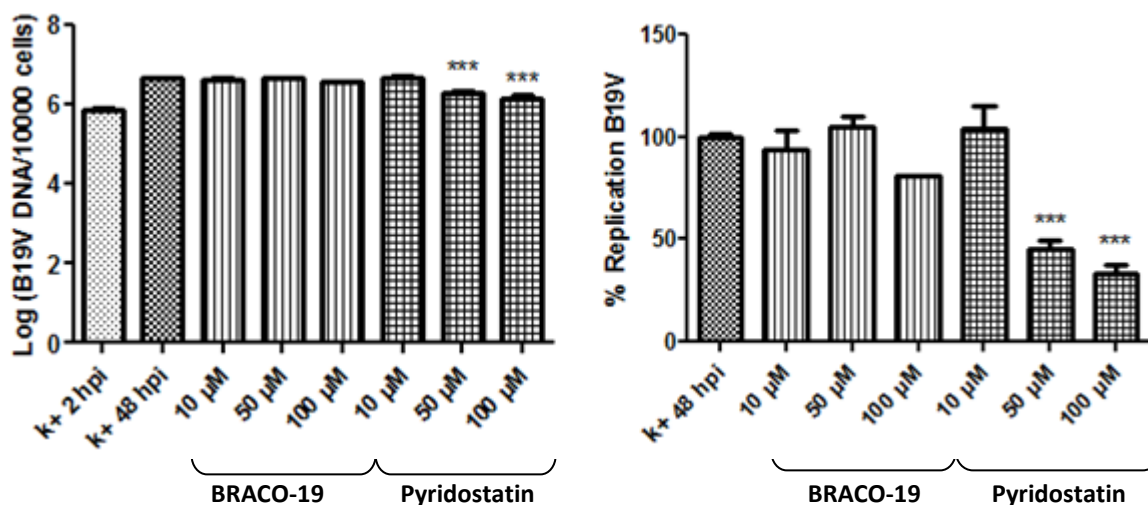
Figure 5.32: Infected UT7/EpoS1 at 48 hpi with B19V at moi = 10^4 geq/cell. Left) qPCR assay of the amount of B19V DNA evaluated in cellular extracts. Mean values are expressed as Log B19V geq/10.000 cells: +5,86 Log for k+ 2 hpi, +6,64 Log for k+ 48 hpi, +6,61 Log for 1 μM, +6,66 Log for 50 μM, +6,55 Log for 100 μM (BRACO-19), +6,66 Log for 1 μM, +6,29 Log for 50 μM, +6,16 Log for 100 μM (PDS); Right) Percentage of B19V replication corrected by the cell viability: data of 50 and 100 μM PDS probably suffer the PDS precipitation in the medium: 10 μM 93,55%, 50 μM 104,84%, 100 μM 81,11% (BRACO-19), 10 μM 104,22%, 50 μM 45,23%, 100 μM 33,46% (PDS) in comparison to the k+ 48 hpi (100% of viability) [*GraphPad Prism 6.0*]. The statistical analysis is done by Dunnett test (variance test based on multiple comparison; *one-way ANOVA*). ***p value < 0.0001.

B19V infected EPCs showed positive cells for VP capsid proteins at the lowest concentrations of both G4 ligands and comparable to the control. A lower number of positive cells were observed at the 50 and 100 μM of the compounds probably due to their cytotoxic effect (figure 5.33).

By qPCR assay, decrease of B19V replication was observed at the highest concentration of both the compounds. The virus infectivity was inhibited in presence of both 50 and 100 μM of the G4 ligands showing amount of B19V DNA comparable to the 2 hpi extract of the control (figure 5.34).

Probably the reduction of viral replication was due to the decreasing of cellular viability in presence of the compounds. Actually, correcting the viral DNA production for the cell viability evaluated by CCK8 assay, the percentages of B19V replication in presence of the highest G4 ligands concentrations increased reaching and overcoming the 100% of replication (control: k+ 48 hpi).
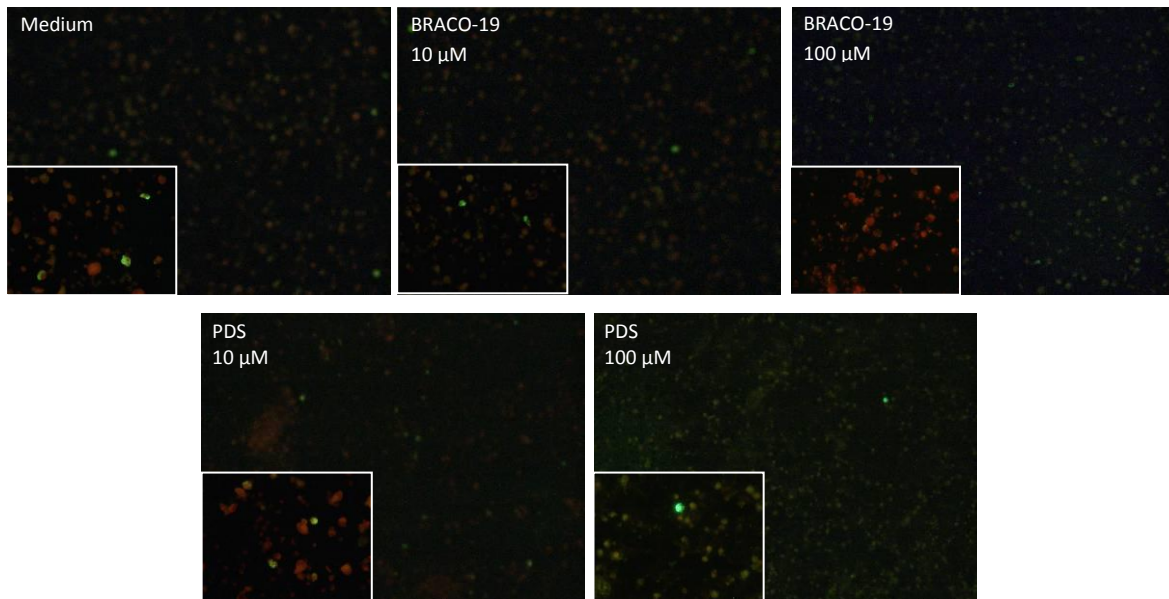
Figure 5.33: Pictures of IIF anti-VP assay for B19V infected EPCs (48 hpi) that are grown in different conditions (10x and 40x magnification) = Medium) EPCs complete culture medium (control); BRACO-19 10 µM) Ligand BRACO-19 at concentration of 10 µM: number of VP positive cells is comparable to the control; BRACO-19 100 µM) Ligand BRACO-19 at concentration of 100 µM: no green positive cells are detected; PDS 10 µM) Ligand Pyridostatin at concentration 10 µM: number of positive cells is comparable to the control; PDS 100 µM) Ligand Pyridostatin at concentration 100 µM: number of positive cells is lower than the control and the negative cells are white in colour for the G4 compound precipitation.
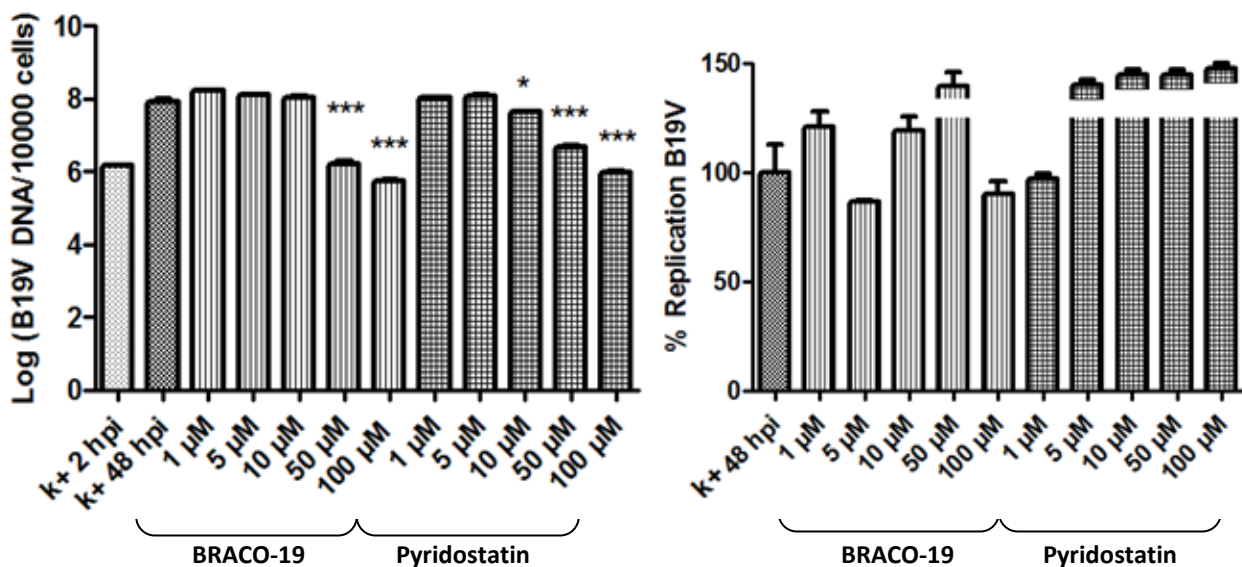
Figure 5.34: Infected EPCs at 48 hpi with B19V at moi = 10^4 geq/cell. Left) qPCR assay of the amount of B19V DNA evaluated in cellular extracts. Mean values are expressed as Log B19V geq/10.000 cells: +6,17 Log for k+ 2 hpi, +7,92 Log for k+ 48 hpi, +8,20 Log for 1 µM, +8,09 Log for 5 µM, +8,03 Log for 10 µM, +6,19 Log for 50 µM, +5,74 Log for 100 µM (BRACO-19), +8,01 Log for 1 µM, +8,07 Log for 5 µM, +7,64 Log for

10 μM, +6,67 Log for 50 μM, +5,97 Log for 100 μM (PDS); Right) Percentage of B19V replication corrected by the cell viability: data of 50-100 μM BRACO-19 and 5-10-50-100 μM PDS probably suffer the very low cellular viability: 1 μM 120,56%, 5 μM 86,87%, 10 μM 119,33%, 50 μM 164,42%, 100 μM 90,25% (BRACO-19), 1 μM 96,79%, 5 μM 353,82%, 10 μM 475,01%, 50 μM >500%, 100 μM 464,79% (PDS) in comparison to the k+ 48 hpi (100% of viability) [*GraphPad Prism 6.0*]. The statistical analysis is done by Dunnett test (variance test based on multiple comparison; *one-way ANOVA*). Plotted values are mean of three experiments; *p value < 0.01-0.05, ***p value < 0.0001.

5.4.5 Discussion

In addition to the screening of libraries, another approach for the identification and investigation of new antiviral agents is based on predictions by bioinformatics tools. Computational analysis by *QGRS Mapper* software allowed to predict G-quadruplex structures within the B19V ITRs. G-quadruplexes regulate human cellular processes (e.g. telomeres [Henderson et al; 2014]) and they are involved during the replication of different viruses, for example they regulate HIV LTR-promoter [Perrone et al; 2013]. Hence, the putative predicted B19V G-quadruplexes could constitute a new target for developing an antiviral therapy.

In order to confirm or not the predictions, both chemical and biological *in vitro* studies in presence of two known G4 ligands (*BRACO-19* and *Pyridostatin*) were performed.

Since the G-quadruplexes have a stable and established structure, their spectra are already investigated by CD assay. Actually, light absorption by the quadruplex stem can be measured with the help of circularly polazired light (CD) [Karsisiotis et al; 2011]. The obtained spectra of the B19V oligonucleotides were compared to those present in literature showing different profiles among them and in comparison to the known G4 spectra. The efficiency and the robustness of CD assay were confirmed by the profiles of the positive control. The CD spectra of the B19V oligonucleotides did not corroborate the G4 predictions by the bioinformatics tool. However, the structure of the B19V ITRs nucleotide sequence are more complex than the basic single-helix DNA in B-form. Actually, CD melting profiles showed different conditions of stability among the B19V oligonucleotides, suggesting different conformations and the presence of different supramolecular structures such as, other folds, loops and bubbles. These DNA structures could interact with the known G4 ligands altering the structure but without a stabilizing effect [Mergny et al; 2003].

Independently from their interactions with the viral oligonucleotides, *BRACO-19* and *Pyridostatin* (PDS) did not show a significant antiviral action against the Human Parvovirus

B19. Inhibition of B19V replication was detected in presence of the higher concentrations of BRACO-19 and from the lower concentrations of PDS. However, these data could be related to the reduction of the cellular viability due to the compounds themselves rather than an antiviral activity.

6. Conclusions

Human Parvovirus B19 is one of the smallest known human pathogenic virus. Although its relatively simply composition with a short ssDNA (5596 nucleotides) enclosed inside a 20-25 nm capsid, it is still not well characterized. Viral proteins structure and functions, mechanism of replication, viral and cellular elements important for B19V infectivity are still not completely understood. A better knowledge of the virus and of its "habits" (such as the narrow tropism) should help to identify viral targets useful to the development of antiviral therapy and vaccine [G. Gallinella; 2013].

Investigations of the virus, its replicative mechanism and its interactions within the cells are important for its better characterization and for identifying targets for new antiviral agents. With this research, a synthetic *reverse genetic* approach was developed allowing to generate functional and mature B19V particles starting from design a *consensus sequence.* The reverse genetic approach could be applied for different studies: for example it was useful to understand the importance of the length of the ITRs and their isomerism for the viral replication. Then, cellular markers were investigated to understand the influence of the erythroid differentiation stage on the narrow tropism of the virus. Finally, different strategies were performed to find new B19V antiviral agents. Among all the tested molecules, the retargeted drug *Hydroxyurea* and in particular *Brincidofovir,* the lipid conjugate of the broad-spectrum antiviral drug *Cidofovir*, showed a potent and selective inhibition of B19V replication.

On the other hand, computational predictions or a "serendipity approach" are both based on the investigation of new molecules, that might not be well characterized and known. In a "serendipity screening approach", newly synthesized molecules, or molecules derived previous ones following a rational chemical approach, can often cause additional and unpredictable effects different from what was hypothesised. Investigation of small libraries could be useful for a first screening, then a putative lead compound might be identified among all the molecules within the library. A "serendipity approach" can be justified in the screening of small libraries when the target is not well known, but may however result expensive both in an economic and in a temporal point of view. Computational tools are useful in the search of new possible targets and for the development of new putative active drugs based on known targets, so knowledge of sequences and structures are required for this rational investigation, but the predictions need to be confirmed or rejected by *in vitro* studies.

In conclusion, the generation of functional viruses from synthetic genome allows to overcome some of the impediments for the study of Human Parvovirus B19. Actually, a synthetic source of virus will lead to become independent from the viremic sera of patients and will guarantee a stable and repetitive system overcoming the variability of the natural genomes. A reverse genetic approach will be also useful for sequence-function studies in order to understand not only the virus but also its interactions with the target cells. The B19V involves cellular elements during its infection and it can efficiently replicate when all the required elements are present in the target cells [Wolfisberg et al; 2013]. Investigations of the virus-cells complex and the biological characteristics of B19V will allow to increase the knowledge of the virus for continuing the development of an antiviral strategy.

7. *Materials and Methods*

7.1 Bioinformatic analysis

 - For the B19 synthetic genome construction: 49 B19V genomic sequences (genotype 1a), that are deposited in the NCBI nucleotide database were aligned and analyzed using ClustalW algorithms implemented within the *Clone Manager 9 Professional Edition Software* (Scientific & Educational Software) and MEGA6 Software (*Molecular Evolutionary Genetics Analysis*) for obtaining a consensus sequence. The selected nucleotide sequences for the analysis include >70% of genomic sequence of B19V and are representative of isolates collected in different settings, ante 2010.

 - For testing the putative antiviral compounds: the presence of G-quadruplex structures within B19V ITRs was predicted using *QGRS Mapper* Software (Ramapo Bioinformatics) [Kikin et al; 2006]. The putative G-quadruplexes were identified by the software using the following motif:

$$G_xN_{y1}G_xN_{y2}G_xN_{y3}G_x$$

 Here, "*x*"= number of guanine tetrads in the G-quadruplex and "*y₁, y₂, y₃*" = length of gaps, that is the length of the loops connecting the guanine tetrads.

 In particular, the parameters which were fixed for the bioinformatic analysis were: i) 30 nucleotides as maximum length of the G4; ii) 2 as minimum number of G and iii) from 0 to 15 nucleotides as length of the loop.

7.2 Bacterial Strains

 Different kinds of bacterial strains were used to fit to the diverse characteristic of the plasmids and to the different purposes:

 - *XL10-Gold Ultracompetent Cells* (Agilent Technologies): it is a strain of *E. Coli* created for transformation of large DNA molecules with high efficiency (yield greater than $5x10^9$ cfu/µg DNA). These cells are tetracycline and chloramphenicol resistant and need NZY$^+$ broth during transformation procedure.

 - *SURE 2 Supercompetent Cells* (Agilent Technologies): it is a strain of *E. Coli* which has been engineered to allow the cloning of certain DNA segments that are "unclonable" in conventional bacteria with ah efficiency greater than $1x10^9$ cfu/µg DNA. The SURE strain

lacks elements that catalyze the rearrangement and deletion of nucleotide sequence's secondary and tertiary structures, such as cruciforms. These cells are kanamycin, tetracycline and chloramphenicol resistant and require NZY$^+$ broth during transformation procedure.

- *BL21(DE3) Competent Cells* (New England BioLabs): it is a strain of *E. Coli* suitable for transformation and protein expression with a transformation efficiency of $1\text{-}5\text{x}10^7$ cfu/µg DNA. These cells need SOC broth during the transformation procedure. Indeed, the strain contained a T7 promoter DNA sequence whose expression is induced by IPTG (Isopropyl β-D-1-thiogalactopyranoside), a molecular mimic of lactose; actually, in this system the gene of interest is under the control of a lac operon. IPTG binds to the lac repressor and releases it from the lac operator allowing the transcription of the genes in the lac operon.

All these strains lack ribonuclease and endonuclease to ensure the stability of the plasmid and to improve the quality of the purified DNA.

7.3 Bacterial Media

In order to fit to the diverse steps of the experiment, different media were used:

- LB Agar was a solid medium used to make plates and it was composed of: 1% tryptone, 0,5% yeast extract, 1% NaCl, 100 µL NaOH 1 M in 100 mL of medium, 1,5% agar and antibiotics ([kanamycin]$_{final}$ = [ampicillin]$_{final}$= 50 µg/mL). At the moment of utilization they were preheated at 37°C for about 1 h; thus, the ideal temperature for bacterial growing was reached and the condensation will dry.

- SOC medium or NZY$^+$ broth were added to the bacterial cellular suspension after the transformation for helping them to grow: 1) SOC medium is made of: 2% Tryptone, 0,5% yeast extract, 10 mM NaCl, 2,5 mM KCl, 10 mM MgSO$_4$, 10 mM MgCl$_2$, 20 mM glucose; 2) NZY$^+$ broth is made of: 1% casein digest (NZ amine), 0,5% NaCl, and 0,5% yeast extract. They were both pre-heated at 37°C before the utilization.

- The medium LB is a liquid broth where the bacterial cells grow and amplify their numbers. Its composition is the following: 1% tryptone, 0,5% yeast extract, 1% NaCl, 100 µL NaOH 1 M in 100 mL of LB and antibiotics are added until their final concentration: kanamycin and ampicillin 50 µg/mL. Bacteria grew in this medium at 30°C or 37°C for 16-18 h and in continuous agitation.

7.4 Ligase Reaction and Enzymatic Reaction

Ligase reaction was performed using the T4 DNA ligase enzyme (Roche): vector and insert DNA were incubated together with T4 DNA ligase (1 U) in 1X ligation buffer (50 mM Tris-HCl, 10 mM dithioerythritol, 500 µg/mL BSA, pH 7,6; it contains also ATP as cofactor's enzyme) overnight at 16°C. Both the vector and the insert had sticky ends due to the digestion by the restriction enzymes and they were in a molar ration of 1:3, 1:5 or 1:10 respectively, to ensure a major probability of contact and so, to bind together.

In addition to the reactions between the insert and the vector, a ligase reaction was done with all the reagents except the insert and used as negative control. A negative control is useful to notice if the plasmid (vector) could close itself without insert and have the ability to form colonies after transformation of bacteria.

Enzymatic reaction were performed using restriction digestion enzymes in order to screen the transformed bacteria colonies, to separate the vectors and the inserts for the further ligase reactions or the transfection reactions. Different *FastDigest* enzymes were used that were all provided by *ThermoFisher Scientific*: *AccIII*, *BamHI*, *BssHII*, *DpnI*, *Eco47III*, *EcoRI*, *SacI*, *SalI*, *XbaI*, and *XhoI*. For each digestion reaction, the plasmid DNA was incubated together with the enzyme (1 U) in 1:10 diluted FastDigest buffer (*ThermoFisher Scientific*) and water, till the final volume of 20 µL, at 37°C for at least 30 minutes. Double digestions were performed as the single ones but using multiple enzymes within the same reactions. Following the incubation, the digestions were checked by gel electrophoresis before the further steps.

7.5 Transformation of Bacteria

10 ng of plasmid DNA or 2 µL of a ligase reaction were used to transform 20 µL of bacterial cells. The cell suspension was incubated in ice for 30 minutes then shocked at 42°C for 30-45 seconds and finally kept in ice for 2 minutes. After the shock, SOC or NZY$^+$ medium (depending on the bacterial strain used) was added to the suspension and the cells were incubated at 37°C for 1 h and in agitation. 100 µL of the cellular suspension was disseminated on a Petri plate containing selective medium and incubated at 30°C or 37°C for 16-18 h.

7.6 Bacterial Cells Growth

Transformed bacterial colonies, that were grown on selective LB agar medium, were recovered from the plate and expanded in 5 mL of LB liquid broth with antibiotics (kanamycin or ampicillin). Selected colonies were further expanded in 200 mL of LB liquid broth with antibiotics for medium-scale plasmid preparation.

7.7 Plasmid Miniprep/Midiprep Systems

Both *PureYield^{TM} Plasmid Miniprep Sistem* and *PureYield^{TM} Plasmid Midiprep Sistem* (Promega) provide a rapid method to purify plasmid DNA using a silica-membrane column. They differ only for the culture volumes they process and so, for their different purposes: the Miniprep System purifies maximum 3 mL of culture volume while the Midiprep System purifies since 50 to 250 mL culture volume.

The smaller culture volume was used for an early screening of the transformed bacterial colonies recovered from the plates; instead, the bigger culture volume was important to expand the bacterial colony, which was selected with the screening, and its purified DNA was used for the further eukaryotic transfection.

The isolated and purified plasmid DNAs were checked by cutting with restriction enzymes and the size of the obtained fragments were evaluated by agarose gel electrophoresis. In addition, as further confirmation, plasmid DNAs were sequenced.

7.8 Cells

Different kinds of eukaryotic systems were used:

- UT7/EpoS1 cells: it is a suspension cancer cell line derived by a human adult acute megakaryoblastic leukemia. They were cultured in IMDM (Lonza) supplemented with 10% FCS, 1% L-Glutamine, 1% streptomycin/penicillin and 2 U/mL Epo (NeoRecormon, Roche) at 37°C and 5% CO_2. Cells were used for transfection experiments, for testing putative antiviral compounds and for investing the cell susceptibility and permissiveness.

- Erythroid progenitor cells (EPCs) were generated *in vitro* from peripheral blood mononuclear cells (PBMC) obtained from leukocyte-enriched buffy coats of healthy blood

donors, available for institutional research purposes according to the policy approved by the local Ethical Committee (S.Orsola-Malpighi University Hospital). PBMCs were isolated using centrifugation in Ficoll-Plaque Plus (GE Healthcare Bio-Sciences AB) and cultured in IMDM (Lonza) supplemented with 20% serum substitute BIT 9500 (StemCell Technologies), enriched with 900 ng/mL ferrous sulphate, 90 ng/mL ferric nitrate, 1 μM hydrocortisone (Sigma), 3 U/mL Epo (NeoRecormon, Roche), 5 ng/mL IL-3, 20 ng/mL Stem Cell Factor (SCF; Life Technologies), 2 mM L-Glutamine and 1% streptomycin/penicillin. Cells were used for infection experiments and for testing the putative antiviral compounds when at day 8 of *in vitro* growth and differentiation; while, they were used at different days of *in vitro* differentiation for studying the cell susceptibility and permissiveness.

- HuDEP cells (Human umbilical cord blood-Derived Erythroid Progenitors): CD34^{+} hematopoietic stem/progenitor cells derived from umbilical cord blood were induced to immortalized erythroid progenitor cell line by lentiviral transduction.

The HuDEP cells were cultured in the presence of 1 μg/mL doxycycline (DOX; it activates the inducible system for erythropoietic phenotype), 50 ng/mL SCF and 3 IU/mL EPO [Kurita et al; 2013].

- HiDEP cells (Human iPS cell-Derived Erythroid Progenitors): iPS obtained from fibroblasts were induced to immortalized erythroid progenitor cell line by two lentiviral transductions. The first one for the introduction of the TAL1 gene and the second one for its expression.

The HiDEP cells were cultured in the presence of 1 μg/mL doxycycline (DOX; it activates the inducible system for erythropoietic phenotype), 3 IU/mL EPO and 1 μM dexamethasone (DEX) [Kurita et al; 2013].

7.9.Transfection

UT7/EpoS1 cells were transfected by the *Amaxa Nucleofector System* (Lonza), using the kit V Nucleofector Reagent and the T20 program. In particular before the transfection, the B19V inserts were excised from each clones by SacI digestion or amplified by PCR (LONGPAN program) using the *Expand High Fidelity PCR System* (Roche) and, purified recovering from agarose gel using the *Wizard SV Gel and PCR clean-up System* (Promega).

STEP	T (°C)	Time	n° cycles
Initial Denaturation	94°C	2 min	1
Denaturation	94°C	15 sec	
Annealing	55°C	30 sec	x 10 times
Extension	68°C	4 min	
Denaturation	94°C	15 sec	
Annealing	55°C	30 sec	x 20 times
Extension	68°C	4 min + 5 sec/cycle	
Final Extension	68°C	7 min	1
Hold	10°C	o/n	

Primers	Sequence
HJ0	TGTCTTCTTTAAATTTT
HI0	TCCGGAAGTCCCGCCC
HH0	GCGCGCCGCTTGATCTTAGTGG
HH1	GCGCGCCGCTTGTCTTAGTGTC

Composition Mix	Final conc.
Buffer 5x	1x
dNTPs (10 mM)	0,2 mM
Primer For (10 µM)	0,4 µM
Primer Rev (10 µM)	0,4 µM
Expand (5 U/µL)	2,5 U
Template	5 ng
H$_2$O	till volume
	V$_F$ = 50 µL

The linearized and purified B19V genomes were used to transfect UT7/EpoS1 cells with a ration of 1 µg of insert DNA for 1x10^6 cells. Following the transfection, the cells were incubated at 37°C in complete medium at an initial density of 10^6 cells/mL. Constant amounts of cells and supernatants were collected at different days post-transfection (dpt) and used for analysis and for successive infection experiments.

7.10 Infection

- For the B19V synthetic genome experiments: cell-free supernatants obtained from transfected UT7/EpoS1 cells at different time-points were used to infect EPCs at a ratio of 100 µL of supernatant for 1*10^6 cells. As control, EPCs were infected also by B19V from a serum sample at a moi of 10^4 geq/cell (moi = multeplicity of infection; geq = equivalent genomes that is the viral concentration inside the sample which was evaluated by real-time PCR). The infection was carried out at 37°C for 2 h, then cells were washed from inoculum and expanded in complete medium at a density of 10^6 cells/mL. Constant amounts of cells and cell-free supernatants were collected at 2 and 48 h post infection (hpi) and at 6 days post-

infection (dpi), then used for analysis or for a successive infection experiments. Actually, cell-free supernatants obtained from infected EPCs were used to infect other EPCs for a second round of infection in order to propagate and increase the recovered stock virus.

 - For testing the putative antiviral compounds: UT7/EpoS1 cells and/or EPCs were infected by B19V from a serum sample at a moi of 10^4 geq/cell for 2 h at 37°C. Then the cells were washed of inoculums and expanded in the respective complete medium at a density of 10^6 cells/mL and in presence of compounds at different concentrations. Constant amounts of cells were collected at 2 and 48 h post-infection (hpi) and then used for successive analysis. Different controls were performed in order to evaluate the activity of the compounds: i) B19V infected cells were expanded in complete medium without compounds; ii) B19V infected cells were expanded in complete medium and in presence of DMSO 1% (medium which was used for the solubilization of some of the putative antiviral molecules); iii) B19V infected cells were expanded in complete medium and in presence of CDV (this last is an already known B19V antiviral drug).

7.11 Indirect Immunofluorescence for VP capsid proteins (IIF)

100.000 transfected or infected cells at different time points were collected, washed and let them dry on glass slides. After fixation and permeabilization by Methanol/Acetone 1:1 for 10 minutes and -20°C, they were incubated with the primary antibody *MAb 8293* (Mouse monoclonal antibody; Chemicon International), which was diluted 1:200 in PBS/BSA 1%. This primary antibody is directed against a VP epitope in common between VP1 and VP2 capsid proteins. The incubation was performed inside a humid chamber for 1 h at 37°C. Then, the cells were washed three times, for 2 minutes each one, with PBS and incubated with the secondary antibody *Alexa Fluor-488* conjugated Goat anti-Mouse IgG (Life Technologies). The secondary antibody has been diluted 1:1000 in PBS/BSA 1% and the incubation was performed inside a humid chamber for 1 h at 37°C and protected from light. After 3 washes for 2 minutes each one with PBS, the cells were stained with Evans Blue 0,0005% solution for 8 - 10 minutes at RT, to label in red the negative cells. Finally after wash with PBS and water, the slides were mounted by PBS/glycerin 1:1 and visualized with the *Nikon Eclipse E400* fluorescence microscope.

7.12 FISH assay

100.000 cells collected at different time points following transfection or infection were processed by on slide FISH assay for the detection of viral nucleic acids [Manaresi et al; 2015]. Cells were washed, spotted and let them dry on glass slides. After fixation with PBS/para-formaldehyde 0,5% at 4°C for 30 minutes, the cells were permeabilized with PBS/Saponin 0,2% for 45 minutes at RT. For the hybridization reaction, 20 ng of a digoxigenin labeled, random primed full-length genomic probe (Dig High Prime; Roche) in 25 µL of a hybridization solution was added to the cells. The viral DNA and the probe was denatured together by heating at 95°C for 5 minutes and then incubated at 37°C over night. Following hybridization, the cells were washed twice with a mixture of SSC 2x − formamide 50% (300 mM NaCl, 30 mM sodium citrate; pH 7.0) at 37°C and twice with SSC 2x buffer at RT, for 10 minutes each one. Detection of the hybrids was performed with a FITC-conjugate anti-digoxigenin antibody (Roche) which was diluted 1:20 in PBS/BSA 1%. The incubation occurred for 1 h at 37°C and protected from light; then, after wash with PBS, the cells were stained with Evans Blue 0,0005% solution, mounted with PBS/glycerin 1:1 and observed with the *Nikon Eclipse E400* fluorescence microscope.

7.13 Flow cytometric analysis

Cells were collected and characterized for the erythroid lineage differentiation markers and their cell cycle by using *FACSCalibur* flow cytometer (Beckton Dickinson). For cells surface analysis, 500.000 cells were incubated with CD36-PE, CD71-PE and CD235a-FITC (BD Biosciences) diluted 1:20 in PBS/FCS 2% for 30 minutes at 4°C with agitation. Following two washes by centrifugation with 500 µL of PBS, the cells were resuspended by 500 µL of PBS and analyzed. For cell cycle analysis, 500.000 cells in 100 µL of cold PBS were permeabilized by 900 µL of 70% ethanol for 2 hours at 4°C without agitation. After two washes by centrifugation with cold PBS, the cells were incubated in a propidium iodide (PI) staining solution containing 0,1% Triton X-100 (Sigma-Aldrich), 50 µg/mL PI and 100 µg/mL RNase in PBS, for 30 minutes at 37°C. No stained cells were treated as the stained ones and used as controls to set the parameters for the subsequent analyses. Samples were gated on the forward light scatter (FSC) vs side light scatter (SSC) plot to exclude cellular debris and were analyzed using the *Cell Quest Pro* software (Becton Dickinson).

7.14 Extraction of Nucleic Acids

Viral nucleic acids purification from the transfected and infected cells and their respective cells-free supernatants was performed by using two systems: 1) BIOrobot EZ1 (Qiagen); 2) Maxwell (Promega). These instruments provide an automated procedure which combines the speed and efficiency of silica-based nucleic acid purification with the convenient handling of magnetic particles. The purification procedure comprises 4 steps: 1) lysis; 2) binding to magnetic particles; 3) washing of bound nucleic acids; 4) elution of purified nucleic acids.

100.000 cells or 60 µL of cells-free supernatant were collected at the appropriate time points and processed in order to obtain a total nucleic acid fraction in elution volumes of 100 µL. Volumes of 10 µL were used in the subsequent qPCR assays for the quantitative evaluation of target viral nucleic acids. For the analysis of supernatants, a benzonase treatment was also carried out by incubating 10 µL of supernatants with 1 µL of enzyme (Novagen) for 4 h at 37 °C to distinguish and quantify the amount of viral nucleic acids that were incapsidated and so protected from the degradation by benzonase.

7.15 qPCR

qPCR was carried out with the instrument *Rotor Gene-Q* (Qiagen). For the reaction, the *Maxima Sybr Green qPCR Master Mix 2X* (ThermoScientific) was used, that is a master mix 2X containing = a) *Hot Start Taq DNA polymerase*, which is activated by an incubation at 95°C for 10 minutes; b) *SYBR Green qPCR Buffer*; c) *SYBR Green I* as fluorescent dye ($\lambda_{excitation}$= 494 nm and $\lambda_{emission}$= 521 nm), which intercalates in the double helix of DNA; d) dNTPs. For each sample 10 µL master mix, 0,3 µM primers, 5 µL extract (1:2 diluted) and water to 20 µL final volume was used. Each sample was analyzed twice.

In order to fit to diverse purposes, different primers pairs were used:

- for the B19V DNA genome amplification:

2210: CGCCTGGAACACTGAAACCC (Forward primer)

2355: GAAACTGGTCTGCCAAAGGT (Reverse primer)

- for the cellular ribosomal DNA amplification (in order to normalize the obtained signal):

5.8S (Forward): CTCTTAGCGGTGGATCACTC (Forward primer)
5.8S (Reverse): GTGCGTTCGAAGTGTCGATG (Reverse primer)

Amplification profile:

	T(°C)	Time	Cycles
Initial Taq Activation	95 °C	10 min	1
Denaturation	95 °C	15 s	40
Annealing	60 °C	30 s	
Elongation + Acquiring of signal	72 °C	30 s	

To confirm amplification specificity, the PCR products were subjected to a slow denaturation ("melting curve analysis"). The melting point (T_m) was evaluated by a different profile: from 95°C the temperature was reduced to 65°C then increased to 95°C with a shift of 0,1°C/sec. Cycle to cycle fluorescence readings were plotted and at the end of each run, fluorescence data were analyzed by setting a noise band to remove background fluorescence. In this way, an interpolated value was obtained where the best-fit line through the log-linear portion of the amplification curve intersected the noise band (crossing point). Values previously obtained for external standards were employed to construct a reference curve; for each sample, the concentration was calculated by interpolation within this reference curve. The program GraphPad Prism version 5.00 for Windows (GraphPad Software, San Diego California, USA) was used to carry out data analysis.

7.16 Benzonase Nuclease Treatment

In order to distinguish not enclosed viral DNA molecules inside a capsid from the enclosed ones, transfected/infected cellular supernatants were digested by *Benzonase Nuclease* (Novagen).

Benzonase is a genetically engineered endonuclease from *Serratia marcescens* which attacks and degrades all forms of unprotected DNA and RNA (single-double stranded, circular and linear). 10 μL of sample were treated by 1 μL of enzyme ([benzonase nuclease]$_F$ = 25 U/μL) for 4 h at 37°C; then the viral nucleic acids were extracted and quantified by qPCR.

7.17 Southern Blot

Viral extracts from transfected and infected cells were analyzed by Southern Blot assay. The samples were digested by restriction enzymes to evaluate different characteristics of the genomic clones, such as the length of the ITRs and the maintenance of the isomerism. In addition, a DpnI enzyme digestion was carried out to distinguish de novo synthesized viral DNA based on different Dam methylation pattern. Following cleavage, the DNA fragments were separated by an electrophoresis agarose gel run. For denaturing and preparing the DNA before the transfer, the gel was washed twice by Gel Denaturation solution for 20 minutes each one at RT and one time in Gel Transfer solution for 20 minutes at RT. For transblotting, the DNA molecules were transferred by capillarity from the gel to a positive charge nylon membrane for 90 minutes at RT and fixed by UV for 3 minutes. Then, the membrane was washed for 10 minutes by STE 1X on shaker and hybridized with 50 ng of DIG labeled-B19V probe which was diluted in 5 mL of hybridization solution (*DIG Easy Hyb Granules*; Roche) over night at 45°C in hybridizer. Before the addition, the DIG labeled-B19V probe was denatured at 95°C for 5 minutes.

The following day, the membrane was washed twice by "1° wash-Buffer" for 10 minutes each one at RT on shaker, twice by "2°-wash-Buffer" for 30 minutes each one at 65°C in hybridizer and after that, it was incubated with anti-DIG AP conjugated (Alkaline Phosphatase) antibody diluted 1:10.000 in Buffer 2 for 30 minutes at RT on shaker. The surplus of antibody was removed by two washes with Buffer 1 for 30 minutes each one on shaker. A wash (30 minutes) with Buffer 3 at RT was performed before adding NBT/BCIP (substrate of the alkaline phosphatase enzyme), in order to increase the pH; actually, the enzyme works at pH = 9. Then, the membrane was incubated with NBT/BCIP diluted 1:50 in Buffer 3. The DNA fragments were detected as purple bands on the membrane due to the reaction of the alkaline phosphatase with its substrate (figure 7.1). Finally, the enzyme reaction was stopped by water.

DNA molecules length was evaluated by comparison with the bands of the *DIG labeled-Marker III* (Roche).
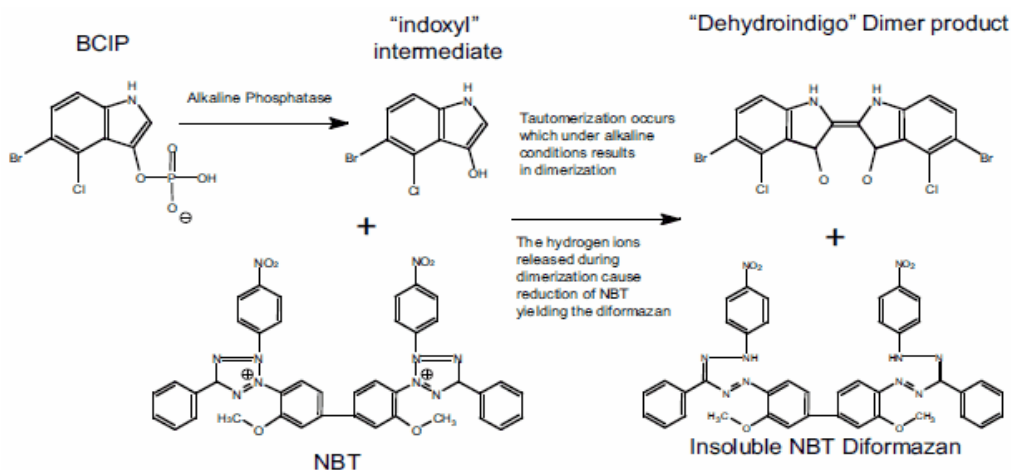
Figure 7.1: The alkaline phosphatase enzyme removes the phosphate group of 5-bromo-4-chloro-3-indolyl phosphate (BCIP). The resulting molecule can dimerize in oxiding condition giving 5,5'-dibromo-4-dichloro-indigo (an insoluble indigo product). Indigo color is amplified by presence of NBT (nitroblue tetrazolium chloride): indolyl group reduces NBT which gives a blue formazan NBT.

7.18 Proteins Purification

ΔC128 and ΔN29/C128 proteins codified for the VP1u region and were previously synthesized within the laboratory of Prof. Ros (University of Bern; Switzerland). For their purification, bacteria were transformed with plasmids codifying the respective protein. The screening of the selected colonies was carried out by restriction enzyme digestions and PCR amplifications for the VP1u region. For the PCRs, *Q5 High-Fidelity 2x Mix* (NEB) was used:

Composition Mix	Final Conc.
Q5 High Fidelity 2x	1x
FLAG Forw (10 μM)	0,5 μM
pTAC Rev	0,5 μM
DNA template	5 ng
H₂0	till volume
	V$_F$= 25 μL

STEP	T (°C)	time	n°cycles
Initial Denaturation	98°C	30 sec	1
Denaturation	98°C	10 sec	x35 times
Annealing	63°C	20 sec	
Extension	72°C	25 sec	
Final Extension	72°C	2 min	1
Hold	4°C	o/n	

Primer	Sequence
FLAG Forw	CTATCATGCCATACCGCGAAAG
pTAC Rev	GAGAAGATTTTCAGCCTGATACAG

140

5-10 mL of the selected colonies were added to 100 mL of LB Broth containing ampicillin for 80 minutes at +37°C with agitation at 220 rpm. When the density of the grown bacteria reached an OD value major than 0,40, 0,025 g IPTG [isopropyl-β-D-thiogalactopyranoside] was added to obtain its final concentration of 1 mM. IPTG (*QIAexpressionist™ Kit;* Qiagen) induced the protein production and after its adding, the bacteria were incubated for other 4 hours at 37°C with agitation at 220 rpm. Following the incubation, the bacteria cultures were collected by centrifugation at 3000 rpm for 5 minutes at +15°C; then, the pellets were stored at -20C.

The following day, three freeze-thaw cycles from -80°C to +25°C were performed to break the cells. Pellets were resuspended with 3 mL of PBS for combining them and then, they were subjected to sonication for fifteen times 8 seconds each time, in order to further lyse the cells. The supernatants containing the proteins were collected after centrifugation at 10000 rpm for 30 minutes at +4°C. After that, 150 µL of pre-washed *Ni-NTA Agarose Beads* (*QIAexpressionist™ Kit*; Qiagen) and 75 µL of 10 mM Imidazole Solution (Sigma) were added to the supernatants and incubated for 1 hour at +4°C on shaker then 10 minutes at 25°C, for allowing the bond among the His-tag of the proteins and the Nickel beads. For removing all the supernatants, the beads were put inside a column (*QIAexpressionist™ Kit*; Qiagen) and they were washed three times with 5 mL of PBS. Then, the elution of the proteins was carried out by adding 250 µL of 250 mM Imidazole Solution (Sigma), mixing and incubating for 5 minutes with the column closed. Opening the column, the solution for the elution was collected within a tube by gravity; this step was repeated four times to ensure the correct and complete elution. The obtained proteins were further cleaned by a second bond and incubation step with 150 µL of pre-washed *Ni-NTA Agarose Beads*, overnight at +4°C on shaker. Following the incubation, the beads were washed twice with 10 mL of PBS using a column for collecting them, as previously. Finally, the proteins were eluted by four wash/incubation-passages for 5 minutes with 250 µL of 250 mM Imidazole Solution (Sigma) and collected within a tube.

7.19 Cellular Markers Expression

The expression of different markers was evaluated by an Indirect Immunofluorescence assay (IIF). In particular, various factors of susceptibility and permissiveness were tested applying

two different protocols. Both a "Binding" and an "Internalization" IIF assay was developed for the following markers:

1) VP1u protein = two different peptides were analyzed: ΔC128 and ΔN29/C128. They were studied and provided by the group of Professor C. Ros (University of Bern; Switzerland) and were truncated versions of the "unique region" of the B19V VP1 protein. ΔC128 had a deletion of 128 aa at C-terminus; while ΔN29 had both the 128 aa deletion at C-terminus and a deletion of 29 aa at N-terminus. This last one did not allow the ΔN29/C128 binding to VP1u receptor, so it worked as negative control (ΔC128 binds the VP1u receptor). Both the proteins had a MAT-tag and a FLAG-tag. The MAT-tag was used for their purification from bacteria, while the FLAG-tag was used as target for the primary antibody of the IIF assay.

75 ng of the VP1u peptides (ΔC128 or ΔN29/C128) were labeled to 300 ng primary antibody *Rat monoclonal anti-FLAG [DYKDDDDK]* (Stratagene) for 15 minutes at 4°C or 37°C, before their addition to the cells. For the IIF assay development, a *Goat anti-Rat conjugated to Alexa Fluor-488* or *Goat anti-Rat conjugated to Alexa Fluor-594* were used as second antibodies diluted 1:500.

2) Holo Transferrin-FITC = This is the iron saturated form of the Human Transferrin which binds its receptor. It was used as marker of the endocytosis pathway. The Holo Transferrin-FITC was directly linked at the FITC fluorophore, so it was added to the cells at the dilution of 1:10 from the stock solution (it was provided by the Professor C. Ros' group). After the incubation, the cells were directly fixed for the visualization.

3) globoside (Gb4Cer) = two different first antibodies and their respective second antibodies were used for the IIF assay anti-globoside. a) *Rabbit polyclonal anti-globoside* (Matreya) diluted 1:100 as first antibody and *Goat anti-Rabbit conjugated to DyLight-488* (ImmunoReagents) or *Goat anti-Rabbit conjugated to DyLight -633* diluted 1:500 as second antibody (ImmunoReagents); b) *Chicken anti-globoside* diluted 1:100 as first antibody and *Goat anti-Chicken conjugated to Alexa-Fluor-594* (ThermoFisher Scientific) as second antibody. Only the binding IIF assay was evaluated for globoside.

4) p-STAT5 (Tyr694) = STAT5 is a marker of the Epo pathway and it is phosphorilated at Tyrosine 694 when the pathway is activated by the binding of Epo to its receptor. STAT5 is an internal cellular factor, so for its IIF assay: cells were fixed with methanol/acetone and then incubated with the first antibody following by the second antibody before the visualization (see protocol at point 3.12: IIF for VP capsid proteins). *Rabbit monoclonal anti-phospho STAT5 (Tyr 694)* (CellSignaling Technology; clone D47E7) [Ganaie et al; 2017] was

used as first antibody at 1:100 dilution; *Goat anti-Rabbit conjugated to DyLight-488* was used as second antibodies at dilution 1:100, respectively.

Secondary antibodies conjugated to different fluorophores were used due to the various combinations of the markers that were analyzed at the same time. In this way, more factors (label by different colors) could be showed on/in the same cell.

The Binding and Internalization IIF protocols were performed as following:

a) BINDING: 200.000 − 300.000 cells were washed twice with PBS by centrifugation at 4.000 rpm for 5 minutes at 4°C and incubated with PBS/goat serum 10% for 20 minutes at 4°C with shaking, in order to block the non-specific sites of antibodies. To remove the solution, the cells were washed with cold PBS by centrifugation at 4.000 rpm for 5 minutes. The first antibody was added at the necessary dilution, due to the marker of interest, in PBS/goat serum 2% and incubated for 1 h at 4°C with shaking. After two washes with cold PBS by centrifugation at 4°C, the respective second antibody diluted in PBS/FCS 2% was added and incubated for 1 h at 4°C with shaking. Then, the cells were washed twice with cold PBS and spotted on a previously cleaned round-coverslip. Their fixation and permeabilization was performed with Methanol/Acetone 1:1 solution for 3 minutes at -20°C and after rinsing with PBS, the cells were stained with DAPI diluted 1:10.000 in PBS. Finally, coverslips were washed with water and ethanol 100% and put on a slide for visualization at *Nikon Eclipse E400* fluorescence microscope.

All the incubations and washes were performed at 4°C before the fixation/permeabilization step, in order to keep the factor-receptor complex on the cellular membrane. When the cells were spotted, all the following steps were performed with coverslips within wells of a 12-wells plate.

For the VP1u IIF assay, ΔC128 and ΔN29/C128-Rat anti-FLAG [DYKDDDDK] (first antibody) complexes were added to the cells to increase the fluorescence signals, as established by previous tests.

b) INTERNALIZATION: 200.000 − 300.000 cells were washed twice with PBS by centrifugation at 4.000 rpm for 5 minutes at RT and incubated with PBS/goat serum 10% for 20 minutes at 37°C with shaking, in order to block the non-specific sites of the antibodies. To remove the solution, the cells were washed twice with PBS by centrifugation at 4.000 rpm for 5 minutes. The first antibody was added at the necessary dilution, due to the marker of interest, in PBS/goat serum 2% and incubated for 30 minutes at 37°C with shaking. After two washes with PBS by centrifugation, the non-internalized factor-receptor complexes were removed by the treatment with trypsine enzyme. Cells were incubated in trypsin/EDTA 1X

solution for 4 minutes at 37°C and then, the enzyme action was stopped by the addition of medium containing 10% serum. After two washes with PBS by centrifugation at 4.000 rpm for 5 minutes, the cells were spotted on a previously cleaned round-coverslip. Their fixation and permeabilization was performed with Methanol/Acetone 1:1 solution for 3 minutes at -20°C and after rising with PBS, the non-specific sites were blocked again by an incubation with PBS/goat serum 10% for 20 minutes at RT on shaker. Then, the cells were washed twice with PBS and incubated with their respective second antibody diluted in PBS/goat serum 2% for 1 h at RT on shaker. After three washes with PBS for 10 minutes each one at RT on shaker, the cells were stained with DAPI diluted 1:10.000 in PBS. Finally, coverslips were washed with water and ethanol 100% and put on a slide for visualization at *Nikon Eclipse E400* fluorescence microscope.

Before the fixation/permeabilization step, all the incubations and washes were performed at 37°C in order to allow the internalization of the factor-receptor complex. When the cells were spotted, all the following steps were performed with coverslips within wells of a 12-wells plate.

For the VP1u IIF assay, ΔC128 and ΔN29/C128-Rat anti-FLAG [DYKDDDDK] (first antibody) complexes were added to the cells to increase the fluorescence signals, as established by previous tests.

7.20 Putative Antiviral Compounds

Different compounds were investigated for their inhibitory effects against B19V replication:
- *Hydroxyurea*: it is a S-phase specific inhibitor of DNA synthesis. It was purchased as powder at purity degree >98% (Sigma-Aldrich), solubilized in water and filter sterilized.
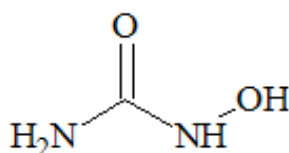
- *Cidofovir* (CDV) and *Brincidofovir* (BCV): BCV was provided by Chimerix (Chimerix, Inc., Durham, USA). Unless stated, BCV refers to the S-enantiomer (CMX001) as opposed to the R-enantiomer (CMX029). CDV was purchased from *Sigma-Aldrich* at a purity of >98%. In all cases, dry powder was resuspended in phosphate buffered saline (PBS), pH 11.6, at 10mM and filter sterilized.
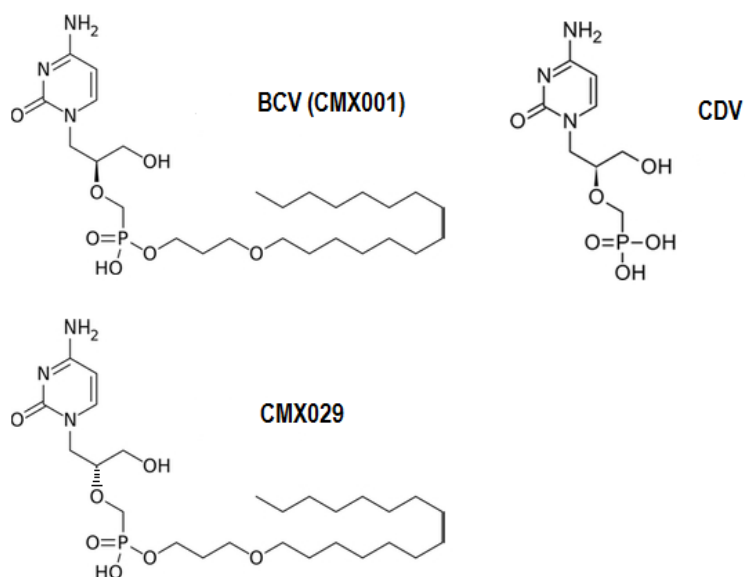
- 8 newly different compounds (named from A to H), whose chemical structures are shown below, were tested in this study to evaluate their putative antiviral activities against the Human Parvovirus B19. The newly synthesized compounds were provided by the group members of Professors: A. Locatelli, A. Leoni, R. Morigi, M. Rambaldi (FaBiT, University of Bologna).

All the compounds were characterized by planar structures, rich in heterocycles and of available positive charges. Due to the structural characteristics and the reference molecules for their synthesis, they could be divided into different groups:

1. A, B, E, F = molecules that were comparable to "BRACO-19". They had symmetric structures with protonable and symmetric lateral chains, like the G4 ligand [Perrone et al, 2014].

2. C = compound without a reference molecule so, which was not defined for its structure and activity.

3. D = Coumarin derivative.

4. G, H = molecules that were analogues of cyclic hydroxyurea.

All these 8 molecules were provided as powder, they were solubilized in DMSO (dimethylsulphoxide) and filtered before their using.

1 BIS ARPy2G.2HCl
(A) PM 564,47

2 AR24EGG.2HCl
(B) PM 501,39

3 MM-67IFUR
(C) PM 371,77

4 AR-CUM
(D) PM 268,29

5 IS-INDIND
(E) PM 363,42

6 5M-BIM
(F) PM 382,46

7 IND-5Cl-NMet-34-PIRIMEt
(G) PM 347,80

8 ARCl-34-PIRIMEtAL
(H) PM 420,91
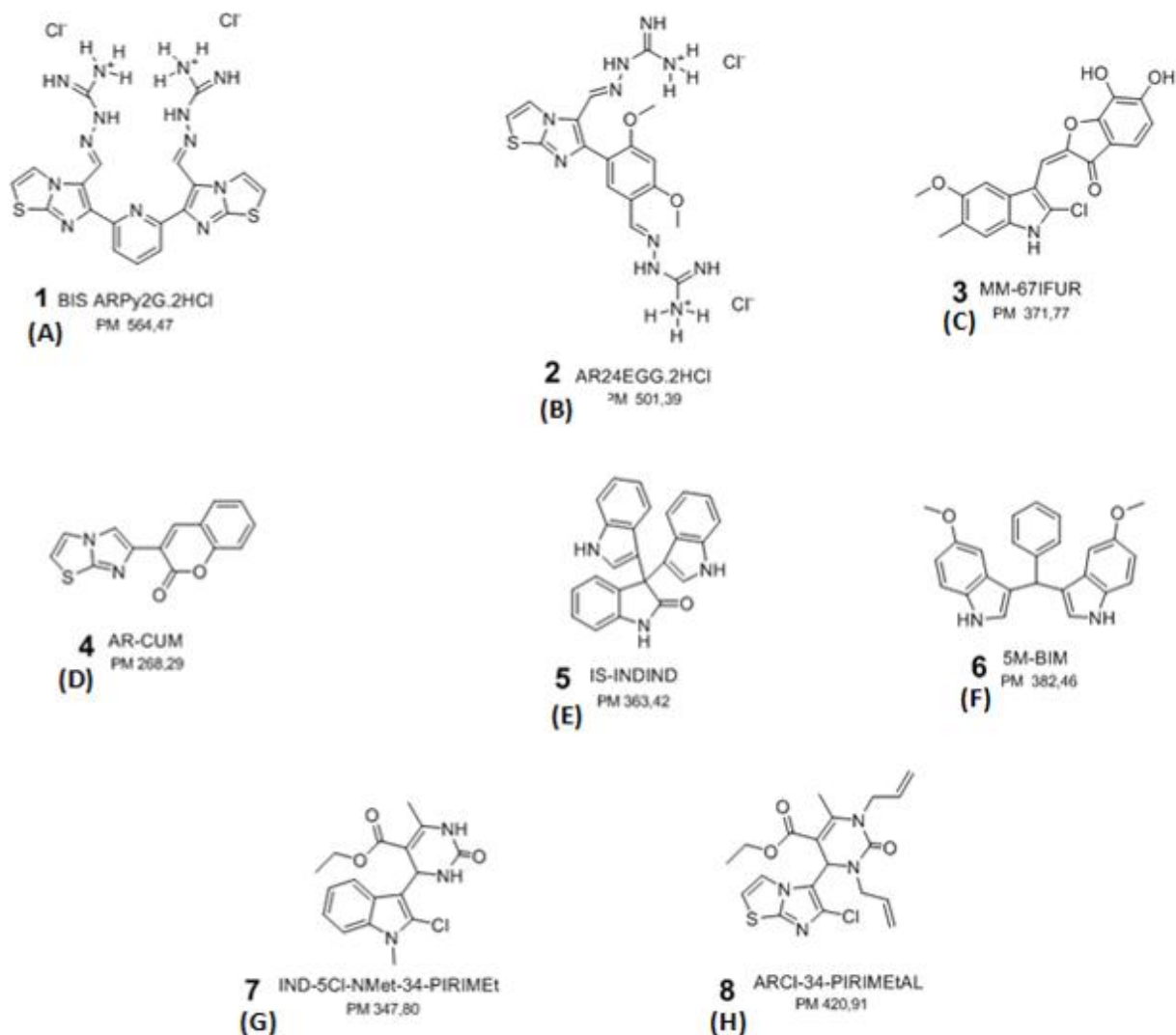
- From the leader "compound 4 or compound D" (ARCUM), other 8 molecules were synthesized by the group members of Professors: A. Locatelli, A. Leoni, R. Morigi, M. Rambaldi (FaBiT, University of Bologna). In particular, they were all coumarin derivatives, named from 4a to 4h, that were characterized by planar structures and rich of heterocycles

Figure 7.2: Chemical structure of Coumarin.

Coumarins (benzo-α-pyrone) are naturally compounds, easy to synthesize and already use as therapeutic agents (figure 7.2). Studies showed their antiproliferative action on tumoral cells and immunomodulatory activity. For example, scopoletin which was isolated from different plants and induced apoptosis on adenocarcinoma cells and lymphocytic leukemia; while it enhanced cell proliferation of normal macrophages and lymphocytes [Manuele et al; 2006]. Some of co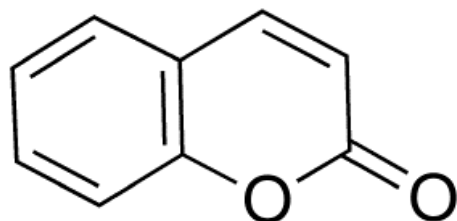umarins analogues also showed antiviral activity, such as chapelin which was isolated from *Ruta angustfolia* leaves and inhibited HCV (hepatitis C virus) RNA replication probably blocking its RNA polymerase and viral protein synthesis [Wahyuni et al; 2014].

4
ARCUM
PM: 268,29

4a
ARCUM-A
PM: 296,30

4b
ARCUM-H
PM: 411,44

4c
ARCUM-5M
PM: 441,46

4d
2MCUM
PM: 282,32

4e
2MCUM-A
PM: 310,33

4f
2MCUM-H
PM: 425,46

4g
2MCUM-5M
PM: 455,49

4h
2MCUM-67
PM: 475,52
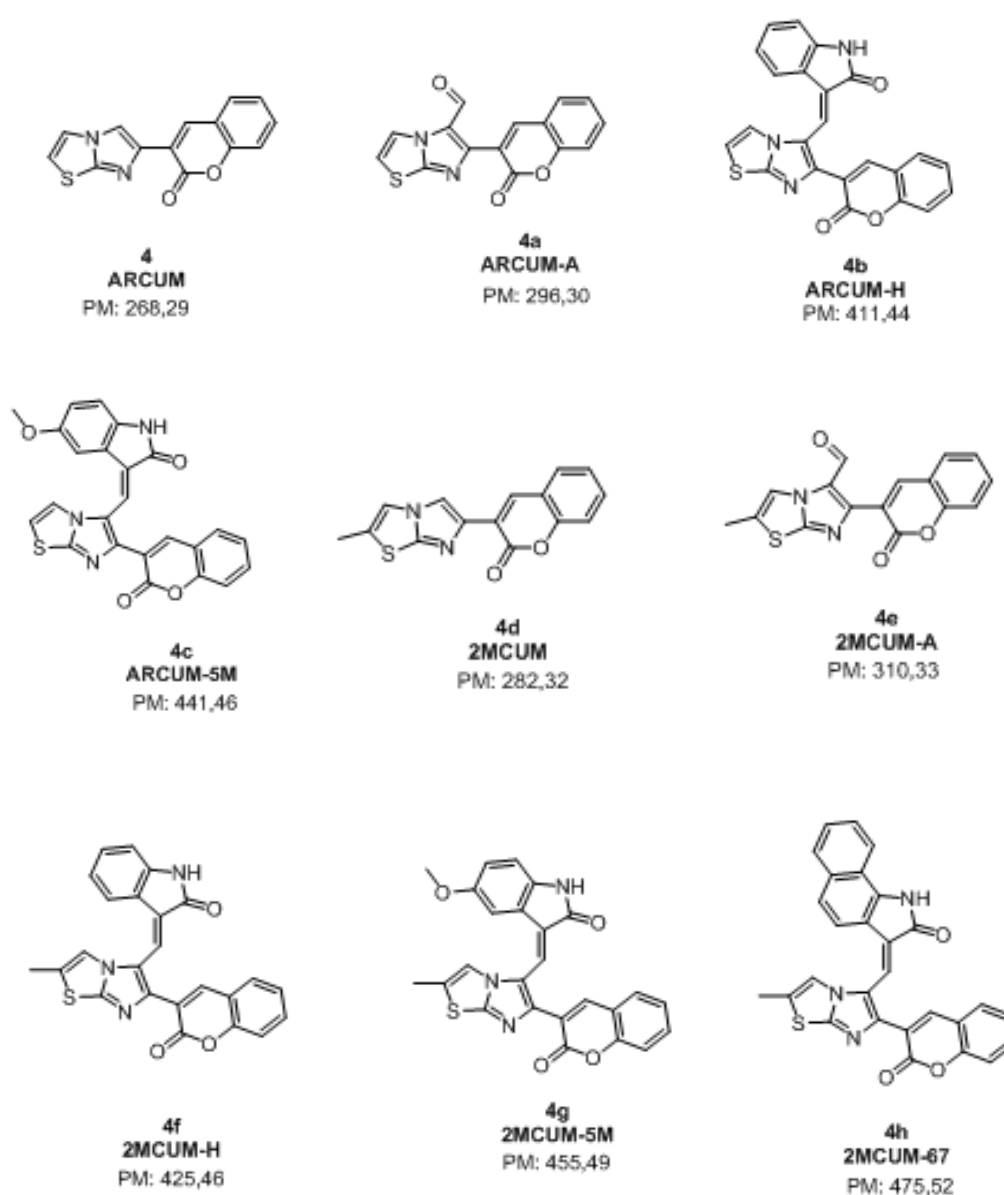
Moreover, some derivatives of coumarins have been reported to possess increased inhibitory effects on HIV replication acting at different steps during its replicative cycle [Zhou et al; 2012].

147

- Other two compounds were tested for a putative antiviral activity against B19V (their chemical structures are shown below). They were the known G4 ligands: BRACO-19 (*Braco-19 hydrochloride*; purity degree >96%, Sigma-Aldrich) and PDS (*Pyridostatin trifluoroacetate salt*; purity degree >98%, Sigma-Aldrich). Following the instructions, they were solubilized in H_2O till the final concentration of 5 mg/mL for BRACO-19 and 15 mg/mL for PDS and filter sterilized.
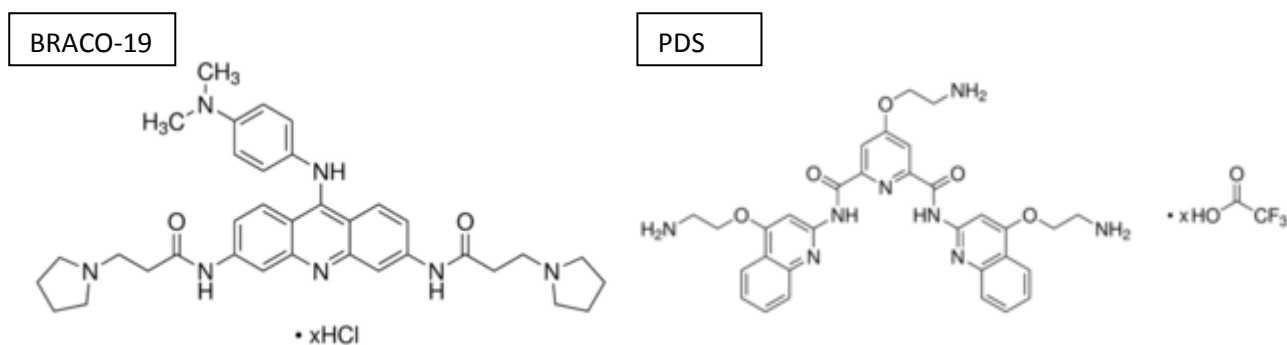
7.21 Cell Viability and Proliferation Assays

-CCK8 assay: *Cell Counting Kit 8* (CCK8; Dojindo Molecular Technologies) is a colorimetric analysis which allow to determine the number of living cells during a cellular cytotoxic test. The WST-8 tetrazolium salt (which is soluble in water) is reduced by dehydrogenase enzyme inside the cells forming an orange product (WST-8 formazan). The amount of WST-8 formazan is directly proportional to the number of the living cells (figure 7.3).
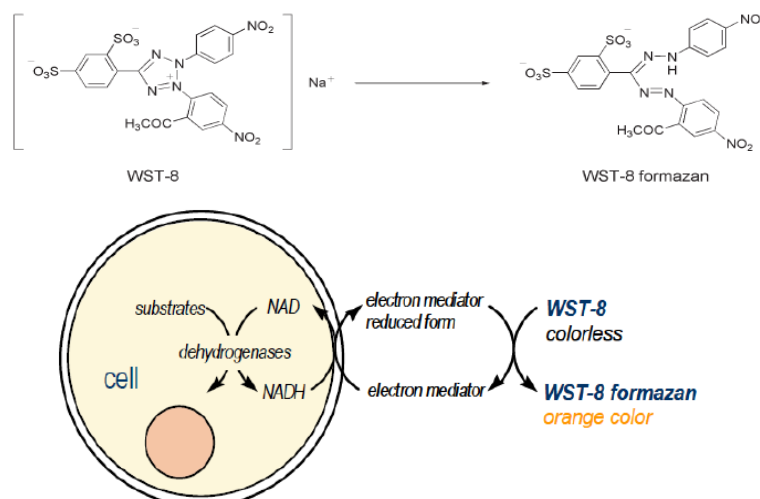
Figure 7.3: Top) Schematic representation of water soluble WST-8 tetrazolium salt and its product (WST-8 formazan), which is soluble in cellular medium. Bottom) Reduction reaction of colorless WST-8 to orange WST-8 formazan.

50.000 cells in a volume of 100 μL were distributed in each well of a 96-wells plate. The cells were resuspended in cellular medium containing the tested compound at different concentrations; a triplicate of each condition was done. The compounds were not colorless so they could influence the absorbance measurement of the orange WST-8 formazan; to overcome this problem, a well containing 100 μL cellular medium in presence of the molecules but without cells was prepared.

After 46 h in incubator at 37°C and 5% CO_2, 10 μL of CCK8 reagent was added to each well ($[CCK8]_i = 10X$) and the cells were maintained in this condition for other 2 hours (46 + 2 = 48 h is the total time to mimic the infection) for UT7/EpoS1 cells while 7-8 hours for EPCs. The absorbance measurements were read by the ELISA plate reader (*Multiskan Ascent, Thermo Electron Corporation*) at different time points after the adding of the CCK8 reagent and at two wavelengths: 450 (corresponding to formazan absorbance) and 630 nm (to delete interferences such as bubbles or a turbid cellular suspension). The percentage of the living cells was obtained with the following formulae:

$$A_{living\ cells} = (A_{450} - A_{630})_{cells} - (A_{450} - A_{630})_{media}$$

$$\%\ _{living\ cells} = (A_{living\ cells} / A_0) * 100$$

Here, $A_{450\ cells}$ and A_{630} are the absorbance measures that are read at λ 450 or 630 nm of the well containing cells/medium/compound (cells) or only medium/compound (media; without cells), respectively. A_0 is the absorbance measure of the well containing only the cells and medium (without compound), where the 100% of cell viability is assumed.

-<u>LDH assay</u>: *Cytotoxicity LDH Assay kit-WST* (Dojindo Molecular Technologies) is a colorimetric assay for determination of cytotoxicity by measuring a lactate dehydrogenase (LDH) activity released from damaged cells. LDH is cytoplasmic enzyme presented in all cells which is released into the cell culture medium through damaged plasma membrane. The released LDH reduces NAD to NADH catalyzing the dehydrogenation of lactate to pyruvate. NADH reduces a water-soluble tetrazolium salt (WST) in the presence of an electron mediator to produce an orange formazan dye (figure 7.4). Hence, the amount of this latter is proportional to the released LDH, which is an indication of cytotoxicity.
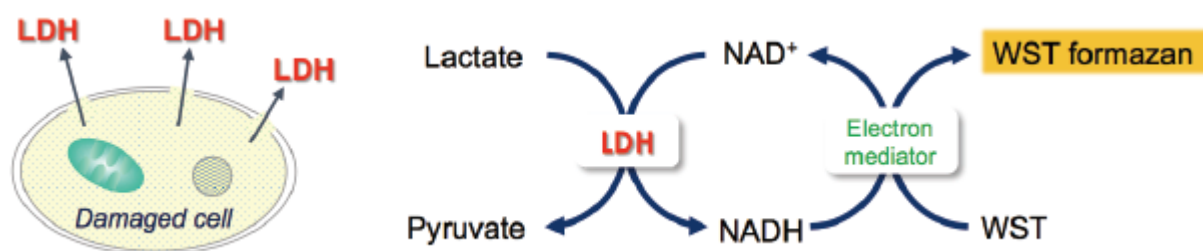
Figure 7.4: Schematic representation of functioning of the LDH assay.

50.000 cells in a volume of 100 µL were distributed in each well of a 96-wells plate. The cells were resuspended in cellular medium containing the tested compound at different concentrations; a triplicate of each condition was done. Following 48 hours of incubation, the cell free supernatants were recovered after centrifugation of the plate at 1000 rpm for 10 minutes and transferred to a new clear 96-well plate. 100 µL of the "Working Solution" was added to each well. After the incubation for 30 minutes at 25°C and protected from light, 50 µL of the "Stop Solution" was added and the absorbance was measured at 450 nm by ELISA plate reader (*Multiskan Ascent, Thermo Electron Corporation*). 50.000 cells in a volume of 100 µL of cellular medium adding 10 µL of "Lysis Buffer" 30 minutes before the absorbance reading and 100 µL of only cellular medium were used as "High control" and "Low control", respectively. The cytotoxicity percentage was calculated by using the following formulae:

$$\text{Cytotoxicity (\%)} = [(A-A_L)/(A_H-A_L)] \times 100$$

Here, A is absorbance of the interested samples (supernatants from well containing cells/medium/compound), A_L is the absorbance of the "Low control" and A_H is the absorbance of the "High control".

-<u>BrdU assay</u>: *Cell Proliferation ELISA, BrdU colorimetric* (Roche) kit is an immunoenzymatic assay which allows to quantify the cellular proliferation due to the BrdU (5-Bromine-2'-deoxyuridine) incorporation during the DNA synthesis. Actually, proliferating cells add this pyrimidine analogue instead of tymidine in the newly synthesized DNA.

50.000 cells in a volume of 100 µL were distributed in each well of a 96-wells plate. The cells were resuspended in cellular medium containing the tested compound at different concentrations; a triplicate of each condition was done. After 44 hours of incubation, 10 µL of BrdU solution diluted 1:100 from the stock solution was added to each well and incubated for other 4 hours (total of 48 hours of incubation). Then, the cells were adhered to the plate by centrifugation at 1000 rpm for 10 minutes at 25°C; the supernatants were removed and the cells were dried for 1 hours at 60°C in *ThermoMixer*. After that, 200 µL of "FixDenat Solution" (for fixation and denaturation) was added and following incubation for 30 minutes, cells were incubated with 100 µL of peroxidase conjugated anti-BrdU antibody for 90 minutes. After three washes with 200 µL for each well of "Washing Solution", 100 µL of "Substrate Solution" was added and incubated for 15 minutes protected from light. Finally, the reaction of the peroxidase enzyme was blocked by adding 25 µL of H_2SO_4 1 M leading to change from the blue colour to the yellow colour of the solution (figure 7.5). Triplicate of 50.000 cells in 100 µL of cellular medium without BrdU was used as control.

The absorbance measurements were read by the ELISA plate reader (*Multiskan Ascent, Thermo Electron Corporation*) at 450 and 630 nm (yellow colour and blue colour absorbance, respectively). The percentage of proliferation was calculated by using the following formulae:

$$A = (A_{450} - A_{630})$$

$$\%_{\text{proliferating cells}} = (A / A_0) * 100$$

Here, the 450 nm measured absorbance is subtracted to the 630 nm one and the obtained result is divided for the absorbance of the control (A_0 is the absorbance of cells/medium well which is assumed to have 100% of proliferation).
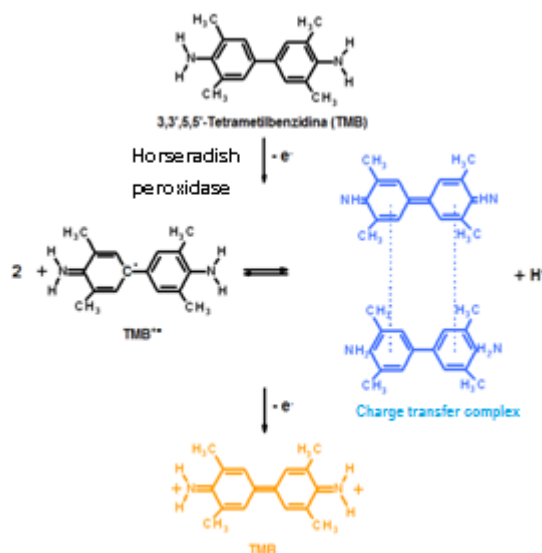
Figure 7.5: Schematic representation of peroxidase enzyme action = TMB substrate acts as electrons donor by horseradish peroxidase assuming a blue colour staining ($\lambda = 630$ nm). Following H_2SO_4 addition, a complex of two TMB molecules is done at first and within it, each TMB transfers charge to the other one. The yellow final product is obtained after the completely oxidation of the complex ($\lambda = 450$ nm).

7.22 Circular Dichroism Analysis

Circular dichrosim (CD) is a phenomen originating from interactions of chiral molecules with circularly polarized electromagnetic rays. Absorption of right- and left-handed circularly polarized light by chiral molecules differs and the difference is called ellipticity (θ; it is expressed in degrees).

The theoretical description of large molecules such as DNA is very complex, so the method is not able to provide structural information on the molecules at atomic level. For this reason, CD spectroscopy is primarily used empirically in studies of DNA. However, CD spectroscopy has many advantages: 1) it is extremely sensitive, permitting to work with low amount of DNA which is advantageous in studies of samples with low solubility or of those that tend to aggregate under extreme solvent conditions; 2) the studied molecules can be not only short (oligonucleotides) but also long; 3) the samples can be titrated with various agents (like salts, alcohols or acids) that induce conformational isomerizations in DNA allowing to map the whole conformational space of the studied molecules, and not a single structure; 4) CD spectroscopy distinguishes two state conformational isomerizations between distinct conformers from gradual changes within arrangements characterized by a single energetic

minimum; 5) CD can analyze not only solutions but also films; 6) CD measurements are fast and relatively inexpensive [Kypr et al; 2009].

As mentioned previously, different topologies of G-quadruplex structures could be identified and CD spectroscopy is widely used for distinguishing a single topology, the parallel stranded (group I), from all the others (antiparallel quadruplexes). The spectra show at least three distinctive features in the spectral range of interest, in which guanine absorbs: bands centered at 235-245 nm, 264-270 nm and 280-297 nm (figure 7.6).

- Group I (parallel): an intense CD band at approximately 264 nm, and a negative band at approximately 245 nm, while the dichroic signal around 290 nm is negligible.

- Group II (antiparallel): CD spectrum shows a positive band at 290 nm and a negative band at 264 nm, in addition to a negative band at 245 nm.

- Group III (antiparallel): CD spectrum shows a positive band at 290 nm as for group II, but it show the reverse for the other two bands respect to the group II. So, it has a positive band at 245 nm and a negative band at 264 nm.

Quadruplexes may be part of higher-order architectures with additional supramolecular features such as double helix, triads, hairpins, further stacking of any base (such as poly T) and mismatches. So caution should be exercised in assigning a G4 topology from a CD spectrum in systems for which extensive base stacking is expected [Karsisiotis et al; 2011].
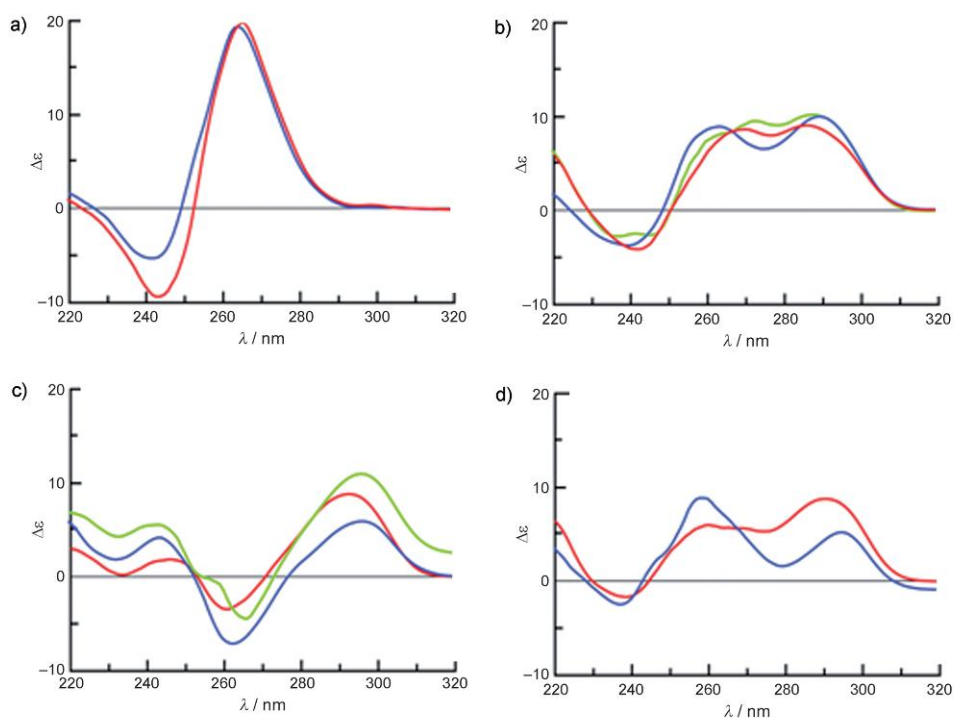
Figure 7.6: CD spectra of standard structurally characterized quadruplex topologies = a) parallel G4; b) antiparallel G4 (group II); c) antiparallel G4 (group III); d) example of a outlier: antiparallel G4 (group III) although it shows a group II CD spectrum (the nucleotide sequence is rich of additional stacking in addition to the guanine tetrads).

The CD measurements and the data processing were done by D. Tedesco and the other group members of Professor M. Bartolini (FaBiT, University of Bologna).

CD analyses were carried out at 25°C on a Jasco (Tokyo, Japan) J-810 spectropolarimeter equipped with a PTC-423S Peltier-type temperature control system. Measurements were performed using a micro-volume QS quartz cell with black walls (1cm pathlength, 500 μL volume; Hellma Italia, Milan, Italy). The wavelength was varied from 420 to 210 nm.

Stock solutions of oligonucleotides (100 μM) and *BRACO-19* or *Pyridostatin* (50 μM) were prepared in analysis buffer (potassium acetate 20 mM pH 6.8 + potassium chloride 70 mM). All samples (500 μL) were prepared at a 2 μM concentration of oligonucleotide by dilution with analysis buffer; samples with *BRACO-19* or PDS were prepared at a 10-20 μM concentration of ligand (5:1 or 10:1 stoichiometry, respectively). Samples were annealed at 95 °C for 5 min and equilibrated at the starting temperature of the assay for additional 30 min. BRACO-19 and PDS were added at different concentrations after the denaturation step.

CD spectra were collected in the 420-220 nm spectral range at 25°C using a 100 nm/min scanning speed at several time points after the denaturation step (1 h e 16 h). Data were

analyzed and processed using the *Jasco Spectra Manager 2* software package. The sample spectra were substracted by the buffer spectrum and smoothed.

7.23 CD Melting assay

Melting analyses were carried out at 25°C on a Jasco (Tokyo, Japan) J-810 spectropolarimeter equipped with a PTC-423S Peltier-type temperature control system. The measurements and data processing were done by D. Tedesco and the other group members of Professor M. Bartolini (FaBiT, University of Bologna).

Measurements were performed using a micro-volume QS quartz cell with black walls (1cm pathlength, 500 μL volume; Hellma Italia, Milan, Italy). Spectra were obtained at 265 nm at 5°C steps starting at 15°C and ending at 95°C using a quartz cuvette ("heating curve"); to confirm the analyses, "cooling curves" were performed at 265 nm decreasing the temperature from 95°C to 15°C.

Stock solutions of oligonucleotides (100 μM) and Braco-19 (50 μM) were prepared in analysis buffer (potassium acetate 20 mM pH 6.8 + potassium chloride 70 mM). All samples (500 μL) were prepared at a 2 μM concentration of oligonucleotide by dilution with analysis buffer; samples with *BRACO-19* were prepared at a 10 μM concentration of ligand (5:1 stoichiometry). Samples were annealed at 95 °C for 30 min and equilibrated at the starting temperature of the ramp for additional 30 min.

CD spectra were collected in the 330–230 nm spectral range between 15 °C and 95 °C for both heating and cooling ramps, using a 0.25 °C/min temperature gradient, a 5 °C sampling frequency, a 100 nm/min scanning speed, a 0.2 nm data interval, a 2 sec data integration time and a 4 nm spectral bandwidth. Spectra were first solvent-corrected with blank measurements carried out in the same temperature range, then converted to molar units per residue ($\Delta\varepsilon_{res}$, in $M^{-1} cm^{-1}$).

CD melting curves for each oligonucleotide were obtained by plotting the $\Delta\varepsilon_{res}$ values at the wavelength of maximum difference between the CD spectra at 15 and 95 °C ($\lambda_{\Delta max}$) as a function of temperature (T). Mid-transition temperatures (T_m) for both heating and cooling ramps were calculated by global fitting on the CD melting curves based on non-linear regression to a 6-parameter logistic function [Mergny et al; 2009]:

$$\Delta\varepsilon_{res} = (a_1 + b_1 T) + \frac{(a_2 + b_2 T) - (a_1 + b_1 T)}{1 + e^{k(T_m - T)}}$$

where a_1 and b_1 are the *y*-intercept and slope of the asymptote for the CD response of the oligonucleotide in the folded state, a_2 and b_2 are the *y*-intercept and slope of the asymptote for the CD response of the oligonucleotide in the unfolded state, and k is the steepness of the melting curve.

7.24 Statistical Analysis

For the statistical analysis: results are represented as the mean values corrected by standard error of at least two experiments, except when indicated. One-way analysis of variance (ANOVA) followed by "Dunnet's Multiple comparison test" was used to compare data among the different experimental conditions; statistically significant differences were determined at $p < 0.01\text{-}0.05$. Values were determined and plotted using the program *GraphPad Prism 6.00* for Windows (GraphPad Software, San Diego California, USA).

50% of effective concentration (EC_{50}) and 50% of cytotoxic concentration (CC_{50}) values were obtained by plotting the percentage values of the inhibition of B19V replication or the percentages values of the inhibition of cell viability/proliferation vs the concentration of the compound, respectively.

8.*References*

1. **Andreoletti L., Leveque N., Boulagnon C., Brasselet C., Fornes P.** "Viral causes of human myocarditis" Archives of Cardiovascular Diseases, vol 102, n° 6-7, pp 559-568 (2009).
2. **Artusi S., Perrone R., Lago S., Raffa P., Di Iorio E., Palù G., Richter S. N.** "Visualization of DNA G-quadruplexes in herpes simplex virus 1-infected cells" Nucleic Acid Research, vol 44, n°21, 10343-10353 (2016).
3. **Astell C. R.** "Terminal hairpins of parvovirus genome and their role in DNA replication" Handbook of Parvoviruses, CRC Press, INC, Boca Raton, Fla, pp 59-80 (1990).
4. **Ballou W. R., Reed J. L., Noble W., Young N. S., Koenig S.** "Safety and immunogenicity of a recombinant parvovirus B19 vaccine formulated with MF59C.1" Journal of Infectious Diseases, vol 187, n°4, pp 675-678 (2003).
5. **Berns, K. I., Bohenzky R. A.** "Adeno-associated viruses: an update" Adv. Virus Res.32:243-306 (1987).
6. **Bernstein D. I., El Sahly H. M., Keitel W. A.** "Safety and immugenicity of a candidate parvovirus B19 vaccine" Vaccine, vol 29, pp 7357-7363 (2011).
7. **Biffi G., Tannahill D., McCafferty J., Balasubramanian S.** "Quantitative visualization of DNA G-quadruplex structures in human cells" Nature Chemistry, vol 5, n°3, pp 182-186 (2013).
8. **Blumel J., Burger R., Drosten C.** „Parvovirus B19-revised" Transfusion Medicine and Hemotheraoy, vol 37, pp 339-350 (2010).
9. **Bock C. T., Klingel K., Kandolf R.** "Human parvovirus B19-associated myocarditis" The New England Journal of Medicine, vol 362, n°13, pp 1248-1249 (2010).
10. **Bonsch C., Zuercher C., Lieby P., Kempf C., Ros C.** "The globoside receptor triggers structural changes in the B19V virus capsid that facilitate virus internalization" Journal of Virology, vol 84, n°22, pp 11737-11746 (2010).
11. **Bonvicini F., Bua G., Gallinella G.** "Parvovirus B19 infection in pregnancy – awareness and opportunities" Current Opinion in Virology, vol 27, pp 8-14 (2017).
12. **Bonvicini F., Bua G., Conti I., Manaresi E., Gallinella G.** "Hydroxyurea inhibits parvovirus B19 replication in erythroid progenitor cells" Biochemical Pharmacology, vol 136, pp 32-39 (2017).
13. **Bonvicini F., Bua G., Manaresi E., Gallinella G.** "Enhanced inhibition of oparvovirus B19 replication by cidofovir in extendendly exposed erythroid progenitor cells" Virus Research, vol 220, pp 47-51 (2016).
14. **Bonvicini F., Bua G., Manaresi E., Gallinella G.** "Antiviral effect of cidofovir on parvovirus B19 replication" Antiviral Research, vol 113, pp 11-8 (2015).
15. **Bonvicini F, Filippone C., Delbarba S.** "Parvovirus B19 genome as a single, two-state re plicative and transcriptional unit" Virology, vol 347, n°2, pp 447-454 (2006).
16. **Bonvicini F., Filippone C., Manaresi E., Zerbini M., Musiani M., Gallinella G.** "Functional analysis and quantitative determination of the expression profile of human parvovirus B19" Virology, vol 381, n°2, pp 168-177 (2008).
17. **Bonvicini F, Manaresi E., Di Furio F., De Falco L., Gallinella G.** "Parvovirus B19 DNA CpG di nucleotide methylation and epigenetic regulation of viral expression" PLoS ONE, vol 7 (2012).
18. **Brown K. E.** "The genus Erythrovirus" In Kerr (ed) Parvoviruses (Hodder Arnold, Londono, United Kingdom), pp 25-45 (2005).
19. **Brown E. K., Hibbs J. R., Gallinella G., Anderson S. M., Lehman E. D., McCarthy P., Young N. S.** "Resistance to Parvovirus B19 infection due to lack of virus receptor (erythrocyte P antigen)" New England Journal of Medicine, vol 330, pp 1192-1196 (1994).
20. **Brown K. E., Young N. S.** "Parvovirus B19 infection and hematopoiesis" Blood Reviews, vol 9, n°3, pp 176-182 (1995).
21. **Brown C. S., Van Lent J. W. M., Vlak J. M., Spaan W. J. M.** "Assembly of empty capsids by using baculovirus recombinants expressing human parvovirus B19 structural proteins" Journal of Virology, vol 65, n°5, pp 2702-2706 (1991).
22. **Bua G., Conti I., Manaresi E., Sethna P., Foster S., Bonvicini F., Gallinella G.** "Antiviral activity of brincidofovir on parvovirus B19" Antiviral Research, vol 162, pp 22-29 (2019).

23. **Bua G., Gallinella G.** "How does parvovirus B19 DNA achieve lifelong persistence in human cells?" Future Virology (2017).

24. **Bua G., Manaresi E., Bonvicini F., Gallinella G.** "Parvovirus B19 replication and expression in differentiating erythroid progenitor cells" PLoS One, vol 11 (2016).

25. **Cahoon L. A., Manthei K. A., Rotman E., Keck J. L., Seifert H. S.** "Neisseria gonorrhoeae RecQ helicase HRDC domains are essential for efficient binding and unwiding of the pile guanine quartet structure required for pilin antigenic variation" Journal of Bacteriology, vol 195, pp 2255-2261 (2013).

26. **Candotti D., Etiz N., Parsyan A., Allain J. P**. "Identification and characterization of persistent human erythrovirus infection in blood donor samples" Journal of Virology, vol. 78, n°22, pp 12169–12178 (2004).

27. **Chandramouli S., Medina-Selby A., Coit D., Schaefer M., Spencer T., Brito L. A., Zhang P., Otten G., Mandl C. W., Mason P. W., Dormitzer P. R.** "Generation of a parvovirus B19 vaccine candidate" Vaccine, vol 31, pp 3872–3878 (2013).

28. **Chen A. Y., Guan W., Lou S., Liu Z., Kleiboeker S., Qiu J.** "Role of erythropoietin receptor signaling in parvovirus B19 replication in human erythroid progenitor cells" Journal of Virology, vol 84, pp 12385-12395 (2010).

29. **Chen A. Y., Kleiboeker S., Qiu J.** "Productive parvovirus B19 infection of primary human erythroid progenitor cells at hypoxia is regulated by STAT5A and MEK signaling but not HIF alpha" PLoS Pathogens (2011).

30. **Chen A. Y., Zhang E. Y., Guan W., Cheng F., Kleiboeker S., Yankee T. M., Qiu J.** "The small 1 kDa non-structural protein of human parvovirus B19 plays a key role in inducing apoptosis during B19 virus infection of primary erythroid progenitor cells" Blood, vol 115, pp 1070-1080 (2010).

31. **Chipman P. R., Agbandje-McKenna M., Kajigaya S., Brown K. E., Young N. S., Bayer T. S., Rossmann M. G.** "Cryo-electron microscopy studies of empty capsids of human parvovirus B19 complexed with its cellular receptor" Proceedings of the National Academy of Sciences USA, vol 93, pp 7502-7506 (1996).

32. **Chorba T., Coccia P., Holman R. C.** "The role of parvovirus B19 in aplastic crisis and erythema infectiosum (fifht disease)" Journal of Infectious Diseases, vol 154, n°3, pp 383-393 (1986).

33. **Cihlar T., Chen M. S.** „Identification of enzymes catalyzing two-step phosphorylation of cidofovir and effect of cytomegalovirus infection on their activities in host cells" Molecular Pharmacology, vol 50, pp 1502-1510 (1996).

34. **Cohen B. J., Field A. M., Mori J.** "Morphology and antigenicity of recombinant B19 parvovirus capsids expressed in transfected COS-7 cells" Journal of General Virology, vol 76, n°5, pp 1233-1237 (1995).

35. **Cohen B. J., Mortimer P. P., Pereira M. S.** "Diagnostic assays with monoclonal antibodies for the human serum parvovirus like virus (SPLV)" Journal of Hygiene, vol 91, n°1, pp 113-130 (1983).

36. **Connelly M. C., Robbins B. L., Fridland A.** "Mechanism of uptake of the phosphonate analog (S)-1-(3-hydroxy-2-phosphonylmethoxpropyl)cytosine (HPMPC) in Vero cells" Biochemecal Pharmacology, vol 46, pp 1053-1057 (1993).

37. **Corcioli F., Zakrzewska K., Rinijeri A., Fanci R., Innocenti M., Civinini R., De Giorgi V., Di Lollo S., Azzi A.** "Tissue persistence of parvovirus B19 genotypes in asymptomatic persons" Journal of Medical Virology, vol 80, pp 2005-2011 (2008).

38. **Cossart Y. E., Field A. M., Cant B., Widdows D.** "Parvovirus-like particles in human sera" Lancet, vol 305, pp 72-73 (1975).

39. **Cotmore S. F., Agbandje-McKenna M., Chiorini J. A., Mukha D. M., Pintel D. J., Soderlund-Venermo M., Tattersali P., Tijssen P., Gatherer D., Davison A. J.** "The family Parvoviridae" Archives of Virology, vol 159, pp 1239-1247 (2014).

40. **Cotmore S. F., McKie V. C., Anderson L. J.** "Identification of the major structural and nonstructural proteins encoded by human parvovirus B19 and mapping of their genes by procaryotic expression of isolated genomic fragments" Journal of Virology, vol 60, n°2, pp 548-557 (1986).

41. **Cotmore S. F., Tattersall P.** "Characterization and molecular cloning of a human parvovirus genome" Science, vol 226, pp 1161-1165 (1984).

42. **Cotmore S. F., Tattersall P.** "Parvoviruses: small does not mean simple" Annual Review of Virology, vol 1, pp 517-537 (2014).

43. **Crabol Y., Terrier B., Rozenberg F.** "Intravenous immunoglobulins therapy for pure red cell aplasia related to human parvovirus B19 infection: a retrospective study of 10 patients and review of the literature" Clinical Infectious Diseases, vol 56, n°7, pp 968-977 (2012).

44. **De Clercq E.** "Acyclic nucleoseide phosphonates: a new dimension to the chemotherapy of DNA virus and retrovirus infections" Journal of Medical Microbiology, vol 47, n°1, pp 1-3 (1998).

45. **De Clercq E., Holy A.** "Acyclic nucleoside phosphonates: a key class of antiviral drugs" Nature Reviews Drug Discovery, vol 4, pp 928-940 (2005).

46. **De Clercq E.** "The acyclic nucleoside phosphonates from inception to clinical use: historical perspective" Antiviral Research, vol 75, pp 1-13 (2007).

47. **De Clercq E., Li G.** "Approved antiviral drugs over the past 50 years" Clinical Microbiology Reviews, vol 29, n°3, pp 695-747 (2016).

48. **Deiss V., Tratschin J. D., Weitz M., Siegl G.** "Cloning of the human parvovirus B19 genome and structural analysis of its palindromic termini" Virology, vol 175, n°1, pp 247-254 (1990).

49. **Domingo E., Sheldon J., Perales C.** "Viral quasispecies evolution" Microbiology Molecular Biology Review, vol 76, n°2, pp 159-216 (2012).

50. **Dong Y., Huang Y., Wang Y.** "The effects of the 11 kDa protein and the putative X protein on the p6 promoter activity of parvovirus B19 in Hela cells" Virus Genes, vol 46, n°1, pp 167-169 (2012).

51. **Duffy S., Shackelton L. A., Holmes E. C.** "Rates of evolutionary change in viruses: patterns and determinants" Nature Reviews Genetics, vol 9, pp 267-276 (2008).

52. **Ekman A.**, Hokynar K., Kakkola L. "Biological and Immunological relations among human parvovirus B19 genotypes 1 to 3" Journal of Virology, vol 81, n°13, pp 6927-6935 (2007).

53. **Enders M., Klingel K., Weidner A., Baisch C., Kandolf R., Schakasta G., Enders G.** "Risk of fetal hydrops and non-hydropic late intrauterine fetal death after gestational parvovirus B19 infection" Journal of Clinical Virology, vol 49, pp 163-168 (2010).

54. **Fan M. M. Y., Tamburic L., Shippam-Brett C., Zagrodney D. B., Astell R.** "The small 11-kDa protein from B19 parvovirus binds growth factor receptor-binding protein 2 in vitro in Src homology domain/ligand-dependet manner" Virology, vol 291, n°2, pp 285-291 (2001).

55. **Filippone C., Franssila R., Kumar A.** "Erythorid progenitor cells expanded from peripheral blood without mobilization or preselection: molecular characteristics and functional competence" PLoS ONE, vol 5, n°3 (2010).

56. **Franssila R., Hokynar K., Hedman K.** "T helper cell-mediated in vitro responses of recently and remotely infected subjects to a candidate recombinant vaccine for human parvovirus B19" Journal of Infectious Diseases, vol 183, n°5, pp 805-809 (2001).

57. **Franssila R., Hedman K.** "T-helper cell-mediated interferon-γ, interleukin-10 and proliferation responses to a candidate recombinant vaccine for human parvovirus B19" Vaccine, vol 22, n°27-28, pp 3809-3815 (2004).

58. **Franssila R., Auramo J., Modrow S.** "T helper cell-mediated interferon-gamma expression after human parvovirus B19 infection: persisting VP2-specific and transient VP1u-specific activity" Clinical and Experimental Immunology, vol 142, n°1, pp 53-61 (2005).

59. **Gadage V S., Viswanathan S., Kunal s., Subramanian P. G., Gujral S.** "Parvovirus B19 presenting with persisten pancytopenia in a patient of T-ALL post induction chemotherapy diagnosed on bone marrow examination" Indian Journal of Pathology and Microbiology, vol 54, pp 603-605 (2011).

60. **Gallinella G.** "Parvovirus B19 Achievements and Challenges" Review Article, 2013.

61. **Gallinella G., Bonvicini F., Filippone C**. "Calibrated real-time PCR for evaluation of parvovirus B19 viral load" Clinical Chemistry, vol 50, n°4, pp 759-762 (2004).

62. **Ganaie S., Qiu J.** "Recent advances in replication and infection of human parvovirus B19" Frontiers in Cellular and Infection Microbiology, vol 8, n°166 (2018).

63. **Ganaie S. S., Xu P., Deng X., Kleiboeker S., Qiu J.** "Phosphorilated STAT5 directly facilitates parvovirus B19 DNA replication in human erythroid progenitors through interaction with the MCM complex" PLOS Pathogens, vol 13, n°5 (2017).

64. **Gellert M., Lipsett M. N., Davies D. R.** "Helix formation by guanylic acid" Proceedings of the National Academy of Science of the USA, vol 48, pp 2013-2018 (1962).

65. **Gigler A., Dorsch S., Hemauer A.** "Generation of neutralizing human monoclonal antibodies against parvovirus B19 proteins" Journal of Virology, vol 73, n°3, pp 1974-1979 (1999).

66. **Gowan S. M., Harrison J. R., Patterson L., Valenti M., Read M. A.** "A G-quadruplex interactive potent small-molecule inhibitor of telomerase exhibiting in vitro and in vivo antitumor activity" Molecular Pharmacology, vol 61, pp 1154-1162 (2002).

67. **Green N. S., Barral S.** "Emerging science of hydroxyurea therapy for pediatric sickle cell disease" Pediatric Research, vol 75, pp 196-204 (2014).

68. **Guan W., Cheng F., Yoto Y.** "Block to the production of full-length B19 virus transcripts by internal polyadenilation is overcome by replication of the viral genome" Journal of Virology, vol 82, n°20, pp 9951-9963 (2008).

69. **Guan W., Cheng F., Huang Q., Qiu J.** "Inclusion of the central exon of parvovirus B19 precursor mRNA is determined by multiple splicing enhancers both in the exon and the downstream intron" Journal of Virology, vol 85, pp 2463-2468 (2011).

70. **Guan W., Huang Q., Cheng F., Qiu J.** "Internal polyadenylation of the parvovirus B19 precursor mRNA is regulated by alternative splicing" Journal of Biological Chemistry, vol 286, pp 24793-24805 (2011).

71. **Guan W., Wong S., Zhi N., Qiu J.** "The genome of human parvovirus B19 can replicate in nonpermissive cells with the help of adenovirus genes and produces infectious virus" Journal of Virology, vol 83, n°18, pp 9541-9553 (2009).

72. **Hankins J. S., Penkert R.P., Lavoie P.** "Parvovirus B19 infection in children with sickle cell disease in the hydroyurea era" Experimental Biology and Medicine, vol 241, pp 749-754 (2016).

73. **Harris L. M., Merrick C. J.** "G-quadruplexes in pathogens: a common route to virulence control?" PLOS Pathogens, vol 11, n°2 (2015).

74. **Hassan , Osman H., Ali M., Ahsan M.** "Therapeutic potential of coumarins as antiviral agents" European Journal of Medical Chemistry (2016).

75. **Heegaard E. D., Brown K. E.** "Human Parvovirus B19" Clinical Microbiology Reviews, vol 15, pp 485-505 (2002).

76. **Hemauer A., von Poblotzki A., Gigler A., Cassinotti P., Siegl G., Wolf H., Modrow S.** "Sequence variabiliy among different parvovirus B19 isolates" Journal of General Virology, vol 77, pp 1781-1785 (1996).

77. **Henderson A., Wu Y., Huang Y. C., Chavez E. A., Platt J., Johnson F. B., Brosh R. M., Sem D., Lannsdorp P. M.** "Detection of G-quadruplex DNA in mammalian cells" Nucleic Acid Reearch, vol 42, n°2, pp 860-869 (2014).

78. **Hsu G. J., Tzang B. S., Tsai C. C., Chiu C. C., Huang C. Y., Hsu T. C.** "Effects of human parvovirus B19 on expression of defensins and Toll-like receptors" The Chinese Journal of Physiology, vol 54, pp 367-376 (2011).

79. **Hubschen J. M., Mihneva Z., Mentis A. F., Schneider F., Aboudy Y., Grossman Z., Rudich H., Kasymbekova K., Sarv I., Nedelikovic J., Tahita M. C., Tamagda Z., Ouedraogo J. B., Gerasimonova A. G., Moskaleva T. N., Tikhonova N. T., Chitadze N., Forbi J. C., Faneye A. O., Otegbayo J. A., Charpentier E., Muller C. P.** "Phylogenetic analysis of human parvovirus B19 sequences from eleven different countries confirms the predominance of genotype 1 and suggests the spread of genotype 3b" Journal of Clinical Microbiology, vol 47, pp 3735-3738 (2009).

80. **Huppert J. L., Balasubramanian S.** "Prevalence of quadruplexes in the human genome" Nucelic Acid Research, vol 33, pp 2908-2916 (2007).

81. **International Committee on Taxonomy of Viruses** "Virus taxonomy: classification and nomenclature of viruses. Seventh report of the International Committee on Taxonomy of Viruses" Springer-Verlag, Vienna, Austria (2000).

82. **Isa A., Lundqvist A., Lindblom A., Tolfvenstam T., Broliden K.** "Cytokine responses in acute and persistent human parvovirus B19 infection" Clinical and Experimental Immunology, vol 147. n°3, pp 419-425 (2007).

83. **Isa A., Norbeck O., Hirbod T.** "Aberrant cellular immune responses in human infected persistently with parvovirus B19" Journal of Medical Virology, vol 78, n°1, pp 129-133 (2006).

84. **Jain P., Das N., Ranjan A., Chaudhary R., Pandey K.** "Comparative study for the efficacy, safety and quality of life in patients of chronic myeloid leukemia treated with Imatimib or Hydroxyurea" Journal Research Pharmacological Practice, vol 2, n°4, pp 156-161 (2013).

85. **Kajigaya S., Shimada T., Fujita S., Young N. S.** "A genetically engineered cell line that produces empty capsids of B19 (human) parvovirus" Proceeding of the National Academy of Sciences of the USA (1989).

86. **Karsisiotis A. I., Hessari N. M., Novelluno E., Spada G. P., Randazzo A., Webba de Silva M.** "Topological characterization of nucleic acid g-quadruplexes by UV absorption and circular dichroism" Angewandte Chemie International Edition, vol 50, pp 10645-10648 (2011).

87. **Kaufmann B., Chipman P. R., Kostyuchenko V. A., Modrow S., Rossmann M. G.** "Visualization of the externalized VP2 N termini of infectious human parvovirus B19" Journal of Virology, vol 82, n°15, pp 7306-7312 (2008).

88. **Kaufmann B., Simpson A. A., Rossmann M. G.** "The structure of human parvovirus B19" Proc Natl Acad Sci U.S.A, vol 101, n°32, pp 11628-11633 (2004).

89. **Kawase M., Momoeda M., Young N. S., Kajigaya S.** "Most of the VP1 unique region of B19 parvovirus is on the capsid surface" Virology, vol 211, n°2, pp 359-366 (1995).

90. **Kikin O., D'Antonio L., Bagga P. S.** "QGRS Mapper: a web-based server for predicting G-quadruplexes in nucleotide sequenze" Nucleic Acid Research, vol 34, pp 676-682 (2006).

91. **Knipe D. M., Howley P. M.** "Fields Virology, 5th edition" Wolters Kluwer, pp 2442-2444 (2007).

92. **Koduri P. R.** "Novel cytomorphology of the giant proerythroblasts of parvovirus B19 infection" American Journal Hematology, vol 58, pp 95-99 (1998).

93. **Kooistra K., Mesman H. J., de Waal M., Koppelman M. H., Zaaijer H. L.** "Epidemiology of high-level parvovirus B19 viraemia among Dutch blood donors, 2003-2009" Vox Sang, vol 100, pp 261-266 (2011).

94. **Kramata P., Votruba I., Otovà B., Holy A.** "Different inhibitory potencies of acyclic phosphonomethoxyalkyl nucleotide analogs toward DNA polymerases alpha, delta and epsilon" Molecular Pharmacology, vol 49, n°6, pp 1005-1011 (1996).

95. **Kypr J., Kejnovska I., Renciuk D., Vorlickova M.** "Circular dichroism and conformational polymorphism of DNA" Nucleic Acid Research, vol 37, n°6, pp 1713-1725 (2009).

96. **Kurita R., Suda N., Sudo K., Miharada K., Hiroyama T., Miyoshi H., Tani K., Nakamura Y.** "Establishment of immortalized human erythroid progenitor cell lines able to produce enucleated red blood cells" PLOS ONE, vol 8, n°3 (2013).

97. **Lane A. N., Chaires J. B., Gray R. D., Trent J.** "Stability and kinectics of G-quadruplex structures" Nucleic Acid Research, vol 36, n°17, pp 5482-5515 (2008).

98. **Lanier R., Trost ., Tippin T., Lampert B., Robertson B., Foster S., Rose M., Painter W., O'Mahony R., Almond M., Painter G.** "Development of CMX001 for the treatment of Poxvirus infections" Viruses, vol 2, pp 2740-2762 (2010).

99. **Lassen J., Bager P., Wohlfahrt J., Bottiger B., Melbye M.** "Parvovirus B19 infection in pregnancy and subsequent morbidity and mortality in offspring" International Journal of Epidemiology, vol 42, pp1070-1076 (2013).

100. **Lehmann H. W., Von Landenberg P., Modrow S.** "Parvovirus B19 infection and autoimmune disease" Autoimmunity Reviews, vol 2, n°4, pp 218-223 (2003).

101. **Leisi R., Di Tommaso C., Kempf C., Ros C.** "The receptor-binding domani in the VP1u region of Parvovirus B19" Viruses, vol 8, n°61 (2016).

102. **Leisi R., Ruprecht N., Kempf C., Ros C.** "Parvovirus B19 uptakes is a highly selective process controlled by VP1u, a novel determinant of viral tropism" Journal of Virology, vol 87, n°24, pp 13161-13167 (2013).

103. **Leisi R., Von Nordheim M., Ros C., Kempf C.** "The VP1u receptor restricts Parvovirus B19 uptake to permissive erythroid cells" Viruses, vol 8, n°265 (2016).

104. **Levy H. C., Browman V. D., Govindasarmy L., McKenna R., Nash K., Warrington K., Chen W., Muzyczka N., Yan X., Baker T. S., Agbandje-McKenna M.** "Heparin binding induces conformational changes in adeno-associated virus serotype 2" Journal of Structural Biology, vol 165, pp 146-156 (2009).

105. **Lopes J., Piazza A., Bermejo R., Kriegsman B., Colosio A.** "G-quadruplex-induced instability during leading-strand replication" EMBO Journal, vol 30, pp 4033-4046 (2011).

106. **Lori F., Malykh A., Cara A., Sun D., Weinstein J. N., Lisziewicz J., Gallo R. C.** "Hydroxyurea as an inhibitor of human immunodeficiency virus-type 1 replication" Science, vol 266, n°5186, pp 801-805 (1994).

107. **Lou S., Luo Y., Cheng F., Huang Q., Shen W., Kleiboeker S., Tisdale J. F., Liu Z., Qiu J.** "Human parvovirus B19 DNA replication induces a DNA damage response that is dispensable for cell cycle arrest at G2/M phase" Journal of Virology, vol 86, pp 10748-10758 (2012).

108. **Luo W., Astell C.R.** "A novel protein encoded by small RNAs of parvovirus B19" Virology, vol 195, pp 448-455 (1993).

109. **Luo Y., Lou S., Deng X., Liu Z., Kleiboeker S., Qiu J.** „Parvovirus B19 infection of human prmiary erythroid progenitor cells triggers ATR-Chk1 signaling, which promotes B19 virus replication" Journal of Virology, vol 85, pp 8046-8055 (2011).

110. **Luo Y., Kleiboeker S., Deng X., Qiu J.** "Human parvovirus B19 infection causes cell cycle arrest of human erythroid progenitors at late S phase that favors viral DNA replication" Journal of Virology, vol 87, pp 12766-12775 (2013).

111. **Magee W. C., Evans D. H.** "The antiviral activity and mechanism of action of (S)-[3-hydroxy-2-(phosphonomethoxy)propyl] (HPMP) nucleosides" Antiviral Research, vol 96, n°2, pp 169-180 (2012).

112. **Maage W. C., Hostetler K. Y., Evans D. H.** Mechanism of inhibition of vaccinia virus DANN polymerase by cidofovir diphosphate" Antimicrobiological Agents Chemoterapy, vol 49, pp 3153-3162 (2005).

113. **Madaan K., Kaushik D., Verma T.** "Hydroxyurea: a key player in cancer chemotherapy" Anticancer Therapy, vol 12, n°1, pp 19-29 (2012).

114. **Manaresi E. Conti I., Bua G., Bonvicini F., Gallinella G.** " A Parvovirus B19 synthetic genome: sequence features and functional competence" Virology, vol 508, pp 54-62 (2017).

115. **Manaresi E., Bua G., Bonvicini F., Gallinella G.** "A flow-FISH assay for the quantitative analysis of parvovirus B19 infected cells" Journal of Virology Methods, vol 223, pp 50-54 (2015).

116. **Manaresi E., Gallinella G., Venturoli S., Zerbini M., Musiani M.** "Detection of Parvovirus B19 IgG: choice of antigens and serological tests" Journal of Clinical Virology, vol 29, n°1, pp 51-53 (2004).

117. **Manaresi E., Zuffi E., Gallinella G.** "Differential IgM response to conformational and linear epitome of parvovirus B19 VP1 and VP2 structural proteins" Journal of Medical Virology, vol 64, n°1, pp 67-73 (2001).

118. **Mani B., Gerber M., Lieby P., Boschetti N., Kempf C., Ros C.** "Molecular mechanism underlying B19 virus inactivation and comparison to other parvoviruses" Transfusion, vol 47, pp 1765-1774 (2007).

119. **Manning A., Willey S. J., Bell J. E., Simmonds P.** "Comparison of tissue distribution, persistence and molecular epidemiology of parvovirus B19 and novel human parvoviruses PARV4 and human bocavirus" journal of Infectious Diseases, vol 195, m°9, pp 1345-1352 (2007).

120. **Manuele M. G., Ferraro G., Barreiro Arcos M. L., Lopez P., Cremaschi G., Anesini C.** "Comparative immunomodulatory effect of scopole tin on tumoral and normal lymphocytes" Life Sciences, vol 79, pp 2043-2048 (2006).

121. **Matsuda H., Sakaguchi K., Shibasaki T., Takahashi H., Kawakami Y., Furuya K.** "Intrauterine therapy for parvovirus B19 infected symptomatic fetus using B19 igG-rich high titer gammaglobulin" Journal of Perinatal Medicine, vol 33, pp 561-563 (2005).

122. **Melamed N., Whittle W., Kelly E. N., Windrim R., Seaward P. G., Keunen J., Keating S., Ryan G.** "Fetal thrombocytopenia in pregnancies with fetal human parvovirus-B19 infection" American Journal Of Obstetrics & Gynecology, vol 212, n°793 (2015).

123. **Mergny J. L., Lacroix L.** "UV Melting of G-Quadruplexes" Current Protocols in Nucleic Acid Chemistry, vol 37 (2009).

124. **Mergny J. L., Lacroix L.** "Analysis of thermal melting curves" Oligonucleotides, vol 13, pp 515-537 (2003).

125. **Mergny J. L., Phan A. T., Lacroix L.** "Following G-quartet formation by UV-spectroscopy" Federation of European Biochemical Societies, Letters 435, pp 74-78 (1998).

126. **Miyagawa E., Yoshida T., Takahashi H.** "Infection of the erythroid cell line, KU812Ep6 with human parvovirus B19 and its application to titration of B19 infectivity" Journal of Virological Methods, vol 83, n°1-2, pp 45-54 (1999).

127. **Mitchell T. J., John S.** "Sugnal transducer and activator of transcription (STAT) signaling and T-cell lymphomas" Immunology, vol 114, pp 301-312 (2005).

128. **Moffatt S., Tanaka N., Tada K.** "A cytotoxiv nonstructural protein, NS1, of human parvovirs B19 induces activation of interleukin-6 gene expression" Journal of Virology, vol 70, n°12, pp 8485-8491 (1996).

129. **Momoeda M., Wong S., Kawase M., Young N. S., Kajigaya S.** "A putative nucleoside triphosphate-binding domain in the nonstructural protein of B19 parvovirus is required for cytotoxicity" Journal of Virology, vol 68, n°12, pp 8443-8443 (1994).

130. **Morey A. I., Ferguson D. J. P., Fleming K. A.** "Ultrastructural features of fetal erythroid precursors infected with Parvovirus B19 in vitro: evidence of cell death by apoptosis" Journal of Pathology, vol 169, n°2, pp 213-220 (1993).

131. **Mori J., Beattie P., Melton D. W., Cohen B. J., Clewlet J. P.** "Structure and mapping of the DNA of human parvovirus B19" Journal of General Virologu, vol 68, pp 2797-2806 (1987).

132. **Morita E., Tada K., Chisaka H.** "Human Parvovirus B19 induces cell cycle arrest at G2 phase with accumulation of mitotic cyclins" Journal of Virology, vol 75, n°16, pp 7555-7563 (2001).

133. **Mortimer P. P., Humphries R. K., Moore J. G., Purcell R. H., Young N. S.** " A human parvovirus-like virus inhibits haematopoietic colony formation in vitro" Nature, vol 302, pp 426-429 (1983).

134. **Munakata Y., Saito-Ito T., Kumura-Ishii K., Kodera T., Ishii T., Hirabayashi Y., Koyanagi Y., Sasaki T.** "Ku80 autoantigen as a cellular coreceptor for human parvovirus B19 infection" Blood, vol 106, pp 3449-3456 (2005).

135. **Munshi N. C., Zhou S., Woody M. J., Morgan D. A., Srivastava A.** Succesfull replication of parvovirus B19 in the human megakaryocytic leukemia cell line MB-02" Journal of Virology, vol 67, pp 562-566 (1993).

136. **Murat P., Zhong J., Lekieffre L., Cowieson N. P., Clancy J. L.** "G-quadruplexes regulate Epstein-Barr virus-encoded nuclear antigen 1 mRNA translation" Nature Chemical Biology, vol 10, pp 358-364 (2014).

137. **Murray P., Rosenthal K., faller M.** "Medical Microbiology, 5th edition" Mosby (2005).

138. **Musiani M., Zerbini ;., Gentilomi G., Plazzi M., Gallinella G., Venturoli S.** "Parvovirus B19 clearance from peripheral blood after acute infection" Journal of Infectious Diseases, vol 172, n°5, pp 1360-1363 (1995).

139. **Nakashima A., Tanaka N., Tamai K.** "Survival of parvovirus B19-infected cells by cellular autophagy" Virology, vol 349, n°2, pp 254-263 (2006).

140. **Nguyen Q. T., Sifer C., Schneider V., Bernaudin F., Auguste V., GarbargChenon A.** "Detection of an erythrovirus sequence distinct from B19 in a child with acute anaemi" Lancet vol 352, pp 1524 (1998).

141. **Nichols D. B., Leao R. A., Basu A., Chudayeu M., de Morades Pde F., Talele T. T., Costa P. R., Kaushik-Basu N**. "Evaluation of coumarin and neoflavone derivatives as HCV NS5B polymerase inhibitors" Chemical Biology & Drug Design, vol 8, n°5, pp 607-614 (2013).

142. **Norja P., Hokynar K., Aaltonene L. M.** "Bioportfolio: lifelong persistence of variant and prototypic erythrovirus DNA genomes in human tissue" Proceeding of the National Academy of Sciences of the United States of America, vol 103, n°19, pp 7450-7453 (2006).

143. **O'Sullivan M. G., Anderson D. K., Goodrich J. A. Tulli H., Green S. W., Young N. S., Brown K. E.** "Experimental infection of cynomolgus monkeys with simian parvovirus" Journal of Virology, vol 71, pp 4517-4521 (1997).

144. **O'SUllivan M. G., Feeney D. A.** "Abstract VIIIth Parvovirus Workshop" abstract 13.5 (2000).

145. **Ogawa M.** "Differentiation and proliferation of hematopoietic stem cells" Blood, vol 81, pp 2844-2853 (1993).

146. **Okochi K., Mori R., Miyazaki M., Cohen B. J., Mortimer P. P.** " Nakatani antigen and human parvovirus (B19)" Lancet, vol 323, pp 160-161 (1984).

147. **Paeschke K., Bochman M. L., Garcia P. D., Cejka P., Friedman K. L.** "Pif1 family helicases suppress genome instability at G-quadruplex motifs" Nature, vol 497, pp 458-462 (2013)

148. **Painter W., Robertson A., Trost L. C., Godkin S., Lampert B., Painter G. "**First pharmacokinetic and safety study in humans of the novel lipid antiviral conjugate CMX001, a broadspectrum oral drug active against double-stranded DNA viruses" Antimicrobil Agents Chemotherapy, vol 56, pp 2726-2734 (2012).

149. **Parsyan, A., Szmaragd C., Allain, J. P., Candotti D.** "Identification and genetic diversity of two human parvovirus B19 genotype 3 subtypes" Journal of General Virology, vol. 88, n° 2, pp 428–431 (2007).

150. **Perrone R. Nadai M., Frasson I., Poe J. A., Butovskaja E.** "A dynamic G-quadruplex region regulates the HIV-1 long terminal repeat promoter" Journal of Medical Chemistry, vol 56, pp 6521-6530 (2013).

151. **Perrone R., Butovskaya E., Daelemans D., Palù G., Pannecouque C., Richter S.** "Anti-HIV-1 activity of the G-quadruplex ligand BRACO-19" Journal of Antimicrobial Chemotherapy, vol 69, pp 3248-3258 (2014).

152. **Perrone R., Doria F., Butovskaya E., Frasson I., Botti S., Scalabrin M., Lago S., Grande V., Nadai M., Freccero M., Richter S. N.** "Synthesis, binding and antiviral properties of a potent core-extended naphtalene diimides targeting the HIV-1 long terminal repeat promoter G-quadruplexes" Journal of Medicinal Chemistry, vol 58, pp 9639-9652 (2015).

153. **Pillet S., Annan Z., Fichelson S., Morinet F.** "Identification of a nonconventional motif necessary for the nuclear import of the human parvovirus B19 major capsid protein (VP2)" Virology, vol 306, n°1, pp 25-32 (2003).

154. **Pillet S., Le Guyader N., Hofer T.** "Hypoxia enhances human B19 erythrovirus gene expression in primary erythroid cells" Virology, vol 327, n°1, pp 1-7 (2004).

155. **Pule D., Mowla S., Novitzky N., Wiysonge C. S., Wonkam A**. "A systematic review of known mechanisms of hydroxyurea-induced fetal hemoglobin for treatment of sickle cell disease" Hematology, vol 1, pp 1-11 (2015).

156. **Quattrocchi S., Ruprecht N., Bonsch C., Bieli S., Zurhcer C., Boller K., Kempf C., Ros C.** "Characterization of the early steps of human parvovirus B19 infection" Journal of Vitology, vol 86, n°17, pp 9274-9284 (2012).

157. **Raab U., Bauer B., Gigler A., Beckenlehner K., Wolf H., Modrow S.** "Cellular transcription factors that interact with p6 promoter elements of parvovirus B19" Journal of General Virology, vol 82, n°6, pp 1473-1480 (2001).

158. **Rachwal P. A., Fox K. R.** "Quadruplex melting" Methods, vol 43, pp 291-301 (2007).

159. **Rodriguez R., Miller K. M., Forment J. V., Bradshaw C. R., Nikan M., Britton S., Oelsclaegel T., Xhemalce B., Balasubramanian S., Jackson S.** "Small molecule-induced DNA damage identifies alternative DNA structure in human genes" Nature Chemical Biology, vol 8, n°3, pp 301-310 (2012).

160. **Ros C., Gerber M., Kempf C.** "Conformational changes in the VP1-unique region of native human parvovirus B19 lead to exposure of internl sequenced that play a role in virus neutralization and infectivity" Journal of Virology, vol 80, pp 12017-12024 (2006).

161. **Schneider B., Hone A., Tolba R. H., Fischer H. P., Blumel J., Eis-Hubinger A. M.** "Simultaneous persistence of multiple genome variants of human parvovirus B19" Journal of General Virology vol 89, n°1, pp 164-176 (2008).

162. **Schwarz T. F., Serke S., Hottentrager B.** "Replication of parvovirus B19 in hematopoietic progenitor cells generated in vitro from normal human peripheral blood" Journal of Virology, vol 66, n°2, pp 1273-1276 (1992).

163. **Servant A., Laperche S., Lallemand F., Marinho V., De Saint M. G., Meritet J. F., Garbarg-Chenon A.** "Genetic diversity within human erythroviruses: identification of three genotypes" Journal of Virology vol 76, pp 9124–9134 (2002).

164. **Shade R. O., Blundell M. C., Cotmore S. F., Tattersall P., Astell C. R.** "Nucleotide sequence and genome organization of human parvovirus B19 isolated from the serume of a child during aplastic crisis" Journal of Virology vol 58, pp 921-936 (1986).

165. **Shimomura S., Komatsu N., Frickhofen N., Anderson S., Kajigaya S., Young N., S.** "First continuous propagation of B19 parvovirus in a cell line" Blood, vol 79, n°1, pp 18-24 (1992).

166. **Shimomura S., Wong S., Brown K. E., Komatsu N., Kajigaya S., Young N. S.** "Early and late gene expression in UT-7 cells infected with B19 parvovirus" Virology, vol 194, n°1, pp 149-156 (1993).

167. **Siddiqui-Jain A., Grand C. L., Bearss D. J., Hurley L. H.** "Direct evidence for a G-quadruplex in a promoter region and its targeting with a small molecule to repress c-MYC transcription" Proceedings of the National Academy of Science of USA, vol 99, pp 11593-11598 (2002).

168. **Siegl G, Bates R. C., Berns K. I., Carter B. J., Kelly D. C., Kurstak E., Tattersall P.** "Characteristics and taxonomy of Parvoviridae" Intervirology vol 23, pp 61-73 (1985).

169. **Singh M. K., Shweta H., Sen S.** "Dispersed dynamics of salvation in G-quadruplex DNA: comparison of dynamic Stokes shifts of probes in parallel and antiparallel quadruplex structures" Methods and Applications in Fluorescence, vol 4, n°3 (2016).

170. **Smith J. S., Chen Q., Yatsunyk L. A. Nicolodius J. M., Garcia M. S.** "Rudimentary G-quadruplex-based telomere capping in Saccharomyces cerevisiae" Naturae Structure & Molecular Biology, vol 18, pp 478-485 (2011).

171. **Sol N., Le Junter J., Vassias I.** "Possible interactions between the NS-1 protein and tumor necrosis factor alpha pathways in erythroid cell apoptosis induced by human parvovirus B19" Journal of Virology, vol 73, n°10, pp 8762-8770 (1999).

172. **Srivastava C. H., Samulski R. J., Lu L., Larsen S. H., Srivastava A.** "Construction of a recombinant human parvovirus B19: adenoassociated virus 2 (AAV) DNA inverted terminal repeats are functional in an AAV-B19 hybrid virus" Proceedings of the National Academy of Science of the USA, vol 86, pp 8078-8082 (1989).

173. **Srivastava C. H., Zhou S., Munshi N. C., Srivastava A.** "Parvovirus B19 replication in human umbilical cord blood cells" Virology, vol 189, n°2, pp 456-461 (1992).

174. **St Amand J., Astell C. R.** "Identification and characterization of a family of 11-kDa proteins encoded by the human oarvovirus B19" Virology, vol 192, pp 121-131 (1993).

175. **Sun D., Hurley L. H.** "The importance of negative superhelicity in inducing the formation of G-quadruplex and i-motif structures in the c-MYC promoter: implication for drug targeting and control of gene expression" Journal of Medicinal Chemistry, vol 52, pp 2863-2874 (2009).

176. **Suzuki M., Yoto Y., Ishikawa A., Tsutsumi H.** "Analysis of nucleotide sequenze of human parvovirus B19 genome reveals two different modes of evolution, a gradual alteration and a sudden replacement: a retrospective study in Sapporo, Japan, from 1980 to 2008" Journal of Virology, vol 83, n°21, pp 10975-10980 (2009).

177. **Takahashi T., Ozawa K., Takahashi K., Asano S., Takaku F.** "Susceptibility of human erythropoietic cells to B19 parvovirus in vitro increases with differentiation" Blood, vol 75, pp 603-610 (1990).

178. **Takahashi T., Ozawa K., Takahashi K., Okuno Y., Muto Y., Takaku F., Asano S.** "DNA replication of parvovirus B19 in a human erythroid leukemia cell line (JK-1) in vitro" Archives of Virology, vol 131, pp 201-208 (1993).

179. **Tewary S. K., Zhao H., Deng X., Qiu J., Tang L.** "The human parvovirus B19 non-structural protein 1 N-terminal domain specifically binds to the origin of replication in the viral DNA" Virology, vol 449, pp 297–303 (2014).

180. **Toan N. L., Duechting A., Kremsner P.G.** "Philogenetic analysis of human parvovirus B19, indicating two subgroups of genotype 1 in Vietnamese patients" Journal of General Virology, vol 87, n°10, pp 2941-2949 (2006).

181. **Toppinen M., Perdomo M. F., Palo J. U., Simmonds P., Lycett S. J., Soderlund-Venemo M., Salatila A., Hedman K.** "Bones hold the key to DNA virus history and epidemiology" Sci Rep vol 5, pp 17226 (2015).

182. **Trigg B. J., Ferguson B. J.** "Funtions of DNA damage machinery in the innate immune response to DNA virus infection" Current Opinion in Virology, vol 15, pp 56-62 (2015).

183. **Tsay S. C., Lin S. Y., Huang W. C., Hsu M. H., Hwang K. C., Lin C. C., Hrong J. C., Chen I. C., Hwu J. R., Shieh F. K., Leyssen P., Neyts J.** "Synthesis and structure activity relationships of imidazole-coumarin conjugates against hepatitis C virus" Molecules, vol 21 (2016).

184. **Tsuikawa M., Nishigaki H., Yoshikawa M., Furuki R., Takahashi K., adan-Kubo J., Shimamura Y., Urayama T., Hattori S., Sakai K., Yunoki M., Ikuta K.** "Variability of parvovirus B19 genotype 2 in plasma products with different compositions in the inactivation sensitivity by liquid-heating" Vox Sang vol 102, pp 93-99 (2012).

185. **Tuckova K., Marusic M., Tothova P., Bauer L., Sket P.** "Human Papillomavirus G-quadruplexes" Biochemistry, vol 52, pp 7207-7216 (2013).

186. **Venturoli S., Gallinella G., Manresi E., Gentilomi G., Musiani M., Zerbini M.** "IgG response to the immunoreactive region of parvovirus B19 nonstructural protein by immunoblot assay with a recombinant antigen" Journal of Infectious Diseases, vol 178, pp 1826-1829 (1998).

187. **Von Kietzell K., Pozzuto T., Heilbronn R., Grossi T., Fechner H., Weger S.** "Antibody-mediated enhancement of parvovirus B19 uptake into endothelial cells mediated by a receptor for complement factor C1q" Journal of Virology, vol 88, pp 8102-8115 (2014).

188. **Wahyuni T. S., Widyawaruyanti A., Lusida M. I., Fuad A., Soetjipto, Fuchino H., Kawahara N., Hayashi Y., Aoki C., Hotta H.** "Inhibition of hepatitis C replication by chapelin and pseudane IX isolated from Ruta angustifolia leaves" Fitoterapia, vol 99, pp 276-283 (2014).

189. **Wan Z., Zhi N., Wong S.** "Human parvovirusB19 causes cell cycle arrest of human erythorid progenitors via deregulation of the E2F family of transcription factors" Journal of Clinical Investigation, vol 120, n°10 pp 3530-3544 (2010).

190. **Wegner C. C., Jordan J. A.** „Human parvovirus B19 VP2 empty capsids bind to human villous trophoblast cells in vitro via the globoside receptor" Infectious Disease in Obstetrics and Ginecology, vol 12, n°2, pp 69-78 (2004).

191. **Weigel-Kelley K. A., Yoder M. C., Chen L., Srivastava A.** "Role of integrin cross-regulation in parvovirus B19 targeting" Human Gene Therapy, vol 17, n°9, pp 909-920 (2006).

192. **Weigel-Kelley K. A., Yoder M. C., Srivastava A.** "Recombinant human parvovirus B19 vectors: erythrocyte P antigen is necessary but not sufficient for successful transduction of human hematopoietic cells" Journal of Virology, vol 75, pp 4110-4116 (2001).

193. **Weigel-Van Aken K. A. K.,** "Pharmacological activation of guanine nucleotide exchange factors for the small GTPase Rap1 recruits high-affinity b1 integrase as coreceptors for parvovirus B19: improved ex-vivo gene transfer to human erythroid progenitor cell" Human Gene Therapy, vol 20, n°12, pp 1665-1678 (2009).

194. **Wong S., Brown K. E.** "Development of an improved method of detection of infectious parvovirus B19" Journal of Clinical Virology, vol 35, n°4, pp 407-413 (2006).

References

195. **Wolfisberg R., Ruprecht N., Kempf C., Ros C. "**Impaired genome encapsidation restrict the in vitro propagation of human parvovirus B19" Journal Of Virology Methods, vol 193, pp 215-225 (2013).

196. **Xiong X., Smith J. L., Chen M. S.** "Effect of incorporation of cidofovir into DNA by human cytomegalovirus DNA polymerase on DNA elongation" Antimicrobiological Agents Chemotherapy, vol 41, n°3, pp 594-599 (1997).

197. **Xu P., Zhou Z., Xiong M., Zou W., Deng X., Ganaie S. S., Kleiboeker S., Peng J., Liu K., Wand S., Ye S. Q., Qiu J.** "Parvovirus B19 NS1 protein induces cell cycle arrest at G2-phase by activating the ATR-CDC25C-CDK1 pathway" PLoS Pathogen vol 13 (2017).

198. **Yaegashi N., Shiraishi H., Takeshita T., Nakamura M., Yajima A., Sugamura K.** "Propagation of human parvovirus B19 in primary culture of erythroid lineage cells derived from fetal liver" Journal of Virology, vol 63, n°6, pp 2422-2426 (1989).

199. **Yoto Y., Qiu J., Pintel D. J.** "Identification and characterization of two internal cleavage and polyadenilation sites of parvovirus B19 RNA" Journal of Virology, vol 80, n°3, pp 1604-1609 (2006).

200. **Young N., Brown K.** "Parvovirus B19" New England Journal of Medicine, vol 350, pp 586-597 (2004).

201. **Young N., Harrison M., Moore J.** "Direct demonstration of the human parvovirus in erythroid progenitor cells infected in vitro" Journal of Clinical Investigation, vol 74, n°6, pp 2024-2032 (1984).

202. **Zadori Z., Szelei J., Tijssen P.** "SAT: a late NS protein of Porcine Parvovirus" Journal of Virology, vol 79, n°20 (2005).

203. **Zakrzewska K., Cortivo R., Tonello C.** "Human parvovirus B19 experimental infection in human fibroblasto and endothelial cells culture" Virus Research, vol 11, n° 1-2, pp 1-5 (2005).

204. **Zhi N., Mills I. P., Lu J., Wong S., Filippone C., Brown K. E.** "Molecular and functional analyses of a Human Parvovirus B19 infectious clone demonstrates essential roles for NS1, VP1 and the 11-kilodalton protein in virus replication and infectivity" Journal of Virology, vol 80, n°12 (2006).

205. **Zhi N., Zadori Z., Brown K. E., Tijssen P.** "Construction and sequencing of an infectious clone of the human parvovirus B19" Virology, vol 318, pp 142-152 (2004).

206. **Zhou T., Shi Q., Chen C. H., Huang L., Ho P., Morris-Natschke S. L., Lee K. H.** "Anti-AIDS agents 85. Design, synthesis and evaluation of 1R,2R-dicamphanoyl-3,3-dimethyldihydropyrano-[2,3-c]xanthen-7(1H)-one (DCX) derivatives as novel anti-HIV agents" European Journal of Medicinal Chemistry, vol 47, pp 86-96 (2012).

207. **Zou W., Wang Z., Xiong M., Yun Chen A., Xu P., Ganaie S. S., Badawu Y., Kleiboeker S., Nishimune H., Qing Ye S., Qiu J.** "Human parvovirus B19 utilizes cellular DNA replication machinery for viral DNA replication" Journal of Virology, vol 92, n°5 (2018).

208. **Zuccheri G., Bergia A., Gallinella G., Musiani M., Samorì B.** "Scanning force microscopy study on a single-stranded DNA: the genome of parvovirus B19" ChemBioChem, vol 2, n°3, pp 199-204 (2001).